DIAGENETIC STUDY OF THE LOWER PERMIAN ROTLIEGEND SANDSTONE, LEMAN FIELD, SOUTHERN NORTH SEA

A thesis submitted for the degree of

Doctor of Philosophy

by Morgan David Sullivan

B.A. University of California Santa Barbara

Department of Geology & Applied Geology

University of Glasgow

May 1991

ProQuest LLC.
789 East Eisenhower Parkway
P.O. Box 1346
Ann Arbor, MI 48106 – 1346

Thesis Declaration

The material presented in this thesis is the result of research carried out between January 1987 and May 1991 in the Department of Geology and Applied Geology, University of Glasgow, under the supervision of Dr. Stuart Haszeldine.

This thesis is based on my own independent research and any published or unpublished material used by me has been given full acknowledgement in the text.

Morgan Sullivan
May, 1991

We certify that Morgan Sullivan has undertaken the bulk of the work involved in this thesis. Specifically: background geology, sample preparation, examinations and analyses, and interpretation. We have assisted with advice and help of a general, technical, conceptual nature, as would be expected in the course of normal Ph.D. supervision and advice. Morgan Sullivan has written the thesis and papers within it himself, and is responsible for its content.

R S Haszeldine

A J Boyce

A E Fallick

G Rodgers

ABSTRACT

The Lower Permian aeolian and wadi subarkoses of the Rotliegend Sandstone, UK southern North Sea, are up to 270 m thick and form the reservoir for the economically important Leman gas field. The diagenetic history of these sands was studied using petrographic, geochemical, and isotopic techniques in order to relate the diagenetic sequence to the burial and tectonic history of the field. The earliest authigenic phases consist of hematite and illite clay rims on detrital grains which precipitated soon after deposition from intrastratal alteration of iron silicates by meteoric groundwater. On the basis of oxygen, carbon, sulphur and strontium isotope data, the remainder of the diagenesis occurred in fluids derived from the mixing of waters from the overlying Zechstein evaporites and underlying Carboniferous shales, which displaced the interstitial meteoric porewaters of the Rotliegend. Flushing of the Rotliegend Sandstone by mixed Zechstein/Carboniferous waters produced two generations of pervasive dolomite cement. Oxygen isotope values for the dolomite reflect precipitation at temperatures between 35° and 60°C at a depth of 400 m to 1.2 km during the Late Permian-Early Triassic. This was followed by extensive quartz cementation. Oxygen isotope and fluid inclusion data indicate that the greatest volume of quartz precipitated during the Late Triassic between 75° and 100°C (1.5 to 2km burial) from modified Carboniferous derived meteoric waters. Subsequent illite, chlorite, ankerite, siderite and anhydrite cements further reduced the porosity of the Rotliegend. Oxygen isotope values for the ankerite and anhydrite suggest that these cements precipitated from evolved brines at temperatures between 105° and 140°C. These temperatures correspond to burial depths between 2 and 3.5 km and would have been attained during the deepest burial of the Rotliegend Sandstone in the Leman field. Later migration of acid fluids from the underlying Carboniferous shales produced extensive secondary porosity. Finally, minor precipitation of quartz and illite occurred prior to the emplacement of hydrocarbons, the latter halting further diagenesis.

ACKNOWLEDGEMENTS

I would like to start by thanking Amoco (U.K.) Exploration and Shell/Esso U.K. Exploration and Production for providing the funding of this project and for allowing me access to their data on the Rotliegend Sandstone in the Leman field. At Amoco I would like to thank Dai Jones, Iain Pearson and Grenville Annett, and at Shell I would like to thank John Kantorowicz, Allan Heward, Robert Marskall and John Marshall for all of their assistance during the course of this research.

I thank Stuart Haszeldine for giving me the opportunity to undertake this project, for his supervision throughout the project and for his patience during the final stages. My thanks also go to Tony Fallick, Adrian Boyce and Graeme Rogers, without whose guidance and advice I could not have completed this project. Tony and Adrian are also thanked for the many enlightening (and intoxicating) discussions held at Dukes University on Friday nights. Also many thanks to the staff of the SURRC Isotope Geology Unit for their assistance, especially Terry, Gawen,Paul, Julie, Elisbeth, Alison, Margret, George, Jocelyn, and of course the Three Musketeers.

I am also greatly indebted to the technical staff in the Geology Department for all of their assistance and I would like to thank John, Peter, Robert, Dugie, Murdo, Allan and the rest of the gang. I would especially like to thank the world's greatest photographer (or at least Glasgow's) and good friend Douglas Maclean for all of his help with producing slides for talks and photographs for this thesis, and also Peter Ainsworth for all of his help with mineral separation techniques and assistance with SEM studies. Many, many thanks also to Jamie Gallagher for all of his help and for introducing me to Celtic and the Vicky Bar, both which provided well needed escapes from the drudgery of research. I thank Bob, Roddy, The Management (alias John and Alec) and even Eddie just for being good friends.

I would also like to thank Ed Stephens and Donald Herd at St.

Andrews University for allowing the use of their microprobe facilities, on which the majority of the probe work was completed and BSE photomicrographs taken. I thank Graeme Walker and Eric Lancake at University of Manchester Institute of Science and Technology for allowing me to use their hot-cathodoluminescence microscope on which all of the quartz luminescence work was completed. I am also greatly indebted to Dick Sutherland of the B.G.S. for allowing access to material from the Hydrocarbon Core Store in Edinburgh, and Joe Bulat and Susan Stoker, also of the B.G.S., for informative discussions concerning the burial history of the the Rotliegend in the southern North Sea.

Fellow members of the *"Diaboredom Gang"* John, Calum, Orla, Gordon, Andy, Rachael, Mark (alias *"The Wobbler"*), Robbie and pseudo members Clark, Joe and Peter are all thanked for discussions regarding this project. Neil Clark is also thanked for undertaking the horrible task of editing an early draft of this work and for providing accommodation when I had no where to live.

And finally I would like to thank my Mother, Father and Gareth, without whose understanding, and help, I definitely could not have finished the work. Most importantly though, I would like to thank my fiancée Tina for giving me her full support and waiting four years for me to finish my Ph.D.

CONTENTS

CHAPTER 1

CHAPTER 1 INTRODUCTION

1.1 ORIGINAL AIMS OF THE PROJECT

Diagenesis can be described as the sum of the processes by which a sediment attempts to attain equilibrium with its environment. This includes all of the physical and chemical changes that occur in a sediment from deposition, through burial diagenesis and reservoir filling, to metamorphism. Diagenesis is, therefore, of direct importance to the petroleum industry in their evaluation of reservoir rocks through the examination of textures, fabrics, and minerals, and is used for the prediction of regional trends of rock quality.

In studies of sandstone diagenesis, it is often difficult to interpret the timing of cementation, the controls on cement distribution, and the chemical and hydrologic conditions under which cementation occurred. The aim of this project was, therefore, to document and decipher the diagenetic history of the Rotliegend Sandstone in the Leman field, focusing on the timing, the controls and the distribution of authigenic cements, and the origin of the fluids/ions from which they precipitated, in order to provide answers to some of these important questions concerning sandstone diagenesis in a well documented study. The Lower Permian Rotliegend Sandstone consists of terrigenous clastics that were deposited in aeolian, fluvial and lacustrine environments following the opening of the Southern Permian Basin. The diagenetic history of core material from the Rotliegend Sandstone was studied, applying petrographic, geochemical and isotopic techniques. This work has been built upon the previous diagenetic studies of the Rotliegend Sandstone by Glennie *et al.* (1978), Almon (1981), Lee (1984), Pye & Krinsley (1986), Goodchild & Whitaker (1986), and Arthur *et al.*, (1986). The diagenesis of the aeolian deposits of Lower Permian Penrith Sandstone was also examined in order to compare the origin and three dimensional geometry of quartz cementation in the Rotliegend and Penrith sandstones.

This study was conducted along a number of lines including:

(i) Examination of the depositional and tectonic history of the Rotliegend Sandstone in the Leman field.

(ii) Construction of a burial history curve for the Leman field based on released well data, interval velocity measurements and vitrinite reflectance.

(iii) Establishment of the paragenetic sequence of diagenetic minerals in the Rotliegend Sandstone through petrographic analysis.

(iv) Isotopic analyses of carbonate, silicate and sulphate authigenic minerals in order to determine the source and evolution of diagenetic fluids and temperatures of precipitation.

(v) Assessment of the distribution of, and factors controlling, cement precipitation, such as porosity, permeability, nucleation and growth rates.

(vi) Modelling the movement of fluids from which authigenic cements precipitated.

(vii) Examination of the reservoir quality of the Rotliegend with respect to secondary porosity development and the mechanisms of mineral dissolution.

(viii) Examination of quartz diagenesis of the Penrith Sandstone in NW England in order to evaluate the controls and timing of quartz cementation in this sandstone and compare these results to the data collected for the Rotliegend Sandstone.

1.2 OVERVIEW OF ROTLIEGEND DIAGENESIS

The Rotliegend Sandstone in the Leman field has experienced a long and varied diagenetic history . The generalized sequence of diagenetic events in the Rotliegend Sandstone was compaction of framework grains, dissolution of unstable detrital components, precipitation of authigenic cements, formation of secondary porosity and emplacement of hydrocarbons (Figure 1.1). The sequence of diagenetic events was determined using cement stratigraphy deduced from polarizing microscope, cathodoluminescence, SEM and microprobe studies. The major diagenetic minerals present in the Rotliegend Sandstone in the Leman field are; (1) hematite and mixed layered illite/smectite, (2) dolomite (3) feldspar, (4) quartz, (5) chlorite, (6) illite, (7) ankerite, (8) siderite, and (9) anhydrite. The general paragenetic sequence, observed in the Leman field, is the same for all seven wells examined, although stratigraphic variations occur in the distribution of certain cements.

Compaction

The Rotliegend Sandstone in the Leman field has undergone considerable compaction. This is indicated by the abundance of sutured grain contacts, although, the concavo-convex and long contacts are the most common types. Unstable grains, such as feldspar, which in some cases were partially dissolved prior to deep burial, have been crushed and broken due to mechanical compaction. The majority of the feldspar dissolution, however, occurred at depth. Compaction has also significantly reduced the porosity in these sandstones. Minus cement porosities range from 15% (reworked dune deposits) to 30% (dune deposits), representing a reduction in porosity of approximately 15% from their original pre-compaction values of 40-45% porosity (Beard & Weyl 1973). The finer grained laminae are more compacted than the medium to coarse grained laminae, suggesting that preferential cementation of the

latter, due to their higher permeability and porosity, may have helped prevent their compaction.

Hematite and illite (smectite ?) clay

The first diagenetic minerals to form in the Rotliegend Sandstone were iron oxide and smectitic clay which occur as thin coatings on detrital grains. Studies by Walker (1976) showed that the reddening of sediments in arid environments develops as a result of interstratal alteration and dissolution of unstable iron rich silicates. These deposits are not red at the time of deposition, but subsequently become reddened due to oxidizing pore fluids which alter the iron silicates by hydrolysis. The oxidized iron is then precipitated as hematite or as a precursor which later alters to hematite. Smectitic clays are also formed by the weathering of iron silicates and the early illite observed coating grains is assumed to have been derived in part from the alteration of smectite.

Early dolomite

Two distinct generations of pervasive dolomite cement are recognized in the Rotliegend Sandstone using cathodoluminescence petrography. The first phase is Type I dolomite, which is characterised by brightly luminescent microrhombic (10 to 30 μm) and rhombic (100 to 200 μm) Type I dolomite crystals. Microrhombic dolomite occurs as both coalesced aggregates of crystals and as individual pore lining rhombs. Rhombic dolomite commonly forms blocky, anhedral rhombs, which reflect interfering growth during precipitation. Examination under cathodoluminescence shows that the majority of microrhombic and rhombic dolomite is represented by brightly luminescent Type I dolomite. The uniform luminescence of both grain sizes of rhombic dolomite is consistent with the hypothesis that the fine and coarse grained dolomite are the same generation of cement. The chemistry of the Type I carbonate is also very uniform and is characterized by non-ferroan dolomite.

Type II dolomite is the second generation of dolomite cement recognized in the Leman field. It occurs as poikilotopic patches, corrosive

overgrowths on earlier Type I dolomite, and individual pore lining rhombs. Overgrowths of Type II dolomite on earlier Type I dolomite rhombs indicates that the Type II is a slightly later generation of cement, although it is thought that they both formed during early diagenesis. The Type II dolomite appears dull red to brownish red under cathodoluminescence and is significantly more ferroan (up to 4 mole % iron) than the non-ferroan Type I dolomite.

K-feldspar

Authigenic K-feldspar is a minor cement in the Rotliegend Sandstone occurring as overgrowths on detrital feldspar grains. Microprobe and EDAX analysis of the overgrowths indicate that they are orthoclase and the overgrowths are preferentially developed around detrital cores of K–feldspar. Feldspar overgrowths are separated from detrital cores by a thin rim of authigenic hematite and clay which formed prior to authigenic feldspar. Authigenic feldspar also encloses early Types I and II dolomite cements, indicating that feldspar precipitation post-dates dolomite precipitation.

Authigenic quartz

Two morphologies of early diagenetic quartz are observed in the Leman field; (1) early individual prismatic crystals, and (2) early pore filling syntaxial overgrowths. The earliest generation of quartz cement is represented by by individual prismatic crystals which formed as "outgrowths" (McBride et al., 1987) on detrital grains. These crystals range in size from 10 to 60 μm and are very euhedral. Prismatic quartz was rapidly followed by the formation of large syntaxial quartz overgrowths. Syntaxial overgrowths commonly occlude pores, engulfing earlier prismatic quartz crystals. Intergrowth of pore-filling quartz and early authigenic feldspar indicate that this phase of quartz was also a relatively early diagenetic phase. Additional evidence for its early formation are loose grain packing and lack of pressure solution within well cemented

zones, suggesting that it precipitated prior to significant compaction.

Chlorite

Chlorite is only a minor authigenic cement, but it is observed in nearly all samples from the Rotliegend of the Leman field. It occurs as thin rims of pore-lining and pore-bridging plates on detrital grains and earlier cements. Chlorite crystals range in size from 5 to 10 μm and are euhedral pseudohexagons. In thin section chlorite appears as green flakes growing radially into pores. This type of texture can significantly reduce permeability, and has inhibited the precipitation of later authigenic minerals within these pores. The chlorite precipitated during deep burial and post dates quartz, feldspar and dolomite cements, but formed contemporaneously with the main phase of illite growth. Fibrous illite growing from chlorite plates possibly represents the extended precipitation of illite.

Illite

The earliest development of illite was as mixed layered illite/smectite associated with hematite. This early clay grain coating was extremely thin and with increasing burial the mixed layered clay was transformed to ordered illite. The main phase of illite precipitation, however, was during late burial diagenesis and consists of wispy illite flakes. Illite is observed as thin grain coatings lining pores, and pore bridging illite is also present within some samples. Only grain contacts and later cements are not coated with illite. XRD analysis of illite indicates that it is extremely pure with only a minor amount of mixed layered smectite.

Ankerite (ferroan dolomite)

Ankerite occurs throughout the formation as overgrowths which nucleated onto earlier dolomite cements and as individual pore lining rhombs. Individual crystals range from 50 to 200 μm in size and are

euhedral in shape. Marginal replacement of rhombic and poikilotopic dolomite by ankerite clearly illustrate that the dolomite pre-dates the ankerite. Ankerite is commonly in optical continuity with the partially dissolved dolomite onto which it has nucleated. This texture suggests replacement, and subsequent overgrowth. Much of the ankerite is compositionally zoned, with zones generally becoming more ferroan toward the margins, suggesting that the iron content of the pore fluids increased during ankerite precipitation. The lack of illite and chlorite cement coatings on ankerite crystals suggests that ankerite precipitation post-dated their formation.

Siderite

Siderite is the least abundant of the carbonate minerals in the Leman field. It only occurs in association with fractures mineralized with bladed anhydrite cement, and no siderite is found within the adjoining sandstones. Crystals range in size from 200 to 1000 μm, they are euhedral and are attached to fracture walls. Their euhedral shape suggests that the fractures were open during crystal growth, and indicates that the siderite precipitated before the fracture filling sulphate. Both siderite and ankerite pre-date anhydrite cement indicating that these carbonate cements formed at similar burial depths.

Anhydrite

Anhydrite occurs as both intergranular poikilotopic and fracture-filling cements. Petrographic observations, such as intergranular anhydrite enclosing late authigenic ankerite and pressure solved cemented grains, suggest that anhydrite formed late in the diagenetic history of the Rotliegend. Anhydrite also occurs as a fracture-filling cement. Mineralized fractures contain bladed anhydrite which has grown sub-parallel to the fracture walls and appears to be all of a single generation. Coarse grained laminae completely cemented by anhydrite are observed intersecting the mineralized fractures which suggests that fluids moved from the fractures into high permeability zones within the

sandstones. This textural evidence suggests that the poikilotopic and fracture-filling anhydrite represent the same generation of cementation.

Secondary Porosity

The main phase of mineral dissolution and generation of secondary porosity occurred after the precipitation of late carbonate and sulphate cements and is therefore thought to have been associated with, or following the deepest burial of the Rotliegend Sandstone in the Leman field. Secondary porosity, which makes up approximately a third of the present porosity, formed by the dissolution of plagioclase, dolomite, ankerite and anhydrite. Textural evidence for mineral dissolution includes oversized and elongate pores, floating grains, corroded grain margins and authigenic cements.

Late quartz and illite cements

Locally, an extremely late phase of authigenic quartz overgrowths have precipitated into oversized pores of secondary origin . This late prismatic quartz is fine grained, and crystals are generally in the order of tens of microns in size and euhedral in form. Fibrous illite is often intergrown with the late quartz indicating there was a late phase of illite associated with quartz generation.

Hydrocarbons

The migration of gas into the Rotliegend Sandstone in the Leman field must have occurred shortly after the generation of secondary porosity, and precipitation of late-stage quartz and illite. This is reflected by the preservation of open secondary pores which only contain minor infilling quartz and illite cements. In the absence of hydrocarbons, diagenesis would have continued and the secondary porosity would have been destroyed by cementation and compaction.

1.3 THE THESIS

This thesis comprises four papers, Chapters 2 to 5, which investigate various aspects of the diagenetic history of the Lower Permian Rotliegend Sandstone in the Leman field of the southern North Sea, with comparisons to the diagenesis of the Lower Permian Penrith Sandstone of NW England. It also contains a summary of the conclusions which are presented in Chapter 6. The first paper, Chapter 2, examines the origin of early and late carbonate cements in the Rotliegend Sandstone using petrographic and geochemical techniques. In Chapter 3 the controls and timing of quartz cementation in the Rotliegend Sandstone in the Leman field are examined in detail and comparisons are made with quartz cementation in the Lower Permian Penrith Sandstone of NW England. Chapter 4 discusses the origin of late intergranular and fracture-filling anhydrite cements in the Leman field. Chapter 5 investigates the origin of secondary porosity present in the Rotliegend Sandstone.

1.4 REFERENCES CITED

Almon, W.R. 1981. Depositional environment and diagenesis of Permian Rotliegendes Sandstones in the Dutch Sector of the southern North Sea. *Min. Assoc. Can. Short Course in: Clays and the Resourse Geologist.* Longstaffe, F. (ed), Calgary,119-147.

Arthur, T.J., Pilling, D., Bush, D., and Macchi, L., 1986, The Leman Sandstone Formation in U.K. block 49/28: Sedimentation, diagenesis and burial history. In: *Habitat of Palaeozoic Gas in N.W. Europe.* Brooks, J., Goff, J. and van Hoorne, B. (eds). *Spec. Publs Geol. Soc.* **23,** Scottish Academic Press, 251-266.

Beard, D.C. and Weyl, P.K. 1973. Influence of texture on porosity and permeability of unconsolidated sand. *Bull Amer. Assoc. Petrol. Geol.*, **57**, 334-369

Glennie, K.W., Mudd, G.C. and Nagtegaal, P.J.C. 1978. Depositional environment and diagenesis of Permian Rotliegendes sandstones in Leman Bank and Sole Pit areas of the U.K. Southern North Sea. *Jour. Geol. Soc. Lond.*, **135**, 25-34.

Goodchild, M.W. and Whitaker, J. McD. 1986. A petrographic study of the Rotliegendes Sandstone reservoir (Lower Permian) in the Rough gas field. *Clay Minerals*, **21**, 459-477.

Lee, M. 1984. Diagenesis of the Permian Rotliegendes Sandstone, North Sea : K/Ar, O^{18}/O^{16}, and petrological evidence. Ph. D. thesis, Case Western University, Cleveland, Ohio, 346pp.

McBride, E.F., Land, L.S. and Mack, L.E. 1987. Diagenesis of eolian and fluvial feldspathic sandstones, Norphlet Formation (Upper Jurassic), Rankin County, Mississippi, and Mobile County, Alabama. *Bull. Am. Ass. Petrol. Geol.*, **79**, 1019-1034.

Pye, K. and Krinsley, D.H. 1986. Diagenetic carbonate and evaporite minerals in Rotliegend aeolian sandstones of the southern North Sea : their nature and relationship to secondary porosity development. *Clay Minerals*, **21**, 443-457.

Surdam, R.C., Crossey, L.J., Hagen, E.S., and Heasler, H.P.,1989. Organic-inorganic interactions and sandstone diagenesis. *Bull. Am. Ass. Petrol. Geol.*, **73**, 1-23.

Walker, T.R. 1976. Diagenetic origin of continential red beds. In: *The Continental Permian in West, Central and South Europe*. Falke, H. (ed). *Reidel Publ. Co.*, Dordrecht, Holland, 352.

1.5 FIGURES AND FIGURE CAPTIONS

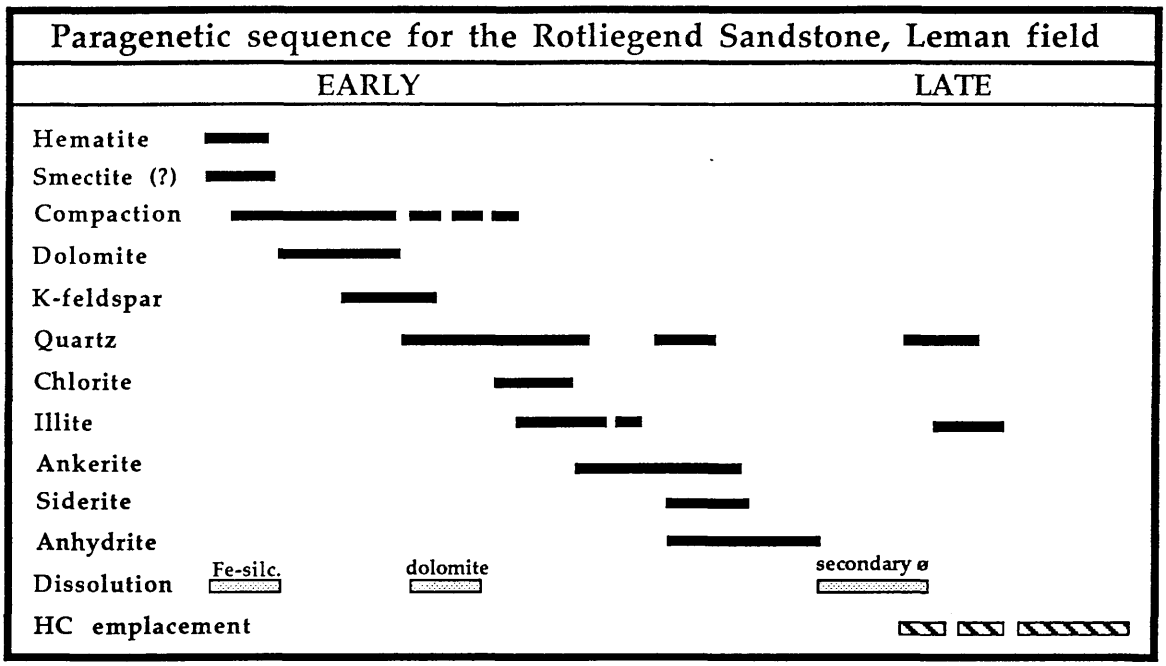

Figure 1.1 Paragenetic sequence showing timing of major diagenetic events in the Lower Permian Rotliegend Sandstone in the Leman gas field.

CHAPTER 2

ORIGIN OF EARLY AND LATE CARBONATE CEMENTS IN THE LOWER PERMIAN ROTLIEGEND SANDSTONE, LEMAN GAS FIELD, UK SOUTHERN NORTH SEA

Morgan Sullivan, R. Stuart Haszeldine
Department of Geology and Applied Geology, University of Glasgow,
Glasgow G12 8QQ, Scotland

Anthony Fallick
Isotope Geology Unit, Scottish Universities Research and Reactor Centre,
East Kilbride, Glasgow G75 0QU, Scotland

2.1 ABSTRACT

Cementation by carbonate is an important feature of the Rotliegend in the Leman gas field. Early carbonate diagenesis is represented by two distinct generations of dolomite; (i) Type I micro-rhombic (10-30 μm crystals) and rhombic (100-200 μm crystals) dolomite and (ii) Type II poikilotopic dolomite. The distribution of dolomite cement in the Leman field suggests variations in the supersaturation of and stratification of porewaters during early diagenesis. Three zones (A,B & C) are observed in the Rotliegend showing variations in the frequency of nucleation sites (crystals) and grain size of dolomite. A later phase of ankerite is developed both as a replacement of the earlier dolomite and as primary pore-filling rhombs, and comprises as much as 12% of the total rock. No systematic variation in ankerite cement with depth was observed in the Rotliegend Sandstone, indicating that the pore fluids were no longer stratified with respect to carbonate.

Carbon and strontium isotope ratios for Type I and II dolomites from unaltered red beds in the Leman field ($\delta^{13}C$ = -2.59 to -0.90‰; $^{87}Sr/^{86}Sr$ = 0.7077 to 0.7087) suggest that a significant portion of the early diagenetic porewaters were of marine origin with a contribution of isotopically light carbon ($\delta^{13}C$ = -10 to -25‰) and radiogenic strontium ($^{87}Sr/^{86}Sr$ = 0.720) derived from thermal maturation of organic matter in the underlying Carboniferous source rocks. $\delta^{13}C$ values for the Type I dolomite from the whitened (altered) beds at the base of the Rotliegend ($\delta^{13}C$ = -5.50 to -3.93‰) are strongly depleted relative to marine bicarbonate, suggesting that this dolomite contains a larger amount of isotopically light carbon derived from thermal maturation of organic matter than that from the unaltered beds. $\delta^{18}O$ results for dolomite from unaltered and altered beds are similar, and reflect precipitation at temperatures between 35° and 60°C from mixed marine/meteoric waters ($\delta^{18}O$ = -2‰) at a depth of 400 m to 1.2 km (1300 to 4000 ft) during the Late Permian to Early Triassic. Carbon and strontium isotope values for the

later ankerite suggest a significant input of basinal fluids derived from the underlying Carboniferous shales. Oxygen isotopes indicate that ankerite precipitation occurred at temperatures between 105° and 125°C from evolved brines ($\delta^{18}O$ = 0‰) at depth of 2.3 km to 3 km (7500 to 10,000 ft).

Cementation of the Rotliegend Sandstone by early Type I microrhombic and rhombic dolomite is interpreted to have been initiated by the influx of marine waters and/or diffusion of ions from the Upper Permian Zechstein marine evaporites during shallow burial, although there also appears to be Carboniferous meteoric component to the fluids at this time. The dominance of compactionally driven meteoric fluids and ions from the Carboniferous at the base of the Rotliegend led to the cementation by Type II dolomite. Precipitation of late phase ankerite occurred from porewaters with a strong Carboniferous component. Siderite is thought to have formed in response to the mixing of of fluids within faults and fractures.

2.2 INTRODUCTION

The Lower Permian aeolian and wadi subarkoses of the Rotliegend Sandstone, southern North Sea are up to 270 m (900 ft) thick and form the reservoir for the economically important Leman gas field (Figures 2.1 & 2.2). These sands overlie 915 m (3000 m) of Upper Carboniferous (Westphalian) mudstones with angular unconformity, and are in turn overlain by 550 m (1800 ft) of Upper Permian Zechstein anhydrite, dolomite and halite evaporites. The petrology and diagenetic history of the Rotliegend Sandstone in the Leman gas field have been described by van Veen (1975), Glennie *et al.* (1978) and Arthur *et al.* (1986). In summary, the formation consists of a lower unit characterized by 30 m to 60 m (100 to 200 ft) of wadi deposits interbedded with aeolian sands. A middle unit consisting entirely of aeolian sands forms the main reservoir and is between 140 m and 200 m (450 and 650 ft) thick. This is overlain by the upper unit, consisting of marine reworked dune deposits,

which is between 6 m and 30 m (20 to 100 ft) in thickness. The dominant reservoir sands are fine- to medium-grained subarkoses with porosities ranging from 5% to 25% (average 15%). The main diagenetic events in the Rotliegend Sandstone in wells 49/26-5, 49/26-25, 49/27-2, 49/27-3, and 49/27-4 (Figure 2.2), summarized in Figure 2.3, are compaction, precipitation of dolomite, quartz, chlorite, illite, ankerite and anhydrite cements, and development of secondary porosity.

2.3 ANALYTICAL METHODS

2.3.1 Carbonate petrography and composition

The petrography of the Rotliegend in the Leman field was studied using a number of techniques. Sixty thin sections from five wells (49/26–5, 49/26–25, 49/27–2, 49/27–3, 49/27–4) were examined using a standard polarizing microscope. Samples were first impregnated with blue epoxy resin, prior to sectioning, to highlight porosity. Staining of thin-sections with Alizarin Red-S and potassium ferricyanide, following the technique described by Dickson (1966), facilitated the recognition of dolomite and ankerite cements. Forty thin sections were point counted in detail, with a minimum of 500 counts per section, in order to determine modal percentages of detrital and authigenic components. Textural relationships and quantitative compositions were examined using a CAMBRIDGE STEREOSCAN 100 scanning electron microscope (SEM) equipped with a LINK Energy Dispersive Analysis of X-rays system (EDAX). A NUCLIDE cold stage LUMINOSCOPE was used for cathodoluminescence examination of carbonate minerals, and aided in the recognition of several generations of carbonate cementation. Precise determinations of bulk mineralogy were accomplished using a PHILLIPS X-Ray Diffractometer (XRD). Investigations of compositional variations in carbonate cements were obtained at St. Andews University using a wavelength dispersive system (WDS) backscatter electron mode (BSEM) equipped JEOL 733 SUPERPROBE (standard operating conditions: 15 KV

acceleration potential, 20 nA sample current, 0.5 -1.0 μm beam diameter) using silicate standards. Due to compositional zoning of carbonate cements the beam was not defocussed as this would have produced average analyses of zoned cements.

2.3.2 Isotopic analyses

Carbon and oxygen analyses:

Carbon and oxygen extractions for carbonate minerals were performed using the method outlined by McCrea (1950). Prior to extraction, separates of dolomite and ankerite were ashed in oxygen plasma at low temperatures to remove any organic contamination. These separates sometimes contained small amounts of quartz and feldspar, but had less than 5% carbonate contamination - i.e. ankerite contamination if the mineral being analyzed was dolomite. Measurements of sample weight before and after ashing indicated only minor weight loss, generally much less than 1%. Extractions of carbon and oxygen were performed by allowing powdered samples, weighing 30 to 45 mg, to react with 5 ml 100% phosphoric acid. Dolomite was left to react for 3 days and ankerite for 5 days at 25.0° ±0.1°C in a thermostatic bath. After each sample had completely reacted, the CO_2 gas was purified in a vacuum extraction line. Firstly, a dry ice-acetone slush trap removed any water vapour. The CO_2 was then frozen down, using liquid nitrogen, and any non-condensible gases were pumped away. The yield of CO_2 was measured on a capacitance manometer and the purified CO_2 gas was then transferred to a sample tube and attached to the mass spectrometer manifold.

The CO_2 gas was analysed on a VG SIRA 10 mass spectrometer with a working standard independently calibrated against international reference standards materials of silicate, carbonate, grahphite and oil. Thirteen duplicate sample analyses of Rotliegend carbonates were made during this study and the standard deviation (σn-1) was ±0.37‰ for $\delta^{13}C$ and ±0.43‰ for $\delta^{18}O$ (see appendix D.1); this high spread is interpreted to

be a result of the inhomogeneity of samples due to slight impurities, but also includes analytical and instrumental effects. $\delta^{13}C$ and $\delta^{18}O$ values for the dolomite and ankerite samples are quoted relative to the PDB (Pee Dee Belemnite) and $\delta^{18}O$ compositions of waters are quoted relative to SMOW (Standard Mean Ocean Water). Replicate analysis of inter-laboratory standard NBS # 20 produced an average $\delta^{18}O$ value of +26.64‰ (SMOW) and a $\delta^{13}C$ value of -1.06‰ (PDB) with a precision of 0.13‰ (1σ).

The $\delta^{18}O$ compositions of the samples were derived from the fractionation between calcite and CO_2 using the fractionation factor

$$\alpha = \frac{(^{18}O/^{16}O)_{CO_2}}{(^{18}O/^{16}O)_{carbonate}}$$

with α= 1.01025 (Friedman & O'Neil, 1977). Dolomite $\delta^{18}O$ compositions were corrected by -0.8‰ (Sharma and Clayton, 1965) and ankerite by –0.72‰ (Becker & Clayton, 1972) due to differences in the fractionation between CO_2 and these minerals at 25°C relative to calcite.

Strontium analyses:

Strontium concentrations and $^{87}Sr/^{86}Sr$ ratios were determined for powdered samples weighing 3 to 11 mg. Strontium was separated using standard cation-exchange chromatography and isotope dilution, with concentrations and $^{87}Sr/^{86}Sr$ ratios determined using solid source mass spectrometry on a VG-Isomass 54E. $^{87}Sr/^{86}Sr$ results were normalized to a $^{87}Sr/^{86}Sr$ value of 0.1194 and l Rb was taken as 1.42 x 10^{-11} a^{-1}. Replicate analyses of NBS #987 gave $^{87}Sr/^{86}Sr$ values of 0.71022 ±2(2σ).

2.4 CARBONATE PETROGRAPHY

Dolomite and ankerite are abundant authigenic cements in the

aeolian and reworked aeolian facies of the Rotliegend Sandstone in the Leman field. They occur in well cemented intervals and form up to 15% of the total rock. These sandstones contain three morphologies of dolomite cement: (1) microrhombic dolomite, (2) rhombic dolomite, and (3) poikilotopic dolomite. These three morphologies are very distinct and can be easily distinguished in thin section. Ankerite occurs both as individual pore filling rhombs and as overgrowths nucleated onto earlier dolomite crystals. The term ankerite is used to describe Ca(Mg,Fe,Mn) carbonates with Mg:Fe + Mn ≤ 4:1, while ferroan dolomite is used if up to 20% of the Mg positions are filled by Fe^{+2} or Mn (Deer, Howie and Zussman 1966). Siderite is also found in these samples, but only in association with mineralized fractures containing anhydrite.

2.4.1 Microrhombic dolomite

Microrhombic dolomite forms 1 to 10% of the total rock and crystals range in size from 10 to 30 μm. These rhombs occur both as cement rims on detrital grains, and as individual crystals lining pores. The dolomite cement rims consist of coalesced aggregates of microrhombic crystals completely surrounding detrital grains (Figures 2.4 & 2.5), and in a number of examples, can be observed replacing margins or whole grains (Figure 2.6). The rimming cement formed by the nucleation of individual rhombs on grain boundaries and the rhombs subsequently grew together enclosing the detrital grains. Where grain replacement has taken place, cementation appears to have been initiated along the boundary and has replaced the grain from the margin, often preserving the early hematite-clay grain coating (Figure 2.6). The pore lining phase of dolomite occurs as individual rhombs that precipitated on grain margins (Figure 2.7), and they also can be observed aggressively replacing the detrital material upon which they have nucleated. Distribution of the dolomite is patchy and it does not appear to have significantly affected the porosity of the sands.

2.4.2 Rhombic dolomite

Rhombic dolomite, 100 to 200 μm in size, comprises up to 10% of the total rock in the samples examined and occurs as both pore filling cement and individual rhombs. The pore filling phase consists of anhedral blocky crystals which completely occlude porosity. This cement formed by the nucleation of several crystals within a single pore, and their blocky anhedral texture reflects their continued and interfering growth during infilling of porosity (Figure 2.8). Euhedral rhombs lining pores are also common and occur where single crystals precipitated within a given pore (figure 2.9). This fine to medium grained cement is aggressive and replaces detrital grains, similar in fashion to the finer grained dolomite. Both the extremely fine grained euhedral dolomite and the coarser blocky dolomite display the same textural relationships, suggesting contemporaneous precipitation.

2.4.3 Poikilotopic dolomite

Dolomite also occurs as patches of poikilotopic cement which range from 1 to 3 mm in size. A cursory examination of the compactional textures within the poikilotopic patches suggests that it was an extremely early cement. Framework grains appear loosely packed often displaying point contacts and, less commonly, floating grains (Figure 2.10). Careful analysis, though, shows that this "apparent" open texture is misleading, and is due to very aggressive replacement of detrital grains. Silt and very fine sand fractions are most corroded or completely absent in cemented zones (Figure 2.11), which is probably due to their high ratio of surface area relative to their size. Coarser detrital grains display lesser degrees of dissolution. Some cemented grains also show evidence of pressure solution (Figure 2.12), and more ductile grains have been deformed due to compaction prior to cementation. Such evidence indicates that, in reality, the poikilotopic dolomite formed after significant compaction. This

suggests that it formed at, or near, the time of the rhombic dolomite precipitation. The poikilotopic phase is best developed along coarser laminae indicating grain size, porosity and permeability were important controls on its precipitation.

2.4.4 Ankerite (ferroan dolomite)

Ankerite occurs throughout the formation as overgrowths which nucleated onto earlier dolomite cements and as individual pore lining rhombs. Individual crystals range from 50 to 200 μm in size and are euhedral (Figure 2.13). Corrosion and overgrowth of rhombic and poikilotopic dolomite by ankerite clearly illustrates that the dolomite pre-dates the ankerite (Figure 2.14). Ankerite is commonly in optical continuity with the partially dissolved dolomite onto which it has nucleated. This texture suggests corrosion, and subsequent overgrowth. In iron-rich fluids, ankerite is more stable than dolomite and this would favour the replacement of dolomite by ankerite (Carpenter, 1985; Dutton & Land, 1988), supporting the textural evidence. Pore filling ankerite is similar in morphology to the pore filling dolomite rhombs and formed by the nucleation of individual ankerite rhombs within uncemented pores. Ankerite also displays similar replacive textures, with respect to detrital and authigenic silicates, as earlier dolomites, due to the aggressive nature of the fluids from which the ankerite precipitated. The lack of illite and chlorite cement coatings on ankerite crystals suggests that ankerite precipitation post-dated their formation.

2.4.5 Siderite

Siderite is the least abundant of the carbonate minerals in the Leman field. It only occurs in association with fractures mineralized with bladed anhydrite cement, and no siderite is found within the adjoining sandstones. Crystals range in size from 200 to 1000 μm, they are euhedral and are attached to fracture walls. Their euhedral shape suggests that the

fractures were open during crystal growth (Figure 2.15), and indicates that the siderite precipitated before the fracture filling sulphate. Both siderite and ankerite texturally pre-date anhydrite cement indicating that these carbonate cements formed at similar burial depths.

2.5 CATHODOLUMINESCENCE PETROGRAPHY

Cathodoluminescence petrography of dolomite and ankerite yielded important information concerning the formation of these carbonate minerals. Three distinct generations of carbonate cementation were recognized, based on variations in luminescent properties. They are; (1) brightly luminescent Type I dolomite, (2) dully luminescent Type II dolomite, and (3) non-luminescent ankerite (Figure 2.16). Siderite was not examined using this method since it is only found in fractures and does not occur in association with other carbonate minerals.

2.5.1 Type I dolomite

The first generation of carbonate cementation is characterized by concentric zones of yellowish-orange and red brightly luminescent dolomite (Figures 2.17 & 2.18). Nearly all of these Type I brightly luminescent rhombic crystals are zoned. The zoned crystals have between 2 and 4 zones consisting of a yellowish-orange core, which commonly displays a mottled or patchy mixture of both yellowish-orange and red luminescent cements. This is usually succeeded by an extremely thin, often only microns thick, red zone, a thicker yellowish-orange zone and an outer rim of red luminescent cement. The outer red zone is usually irregular, due to corrosion and overgrowth by later Type II dolomite and ankerite (Figure 2.18). Unzoned crystals display the same luminescent colour as the outer rims of the zoned rhombs, suggesting that they were precipitated during the last pulse of this cementation. The Type I brightly luminescent zoned cement is characteristic of the majority of both the

microrhombic (Figure 2.17) and rhombic dolomites (Figure 2.18). The similarity of luminescent properties of the two grain sizes of dolomite further supports the textural evidence that the microrhombic and rhombic dolomites are of the same generation (see sections 2.4.1 & 2.4.2). The thickness of the luminescent zones within the rhombic dolomites are proportional to the grain size of the crystals, with the largest zones being observed in the coarser grained rhombic Type I dolomite. Samples containing microrhombic and rhombic dolomite from all of the five wells studied display the same bright luminescence, indicating the high efficiency of the vertical and lateral communication of diagenetic fluids within the Leman field during Type I dolomite precipitation.

2.5.2 Type II dolomite

Unzoned dull red to brownish-red poorly luminescent dolomite represents the second generation of carbonate (Type II dolomite) recognized under cathodoluminescence. It occurs as poikilotopic patches, corrosive overgrowths, and individual pore filling rhombs. The most common occurrence is as mottled dull red luminescent poikilotopic patches (Figure 2.19). Samples dominated by weakly luminescent poikilotopic cement do not contain any brightly luminescent Type I carbonate, typical of the first generation of dolomite. This suggests that, if the earlier dolomite had originally been present, it was dissolved and reprecipitated during the later phase of poikilotopic dolomite precipitation. This is supported by overgrowths of dully luminescent dolomite that have formed with irregular contacts on the host brightly luminescent Type I dolomite, indicating it was partially corroded and overgrown (Figure 2.17). Individual rhombs of Type II dolomite were also recognized under cathodoluminescence (Figure 2.20), although these rhombs are indistinguishable from brightly luminescent Type I cement of the same morphology using a standard polarizing microscope.

2.5.3 Ankerite

The last generation of carbonate cementation is represent by non-luminescent ankerite (ferroan dolomite) which is unzoned under cathodoluminescence (Figures 2.17 & 2.20). Work by Sommer (1972), Meyers (1974) and Pierson (1981) has shown that ferrous iron (Fe^{2+}) acts as a quencher of luminescence in carbonate cements and the dead or non-luminescence of the ankerite in the Rotliegend is therefore due to the high iron concentrations in this mineral. The non-luminescent ankerite is present as overgrowths on both Type I and II dolomites. Commonly the contacts between the earlier dolomite and the aggressive ankerite are irregular and these contacts cut across the brightly luminescent zones and embay the dolomite (Figure 2.17). These textures suggest that the ankerite has corroded and overgrown earlier dolomites probably due to disequilibrium between the ankeritic fluids and the earlier dolomite.

2.6 CHEMISTRY OF CARBONATE MINERALS

The chemistry of the three generations of carbonate cements, recognized using cathodoluminescence petrography, and the siderite from the mineralized fractures was examined using a backscatter electron mode (BSEM) equipped microprobe in order to investigate compositional variations of the different types of cement (Figure 2.21, Table 2.1, & Appendix C.1). Distinct chemical variations are observed for each carbonate type which range from non-ferroan dolomite, slightly ferroan dolomite, ferroan dolomite, ankerite and strongly ferroan siderite.

2.6.1 Type I dolomite

The rhombic dolomite crystals characteristic of Type I carbonate are compositionally very homogeneous as indicated by BSEM and microprobe analyses (Figures 2.21, 2.22 & 2.23; Table 2.1). Both

microrhombic and rhombic dolomites were analyzed and this work indicates that their composition is not stoichiometric dolomite $Ca_{1.00}Mg_{1.00}(C0_3)_2$, as both types have excess calcium. Microprobe traverses were made from core to rim of crystals which displayed zoning under cathodoluminescence, but no variations in composition were observed (Figure 2.23). Iron substitution is uncommon, with the most ferroan composition being only 0.4 mole% $FeCO_3$. Manganese ranges from 0.5 to 1.0 mole% and no systematic variation in concentration could be recognized. The general formula for this dolomite is $Ca_{1.18}Mg_{.80}Mn_{.01-.02}Fe_{0-.01}(CO_3)_2$. Compositional analysis of this generation of dolomite indicates that the concentration of iron and manganese in the diagenetic fluids was extremely low and that pore-fluid chemistry remained constant during this phase of cementation.

2.6.2 Type II Dolomite

Type II dolomite contains higher concentrations of iron than the earlier generation Type I dolomite; and it also displays very little compositional variation (Figure 2.21, Table 2.1). Detailed microprobe traverses were made across poikilotopic cements, replacive overgrowths, and individual rhombic crystals to ascertain if any chemical differences existed between the different morphologies. The composition of the Type II dolomite within a single pore or poikilotopic patch displays very little variation in chemistry (Figures 2.24 & 2.25). Cements analyzed from different pores, and poikilotopic zones, within the same sample, showed only minor differences in iron and manganese concentrations. This suggests that cementation varied slightly from pore to pore and that minor variations in pore fluid chemistry existed on a fine scale. Manganese concentration, in the Type II dolomite, was similar to Type I dolomite, ranging from 0.5 to 1.0 mole%, although substitution for magnesium and calcium by iron increased slightly. Iron concentrations range from 2.2 to 4.0 mole% and the general formula of the Type I dolomite is $Ca_{1.14-1.16}Mg_{.76-.80}Fe_{.04-.08}Mn_{.01-.02}(CO_3)_2$. The higher iron

concentration of this generation of dolomite, relative to the Type I cement, is reflected in its dull luminescence. Iron has a quenching effect on luminescence and is the cause of the poor luminescent properties of iron carbonates (Pierson 1981).

2.6.3 Ankerite

Much of the ankerite, representing the last generation of carbonate cementation, is compositionally zoned. Due to the ankerite's high iron concentrations (Table 2.1), an inhibitor to luminescence, zoning was not observed using cathodoluminescence petrography. Compositional zoning was recognized under BSEM and is characterized by concentric rings of ferroan dolomite and ankerite, which have nucleated as corrosive overgrowths on earlier non-ferroan and slightly ferroan dolomite (Figure 2.26). The replacive overgrowths and individual pore filling rhombs are dominantly ankeritic in composition, although some zones contain strongly ferroan dolomite. The number of zones within each rhomb range from 2 to 10 and consist of alternating zones of variable iron concentrations (Figures 2.26 & 2.27). The zones commonly fluctuate between iron enriched and slightly depleted zones with variations of 2-6 mole% iron between adjacent regions. In general, zones become more ferroan toward the margins, suggesting that the iron content of the pore fluids increased during ankerite precipitation. Iron concentrations for both morphologies of ankerite range from 7-28 mole% $FeCO_3$ with substitution by iron occurring for magnesium and less commonly calcium. The variability in iron compositions between adjacent zones may reflect pulses of iron-rich fluids entering the Rotliegend Sandstone during ankerite precipitation.

2.6.4 Siderite

The siderite observed in mineralized fractures is unzoned

(Figure 2.28) and displays no variation in chemical composition. It has 88 mole% $FeCO_3$ and its formula is $Fe_{1.76}Mg_{0.16}Ca_{0.8}(CO_3)_2$ (Table 2.1). The presence of siderite (iron carbonate) in the fractures indicates that sufficient concentrations of reduced ferrous iron (Fe^{2+}) were available in order for siderite to precipitate. The two main sources for the iron incorporated into the siderite would have been: (1) the reduction of ferric iron (Fe^{3+}) grain coatings in the Rotliegend, and (2) iron-rich porewaters derived from the underlying Carboniferous sediments.

2.7 DISTRIBUTION OF CARBONATE CEMENTS

2.7.1 Dolomite

Three stratigraphic zones are observed in the Rotliegend Sandstone in the Leman field on the basis of variations in grain size and frequency of nucleation sites of early authigenic dolomite; Zone A, at the top of the Rotliegend, which is dominated by microrhombic Type I dolomite; Zone B, in the middle and lower portions of the Rotliegend, which consists of rhombic Type I dolomite; and Zone C, at the base of the Rotliegend, which consists of poikilotopic Type II dolomite (Figures 2.29 & 2.30).

The degree of supersaturation of porewaters is thought to be the dominant control on both the rates of nucleation and crystal growth (Berner 1980), such that both the frequency of nucleation sites and the grain size of precipitates can be greatly affected by minor changes in the supersaturation of the porewaters. The size of diagenetic crystals precipitated can therefore be dependent on the relative rates of nucleation and crystal growth (Berner, 1980; Sibley & Bartlett, 1987; Saigal & Bjørlykke, 1987) with smaller crystals resulting from precipitation at numerous sites due to rapid nucleation from supersaturated fluids. This is because the formation of crystals by precipitation from a solution requires an increase in surface free energy (see Berner, 1980 figure 5.1) and

the process during which the maximum free energy is attained is nucleation. At high rates of nucleation (due to high supersaturation) the total excess dissolved material in solution may precipitate entirely as *"critical nuclei"* which therefore would not have a chance to grow into large crystals. This would result in the precipitation, via nucleation, of numerous extremely fine grained crystals (Berner, 1980). Low supersaturations would thus result in smaller numbers of nucleation sites and therefore would produce fewer and larger crystals as crystal growth became the dominant process. The distribution of the various early dolomite cements, therefore, suggests that vertical and lateral variations in saturation of the pore fluids with respect to dolomite existed during early diagenesis of the Rotliegend sandstone in the Leman field.

Top Rotliegend Sandstone (Zone A)

The top of the Rotliegend Sandstone is characterized by a very high abundance of extremely fine grained microrhombic Type I dolomite which varies in size from 10 to 30 μm (see sections 2.4.1 &2.5.1). This zone is approximately 200 ft (61 m) thick and is recognized in all of the six wells examined (Figure 2.29). It includes the entire lithofacies of the *upper unit* of marine reworked aeolian sandstones and the first 100 to 150 ft of the *middle unit's* aeolian dune sandstones (see section 2.2). Throughout the marine reworked aeolian sandstones this extremely fine grained dolomite is by far the most abundant cement, whereas in the underlying aeolian dune sandstones it is best developed along the bimodal bottom sets (see section 2.4.1).

Due to the relationship (discussed above) between fluid supersaturation and rate of crystal nucleation, the density of nucleation sites was calculated for well cemented sandstones within Zone A in order to evaluate the relative saturation of the pore fluids with respect to dolomite. This was accomplished by point counting the number of dolomite crystals (i.e. nucleation sites) for five separate regions of five thin sections for a 1 mm^2 area viewed in cathodoluminescence (Table 2.2;

Figure 2.30). The average number of dolomite crystals for a 1 mm^2 region in Zone A is 43, which represents a high density of crystals (i.e. nucleation sites). The rate of nucleation, therefore, must have been rapid enough to allow the precipitation of only extremely fine grained crystals, as the solution became quickly depleted with respect to dolomite, due to the formation of numerous nuclei. This indicates that the porewaters in Zone A were initially highly supersaturated with respect to Type I dolomite.

Mid and basal Rotliegend Sandstone (Zone B)

There is an abrupt change in grain size of rhombic dolomite from the extremely fine grained cement (10 to 30μm) of Zone A to the coarser grained (100 to 200 μm) rhombic Type I dolomite (see sections 2.4.1, 2.4.2, & 2.5.1) of Zone B. The thickness of Zone B is approximately 300 ft (90 m) and it occurs below Zone A in the mid to basal portion of the Rotliegend Sandstone (Figure 2.29). In wells 49/26-5 and 49/27-4 this zone of coarse dolomite extends to the base of the Rotliegend, but does not reach the base in the other three wells, where a further change in dolomite grain size occurs in the lower portion of the sequence (Figure 2.29). The occurrence of this coarser grained Type I dolomite is predominantly within the lithofacies of the *middle unit* of aeolian dune sandstones below Zone A (see section 2.2). Coarse grained dolomite is also found in the *lower unit* within the interbedded aeolian sandstones of this mainly fluvial portion of the Rotliegend, but insufficient samples of the fluvial sandstones were examined to determine its distribution in that facies. This coarser grained Type I dolomite occurs most frequently along bottom set beds of the aeolian sandstones in Zone B.

The number of nucleation sites for well cemented samples of the coarser Type I dolomite was estimated using the same point-counting method applied to the much finer grained dolomite of Zone A . The large Type I dolomite crystals in Zone B have fewer nucleation sites, with an average of 10 nuclei per 1 mm^2 (Table 2.2; Figure 2.30), than the extremely fine grained Type I microrhombic dolomite in Zone A for the same area. This suggests a slower rate of nucleation which produced fewer and larger

crystals. Petrographic evidence from cathodoluminescence studies (see section 2.5.1) reveals that growth zones within microrhombic and rhombic Type I dolomites are similar, but that the scales of these zones differ, with the coarser grained rhombic dolomite having larger growth zones. This suggests that all Type I dolomites precipitated within the same time interval, with the growth zones in coarser crystals being larger due to precipitation at fewer nucleation sites. This possibly allowed the dolomite ions in solution in Zone B to be transported faster to the fewer sites of nucleation, therefore producing larger crystals within the same relative period of time. This may be because the extremely high abundance of nucleation sites in Zone A caused a rapid decrease in saturation levels thereby limiting the rate by which ions could be supplied for crystal growth. The observed decrease in the frequency of nucleation sites suggests that the porewaters in Zone B were less supersaturated than in Zone A and that crystal growth was more dominant in Zone B.

The basal sandstones of well 49/26-5, which are dominated by coarse grained Type I rhombic dolomite (see sections 2.4.2 &2.5.1) characteristic of Zone B (Figure 2.29), are white as opposed to the red colouration of most of the Rotliegend Sandstone in the Leman field. The white colour of the sandstones in this portion of the well is thought to be due to the reduction of the ferric (Fe^{3+}) hematite grain coatings to ferrous (Fe^{2+}) by reducing fluids (Glennie *et al.*, 1978). There is no definite textural evidence reflecting the timing of whitening of these beds, but since the dolomite encloses whitened grains the alteration is assumed to have occurred prior to, or possibly associated with, dolomite precipitation. The red sandstones above this whitened region indicate that the hematite grain coatings in the rest of the well have not been affected. Rhombic dolomites in this white discoloured region, are petrographically identical to the other large rhombic Type I crystals, displaying the same luminescent properties, grain size and density of nucleation sites (crystals). The lower portion of well 49/27-4 is also dominated by rhombic Type I dolomite of Zone B (Figure 2.29). The base of this well is still predominantly red and

there are no obvious differences vertically within the unit which may have influenced the formation of the rhombic Type I dolomite.

Basal Rotliegend Sandstone (Zone C)

Zone C characterizes the lower 200 to 300 ft (61 to 91 m) of the Rotliegend Sandstone (Figure 2.29), except in the wells 49/26-5 and 49/27-4, and is dominated by Type II poikilotopic dolomite (see sections 2.4.3 & 2.5.2). This region of the Rotliegend has not been altered and is still red. In this zone the poikilotopic dolomite is best developed along the bimodal bottom sets, as is the rhombic Type I dolomites in Zones A and B (see sections 2.4.1 & 2.4.2). The number of nucleation sites for a 1 mm^2 area of the poikilotopic cemented samples was also calculated using the same technique used to determine the frequency of nucleation in Zones A and B (Table 2.2; Figure 2.30). The average number of nucleation sites was less than 2 per 1 mm^2 due to the large size of poikilotopic crystals (1 to 3 mm). Rates of nucleation are slower at low levels of supersaturation and therefore produce fewer nucleation sites (Berner, 1980). This indicates that the poikilotopic dolomite precipitated from waters less saturated with respect to dolomite than the fluids from which rhombic Type I dolomites of Zones A and B precipitated, which have higher frequencies of nucleation. The lower degree of supersaturation of porewaters in Zone C is interpreted to have greatly reduced crystal nucleation rates and slow crystal growth has become the dominant process controlling precipitation of Type II dolomites. These conditions of low supersaturation would have favoured the precipitation of very coarse grained (poikilotopic) dolomite.

The textural evidence, from petrographic analysis, indicates that the poikilotopic Type II dolomite post-dated the rhombic Type I dolomite (see section 2.5.2). A slow rate of crystal growth produces a high degree of crystallinity, favouring nucleation on existing minerals as syntaxial overgrowths (Burley *et al.*, 1985). This could explain the lack of rhombic dolomite in the deeper portions of the sequence and the dominance of poikilotopic cement in these regions. If the porewaters were not highly

supersaturated with respect to dolomite then poikilotopic Type II dolomite may have nucleated sporadically. Through dissolution and reprecipitation, the rhombic Type I crystals may have been replaced by the coarser grained poikilotopic Type II dolomite, since the latter would be more stable than the finer grained rhombic dolomite in waters of low supersaturation (Berner, 1980). This is supported by the aggressive nature of the replacive overgrowths of Type II dolomite observed in Zones A and B (see section 2.4.3). In these regions, Type II dolomite is significantly less abundant than in the poikilotopic zones and this is probably due to a decrease in the availability of ions for dolomite precipitation, indicating these porewaters were also stratified with respect to dolomite supersaturation. Because of this, Type II dolomite was not as pervasive in the upper portions of the Rotliegend and only partial dissolution and replacement of Type I dolomite occurred.

2.7.2 Ankerite

Ankerite occurs as pore lining rhombs 50 to 200 μm in size and as replacive overgrowths (see section 2.4.4), both of which are evenly distributed throughout the Rotliegend Sandstone in the Leman field. Ankerite is often compositionally zoned and the zoning throughout the field is similar, with iron concentrations generally increasing toward the pore margins (see section 2.6.3). The uniformity of ankerite distribution throughout the full thickness of the Rotliegend in Leman field indicates that the pore fluids were well mixed and no longer stratified with respect to carbonate as they formerly had been during earlier dolomite formation. The distribution of ankerite cement also does not appear to have been controlled significantly by sedimentary lithofacies. Ankerite is marginly more abundant in bimodal dune bottom sets of the wind ripple lithofacies, but this is most likely due to dissolution and in situ reprecipitation of earlier dolomite, which is more common in the bottom sets, by the later ankerite. Otherwise late stage ankerite is usually found in pores not infilled by earlier cements, such as pervasive quartz, regardless of facies

association.

2.7.3 Siderite

Siderite precipitation in the Leman field is limited to the mineralized fractures in the Rotliegend Sandstone (see section 2.4.5). Siderite is present as large euhedral rhombs up to 1000 μm in size. Rhombs are attached to fracture walls, often at the intersection of coarse grained laminae with fractures, and their euhedral shape suggests that fractures were fully open prior to siderite precipitation. These textures and the limited occurrence of the siderite, suggests that its precipitation was controlled by the mixing of fluids in the fractures. Thus geochemical conditions which influenced siderite formation were restricted to the fractures and did not extend into the adjoining sandstones.

2.8 ISOTOPE ANALYSES

2.8.1 Carbon and oxygen isotope analyses

Carbon and oxygen isotope analyses were carried out on thirty-six dolomite and ankerite samples, and the values are shown in Figure 2.31 and Tables 2.3 and 2.4. The results for the carbonate cements in the Leman field cluster into three isotopic groups. The first distinct population (Group 1) consists of the Type I rhombic and Type II poikilotopic dolomites from the unaltered red beds of the Rotliegend. These samples have the highest $\delta^{13}C$ and $\delta^{18}O$ compositions of the carbonate cements analysed. The second population, Group 2, consists of the Type I rhombic dolomite from the discoloured white basal portion of well 49/26-5. Samples from this altered region have the same oxygen isotopic composition as the dolomite in Group 1, but they are significantly more depleted in ^{13}C. The third cluster of isotopic data, Group 3, is formed by the late phase ankerite which is depleted in ^{18}O relative to

dolomites of Groups 1 and 2, but the ankerite has isotopically light carbon compositions similar to Group 2 dolomites.

Group 1 dolomite

The carbon and oxygen isotope ratios of both Type I and II dolomites in the unaltered Rotliegend red beds form a distinct population hereafter referred to as Group 1 (Figures 2.31 & 2.32). $\delta^{13}C$ (PDB) values for these samples vary from –2.59 to –0.90‰ with an average value of –1.53‰ (Table 2.3). The $\delta^{13}C$ values of the dolomite in the Rotliegend can be used to identify the source or sources of dissolved bicarbonate in the pore fluids since they reflect the carbon isotopic composition of the fluids from which dolomite precipitated. Possible sources of the carbon are shown in Figure 2.33 and include; oxidation of methane $\delta^{13}C$ = –100 to –30‰ (Smith & Epstein, 1971; Stahl, 1974, 1977), degradation of organic matter and sulfate reduction $\delta^{13}C$ = -10 to -25‰ (Smith & Epstein, 1971; Irwin *et al.*,1977), atmospheric CO_2 δ^{13} C = -7‰ (Keeling, 1958,1961), freshwater bicarbonate $\delta^{13}C$ = –13 to -2‰ (Keith & Weber, 1964; Salem *et al.*,1980), sea water and dissolution of primary bioclastic or marine carbonate $\delta^{13}C$ = –1 to +2 ‰ (Deuser and Hunt, 1969), although $\delta^{13}C$ values for Late Permian carbonate have been reported as high as +6‰ (Tucker, 1990), and $\delta^{13}C$ results for bacterial fermentation range from +10 to +20‰ (Murata *et al.*,1967).

The carbon isotope compositions of the dolomite in the Rotliegend (–2.59 to –0.90‰) are not characteristic of a specific source, but are similar to what might be expected for modified bicarbonate of inorganic origin derived from seawater or primary marine carbonate dissolution. The basinal meteoric waters that interstitially filled the aeolian deposits of the Rotliegend as it became buried below the water table were unlikely to have contributed significant bicarbonate to the dolomite. This is because meteoric waters in an arid dune environment generally have low dissolved bicarbonate contents, owing to the negligible contribution from organic matter (plants). More probable sources of

carbon for early dolomite precipitation were either basin recharge by the Late Permian Zechstein seas, whose evaporation produced the thick evaporites overlying the Rotliegend, or possibly fluids derived from dewatering of the underlying Upper Carboniferous deltaic organic-rich mudstones. Dewatering of Lower Carboniferous limestones presumably did not contribute to the evolution of the Rotliegend pore waters because of the nearly 1000 m of Upper Carboniferous mudstones these fluids would have had to pass through. The carbon isotope composition of Late Permian seawater is not well constrained so we adopt the estimate of Veizer *et al.* (1980) who have reported $\delta^{13}C$ values for Late Permian and Late Carboniferous seawaters of between 0‰ and +2‰, based on 270 measurements for the Permian and 166 for the Carboniferous, although Tucker, (1990) has reported $\delta^{13}C$ values as high as +6‰ for carbonates from the Zechstein carbonates. These measured values for seawater are enriched, however, relative to the carbon isotope values of the dolomite in the Rotliegend. Although $\delta^{13}C$ compositions of the dolomite implicate a dominantly marine source for the bicarbonate, they do not indicate the particular source.

The 1‰ to 3‰, or possibly more, ^{13}C depletion in the dolomite, relative to either Late Carboniferous or Late Permian seawater, is interpreted to indicate mixing with a contribution of isotopically light carbon derived from early maturation of organic matter in the underlying Upper Carboniferous mudstones. This process produces very light bicarbonate with $\delta^{13}C$ values between -10‰ to -25‰ (Irwin et al., 1977); therefore, it would require only a small amount of this isotopically depleted bicarbonate to produce the observed shift in the carbon isotope values of the dolomite from that of seawater.

$\delta^{18}O$ values of minerals are controlled by both the temperature of precipitation, and the isotopic composition of the pore fluids from which they formed (Urey, 1947). $\delta^{18}O$ values for Type I and II dolomites of isotopic Groups 1 range from -7.48 to -3.56‰ (PDB) (Figure 2.31; Table 2.3). These $\delta^{18}O$ values could have resulted either by, (1) the precipitation of

dolomite from waters strongly depleted in $\delta^{18}O$ at extremely shallow burial or, (2) by relatively enriched fluids at deeper burial and elevated temperatures. Carbon and strontium isotope data indicate that the pore fluids from which the dolomite precipitated had a significant marine component (see sections 2.8.2 & 2.8.3), although the waters appear to have been a mixture of marine waters from the overlying Zechstein evaporites and Carboniferous fluids. The Carboniferous sediments in the southern North Sea were flushed by meteoric waters during the Early Permian uplift, prior to deposition of the Rotliegend Sandstone (Cowan, 1989; Besley, 1990), and therefore would have had a predominantly meteoric oxygen isotope signature. Work by Craig (1961), Craig and Gordon (1965) and Yurtsever (1975) shows that meteoric waters are more enriched in ^{18}O at lower latitudes and have compositions approaching 0‰ (SMOW) at the equator (Figure 2.34). Assuming a palaeolatitude for the Permian Rotliegend Basin of approximately 20°N (Glennie, 1972), and a similar trend in $\delta^{18}O$ with latitude during the Permian as now, then rainfall should have had a $\delta^{18}O$ composition of about -4‰ (SMOW). The oxygen isotope composition of the oceans are relatively enriched in $\delta^{18}O$ (approximately -1 to 0‰ SMOW). The mixing of meteoric fluids derived from the underlying Carboniferous and marine waters from the Zechstein evaporites, therefore, would not have produced $\delta^{18}O$ depleted pore fluids capable of generating the measured oxygen isotope values of the dolomite if precipitation occurred at shallow burial (i.e tens of meters). Petrographic evidence, also, suggests that the dolomite did not precipitate extremely early, so the depleted ^{18}O values of the dolomite must be due to elevated temperatures of precipitation.

The fractionation equation relating isotopic compositions of dolomite and the pore fluid to temperature, as determined by Fritz and Smith (1970) at temperatures between 20° to 80°C, is:

$$(\delta_{dol} - \delta_{w}) = 2.78 \times 10^{6}(T^{-2}) + 0.11$$

where δ_{dol} = oxygen isotope composition of the dolomite (relative to SMOW), δ_w = oxygen isotope composition of the water from which the dolomite precipitated (relative to SMOW) and T = the temperature of formation in degrees Kelvin. If the dolomite in the Rotliegend precipitated from mixed pore waters of meteoric origin (-4‰ SMOW) and Permian seawater (estimated by Given and Lohman, 1985 to be between –1.1 and -0.1 ‰ SMOW), then the resulting fluid should have had an oxygen isotopic composition of between -4 and 0‰ (SMOW). Assuming a fluid with a $\delta^{18}O$ value of -2‰ (SMOW), precipitation would have occurred at temperatures between 35° and 60°C as shown in Figure 2.35. These temperatures would have been attained at a burial depth of approximately 400m to 1.2 km (1300 to 4000 ft), assuming a surface temperature of 15 to 20°C (see Figure 2.36). Examination of the burial history curve for the Leman field suggests this would have occurred during the Late Permian to Early Triassic when the basin was under going rapid burial.

Group 2 dolomite (discoloured beds)

Carbon and oxygen isotopic compositions were analyzed for two samples of large Type I dolomite rhombs from the whitened lower portion of well 49/26-5 (see section 2.7.1). This discoloured region is approximately 140 ft (43 m) thick in this well and one sample was selected from near the top of the zone at a depth of 6925 ft (2110 m) and the other from the base at 7040 ft (2146 m). As discussed, all large Type I dolomite rhombs have the same morphology, luminescent properties and chemistry indicating that they are a single phase of cement (see sections 2.4.1, 2.4.2, 2.5.1 2.6.1). The $\delta^{13}C$ isotopic compositions of the dolomite from the discoloured region, however, are significantly more depleted than the other Type I dolomites, being –3.93‰ for sample 6925 and for–5.50‰ for sample 7040 (Figure 2.31 & 2.32). Although $\delta^{13}C$ values are more negative than those of the other dolomites (both Type I & II), the $\delta^{18}O$ values for the both Group 1 and 2 isotopic populations of dolomite are similar (see Figure 2.31 & Table 2.3). The similarity of oxygen isotope compositions suggests that they formed at

comparable temperatures and depth of burial (see section discussion for isotopic Group 1), supporting the petrographic and geochemical information which indicates that they are same generation of cement.

Often the basal portion of the Rotliegend is white or grayish and Glennie *et al.* (1978) have suggested that the loss of the original red colour was due to reduction of early iron oxide grain coatings by acidic fluids released from the underlying Carboniferous during coalification and maturation of organic matter. Acidic waters generated by the coalification and oxidation of organic matter would release organic CO_2 depleted in $\delta^{13}C$ (Smith & Epstein, 1971; Claypool *et al.*, 1973; Irwin *et al.*,1977). The depleted carbon isotopic compositions of the dolomite from the discoloured region of well 49/26-5 suggest that the movement of reducing, acidic waters containing isotopically light carbon from the underlying Carboniferous Coal Measures into the Rotliegend occurred during or before dolomite precipitation.

If this dolomite had 100% of its carbon derived from the thermal maturation of organic matter it would have had $\delta^{13}C$ values within the range of –10 to –25‰ (Irwin *et al.*,1977). As already discussed, the carbon isotope composition of the Type I dolomite from the unaltered red beds (Group 1) reflects a dominantly marine source with a minor contribution of isotopically light carbon, possibly from early maturation of the underlying source rocks. The measured carbon isotope values of –5.50 to –3.93‰ for the Type I dolomite of isotopic Group 2, however, reflect an input of up to 30% more isotopically light carbon from thermal maturation of the Carboniferous source rocks. The more ^{13}C depleted composition of sample 7040 relative to 6925, is consistent with a trend of ^{13}C depletion with depth. This would be expected if isotopically light (organic) carbon was being derived from below and not being homogeneously mixed with the dominantly inorganic carbon reservoir of the Rotliegend pore fluids. Humic organic matter starts releasing carboxylic acids at temperatures of approximately 50°C (Hunt, 1979), which is near the estimated precipitation temperatures for the dolomite, and at

these low temperatures CO_2 is released due the destruction of carboxylic acids by bacteria (Carothers & Kharaka, 1978). It is, therefore, likely that the source of the isotopically light carbon would have been the maturation of humic organic matter in underlying Carboniferous Coal Measures, which would have been at higher temperatures than the more shallowly buried Rotliegend.

The generation of isotopically depleted organic carbon by thermal maturation of the source rocks appears to have been a limited and localized event during the precipitation of dolomite. This might be expected since only small amounts of CO_2 would be generated during the initial stages of thermal maturation of organic matter by bacterial destruction of carboxylic acids because at temperatures above 60°C thermal destruction of the bacteria occurs and the carboxylic acids are stable until they themselves become thermally unstable at temperatures over 130°C (Carothers & Kharaka, 1978). The strongly negative $\delta^{13}C$ values for Type I dolomite only being observed for the dolomite at the base of well 49/26-5 in the discoloured region, supports this, as does the significant shift in carbon compositions between then two samples analyzed from this region, which were separated only by 115 ft (35 m). Also, if the reduction of the iron oxide grain coatings were associated with dolomite precipitation, then the dissolved iron content of the pore fluids must have remained extremely low because none of the reduced iron was incorporated into the Type I (non-ferroan) dolomite, further suggesting this whitening was a localized event.

Group 3 ankerite

$\delta^{13}C$ compositions for ankerite (isotopic Group 3) are more depleted than those for the earlier dolomite of isotopic Group 1, but are similar to negative values of the Group 2 dolomite from the whitened base of well 49/26-5 (Figures 2.31 & 2.32). $\delta^{13}C$ results for the ankerite range from –4.46 to –3.06‰ (Table 2.4) with an average value of –3.60‰. These values are lower than those of the Group 1 dolomites which have a

dominantly inorganic heavy marine $\delta^{13}C$ signature ($\delta^{13}C$ = -1.5‰). This trend toward more negative (lighter) $\delta^{13}C$ compositions of the ankerite is not consistent with precipitation from a slightly modified marine bicarbonate source and instead it is interpreted to reflect further addition of isotopically light organic carbon. Many workers have found that ^{13}C depleted carbonates, especially iron rich varieties, are commonly associated with generation of isotopically light carbon from thermally induced decarboxylation (Irwin *et al.*, 1977; Curtis, 1978; Woronick & Land, 1985). This is because reduction of iron is often linked with the generation of isotopically light carbon derived from the decarboxylation of organic matter and, under these conditions, the precipitation of iron-rich, isotopically-light carbonate would be favoured (Curtis, 1978).

During the later stages of diagenesis, when the Rotliegend was deeply buried, the amount of isotopically light carbon generated by thermal maturation of organic matter would have been larger than during early low-temperature diagenesis (Irwin *et al.*, 1977, Carothers & Kharaka, 1978), thus producing the observed increased negative shift in $\delta^{13}C$ values of the late phase ankerite relative to the earlier dolomite. The carbon isotope values of the ankerite, however, are too heavy to have been derived entirely from thermal maturation of organic matter and therefore reflect a mixing of relatively isotopically heavy marine carbon ($\delta^{13}C$ = 0‰ to +2‰) with ^{13}C-depleted organic carbon ($\delta^{13}C$ = -10‰ to -25‰). To generate the ankerite $\delta^{13}C$ compositions an additional 25 to 35% of organic carbon with a carbon isotope composition of between -10 and -25‰ must have been added to the predominantly inorganic isotopic carbon reservoir of the Rotliegend (assumed to have remained at approximately -1.5‰). The isotopically heavy carbon component in this ankerite may have been derived from the pore waters within the Rotliegend, or from the dissolution, equilibration, and reprecipitation of in situ dolomite by the later replacive ankerite (see section 2.4.4). The absence of organic material in the Rotliegend means that the isotopically light carbon must have been imported into the system. The uniformity of $\delta^{13}C$ values of the ankerite

throughout the stratigraphic section in all five wells examined indicates that inorganic and organic dissolved bicarbonate components were well mixed, and that the pore fluids had a homogeneous carbon composition during precipitation, as opposed to the generation of Group 2 dolomites. This suggests that the generation of isotopically light organic carbon during or prior to ankerite precipitation was not localized as it was during the precipitation of Group 2 dolomites, but was instead a more extensive event that affected the whole Leman field, and probably an even greater area. The most likely source of the isotopically light carbon incorporated into the ankerite would have been thermal maturation of the extremely thick sequence of organic-rich Upper Carboniferous mudstone source rocks, that underlie the Rotliegend in the Leman field, prior to gas generation.

Oxygen isotopic compositions for ankerite are the most depleted of all the carbonate cements examined and $\delta^{18}O$ values range from –11.70 to –9.60‰ (PDB) (Figure 2.31; Table 2.4). The observed shift in $\delta^{18}O$ values away from the oxygen values of the earlier dolomites could have been the result of precipitation from more $\delta^{18}O$ depleted waters than those from which the earlier dolomite formed or, alternatively, precipitation at higher temperatures. Earlier workers studying oilfield diagenesis indicated that with increasing burial, pore waters generally become isotopically heavier, resulting from ^{18}O-^{16}O exchange with minerals (Craig *et al.*, 1956; Lønøy, 1986; Bjørlykke *et al.*, 1986). This, in combination with petrographic evidence (see section 2.4.4), which indicates that ankerite formed later in the burial history than the dolomite, suggests that the depletion in $\delta^{18}O$ was due to elevated temperatures of precipitation accompanying deeper burial.

The fractionation between ankerite and water, and the effects of iron concentrations on the equilibrium relationship relative to pure dolomite have not been published. Previous isotopic studies of ankerite (Boles, 1978; Dutton & Land, 1985 and Longstaffe & Ayalon, 1987) have used the equilibrium fractionation equation between dolomite and water

proposed by O'Neil *et al.* (1969):

$$(\delta_{dol} - \delta_w) = 2.78 \times 10^6(T^{-2}) + 0.32$$

where δ_{dol} = oxygen isotope composition of dolomite, or in this case ankerite, (relative to SMOW), δ_w = oxygen isotope composition of the water from which the dolomite (ankerite) precipitated (relative to SMOW) and T = the temperature of formation in degrees Kelvin. The isotopic composition of the water can be estimated using data from the intervening phase of illite diagenesis, which pre-dates ankerite precipitation (Figure 2.3). Lee (1984) measured the oxygen isotopic compositions of illite (16.09 to 18.78‰ SMOW) in the Rotliegend Sandstone from wells 49/27-2,49/27-3 and 49/27-4 in the Leman field. Lee also dated illite diagenesis in the Rotliegend Sandstone in the Leman field using K-Ar isotope analysis. The finest fraction of authigenic illite yielded dates of approximately 170 m.y. Combining these data with oxygen isotope measurements of the illite and examination of the burial history of the Rotliegend in the Leman field, suggests that during illite precipitation the waters had an oxygen isotope composition of approximately 0‰ (SMOW). If waters of this composition are used in the calculation of the temperatures for ankerite precipitation, and assuming that the ankerite precipitated from a fluid of fixed isotopic composition, then ankerite formed over a temperature interval of 105 to 125°C (see Figure 2.35). These temperatures would have been attained at burial depths between 2.3 and 3 km (7,500 to 10,000 ft) (Figure 2.36), which is approaching the deepest burial for the Rotliegend in the Leman field estimated by Marie (1975), Glennie *et al.*(1978), and Bulat & Stoker (1987).

2.8.2 Strontium isotope analysis

The strontium isotope compositions of nine carbonate samples from the Rotliegend Sandstone were measured in order to examine the

source and evolution of pore fluids. Four samples of dolomite were selected to investigate $^{87}Sr/^{86}Sr$ compositions of early diagenetic pore fluids. The five samples of late phase ankerite were chosen to ascertain if any changes had occurred in the strontium isotope composition due to fluid-rock interactions with increasing burial. All Strontium ratios have been corrected for radiogenic Rb (see appendix D.3).

Dolomite

The least radiogenic strontium ratios measured were from the early diagenetic dolomite and range from 0.7077 to 0.7087 (Table 2.5), with strontium concentrations between 18 ppm and 225 ppm. These strontium isotope compositions are similar to those of Late Permian seawater, although the measured values of the dolomite are slightly more radiogenic than would be expected if the strontium were derived exclusively from Late Permian seawater (Figure 2.37) ($^{87}Sr/^{86}Sr$ = 0.7068 to 0.7070; Burke *et al.*, 1982). Since rain water contains only negligible concentrations of strontium, any strontium present in the early meteoric Rotliegend pore waters would have been derived from the weathering and subsurface leaching of detrital silicate minerals. These minerals typically have $^{87}Sr/^{86}Sr$ ratios of 0.720, and low strontium concentrations (Faure, 1986). Strontium derived from dewatering of the underlying mudstones would reflect the composition of Late Carboniferous seawater (0.7085) and any interaction of these waters with detrital silicate minerals (0.720), thus producing waters with higher $^{87}Sr/^{86}Sr$ values than measured for the dolomite. Although there is a recognized phase of feldspar dissolution in the Rotliegend, it postdates both dolomite and ankerite precipitation and is unlikely to have supplied strontium to either phase of carbonate (Figure 2.3). Therefore, it is suggested that the diagenetically early strontium in the Rotliegend pore waters was mainly of marine origin, derived from the repeated flooding and evaporation of the Late Permian seas. This strontium was mixed with a very small contribution of more radiogenic strontium, derived from either Late

Carboniferous seawater or, more probably, detrital silicate dissolution in the underlying Carboniferous mudstones. This is supported by petrographic evidence presented by Draxler *et al.* (1986), who described dissolution of feldspar and mica in Carboniferous mudstones and sandstones from the North Sea. The strontium concentration of carbonates is a function of the Sr/Ca ratio of the waters from which they formed and the distribution coefficient (D) of the particular carbonate. The low strontium concentrations of the dolomite suggest that the Sr/Ca ratio of the Late Permian marine waters, which migrated into the Rotliegend from the overlying evaporites, was also low. Based on the data, though, there is no unequivocal explanation of the low strontium contents of the dolomite. One possibility, however, may be that the marine derived formation waters contained negligible strontium and, therefore, perhaps had a low Sr/Ca ratio due to evaporation past the point of halite and anhydrite deposition (Carpenter, 1978; Stueber *et al.*,1984).

Ankerite

Strontium isotope compositions of the diagenetically later ankerite (0.7089 to 0.7112; concentrations 18 ppm to 100 ppm; Table 2.5) reflect a larger input of radiogenic strontium, together with recycled marine strontium derived from the dissolution and reprecipitation of the earlier dolomite (Figure 2.37). Potential sources of radiogenic strontium include the dissolution of detrital silicates (i.e., feldspar, micas) and clay transformations. Strontium generated either by silicate dissolution or clay diagenesis would produce high $^{87}Sr/^{86}Sr$ ratios (average 0.720) with low strontium concentrations (Faure, 1986; Stueber *et al.*, 1984). As mentioned above, the majority of feldspar dissolution in the Rotliegend took place after the precipitation of the ankerite, so this could not have been an important local source for high $^{87}Sr/^{86}Sr$. Also, the Rotliegend is a well sorted and wind blown deposit containing very little muscovite or biotite. The minor amount of mica that is present is very fresh and shows no signs of dissolution. Therefore, the higher $^{87}Sr/^{86}Sr$ values of the ankerite were probably not supplied by diagenetic reactions within the

Rotliegend, but instead were most likely derived from the underlying Upper Carboniferous mudstones. The possibility of the radiogenic strontium having been supplied from any other rock unit is unlikely because the structural setting of the field (Figure 2.1 here & figure 5.28 of Glennie, 1990) precludes direct connections to other formations. The low strontium concentrations of the ankerite are, therefore, interpreted to reflect the mixing of strontium derived from dissolution of dolomite with strontium derived from the dissolution of detrital silicates, both sources having relatively low strontium concentrations.

2.8.3 Coupled carbon and strontium isotopes

There is an excellent linear correlation between the carbon and strontium isotope compositions of both the early dolomite and late ankerite cements in the Rotliegend, the correlation coefficient r = 0.93 being significant at the 99.9% level for seven degrees of freedom (Figure 2.38). This suggests a very strong link between the sources of carbon and strontium incorporated into these cements. Carbon isotope compositions of the dolomite reflect a predominantly marine bicarbonate source, but do not indicate whether it was of Late Carboniferous or Late Permian origin. Strontium isotope values of the dolomite, however, are indicative of a specific starting source, namely Late Permian seawater mixed with a minor component of radiogenic strontium (see section 2.8.2). A distinct linear trend in carbon and strontium isotope compositions of the dolomite is observed moving away from the isotopic composition of Late Permian seawater (Figure 2.39). This trend indicates progressive mixing of Late Permian seawater with fluids from the underlying Upper Carboniferous mudstones. These Carboniferous fluids had negative $\delta^{13}C$ from early thermal maturation of organic matter, and radiogenic strontium derived from diagenetic reactions.

The obvious linearity of Figure 2.38 strongly suggests that the carbon to strontium concentration ratios of Late Permian seawater and

diagenetically modified Late Carboniferous brines were the same within a factor of 2 (see Fig. 1 of Langmuir *et al.*, 1978). This is because the generalized form of the equation for the mixing of two isotopic ratios is a hyperbola whose curvature is dependent on the relative element concentration ratios. If the concentration ratios are equal or nearly equal then the mixing curve is a straight line (i.e., Figure 2.38).

Increasing organic (isotopically negative) carbon and radiogenic strontium in the diagenetically later ankerite, suggest a much stronger influence from the underlying mudstones. The low $\delta^{13}C$ values of the ankerite are consistent with precipitation following the continued mixing of Late Permian marine bicarbonate with a significant amount of diagenetic carbon derived from late-stage thermal maturation of organic matter in the Upper Carboniferous mudstones (Figure 2.37). The strontium isotope ratios of the ankerite are not indicative of a specific radiogenic strontium source, although the preferred hypothesis is that a gradually increasing component of radiogenic strontium was dissolved from detrital silicates ($^{87}Sr/^{86}Sr$ = 0.720) in the Upper Carboniferous mudstones. As with the dolomite, the correlation between the carbon and strontium isotopes in the ankerite suggests an important association between increasing organic carbon and radiogenic strontium. This linear relation between strontium and carbon isotope ratios implies that the radiogenic strontium and organic carbon had the same source, the underlying Upper Carboniferous mudstones. It suggests that the organic acids generated by thermal maturation of organic matter dissolved the detrital silicates in the Upper Carboniferous mudstones, releasing radiogenic strontium. This isotopically negative carbon and radiogenic strontium then migrated up into the Rotliegend by compactional fluid movement of fluids or by diffusion of ions.

2.9 POREWATER EVOLUTION

Authigenic cements reflect the chemistry of the pore fluid from

which they grew and therefore can be explained in terms of the chemical composition and evolution of the pore fluids. Understanding the distributions of these cements and the controls on their precipitation is thus of great importance in modelling the diagenetic history of sedimentary rocks. Petrographic, geochemical and isotopic observations and results are presented here, therefore, in order to evaluate the evolution of pore fluid chemistry during dolomite and ankerite cementation in the Rotliegend Sandstone in the Leman field.

2.9.1 Dolomite

Type I dolomite

Cementation of the Rotliegend Sandstone by early Type I microrhombic and rhombic dolomite is interpreted to have been initiated by the influx of waters and/or diffusion of ions from the marine Upper Permian Zechstein evaporites during shallow burial, although there also appears to be meteoric Carboniferous component to the fluids at this time (Figure 2.40a). The marine contribution to the porewaters is reflected by both the relatively heavy carbon isotope ratios and low radiogenic strontium contents of the early Type I dolomite cement (see sections 2.8.1, 2.8.2 & 2.8.3). The $\delta^{13}C$ values of the early dolomite form the unaltered red beds (–2.59 to –0.90‰), however, are depleted in ^{13}C relative to Late Permian sea water, which may had a $\delta^{13}C$ compositions of 0 to +2‰ (or possibly as enriched as +6‰; Tucker *et al.*, 1990). The ^{13}C depletion in the Type I dolomite relative to Late Permian seawater is interpreted to reflect a contribution of isotopically light carbon derived from the early maturation of organic matter in the underlying Upper Carboniferous source rocks. $\delta^{13}C$ isotope values of Type I dolomite from the the discoloured region (–3.93 to –5.50‰) at the base of 49/26-5 are even more depleted than the other Type I dolomite samples, reflecting a larger input of isotopically light carbon from thermal decarboxylation of organic matter in the underlying Carboniferous source rocks. The strontium isotope

compositions of the Type I dolomite in the Rotliegend (0.7077 to 0.7087) are only slightly more radiogenic than Late Permian seawater (0.7070), suggesting a significant marine component in the early pore fluids. Oxygen isotope compositions of both Type I and Type II dolomites reflect precipitation at temperatures between 35° and 60°C assuming precipitation from mixed marine/meteoric waters with an oxygen isotope composition of -2‰. These temperatures correspond to burial depths of approximately 400 m to 1.2 km (1300 to 4000 ft) assuming a surface temperature of 15 to 20°C and suggest that dolomite cementation occurred during the Late Permian to Early Triassic (Figure 2.36).

The bimodal grain size distribution of the Type I dolomite is consistent with downward migrating fluids and/or ions from the overlying Zechstein evaporites (see section 2.7.1). Zone A of the Rotliegend, at the top of the sequence, is characterized by a high frequency of nucleation sites (i.e. crystals) and extremely fine grained (microrhombic) dolomite. Zone B, located stratigraphically below Zone A, consists of medium to coarse grained dolomite and this coarser cement has a lower frequency of nucleation sites. Studies by Berner (1980), Sibley & Bartlett (1987), and Saigal & Bjørlykke (1987) have shown that rapid nucleation and fine grained precipitates result from highly supersaturated fluids and that with lessening degrees of supersaturation the rate of nucleation decreases and larger crystals are formed. This suggests that the fluid which initiated Type I dolomite precipitation became less supersaturated with depth, which is interpreted to have resulted as the waters or ions controlling carbonate precipitation moved further from their source, the overlying Zechstein, supporting the model of downward movement of marine water.

Type II dolomite

The dominance of compactionally driven evolved meteoric fluids and ions from the Carboniferous at the base of the Rotliegend led to the precipitation of Type II dolomite (Figure 2.40a). The most significant

evidence supporting the upward migration of Carboniferous fluids and/or ions into the Rotliegend, during this generation of cementation, is the stratigraphic distribution of Type II dolomite within the study area (see section 2.7.1). This generation of dolomite is most abundant at the base of the Rotliegend (Zone C) where it occurs as large poikilotopic crystals. In the middle and upper portion of the sequence (Zones A & B), Type II dolomite is much less common and no longer occurs as a pervasive poikilotopic cement (see section 2.7.1). Instead, it forms as minor replacive overgrowths on earlier Type I dolomite rhombs and less commonly as individual pore lining rhombs. The preferential cementation of the base of the Rotliegend by Type II dolomite and the decrease in abundance of this cement in the upper portions of the sequence suggests that the pore fluids were stratified, which is consistent with a model of upwardly migrating fluids and ions from the Carboniferous.

The higher iron concentrations of the Type II dolomite, relative to Type I dolomite, also supports the introduction of fluids from the Carboniferous (see section 2.6.2). Iron concentrations of Type II dolomite range from 2 to 4 mole % $FeCO_3$, whereas the non-ferroan Type I dolomite generally contains less than 0.2 mole % $FeCO_3$ (see section 2.6.1). This indicates that the fluids from which the Type I dolomite precipitated were depleted in dissolved ferrous (Fe^{2+}) iron, whereas the chemistry of the Type II dolomite reflects a significant increase in dissolved iron concentrations of the pore fluid. The increased iron concentrations of the Type II dolomite suggests that porewaters were more reducing than during earlier dolomite precipitation and the most probable source of reducing iron rich fluids would have been the underlying organic rich Carboniferous sediments.

2.9.2 Ankerite

During burial diagenesis the cross-formational movement of fluids or diffusion of ions from the Carboniferous progressively dominated the porewaters of the Rotliegend Sandstone and led to the

precipitation of ankerite cement (Figure 2.40b). The precipitation of the ankerite from Carboniferous derived fluids is suggested by both the $\delta^{13}C$ and $^{87}Sr/^{86}Sr$ values of the ankerite (see sections 2.8.1, 2.8.2 & 2.8.3). The majority of earlier dolomite cement had carbon isotope values close to those of Permian sea water (-2.59 to -0.90‰), whereas the $\delta^{13}C$ values of ankerite (-4.46 to -3.06‰) are more depleted. These lighter carbon isotope values of the ankerite are interpreted as representing an influx of depleted carbon derived from thermally induced decarboxylation of organic matter during the early maturation of the underlying Carboniferous source rocks. The strontium isotope compositions of the ankerite (0.7110) also are much more radiogenic then the strontium compositions of the early dolomite (0.7077) and the strontium isotope compositions of the ankerite are thought to reflect a dominantly radiogenic source derived from the dissolution and diagenesis of silicates. The relationship between increasing organic (light) carbon and more radiogenic strontium concentrations in the ankerite suggests that the source of the radiogenic strontium was diagenetic reactions in the clay-rich Carboniferous sequences which migrated into the Rotliegend along with the organic (light) carbon. Oxygen isotope compositions of the ankerite reflect precipitation at temperatures between 105° and 125°C, assuming precipitation from evolved brines with a $\delta^{18}O$ composition of 0‰, which correspond to burial depths of approximately 2 to 3 km (6600 to 10,000 ft) and suggest ankerite cementation occurred during the Jurassic (Figure 2.36).

The ankerite, which occurs in part as replacive overgrowths on earlier dolomite and in part as pore lining rhombs, displays no vertical or lateral variation in its distribution within the Rotliegend (see sections 2.4.4 & 2.7.2). The ankerite is often compositionally zoned and the zoning throughout the field is the same, with iron concentrations increasing toward crystal margins (2.6.3). This uniformity of distribution and chemistry throughout the nearly 700 ft (200 m) thickness of sandstone, thus, indicates that the stratification of porewaters which existed during

the precipitation of Type I and II dolomites, no longer was present during this later stage of diagenesis.

2.9.3 Siderite

The presence of both siderite and anhydrite cements in mineralized fractures of the Rotliegend suggests that their precipitation was related to fractures and faults formed in response to tectonic stresses in operation prior to basin inversion during the Late Jurassic-Early Cretaceous (Figure 2.40b). Prior to faulting, the porous and permeable Rotliegend would have probably been under-pressured relative the impermeable Zechstein evaporites which sealed it from above. Therefore, fluids may have been capable of entering the Rotliegend from the overlying overpressured evaporites.

The precipitation of siderite is inferred to have been in response to the mixing of of fluids within the tectonically generated faults and fractures. Sibson (1981) has shown that under compressional tectonics, changes in rock volume occur which cause the migration of fluids toward dilatant regions. Therefore, prior to the inversion of the Rotliegend, the compressional tectonics in the region may have caused the migration of fluids into the fractures, with the first fluids to enter these faults and fractures beening Rotliegend porewaters. The movement of waters from the overpressured Zechstein is also thought to have occurred at this time and the mixing the two fluids is thought to have precipitated the siderite, which was the first mineral to form in fractures.

2.10 CONCLUSIONS

Both early and late carbonate cements have significantly modified the porosity of the Rotliegend Sandstone in the Leman field. Early carbonate cementation is represented by two regionally extensive generations of dolomite which can be recognized by their

cathodoluminescence characteristics. The first, Type I dolomite, consists of non-ferroan micro-rhombic (10 to 30 μm) and rhombic (100 to 200 μm) dolomite crystals which are concentrically zoned and brightly luminescent. Type II dully luminescent dolomite is the second generation of dolomite cement recognized in the Leman field and it occurs as poikilotopic patches, corrosive overgrowths on earlier Type I dolomite, and individual pore lining rhombs. Carbon and strontium isotope data indicate that both generations of dolomite were precipitated from fluids with a strong marine component. Dolomite cementation is interpreted to have been initiated by the influx of marine waters and/or diffusion of ions from the Upper Permian Zechstein evaporites during shallow burial (400 m). The bimodal distribution of Type I dolomite suggests that the porewaters which precipitated Type I dolomite became less supersaturated away from Zechstein evaporites, supporting the model of downward movement of waters and/or ions. There also appears to be an important Carboniferous component to the fluids at this time and the addition of compactionally driven evolved meteoric fluids and ions from the Carboniferous at the base of the Rotliegend led to the cementation by Type I dolomite in the altered (whitened) beds and Type II dolomite in the unaltered beds. This is reflected by the strong ^{13}C depletion of the Type I dolomite from the altered beds and the preferential cementation of the base of the Rotliegend by Type II dolomite. The oxygen isotope compositions of both Type I and Type II dolomites reflect precipitation at temperatures between 35° and 60°C from a mixture of marine and evolved meteoric fluids. These temperatures correspond to burial depths of approximately 400 m to 1.2 km (1300 to 4000 ft) and suggest dolomite cementation occurred during the Late Permian to Early Triassic.

Late carbonate cementation in the Rotliegend Sandstone is represented by authigenic ankerite and later siderite. Ankerite is compositionally zoned and occurs as pore lining rhombs and also as replacive overgrowths on earlier Type I and II dolomites. No systematic variation in ankerite cement with depth was observed in the Rotliegend

Sandstone, indicating that the pore fluids were no longer stratified with respect to carbonate as they were during earlier dolomite formation. Carbon and strontium isotope ratios indicate that ankerite precipitated from porewaters with a larger component of Carboniferous waters than the earlier dolomite, suggesting that during burial diagenesis the movement of fluids and/or diffusion of ions from the underlying Carboniferous progressively dominated these waters. The oxygen isotope compositions of the ankerite reflect precipitation at temperatures between 105° and 125°C which correspond to burial depths of approximately 2 to 3 km (6600 to 10,000 ft) and suggest ankerite cementation occurred during the Jurassic. Siderite is uncommon in the Rotliegend and is only found on the sides of mineralized fractures. This suggests that siderite precipitation was controlled by fluids and processes that were restricted to the fractures in the Leman field and which did not extend into the sands themselves.

2.11 ACKNOWLEDGEMENTS

Supported by funds from Amoco (UK) Exploration and Shell/Esso U.K. Exploration and Production. This research was carried out at the Department of Geology and Applied Geology, University of Glasgow, and the Isotope Geology Unit, Scottish Universities Research and Reactor Centre (SURRC). Core was supplied by the British Geological Survey and by Shell/Esso. The authors thank Ed Stephens and Donald Herd of St. Andrews University for the use of microprobe facilities. The authors would also like to thank Douglas Maclean (Glasgow University) for his assistance with the production of photographic plates. The SURRC is supported by Natural Environment Research Council of Britain and the Scottish Universities.

2.12 REFERENCES CITED

Anderson, T.F. and Arthur, M.A. 1983. Stable isotopes of oxygen and carbon and their application to sedimentological and paleoenvironmental problems. Chapter 1 in: *Stable Isotopes in Sedimentary Geology*. Arthur, M.A.,Anderson, T.F., Kaplan, I.R., Veizer, J. and Land, L.S. (eds), *S.E.P.M. Short Course Notes* 10,1-151.

Arthur, T.J., Pilling, D., Bush, D., and Macchi, L., 1986, The Leman Sandstone Formation in U.K. block 49/28: Sedimentation, diagenesis and burial history. In: *Habitat of Palaeozoic Gas in N.W. Europe*. Brooks, J., Goff, J. and van Hoorne, B. (eds). *Spec. Publs Geol. Soc.* **23,** Scottish Academic Press, London, 251-266.

Becker, R.H. and Clayton. R.N. 1972. Carbon isotopic evidence for the origin of a banded iron formation in Western Australia. *Geochim. Cosmochim. Acta,* **36,** 577-595.

Berner, R.A. 1980. Non-marine sediments. In: *Early Diagenesis, a Theoretical Approach.* Princeton Univ. Press, Princeton, N.J., 206-224.

Bjørlykke, K, Aagaard, P., Dypvik, H., Hastings, D.S. and Harper, A.S. 1986. Diagenesis and reservoir properties of Jurassic sandstones from the Haltenbanken area, offshore mid Norway. *Habitat of Hydrocarbons on the Norwegian Continental Shelf.* Norwegian Petrol. Soc., Graham and Trotman, London, 397-406.

Boles, J.R. 1978. Active ankerite cementation in the subsurface Eocene of Southwest Texas. *Contr. Miner. Petrol.,* **68,** 13-22.

Bulat, J. and Stoker, S.J. 1987. Uplift determination from interval velocity studies, UK, southern North Sea. *Petroleum Geology of North West Europe.* Brooks, J. and Glennie, K.W. (eds). Graham and Trotman, London, 293-306.

Burke, W.M., Denison, R.E, Hetherington, E.A., Koepnick, R.B., Nelson, M.F. and Otto, J.B. 1982. Variation of sea-water $^{87}Sr/^{86}Sr$ throughout Phanerozoic time. *Geology* **10,** 516-519.

Burley, S.D., Kantorowitz, J.D. and Waugh, B., 1985. Clastic diagenesis. In: *Sedimentology, Recent Developments and Applied Aspects.* Brenchley, P.J. and Williams, B.J.P. (eds). Blackwell, london, 189-

226.

Carpenter, A.B., 1978, Origin and chemical evolution of brines in sedimentary basins: Oklahoma Geological Survey Circular 79, p. 60-77.

Carpenter,A.B. 1985. Effect of ferrous iron on the stability and nucleation of dolomite. In: *Timing of siliclastic diagenesis* S.E.P.M. , Gulf Coast Section, Sixth Annual Research Conference, 4-5.

Claypool, G.E. and Kaplan, I.R. 1974. The origin and distribution of methane in marine sediments. In: *Natural Gases in Marine Sediments*. Kaplan, I.R. (ed). 99- 139. Plenum Press, New York.

Cope, M.J. 1986. An interpretation of vitrinite reflectance data from the southern North Sea Basin. *Habitat of Palaeozoic Gas in N.W. Europe*. Brooks, J., Goff, J. and van Hoorne, B. (eds). *Spec. Publs Geol. Soc.* **23**, Scottish Academic Press, London, 85-101.

Craig, H. 1963. Isotopic variations in meteoric waters. *Science*, **133**, 1702-1703.

Craig, H., Boato, G. and White, D.E. 1956. *Isotopic Geochemistry of Thermal Waters*. pp. 29-38. National Academy of Sciences, National Research Council Publication, 400.

Craig. H. and Gordon, L.I. 1965. Deuterium and Oxygen-18 variations in the ocean and the marine atmosphere. In: *Stable Isotopes in Oceanographic Studies and Paleotemperatures*. Tongoirgi, E. (ed). Consiglio Nazionale delle Richerche, Laboratorio di Geologia Nucleare, Pisa, 9-130.

Carothers, W.W. and Kharaka, Y.K., 1978. Aliphatic acid ions in oil-field waters—implications for origin of natural gas. *Bull. Am. Ass. Petrol. Geol.* **62**, 2441-2453.

Curtis, C.D. 1978. Possible links between sandstone diagenesis and depth-related geochemical reactions occurring in enclosed mudstones. *Jour. Geol. Soc. Lond.*, **135**, 107-117.

Deer, W.A., Howie, R.A. and Zussman, J. 1966. *An Introduction to the Rock Forming Minerals,* Longmans, London 528 p.

Deuser. W.G. and Hunt, J.M. 1969. Stable isotope ratios of dissolved inorganic carbon in the Atlantic. *Deep-Sea Res.*, **16**,221-225.

Dickson, J.A.D. 1966. Carbonate identification and genesis as revealed by staining: *Jour. Sediment. Petrol.*, **36**, 491-505.

Draxler, J.K. and Edwards, D.P. 1986. Evaluation procedures in the Carboniferous of Nothern Europe. *Habitat of Palaeozoic Gas in N.W. Europe.* Brooks, J., Goff, J. and van Hoorne, B. (eds). *Spec. Publs Geol. Soc.* **23,** Scottish Academic Press, London, 151-168.

Dutton, S.P. and Land, L.S. 1985. Meteoric burial diagenesis of Pennsylvanian sandstones, southwestern Anadarko Basin, Texas. *Bull. Amer. Assoc. Petrol. Geol.*, **69**, 22-38.

Dutton, S.P. and Land, L.S. 1988. Cementation and burial history of a low permeability quartzarenite, Lower Cretaceous Travis Peak Formation, East Texas. *Geol. Soc. Amer. Bull.*, **100**, 1271-1282.

Fairchild, I.J. 1983. Chemical controls on cathodoluminescence of natural dolomites and calcites : new data and review. *Sedimentology*, **30**, 579-583.

Faure, G., 1986, *Principles of Isotope Geology* (second edition): New York, John Wiley & Sons, 183-199.

Friedman, I and O'Neil, J.R. 1977. *Compilation of Stable Isotope Fractionation Factors of Geochemical Interest.* United States Geological Survey Professional Paper 440-KK, 12 pp.

Fritz, P. and Smith, D.G.W., 1970. The isotopic composition of secondary dolomites. *Geochim. Cosmochim. Acta*, **34**, 1161-1173.

Given, R. K. and Lohman, K. 1985. Isotopic evidence for the early meteoric diagenesis of the reef facies, Permian reef complex of west Texas and New Mexico. *Jour. Sediment. Petrol.*,**56**, 183-193.

Glennie, K.W. 1972. Permian Rotliegendes of Northwest Europe interpreted in light of modern desert sedimentation studies. *Bull Amer.Assoc.Petrol.Geol.*, **56**, 1048-1071.

Glennie, K.W. 1990. Lower Permian—Rotliegend. In: *Introduction to the Petroleum Geology of the North Sea* (3rd edition). Glennie, K.W. (ed), Blackwell Scientific Publications, Oxford, 120-152.

Glennie, K.W., Mudd, G.C. and Nagtegaal, P.J.C. 1978. Depositional environment and diagenesis of Permian Rotliegendes sandstones in Leman Bank and Sole Pit areas of the U.K. Southern North Sea. *Jour. Geol. Soc. Lond.*, **135**, 25-34.

Hunt, J.M. 1979. *Petroleum Geochemistry and Geology.* San Francisco, W. H. Freeman & Co., 716p.

Irwin, H., Curtis, C.D. and Coleman, M.L. 1977. Isotopic evidence for source of diagenetic carbonates formed during burial of organic-rich sediments. *Nature*, **269**, 209-213.

Keeling, C.D. 1958. The concentration and isotopic abundance of carbon dioxide in rural areas. *Geochim. Cosmochim, Acta*, **13**, 322-334.

Keeling, C.D. 1961. The concentration and isotopic abundance of carbon dioxide in rural and marine air. *Geochim. Cosmochim, Acta*, **24**, 277-298.

Keith, M.L. and Weber, J.N., 1964. Isotopic composition and environmental classification of selected limestones and fossils. *Geochim. Cosmochim. Acta*,**28**, 1787-1816.

Langmuir, C.H., Vocke, R.D. Jr., Hanson, G.N., and Hart, S.R., 1978, A general mixing equation with applications to Icelandic basalts: *Earth and Planet. Sci. Lett.*, **37**, 380-392.

Lee, M. 1984. Diagenesis of the Permian Rotliegendes Sandstone, North Sea : K/Ar, O^{18}/O^{16}, and petrological evidence. Ph. D. thesis, Case Western University, Cleveland, Ohio, 346pp.

Longstaffe, F.J. and Ayalon, A 1987. Oxygen-isotope studies of clastic rocks in the Lower Cretaceous Viking Formation, Alberta: implications for the role of meteoric water. In: *Diagenesis of Sedimentary Sequences*. Marshall, J.D. (ed). *Geol. Soc. Spec. Publ.***36**, Blackwell Scientific Publications, London, 277-296.

Lønøy, A., Akselsen, J. and Rønning, K. 1986. Diagenesis of a deeply buried sandstone reservoir: Hild field northern North Sea. *Clay Minerals*,**21**, 497-511.

Marie, J.P.P. 1975. Rotliegendes stratigraphy and diagenesis. In: *Petroleum and the Continental Shelf of North West Europe*, Woodland, A.W. (ed.). *Applied Science Publ.*, London, 205-211.

McCrea, J.M. 1950. On the isotope chemistry of carbonates and a paleotemperature scale. *Jour. Chem. Phys.* **18**, 849-857.

Meyers, W.J. 1974. Carbonate cement stratigraphy of the Lake Valley Formation (Mississippian) Sacramento Mountains, New Mexico. *Jour. Sediment. Petrol.*,**44**, 837-861.

Murata, K.J., Friedman, I. and Madsen, B.M. 1967. Carbon-13-rich diagenetic carbonates in Miocene formations of California and Oregon. *Science*, **156**, 1484-1486.

O'Neil, F.R., Clayton, R.N. and Mayeda, T.K. 1979. Oxygen isotope fractionation in divalent metal carbonates. *Jour. Chem. Phys.* **51,** 5547-5548.

Pierson, B.J. 1981. The control of cathodoluminescence in dolomite by iron and manganese. *Sedimentology,* **28,** 601-610.

Saigal, G.C. and Bjørlykke, K., 1987. Carbonate cements in clastic reservoir rocks from offshore Norway—relationships between isotopic composition, textural development and burial depth. In: *Diagenesis of Sedimentary Sequences,* Marshall, J.D. (ed). *Spec. Publs Geol. Soc.* **36,** Blackwell Scientific Publications, London, 313-324.

Salem, O., Visser, J.H., Dray, M. and Gonfiantini, 1980. Groundwater flow patterns in the western Libyan Arab Jamahiriya evaluated from isotopic data. *Arid -Zone Hydrology: Investigations with Isotope Techniques* (Proc. Symp. Vienna 1980) IAEA-158/12, Vienna.

Sibley, D.F. and Bartlett, T.R. 1987. Nucleation as a rate limiting step in dolomitization. In: *Proceedings of the International Meeting on Geochemistry of the Earth's Surface and Processes of Mineral Formation 16-22 March, 1986,* Rodriguez-Clemente, R. and Tardy, Y. (eds). *Consejo Soperior De Investigacinoes Cientificas, Madrid, 1987.,*735-741.

Sibson, R., 1981. Fluid flow accompanying faulting: field evidence and models. In: *Earthquake prediction: an International review,* Simpson, D.W. and Richards, P.G. (eds). Maurice Ewing Series, **4,** *Amer. Geophys. Union,* Washington D.C., 593-603.

Sharma, T. and Clayton, R.N. 1965. Measurement of O^{18}/O^{16} ratios of total oxygen of carbonates. *Geochim et Cosmochim Acta,* **29,** 1347-1353.

Smith, B.N. and Epstein, S. 1971. Two categories of $^{13}C/^{12}C$ ratios for higher plants. *Plant. Physiol.,* **47,** 380-384.

Sommer, S.E. 1972. Cathodoluminescence of carbonates. 1. Characterization of cathodoluminescence from carbonate solid solutions. 2. Geological applications. *Chem. Geol.* **9,** 257-284.

Stahl, W. 1974. Carbon isotope fractionations in natural gases. *Nature,* **251,** 134-135.

Stahl, W.J. 1977. Carbon and nitrogen isotopes in hydrocarbon research and exploration. *Chem. Geol.*, **20**, 121-149.

Stueber, A.M., Pushkar,P., and Hetherington, E.A., 1984. A strontium isotopic study of Smackover brines and associated solids, southern Arkansas: *Geochim. Cosmochim. Acta*, **48**, 1637-1649.

Tucker, M.E., 1990. Dolomites and dolomitization models. In: *Carbonate Sedimentology*, Tucker, M.E. and Wright, P.V. (eds). Blackwell Scientific Publications, Oxford, 365-396.

Urey, H.C., 1947. The thermodynamic properties of isotopic substances. *Jour. Chem. Soc. (London)*, 562-581.

van Veen, F.R. 1975. Geology of the Leman gas field. In: *Petroleum and the Continental Shelf of North West Europe*, Woodland, A.W. (ed.). *Applied Science Publ.*, London, 223-231.

Veizer, J., Holser, W.T. and Wilgus, C.K. 1980. Correlation of $^{13}C/^{12}C$ and $^{34}S/^{32}S$ secular variations. *Geochim. Cosmochim. Acta*, **44**, 579-587.

Woronick, R.E. and Land, L.S. 1985. Late burial diagenesis, Lower Cretaceous Pearsall and Lower Glen Rose Formations, south Texas. In: *Carbonate Cements*. Schneiderman, N and Harris, P. (eds). *S.E.P.M Spec. Publ.* 36, 265-275.

Yurtesever, Y 1975. Worldwide survey of stable isotopes in precipitation. *Rept. Sect. Isotope Hydrol.*, IAEA, November, 1975, 40 p.

2.13 TABLES

Table 2.1 Electron microprobe analyses of carbonate cements from the Rotliegend Sandstone. (1) Type I dolomite, (2) Type II dolomite, (3) ankerite, (4) siderite..

Sample (Well)	6317[1] (27-2)	6737[1] (27-2)	6737[2] (27-2)	6854[2] (26-5)	6737[3] (27-2)	6965[3] (26-25)	6565[4] (26-5)
$CaCO_3$	58.9	58.6	57.3	57.5	54.0	54.9	3.8
$MgCO_3$	39.9	39.8	38.7	39.1	28.7	28.5	7.1
$FeCO_3$	0.2	0.2	3.5	2.9	16.4	16.0	88.6
$MnCO_3$	0.65	0.63	0.5	0.5	1.0	0.6	0.5

Table 2.2 Density of nucleation sites (crystals) per mm^2 for dolomite cements in zones A,B & C in the Leman field, Quadrant 49. Five samples from each zone were examined under cathodoluminescence and five different portions of each sample were examined in order to estimate density of nucleation sites.

Sample (Well)	Number of nucleation sites				
	1	2	3	4	5
Zone A(Type I microrhombic)					
6317' (27-2)	49	37	51	48	42
6351' (27-2)	53	42	47	41	39
6466' (26-5)	47	39	32	57	51
6471' (26-25)	31	46	39	27	45
6560' (27-3)	52	49	41	37	49
Zone B(Type I rhombic)					
6585' (26-5)	7	13	8	9	11
6649' (26-25)	14	8	9	7	13
6681' (27-2)	11	8	14	13	11
6717' (27-3)	12	9	14	11	10
6737' (27-2)	14	7	9	15	13
Zone C(Type II poikilotopic)					
6854' (26-25)	1	2	2	1	2
6892' (27-2)	1	1	3	1	2
6899' (26-25)	2	1	1	1	2
6980' (26-25)	2	1	3	1	1
7002' (27-2)	1	1	2	2	1

Table 2.3 Summary of $\delta^{13}C$ and $\delta^{18}O$ values for Type I and II dolomites from the Rotliegend Sandstone in the Leman field, Quadrant 49 (± values quoted for samples encompass range of replicate analyses-see Appendix D.1)

Well no.	Depth (feet)	$\delta^{13}C$ (‰ PDB)	$\delta^{18}O$ (‰ PDB)	$\delta^{18}O$ (‰ SMOW)	Type of Dolomite
26-5	6566	-2.59 ±0.18	-5.28 ±0.61	+23.41	I
26-5	6670	-1.36	-5.50	+25.19	I
26-5	6925 (*)	-3.93	-5.68	+25.00	I
26-5	7040 (*)	-5.55 ±0.35	-8.47 ±0.30	+22.25	I
26-25	6585	-1.49	-4.54	+26.18	I
26-25	6649	-1.59	-6.14	+24.53	I
26-25	6722	-1.63	-5.85	+24.83	I
26-25	6854	-1.03	-7.43	+23.20	II
26-25	6965	-1.44	-7.48	+23.15	II
27-2	6317	-0.90	-4.60	+26.14	I
27-2	6681	-1.20	-3.56	+27.19	I
27-2	6737	-1.82 ±1.04	-4.22 ±0.4	+26.51	I
27-2	6892	-1.21 ±0.31	-4.82 ±1.1	+25.89	II
27-3	6560	-1.79	-5.64	+25.05	I
27-3	6717	-1.77	-5.90	+24.78	I
27-3	7017	-1.71	-5.32	+25.38	I
27-4	6670	-1.05 ±0.05	-4.80 ±0.20	+25.91	I
27-4	6851	-2.23	-4.92	+25.79	I
27-4	6932	-2.32 ±0.19	-6.83 ±0.22	+24.56	I

(*) samples from the discoloured region at the base of the Rotliegend

Table 2.4 Summary of $\delta^{13}C$ and $\delta^{18}O$ values for ankerite from the Rotliegend Sandstone in the Leman field, Quadrant 49 (± values quoted for samples encompass range of replicate analyses-see Appendix D.1)

Well no.	Depth (feet)	$\delta^{13}C$ (‰ PDB)	$\delta^{18}O$ (‰ PDB)	$\delta^{18}O$ (‰ SMOW)
26-5	6566	-4.32 ±0.02	-11.02 ±0.50	+19.50
26-5	6670	-4.10	-11.78	+18.72
26-5	6925	-3.31	-11.17	+19.35
26-5	7040'	-4.57 ±0.05	-10.06 ±0.40	+20.49
26-25	6585'	-3.45 ±0.03	-9.33 ±0.30	+21.24
26-25	6649'	-3.06	-9.60	+20.96
26-25	6722'	-4.19	-10.17	+20.38
26-25	6854'	-4.68	-10.68	+19.85
26-25	6965'	-3.82 ±0.82	-9.56 ±0.36	+21.04
27-2	6516	-3.10	-10.63	+19.90
27-2	6681	-3.91 ±0.80	-10.27 ±0.20	+20.17
27-2	6737	-3.41 ±0.30	-9.27 ±0.40	+21.30
27-2	6892	-3.12 ±0.30	-10.22 ±0.06	+20.32
27-3	6560	-3.30	-10.43	+20.12
27-3	6717	-3.10	-9.71	+20.85
27-3	6870	-3.51	-10.06	+20.49
27-3	7017	-3.25	-9.83	+20.73

Table 2.5 Summary of data on dolomite and ankerite cement in the Rotliegend Sandstone, Leman field, Quadrant 49.

Well no.	Depth (feet)	Sr (ppm)	$^{87}Sr/^{86}Sr$	$\delta^{13}C$ (‰ PDB)	$\delta^{18}O$ (‰ PDB)	Type of dolomite
Dolomite						
26-5	6670'	86	0.7080	-1.36	-5.50	Type I
27-2	6681'	25	0.7077	-1.28	-3.56	Type I
27-2	6737'	18	0.7084	-1.82	-4.22	Type I
26-25	6965'	225	0.7087	-1.44	-5.25	TYpe II
Ankerite						
26-5	6566'	100	0.7099	-4.32	-11.02	
26-25	6885'	59	0.7089	-3.00	-9.33	
26-25	6854'	76	0.7112	-4.68	-10.68	
27-2	6892'	18	0.7091	-3.11	-10.22	
26-5	7040'	88	0.7101	-4.46	-10.06	

Note: All strontium isotope ratios have been corrected for radiogenic rubidium (see appendix D.2).

2.14 FIGURES AND FIGURE CAPTIONS

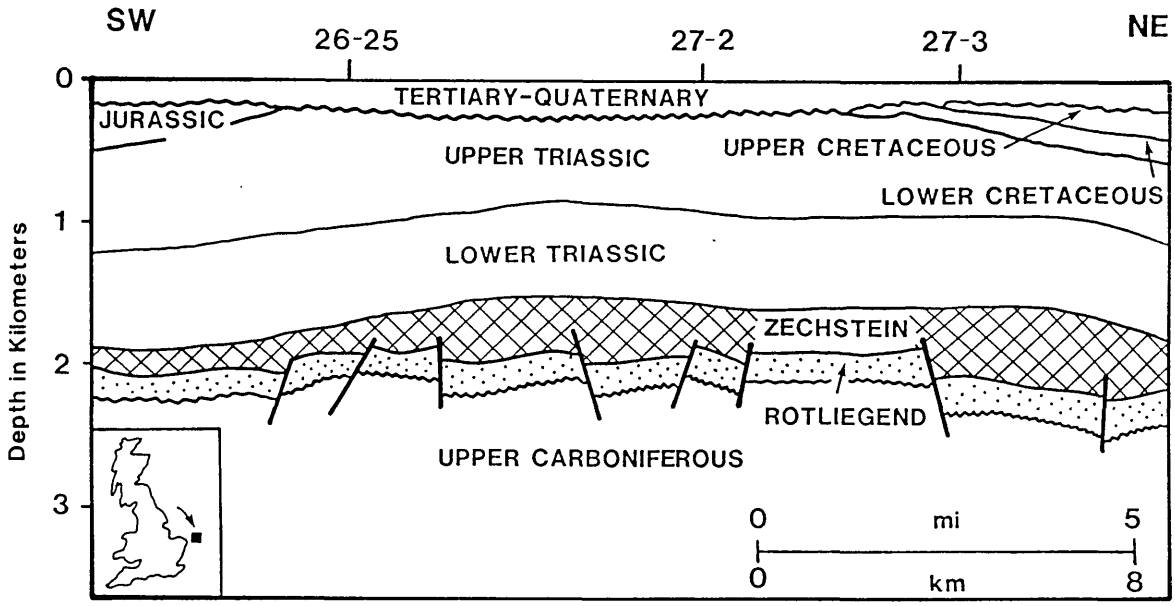

Figure 2.1 Location of Leman gas field (North Sea) and geologic cross section for the Leman region (after Glennie 1990).

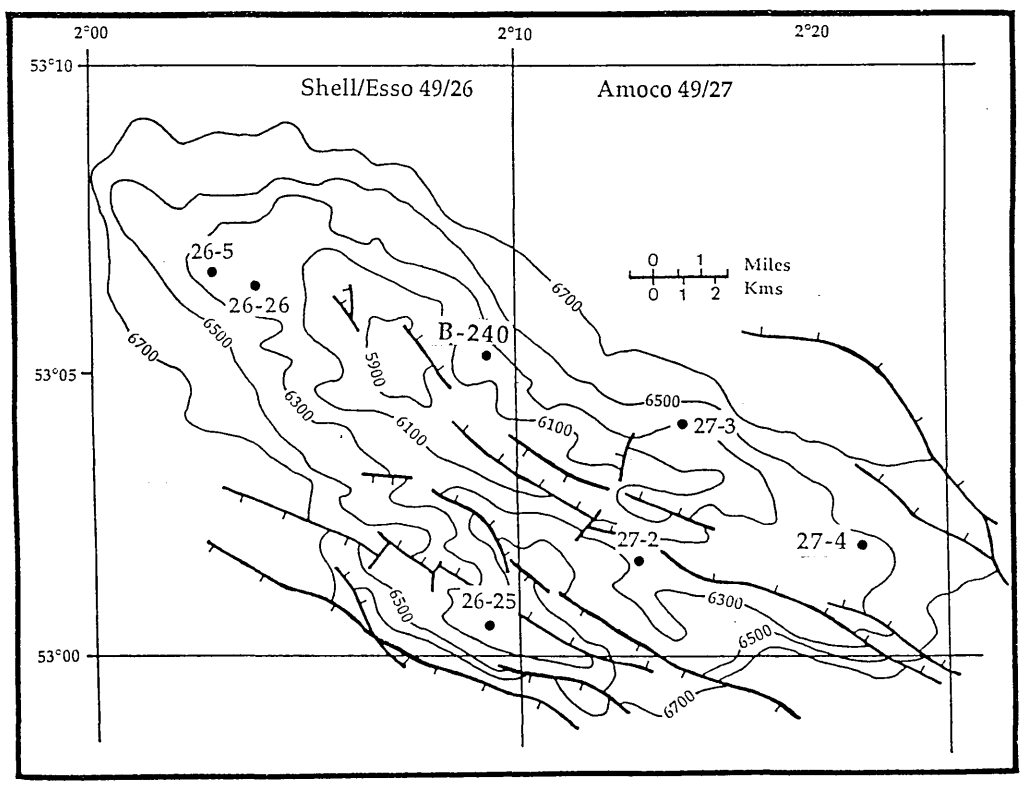

Figure 2.2 Present interpretation of Leman field, showing contours of the the top of the Rotliegend in feet below sea level and locations of wells used in this study (from van Veen, 1975).

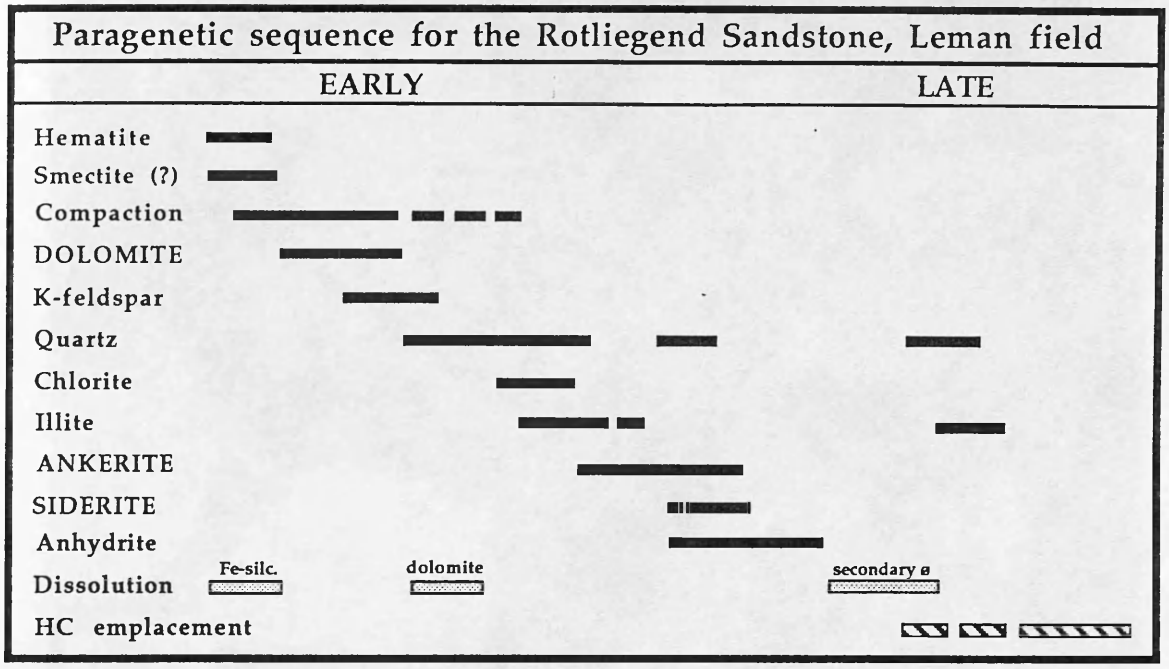

Figure 2.3 Paragenetic sequence showing timing of major diagenetic events in the Lower Permian Rotliegend Sandstone in the Leman gas field.

Figure 2.4 SEM photomicrograph of small rhombic dolomite crystals which have intergrown to form a coalesced aggregate of dolomite. Well 49/26-5, 6466'.

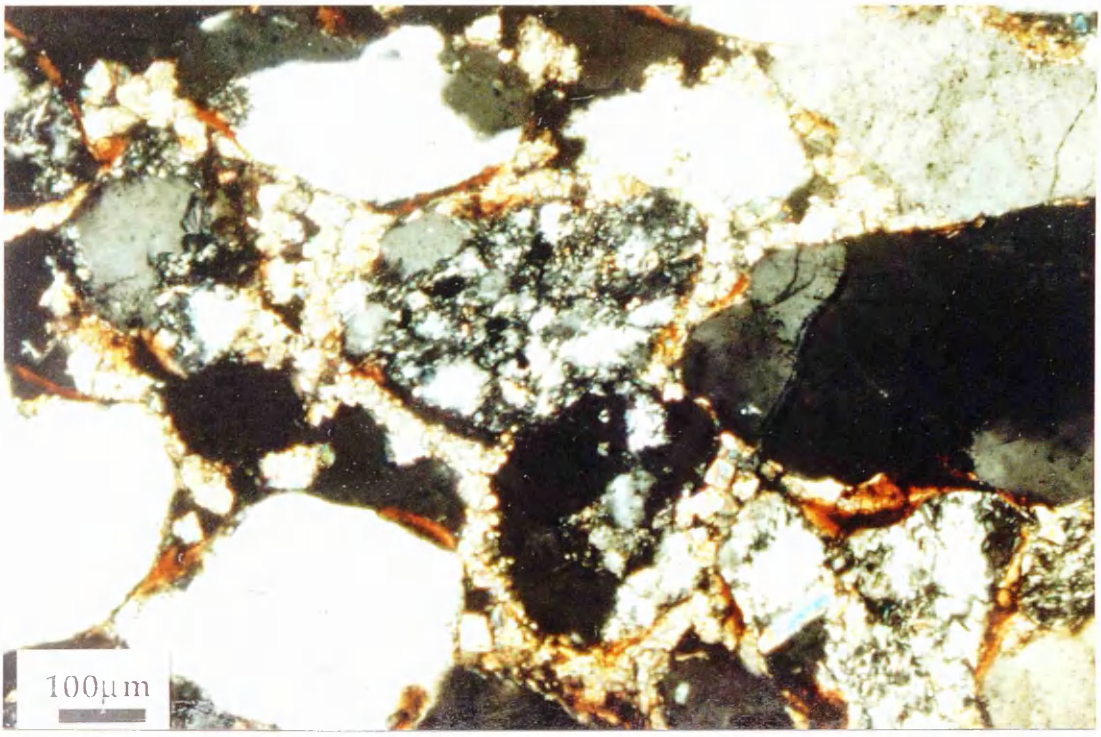

Figure 2.5 Photomicrograph of dolomite rimming cement consisting of intergrown small rhombic dolomite crystals which completely surround detrital grains. Well 49/27-2, 6317'.

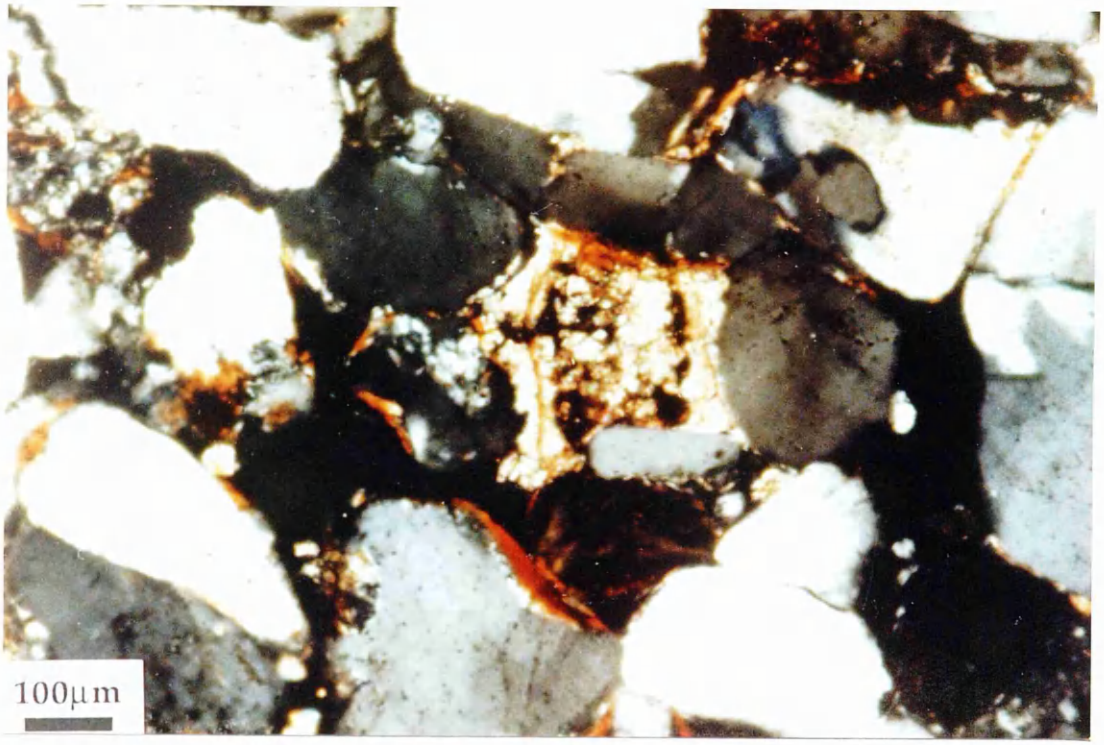

Figure 2.6 Photomicrograph of a detrital grain which has been completely replaced by fine grained dolomite. Note preservation of hematite/clay grain coating which marks the original margin of replaced grain. Well 49/27-2, 6317'.

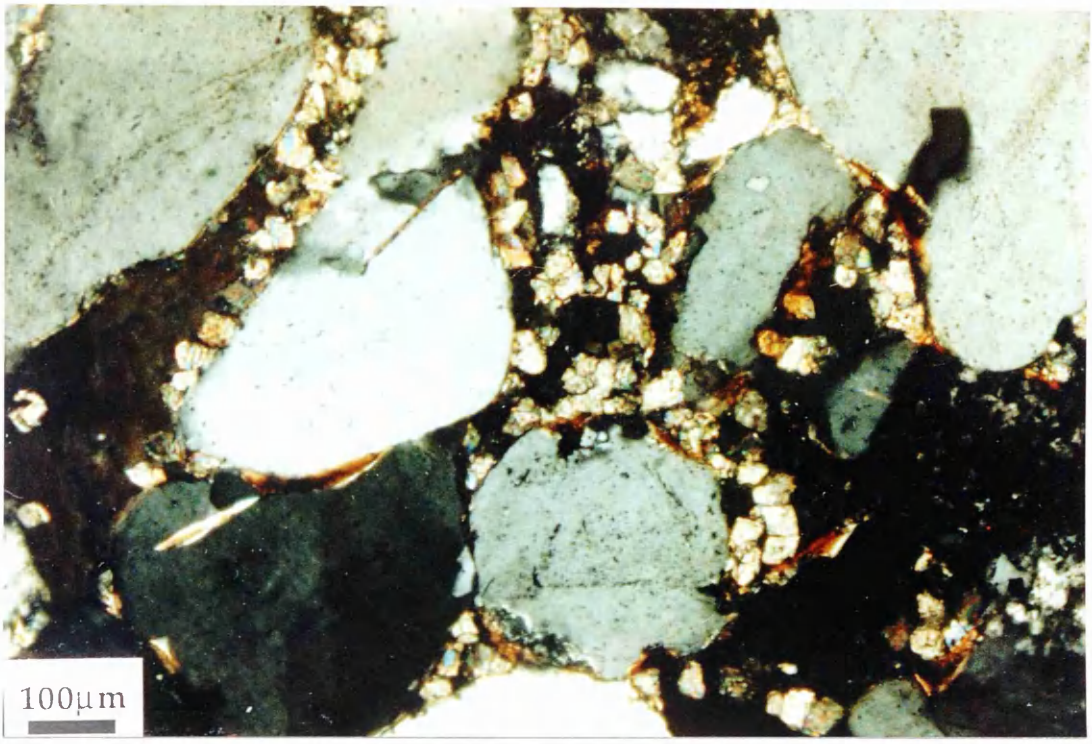

Figure 2.7 Photomicrograph of pore lining phase of small rhombic dolomite crystals. Well 49/26-25, 6466'.

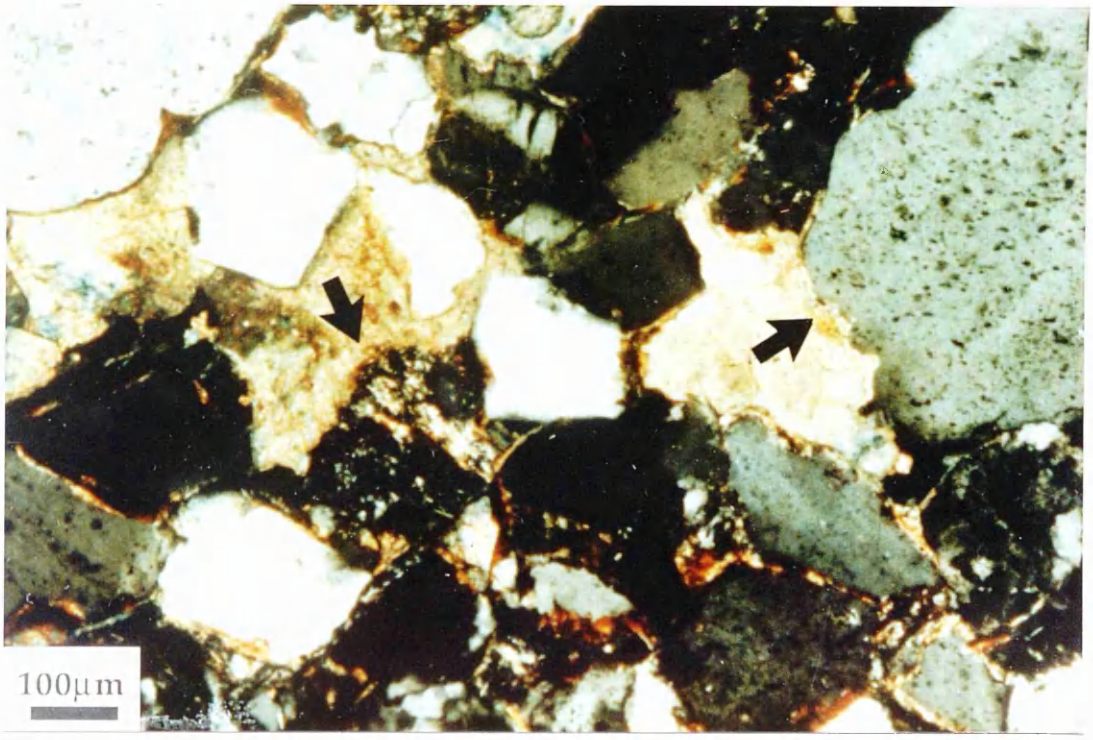

Figure 2.8 Photomicrograph of large blocky anhedral dolomite crystals completely occluding porosity. Note aggressive replacement of detrital grains (arrows). Well 49/27-2, 6737'.

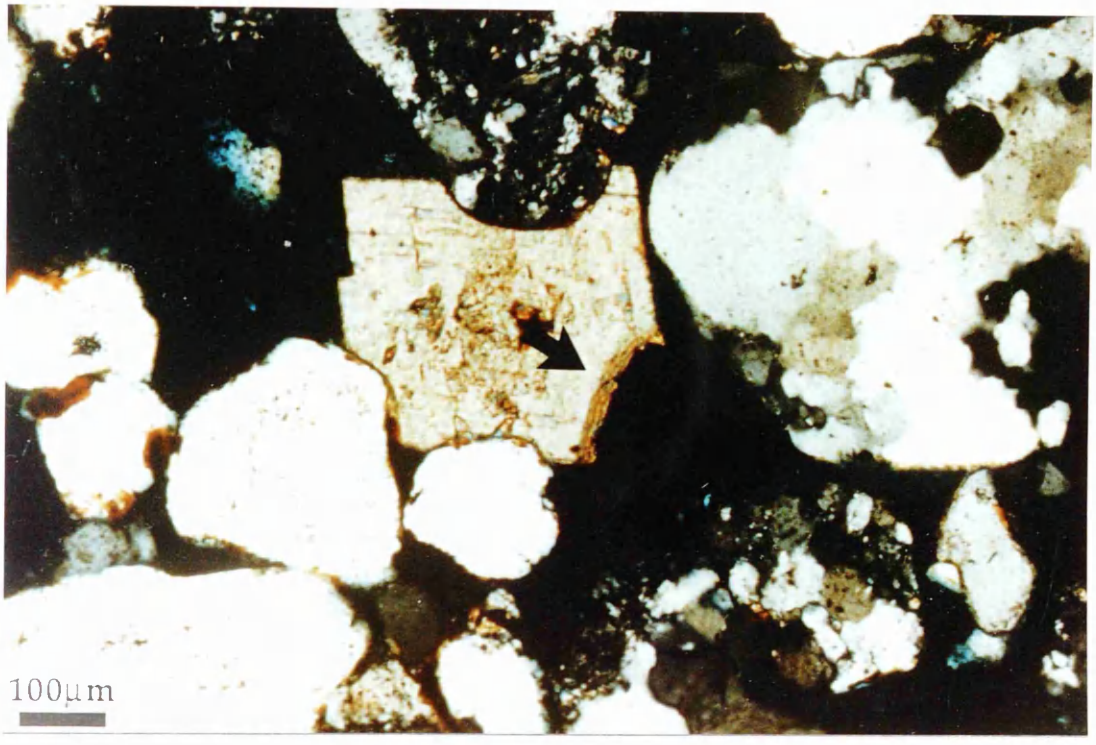

Figure 2.9 Photomicrograph of large dolomite rhomb infilling porosity and aggressively replacing detrital grain (arrow). Well 49/25-25, 6585'.

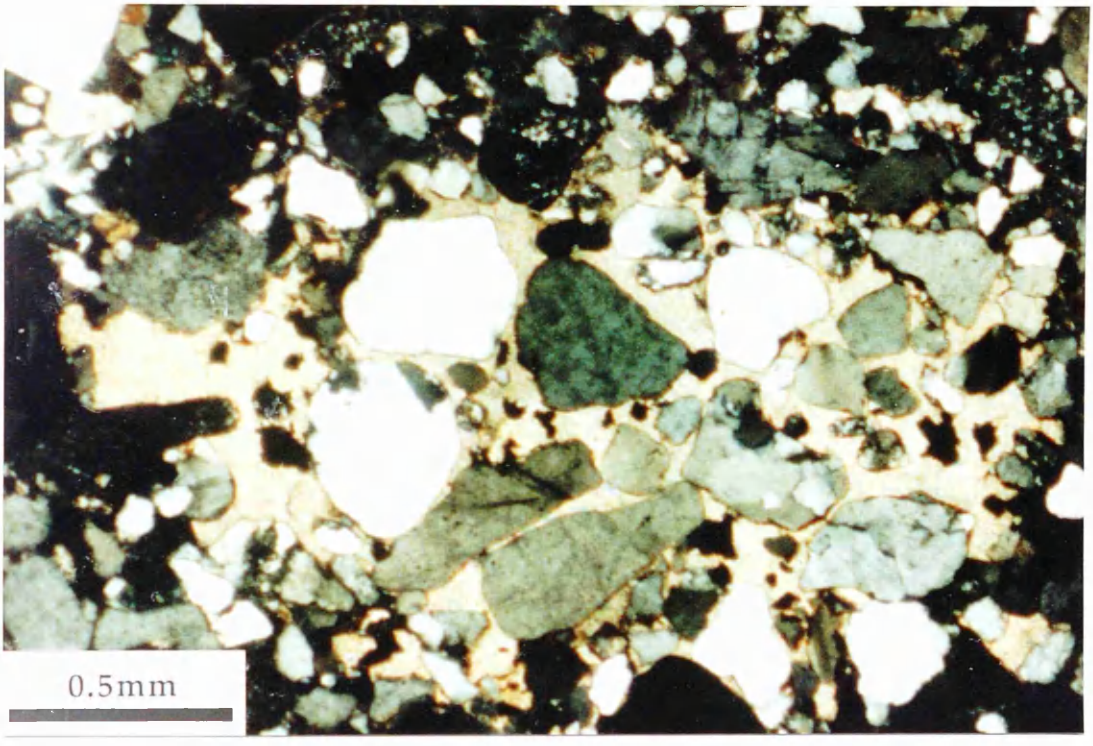

Figure 2.10 Photomicrograph of a large patch of poikilotopic dolomite with cemented framework grains displaying an "apparent" open texture, suggesting very early precipitation of poikilotopic dolomite. Well 49/26-5, 6854'.

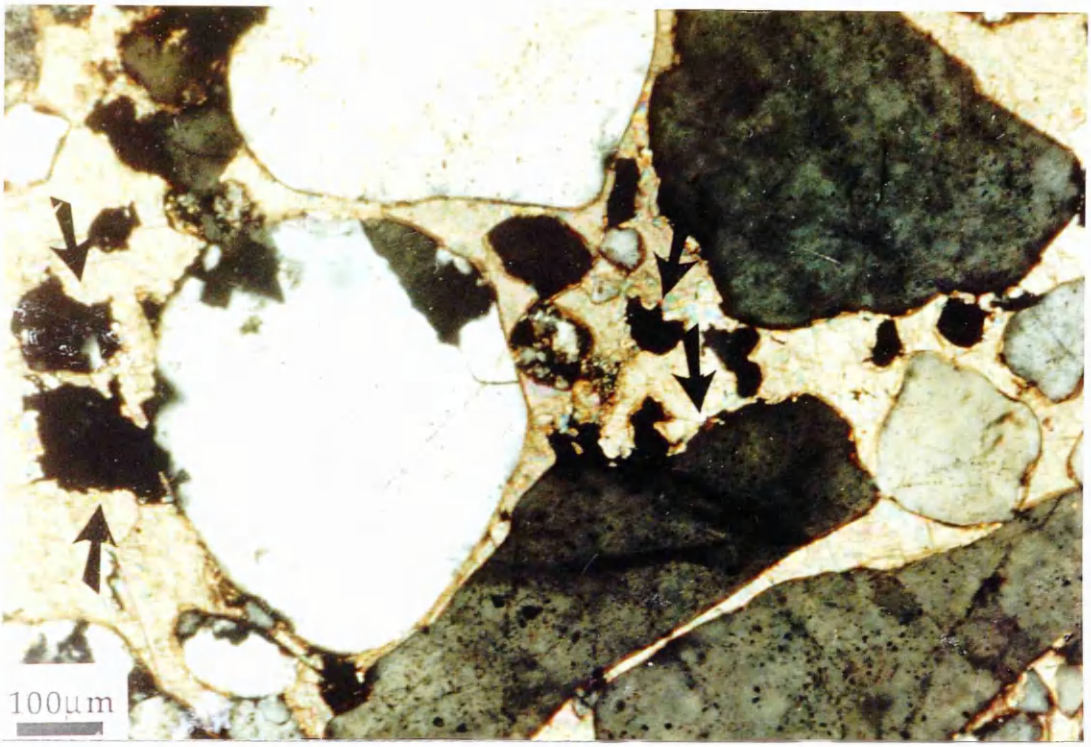

Figure 2.11 Photomicrograph of same poikilotopic patch as shown in Figure 2.9, but at higher magnification. In this close-up view, the aggressive replacement of detrital grains, especially silt size material can be observed (arrows). Well 49/26-5, 6854'.

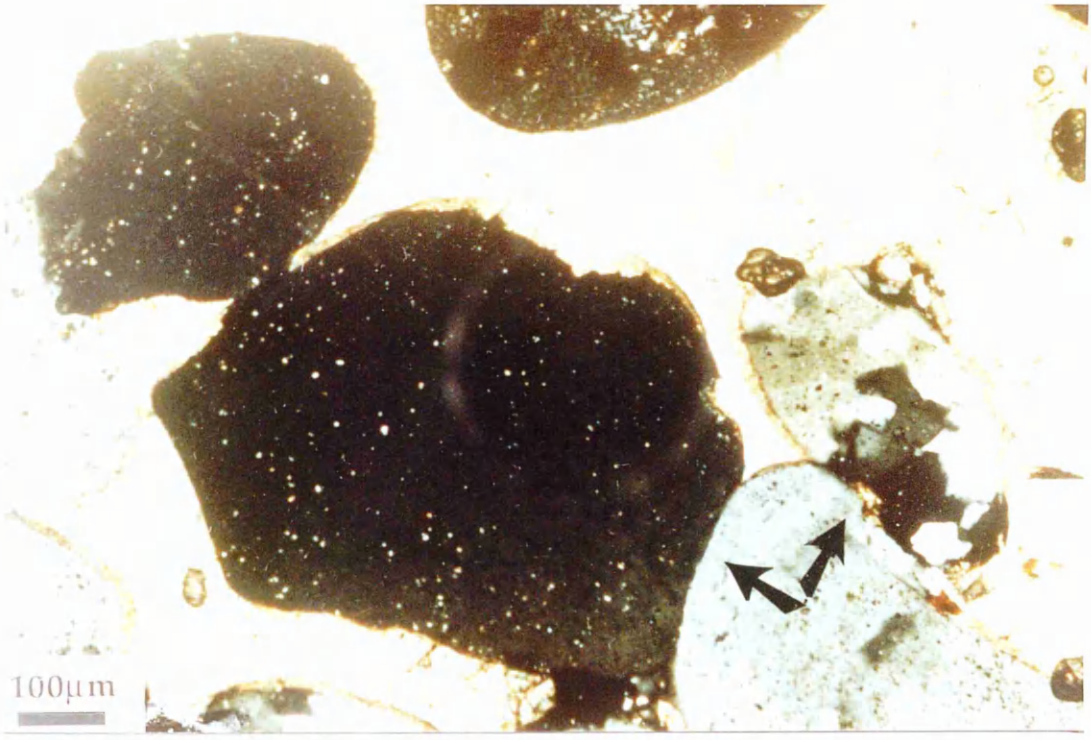

Figure 2.12 Photomicrograph of detrital grains cemented by poikilotopic dolomite. Cemented grains show evidence of pressure solution and some suturing may have taken place (arrows). Well 49/27-2, 6892'.

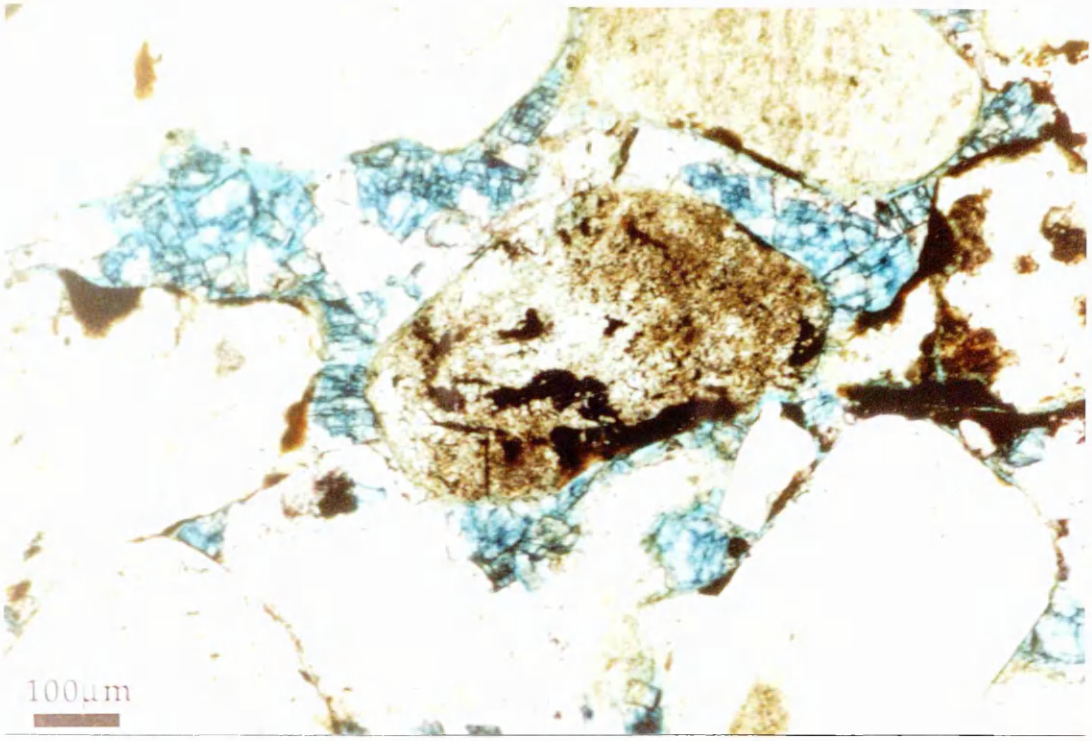

Figure 2.13 Photomicrograph of pore lining ankerite rhombs (stained blue with potassium ferricyanide). Well 49/27-3, 6717'.

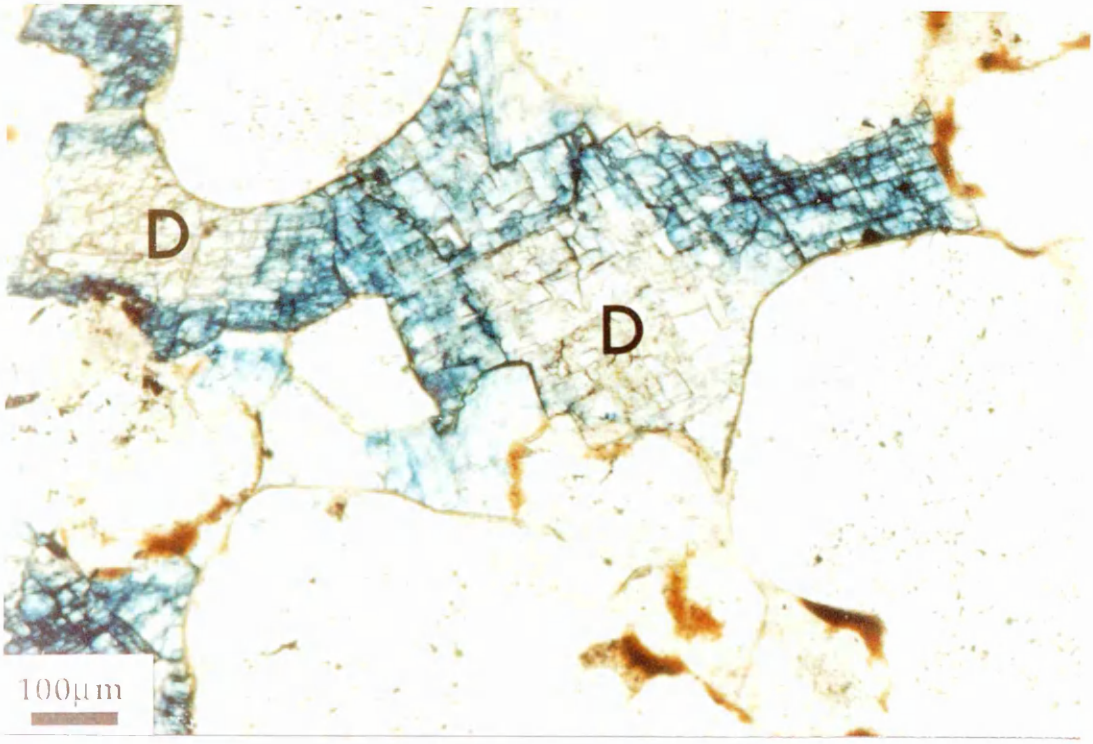

Figure 2.14 Photomicrograph of ankerite (stained blue with potassium ferricyanide) replacing earlier dolomite (unstained, labelled D). Well 49/27-3, 6717'.

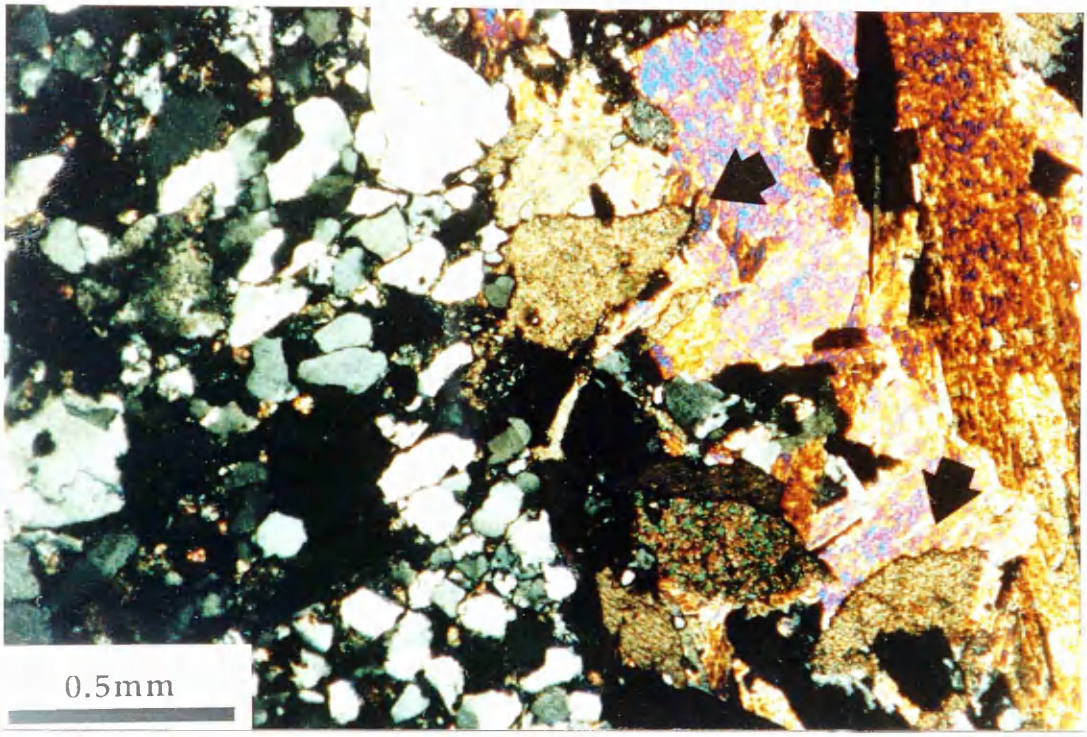

Figure 2.15 Photomicrograph of siderite (arrows) which has precipitated along the wall of mineralized fracture. Mineral filling fracture is anhydrite (blue-yellow birefringent colours). Well 49/26-5, 6565.5'.

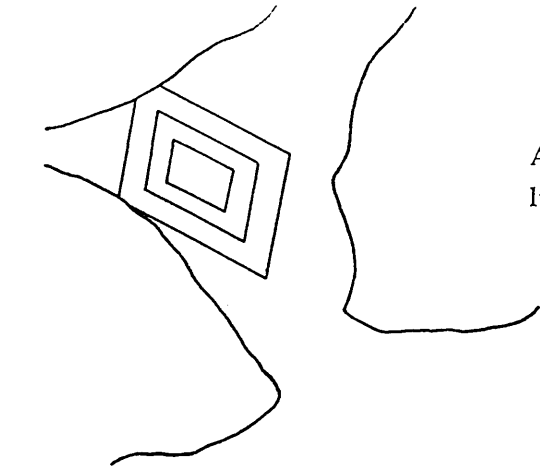

A) Precipitation of brightly luminescent Type I dolomite.

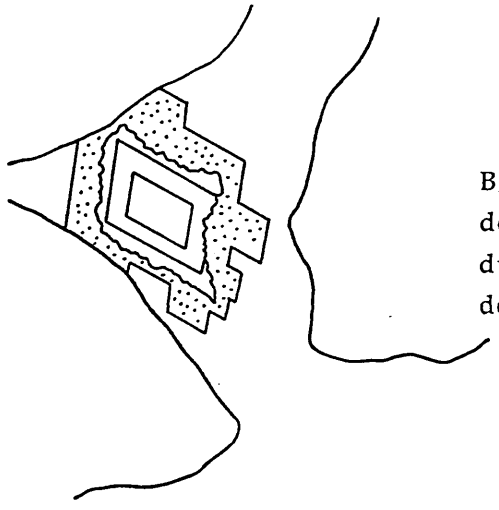

B) Replacement of Type I dolomite and precipitation of dully luminescent Type II dolomite.

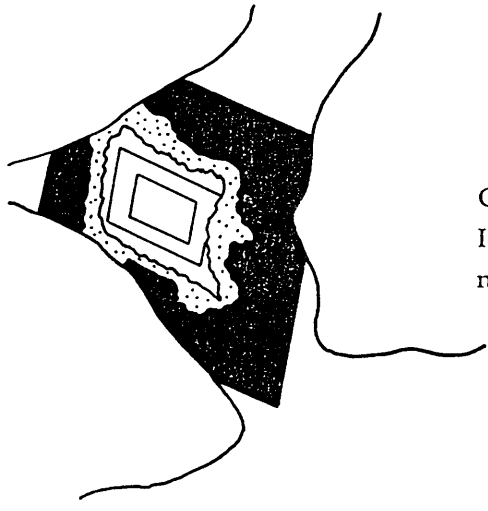

C) Replacement of Type I and II dolomite and precipitation of non-luminescent ankerite.

Type I dolomite

Type II dolomite

Ankerite

Figure 2.16 Summary of Rotliegend carbonate petrography. Type II dolomite and ankerite represent progressive corrosion and overgrowth on earlier Type I and II dolomites.

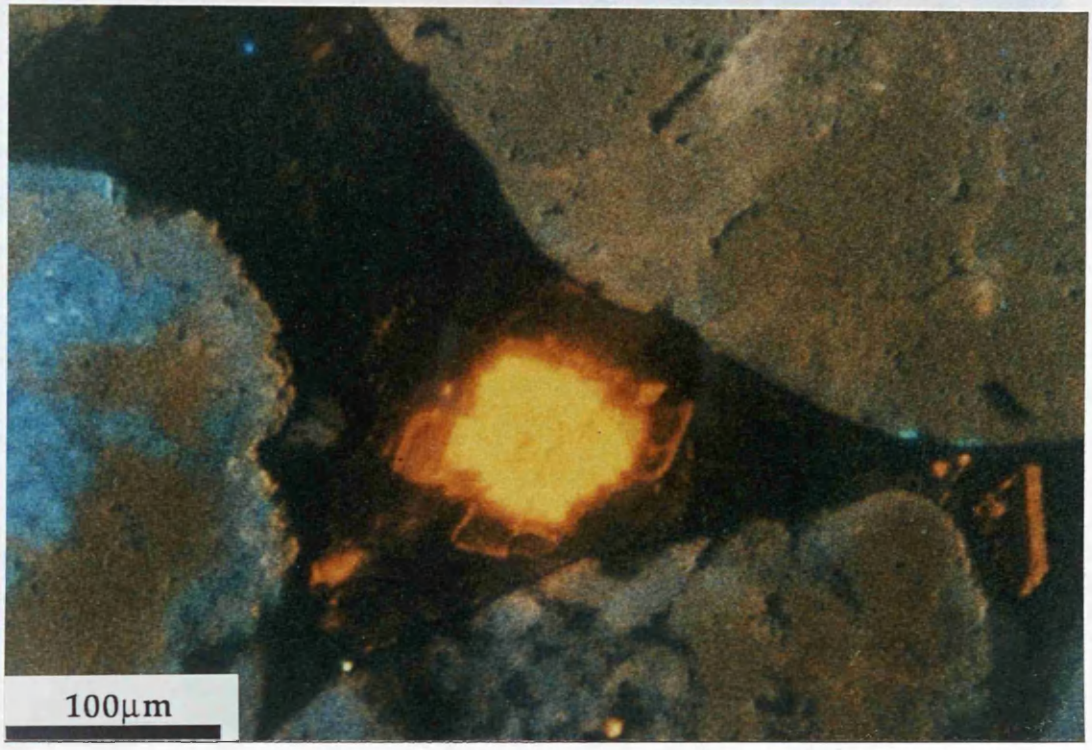

Figure 2.17 Cathodoluminescence photomicrograph of brightly luminescent rhombic Type I dolomite which has been corrroded and overgrown by Type II dolomite and ankerite. Zoning sequence: bright yellow to bright red = Type I dolomite, dull red = Type II dolomite, dead luminescence = ankerite. Well 49/27-2, 6737'. Same pore is shown using BSEM in Figure 2.22.

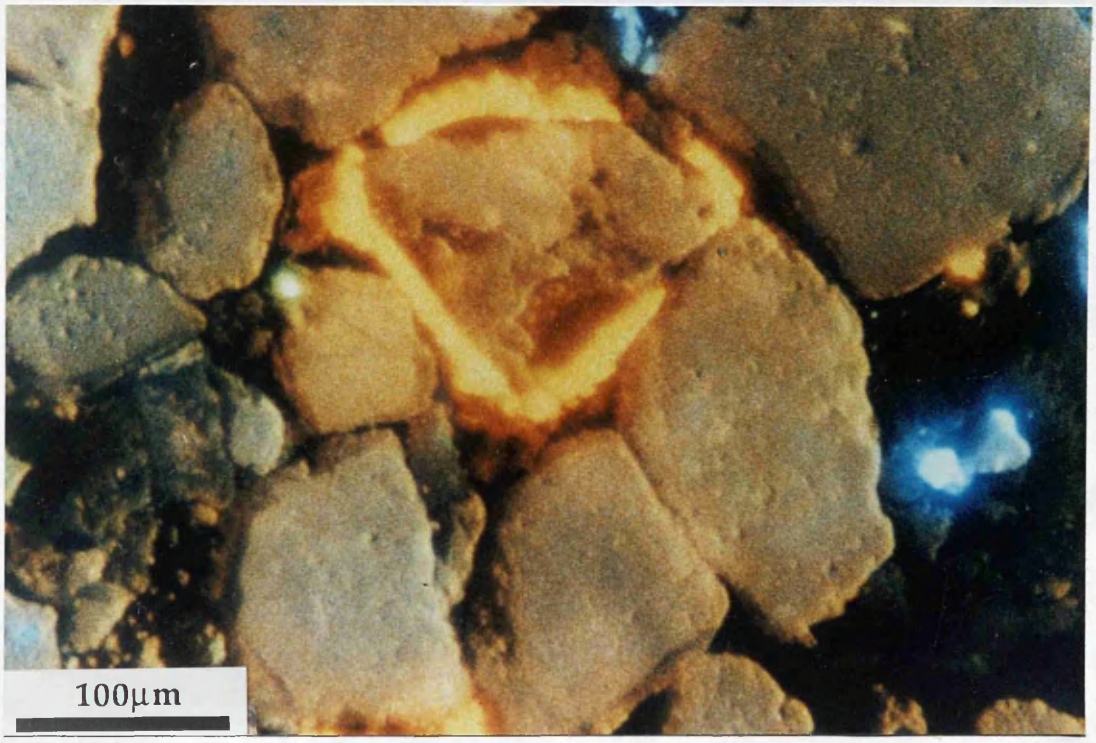

Figure 2.18 Cathodoluminescence photomicrograph of brightly luminescent microrhombic Type I dolomite. Note the small Type I dolomite rhombs have the same luminescence as large Type I dolomite rhombs. Well 49/27-2, 6317'.

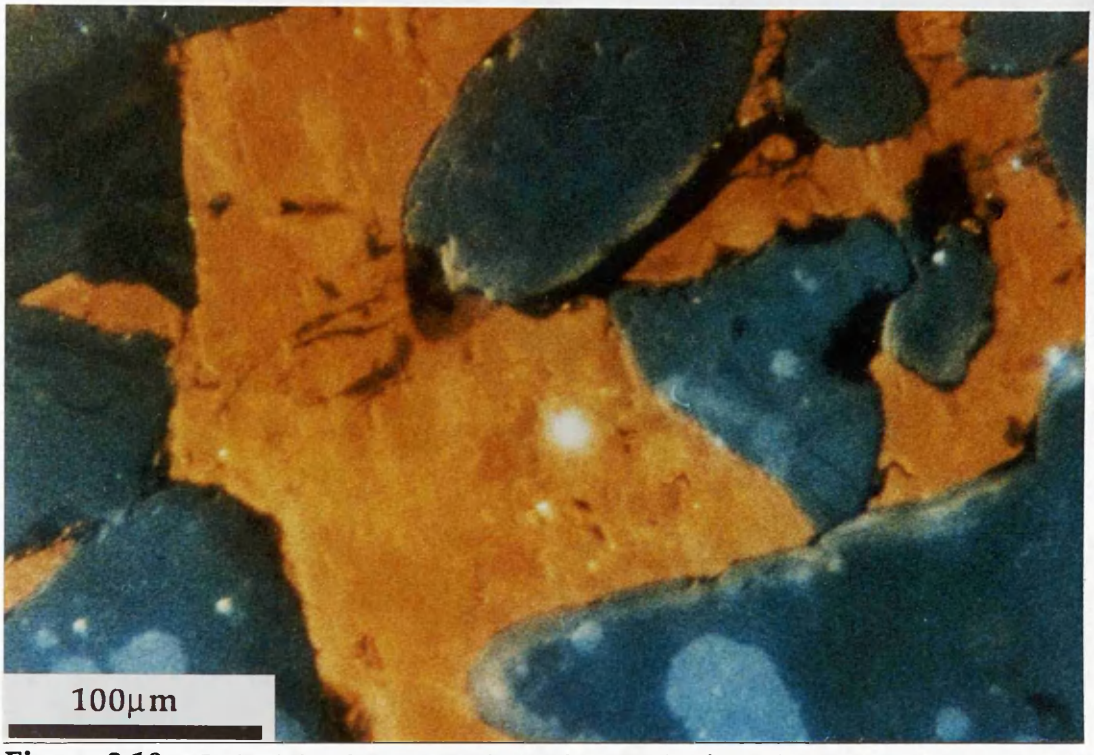

Figure 2.19 Cathodoluminescence photomicrograph of poikilotopic Type II dolomite. Note the duller luminescence of this dolomite compared to Type I dolomite. Well 49/26-5, 6854'.

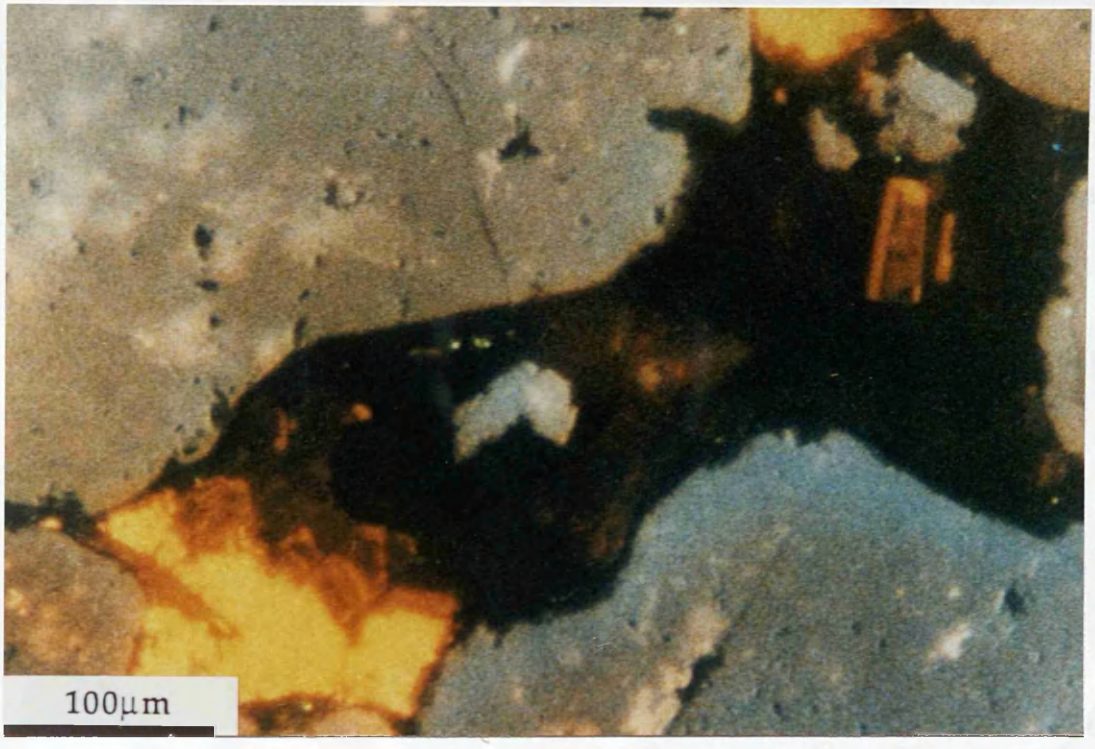

Figure 2.20 Cathodoluminescence photomicrograph of Type II dolomite in pore centre (dull luminescence) which has been corroded and overgrown by ankerite (dead luminescence). There is also Type I dolomite (brightly luminescent) in the southern and northeastern portions of the pore. Well 49/27-2, 6737'. The same pore is shown using BSEM in Figure 2.26.

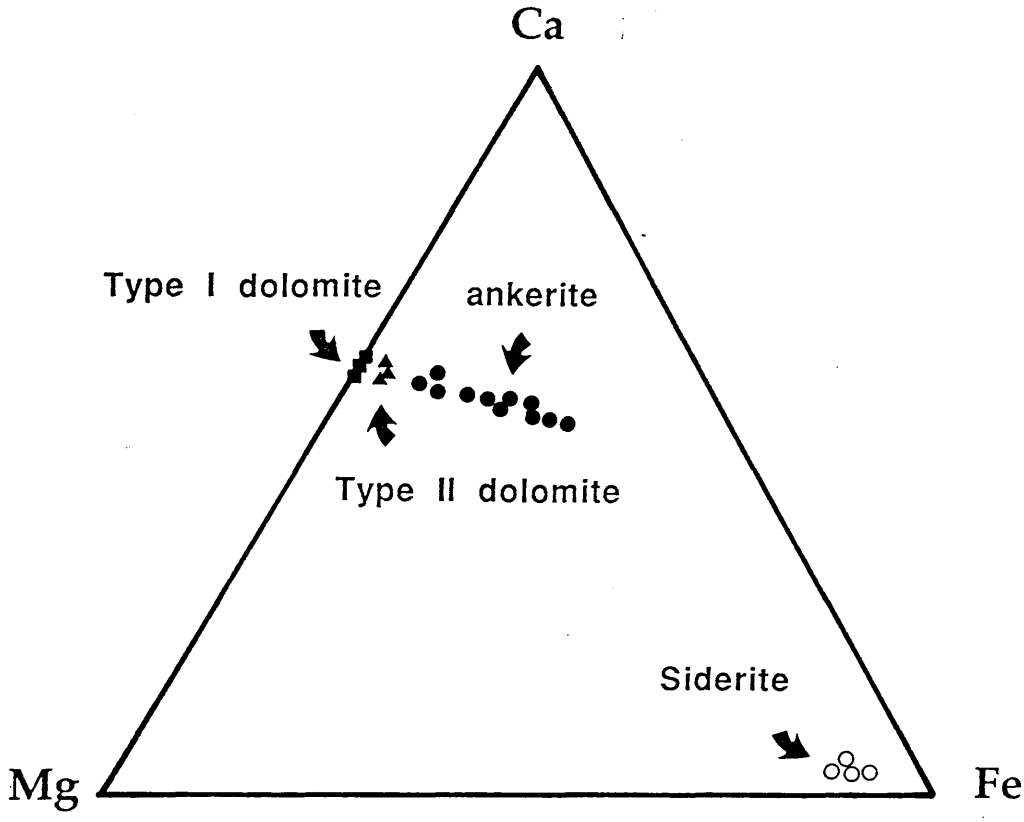

Figure 2.21 Mg: Ca: Fe ratios of carbonate cements in the Rotliegend of the Leman field. (■) Type I dolomite, (▲) Type II dolomite, (●) ankerite and (○) siderite.

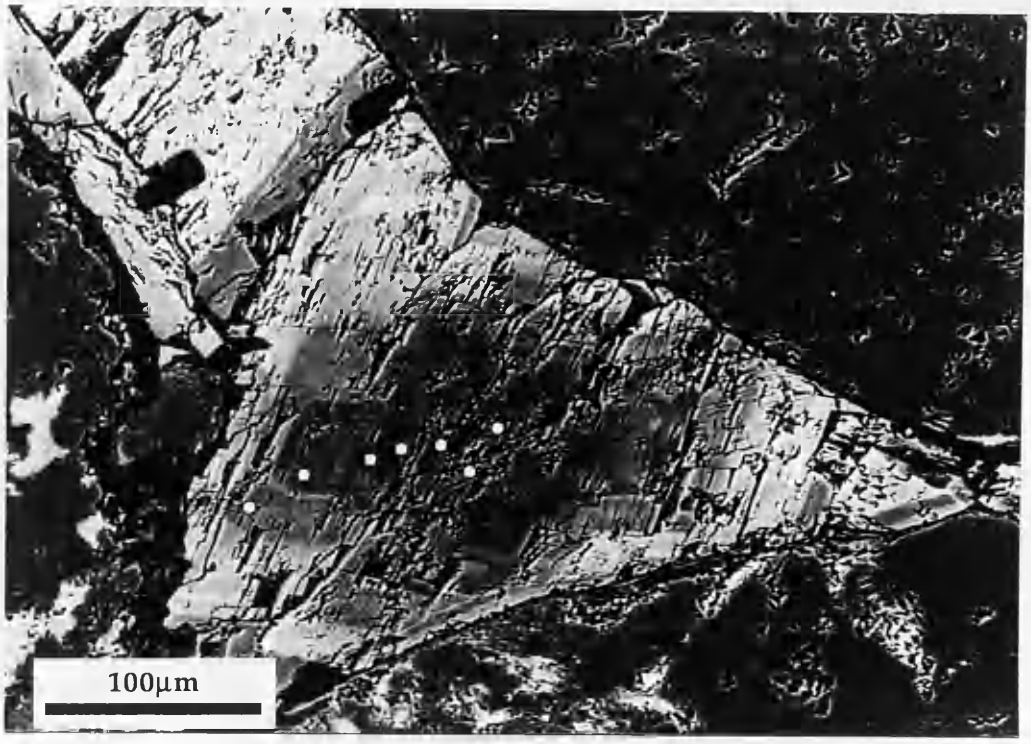

Figure 2.22 BSEM photomicrograph of Type I dolomite (dark) which has been corroded and overgrown by Type II dolomite (lighter) and zoned ankerite. Note irregular contacts between Type I and Type II dolomites. ● represent analysis points of probe traverse represented in Figure 2.23. Well 49/27-2, 6737'.

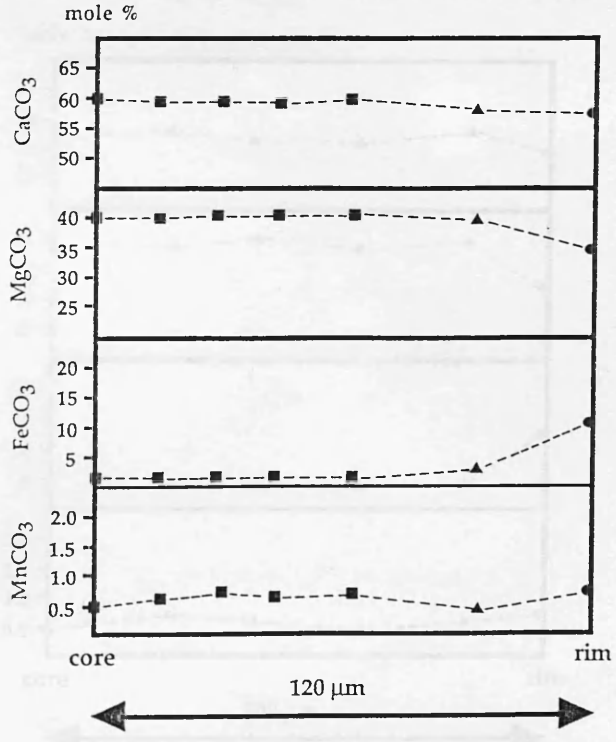

Figure 2.23 Variation in chemistry across an individual Type I dolomite rhomb which has been corroded and overgrown by Type II dolomite and ankerite (see Figure 2.22). (■) Type I dolomite, (▲) Type II dolomite, (●) ankerite. Well 49/27-2, 6737'.

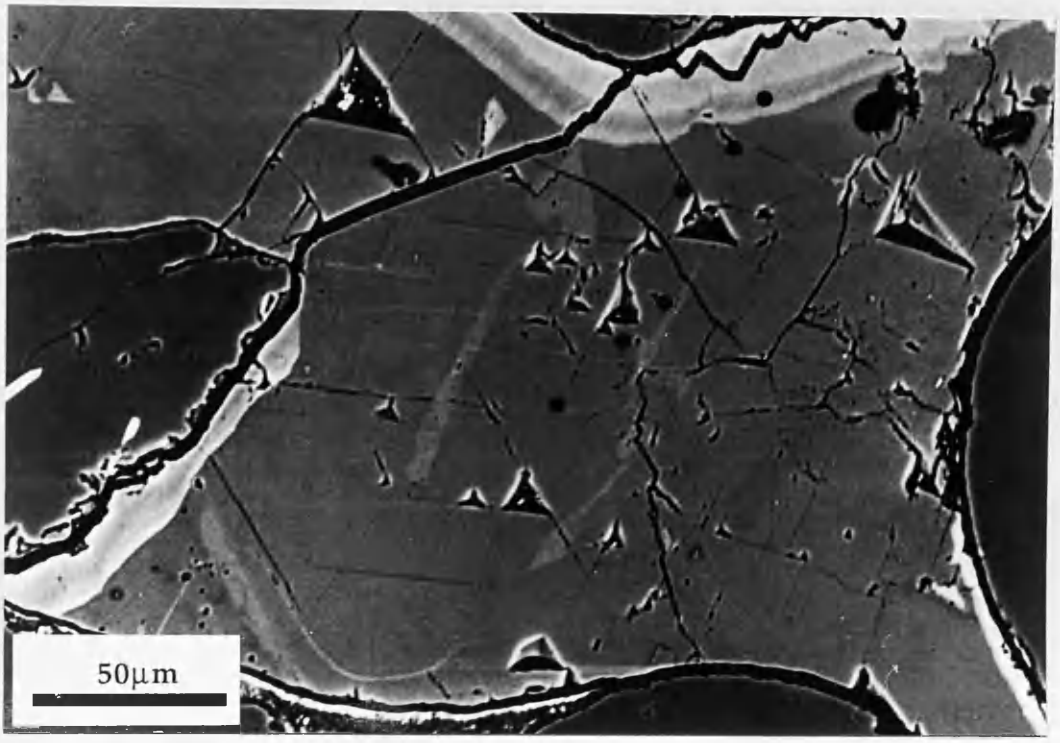

Figure 2.24 BSEM photomicrograph of pore filled with poikilotopic Type II dolomite (dark) which has been overgrown by ankerite (light) at the margins of the pore. ● represent analysis points of probe traverse represented in Figure 2.25. Well 49/26-5, 6854'.

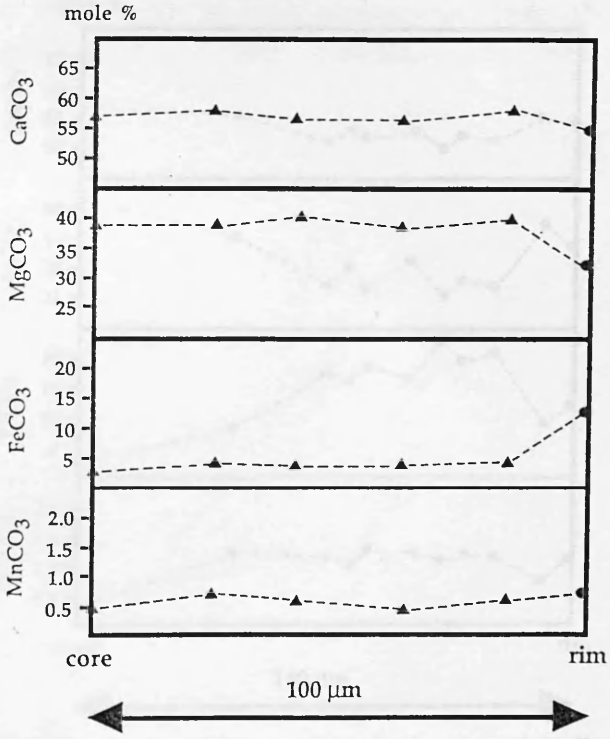

Figure 2.25 Variation in chemistry across pore filled with poikilotopic Type II dolomite which has been corroded and overgrown at the margins of the pore by ankerite (see Figure 2.24). (▲) Type II dolomite, (●) ankerite. Well 49/26-5, 6854'.

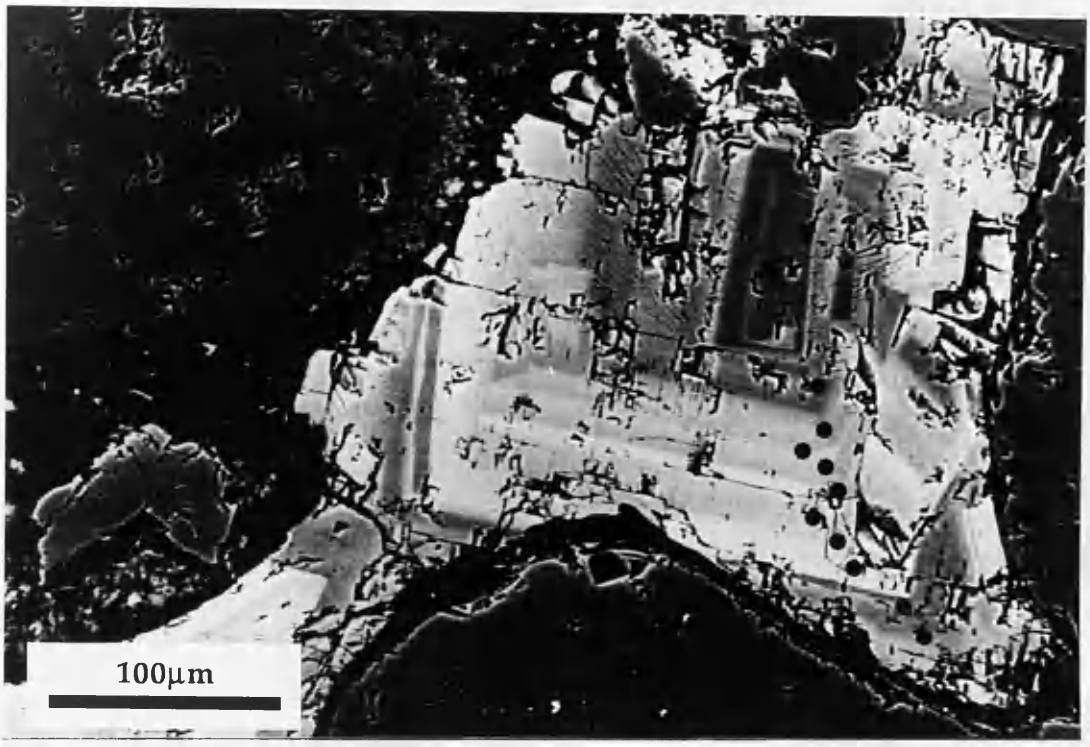

Figure 2.26 BSEM photomicrograph of concentrically zoned ankerite (light) which has overgrown Type II dolomite rhomb (dark) in the centre of the pore. ● represent analyses points shown in Figure 2.27. Well 49/27-2, 6737'.

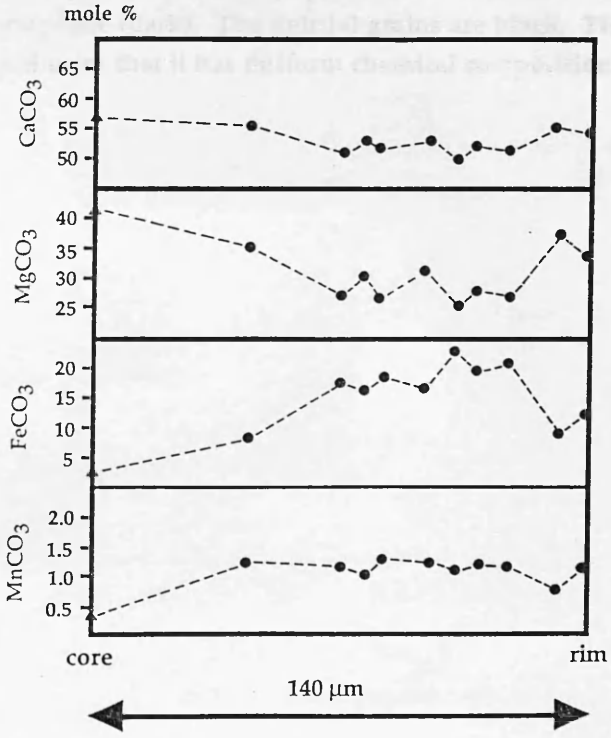

Figure 2.27 Variation in chemistry across a single concentrically zoned ankerite rhomb which has overgrown earlier Type II dolomite (see Figure 2.26). (▲) Type II dolomite, (●) ankerite. Well 49/27-2, 6737'.

Figure 2.28 BSEM photomicrograph of siderite rhombs (light) in mineralized fracture filled with anhydrite (dark). The detrital grains are black. The homogeneous density of the siderite indicates that it has uniform chemical composition. Well 49/26-5, 6565.5'.

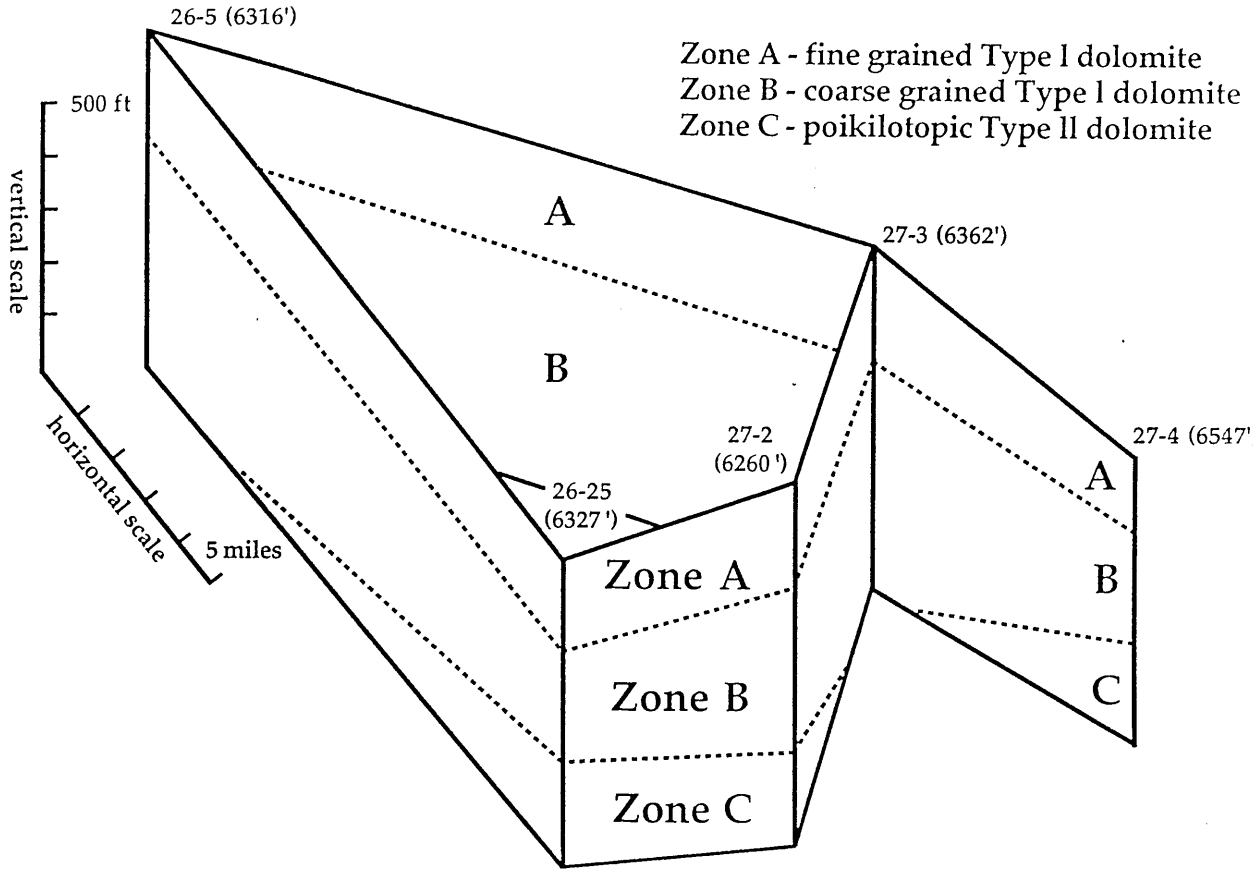

Figure 2.29 Schematic diagram showing the distribution of dolomite cements in the Rotliegend Sandstone in the Leman field.

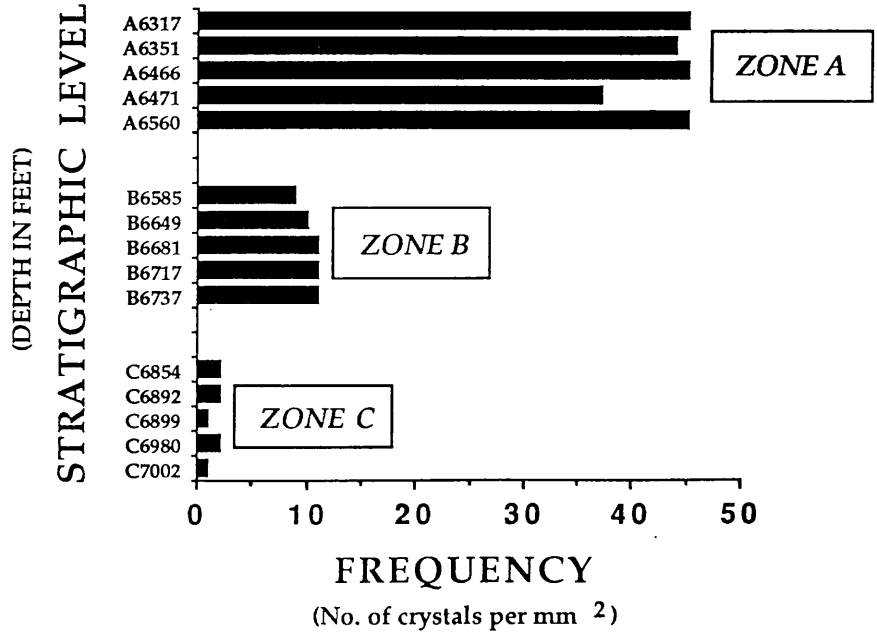

Figure 2.30 Histogram showing the number of crystals (nucleation sites) per mm^2 for the three dolomite cement zones observed in the Rotliegend Sandstone in the Leman field. See Table 2.2 for sample location and point count data for each sample.

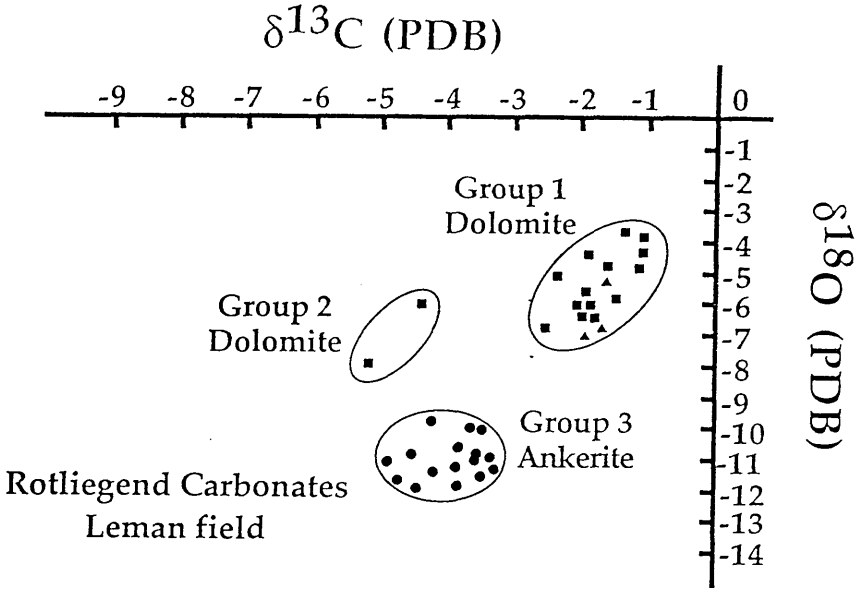

Figure 2.31 Plot of $\delta^{13}C$ against $\delta^{18}O$ for authigenic dolomite and ankerite from the Rotliegend Sandstone, Leman gas field. Isotopic Group 1 consists of dolomite from the unaltered portion of the Rotliegend, Group 2 consists of dolomite from the altered (whitened) basal portion of well 49/26-5, and Group 3 is formed by the late phase ankerite. (■) Type I dolomite, (▲) Type II dolomite, (●) ankerite.

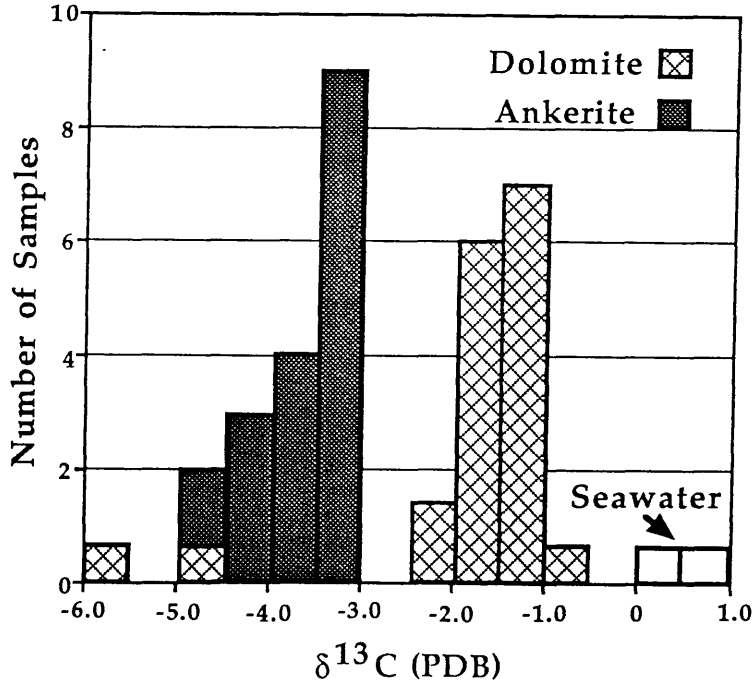

Figure 2.32 Histogram showing the distribution of $\delta^{13}C$ values of authigenic dolomite and ankerite from the Rotliegend Sandstone, Leman gas field. Note the dolomites with the isotopically light carbon values are from the whitened basal portion of well 49/26-5 (isotopic Group 2).

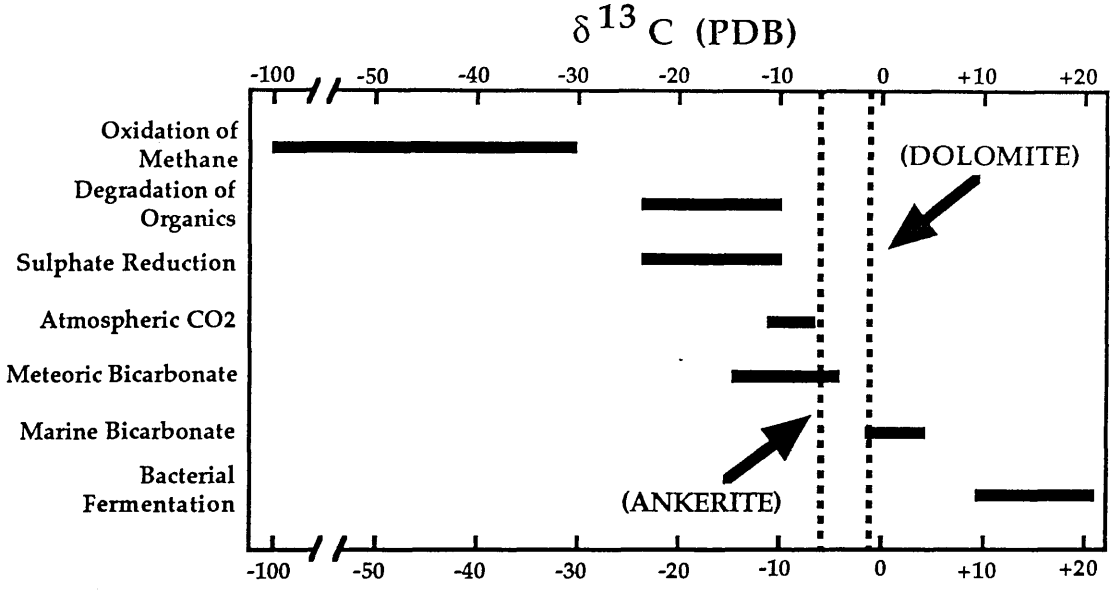

Figure 2.33 Schematic diagram showing the major sources of carbon in the sedimentary environment and their $\delta^{13}C$ values. See discussion for references.

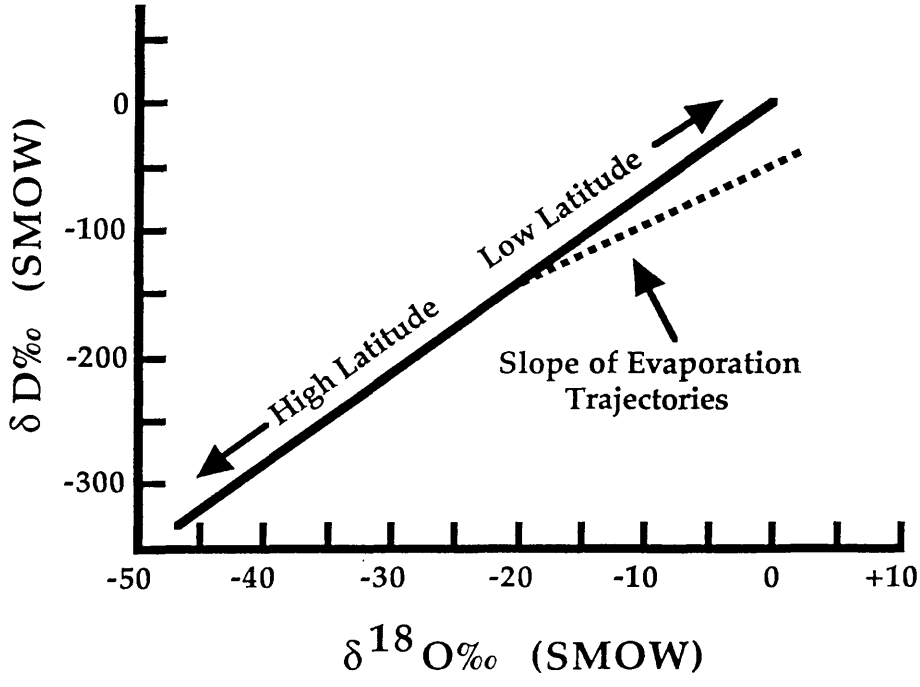

Figure 2.34 The relationship between δD, $\delta^{18}O$ and latitude for meteoric water (modified from Craig, 1961). The linear relationship is the "meteoric water line".

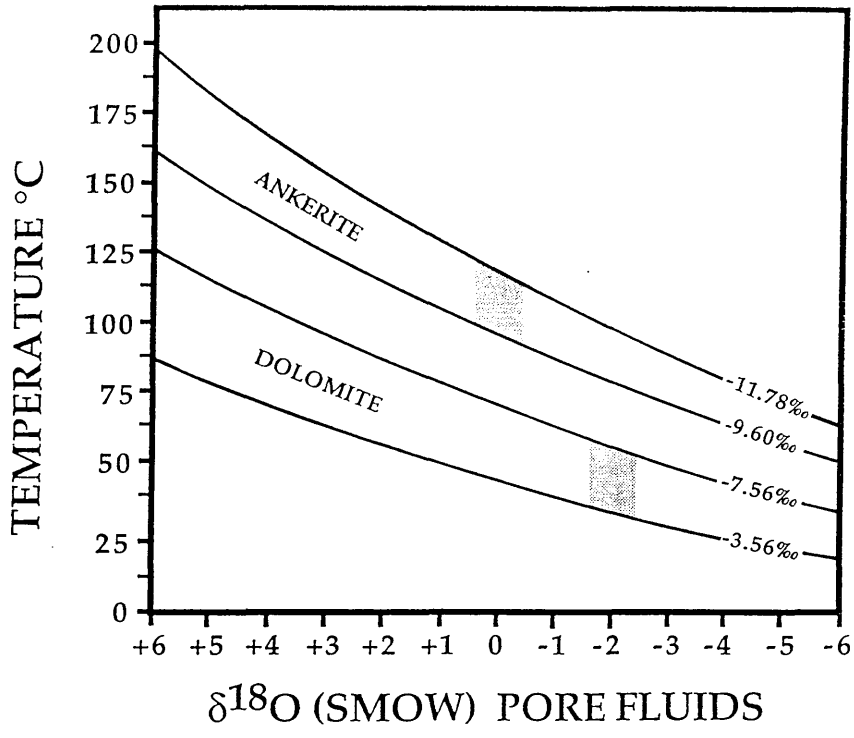

Figure 2.35 Equilibrium relationship between $\delta^{18}O$ of water, $\delta^{18}O$ of mineral and temperature. Dolomite cementation is inferred to have occurred at temperatures between 35° and 60°C from waters with a $\delta^{18}O$ of -2‰ (SMOW), and ankerite is inferred to precipitated at temperatures between 105° and 125°C from waters with a $\delta^{18}O$ of 0‰ (SMOW).

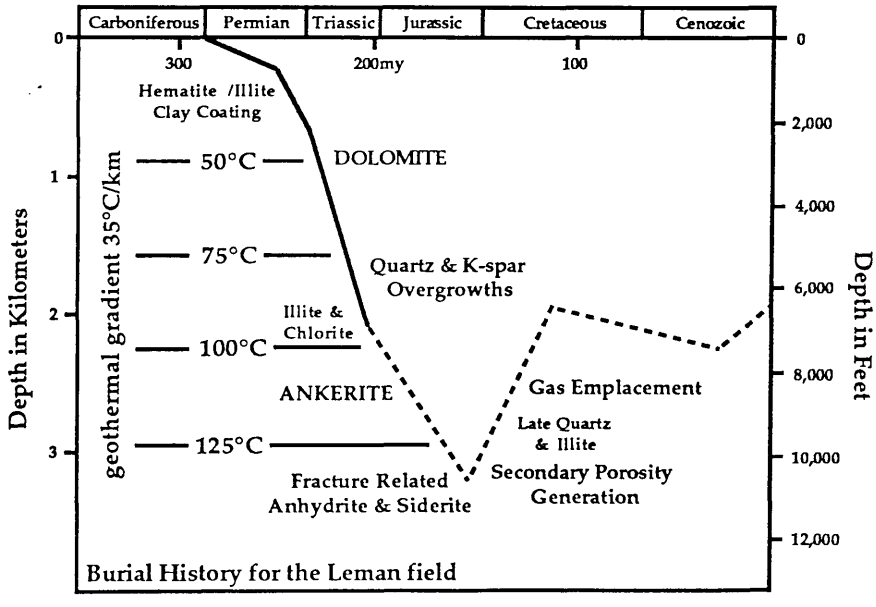

Figure 2.36 Burial curve for the Rotliegend Sandstone in the Leman field showing time and temperature of authigenic mineral precipitation and other major diagenetic events. The reconstructed burial curve is based on well logs 49/27-3 & 49/27-4, interval velocity data from Marie (1975), Glennie et al. (1978) and Bulat & Stoker (1987), and vitrinite reflectance data from Cope (1986).

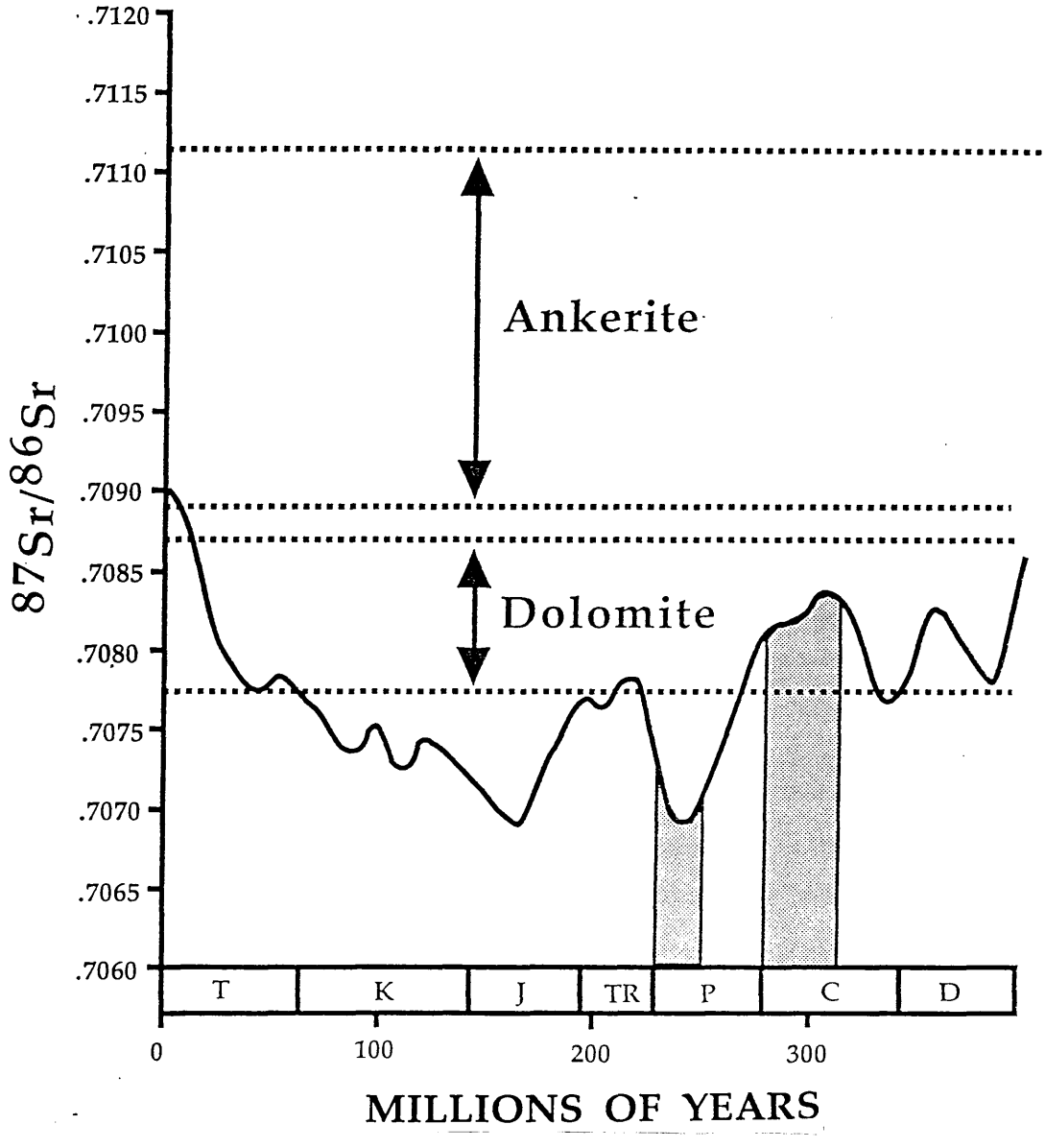

Figure 2.37 Plot of $^{87}Sr/^{86}Sr$ values of dolomite and ankerite minerals vs $^{87}Sr/^{86}Sr$ values of seawater. Isotope values for seawater are from Veizer *et al.* (1980) and Burke *et al.* (1982).

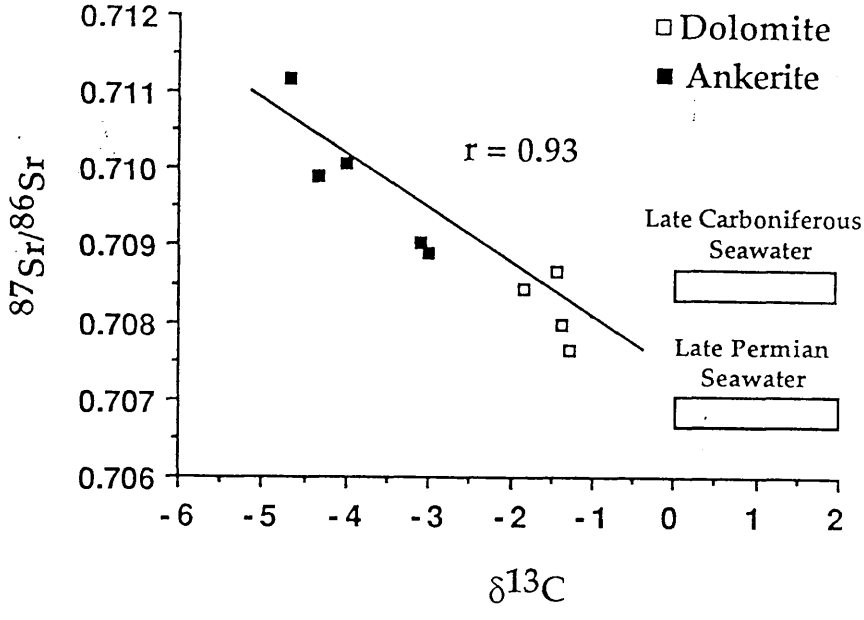

Figure 2.38 Plot of $^{87}Sr/^{86}Sr$ vs $\delta^{13}C$ (PDB) for dolomite and ankerite minerals from the Rotliegend Sandstone. Strong linear correlation illustrated by Sr and C isotope compositions of dolomite and ankerite indicate that sources of these ions were interlinked. Isotope values for Late Permian and Late Carboniferous seawaters are from Veizer *et al.* (1980) and Burke *et al.* (1982).

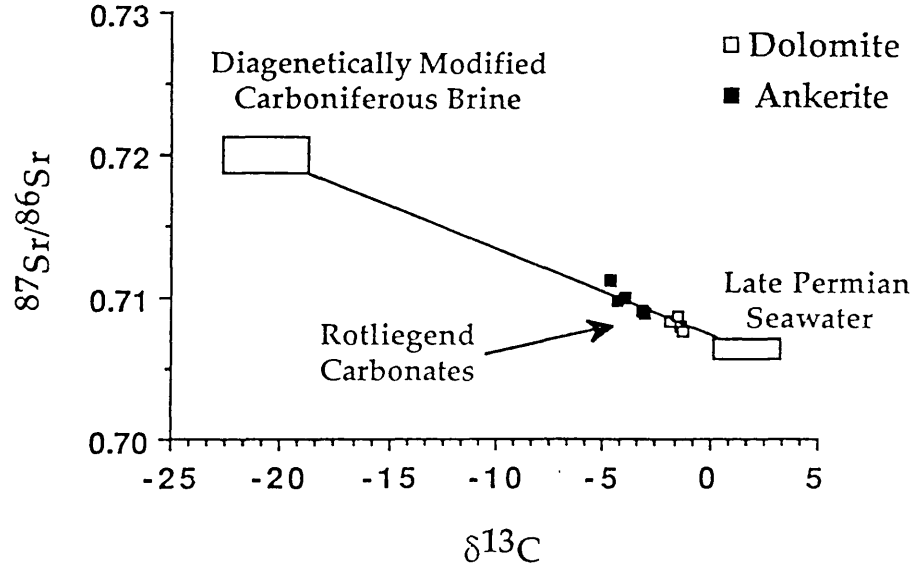

Figure 2.39 Diagram illustrating evolutionary trend through diagenesis, from Sr and C derived from Late Permian seawater during dolomite precipitation, to Sr and C isotope compositions reflecting a significant input from underlying Upper Carboniferous mudstones during ankerite precipitation.

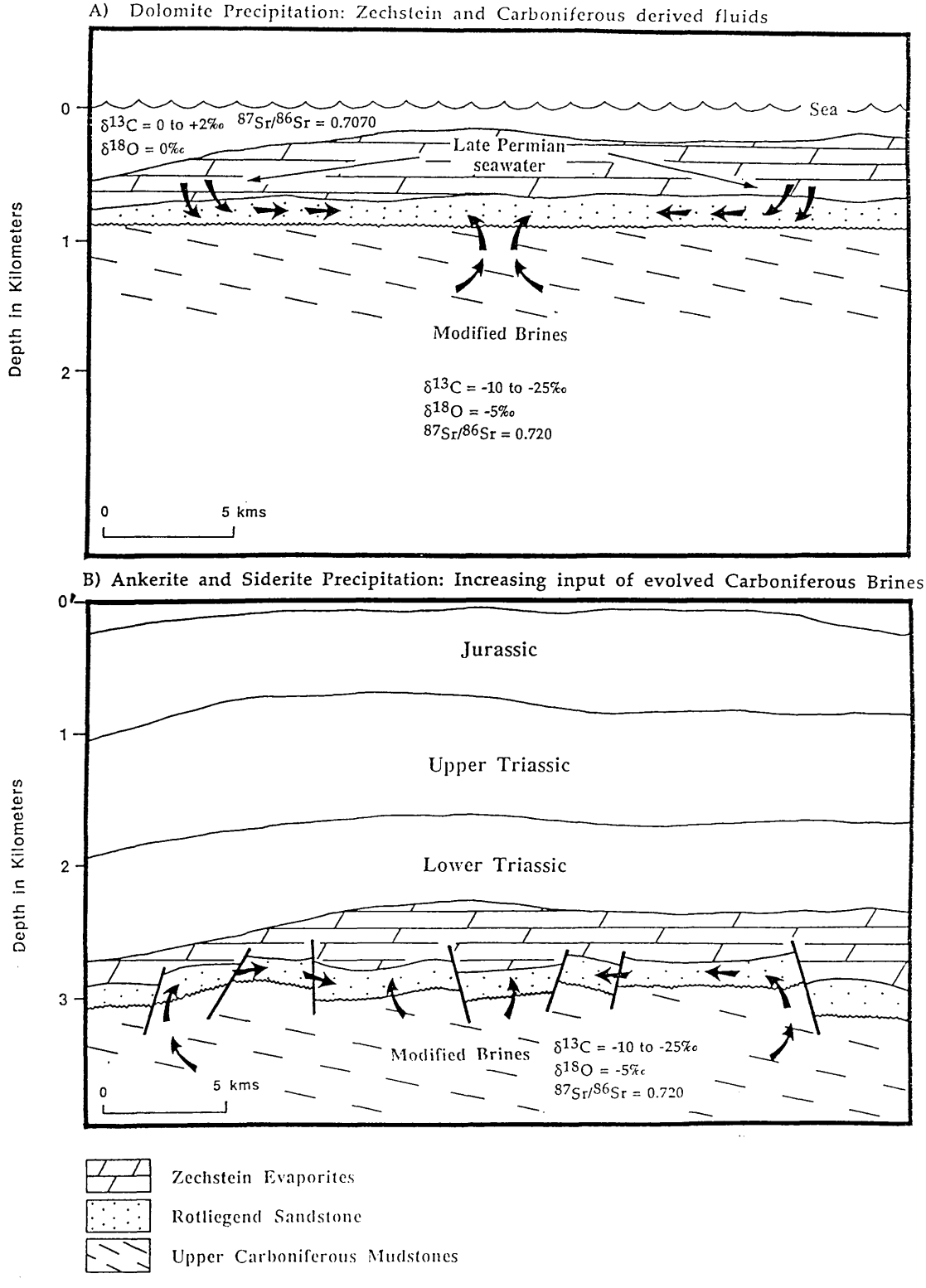

Figure 2.40 **(A)** Model for the precipitation of dolomite from waters and/or ions derived from the Upper Permian Zechstein marine evaporites which mixed with compactionally derived evolved meteoric waters from the underlying Upper Carboniferous shales. **(B)** Model for the precipitation of ankerite and siderite from evolved brines derived from the Upper Carboniferous shales. Note, siderite precipitation was limited to mineralized fractures.

CHAPTER 3

CONTROLS AND TIMING OF QUARTZ CEMENTATION IN THE ROTLIEGEND SANDSTONE, LEMAN FIELD, SOUTHERN NORTH SEA: WITH COMPARISONS TO THE PENRITH SANDSTONE, NW ENGLAND

Morgan D. Sullivan, R. Stuart Haszeldine
Department of Geology and Applied Geology, University of Glasgow, Glasgow G12 8QQ, Scotland

Anthony E. Fallick
Isotope Geology Unit, Scottish Universities Research and Reactor Centre, East Kilbride, Glasgow G75 0QU, Scotland

3.1 ABSTRACT

Authigenic quartz is a pervasive cement in the Lower Permian Rotliegend Sandstone of the Leman field, and where it is an abundant authigenic phase it significantly reduces porosity. It forms up to 30% of the total rock in many samples and two generations of early diagenetic quartz are observed. The earliest generation of quartz is represented by small prismatic outgrowths (30 to 70μm in size) which are commonly enclosed within later pore filling syntaxial overgrowths. The most extensive development of both phases of quartz is along the well sorted, medium to coarse grained beds of cross-stratified dune foresets. Oxygen isotope compositions range from +19.7‰ to +22.3‰ (SMOW) and fluid inclusion data indicate that the greatest volume of quartz precipitated during the Late Triassic between 72° and 97°C (1.5 to 2 km burial) from an evolved meteoric brine with $\delta^{18}O$ composition of -2‰ (SMOW). The lack of sufficient intergranular pressure solution between detrital grains and the late timing of feldspar dissolution (post-dating quartz cementation) precludes the authigenic silica being derived from within the Rotliegend. It is suggested that the quartz cement in the Rotliegend was derived from silica released by diagenetic reactions occurring in deeper-buried Carboniferous shales which directly underlie the Rotliegend in the basin. Textural selectivity of authigenic quartz distribution and thin section petrography indicate that the silica was imported by migrating fluids, rather than diffusion. Importation of silica by advection, however, requires very large volumes of water. Since compaction of underlying shales was not capable of supplying large amounts of water, it is thought is that the silica was imported by deep circulation of highly evolved meteoric waters, possibly in association with Triassic rifting.

Quartz cement is also prevalent in outcrop in the aeolian dune deposits of the Penrith Sandstone of NW England. Diagenetic textures displayed by authigenic quartz in the Penrith Sandstone appear identical to those observed in the Rotliegend Sandstone. The paragenetic sequence of

diagenetic events, including relative timing of quartz cementation, are also very similar for both sandstones. Oxygen isotope compositions of quartz overgrowths from the Penrith Sandstone closely resemble those of the Rotliegend, suggesting that they formed under the same temperature and fluid conditions. In addition, the lack of internal silica sources implies that the quartz cement in the Penrith Sandstone was derived from deep circulation of highly evolved meteoric waters, as suggested for the Rotliegend Sandstone.

3.2 INTRODUCTION

The Lower Permian Rotliegend and Penrith Sandstones are continental red bed sequences deposited in aeolian, fluvial and wadi environments within Early Permian rift basins of NW Europe (Figure 3.1). These formations were deposited in separate basins, the Rotliegend in the Southern Permian Basin and the Penrith in the Solway Basin. Quartz cementation of the Rotliegend Sandstone was studied in cores from the Leman gas field (blocks 49/26 & 49/27) and the Penrith Sandstone at outcrop from NW England (Penrith District) (Figure 3.2) using conventional petrography and stable isotope geochemistry. This study provided an opportunity to (1) evaluate the influence of facies, grain size and sorting on quartz cementation; (2) estimate the amount of silica derived from within the sandstones compared with the volume imported from outside; (3) correlate one dimensional observations in core with two dimensional observations in the field; and (4) compare quartz diagenesis between these two basins.

3.3 METHODS

One hundred and forty thin sections from seven wells (49/26–5, 49/26–25, 49/26–26, 49/26–B240, 49/27–2, 49/27–3, 49/27–4) in the Leman field and 15 thin sections of outcrop material were examined using a

standard polarizing microscope. All samples were impregnated with blue epoxy resin, prior to sectioning, to highlight porosity. Fifty thin sections from the Rotliegend Sandstone and ten from the Penrith Sandstone were point counted, with a minimum of 500 counts per section, in order to determine modal percentages of detrital and authigenic components (see Appendix B.1). Textural relationships and quantitative compositions were examined in detail using a CAMBRIDGE STEREOSCAN 360 scanning electron microscope (SEM) equipped with a LINK energy dispersive analysis of X-rays system (EDS). A NUCLIDE cold stage LUMINOSCOPE was used for cathodoluminescence examination of carbonate cements, and aided in the recognition of several generations of carbonate cementation. Cathodoluminescence of authigenic quartz was studied using a pulsed electron beam (10-15 keV; 1μA mm^{-2}) from a hot-cathode gun at the University of Manchester Instsitute of Scince and Technology. Precise determinations of bulk mineralogy and identification of clay minerals were accomplished using a PHILIPS X-ray difractometer (XRD). Investigations of compositional variations in carbonate cements and other authigenic and detrital minerals were performed using a backscatter electron mode (BSEM) equipped JEOL 733 SUPERPROBE.

Quartz overgrowths were prepared for oxygen isotope analyses using the method outlined by Lee and Savin (1985). This method allowed physical isolation of authigenic quartz from detrital quartz and therefore direct measurement of the $\delta^{18}O$ composition of the overgrowths. Separation of authigenic and detrital quartz was accomplished firstly by etching interfacial material between detrital core and overgrowth. Quartz overgrowths were released from detrital grains by ultrasonic agitation and sieving was then used to concentrate authigenic quartz within narrowly defined particle size ranges. Three or four size separates, depending on the size of authigenic quartz crystals, (<30μm; 30-53μm; 53-85μm; 85-100μm) were analyzed for each sample. The purity (% quartz overgrowths vs % detrital quartz) was determined by detailed point counting of samples using a hot-stage cathodoluminescence microscope. The overgrowths in

the 30 to 53μm size-fractions generally were the purest separates (see Appendix D.3). To determine the $\delta^{18}O$ of the quartz overgrowths, the $\delta^{18}O$ of detrital quartz from the Rotliegend Sandstone was also measured in order to correct for detrital comtamination of separates. Detrital quartz from the Penrith Sandstone was not measured and therefore has been assumed to have the same $\delta^{18}O$ composition as detrital quartz from the Rotliegend Sandstone.

Oxygen extractions were performed using the method of Clayton and Mayeda (1963) modified for oxidation with ClF_3 (Borthwick and Harmon, 1982). Approximately 10 mg of relatively pure authigenic quartz was loaded into the Ni reaction vessels and outgassed at high vacuum at 250°C for 1 hour. The oxygen liberated by fluorination was subsequently converted to CO_2.

The CO_2 gas was analysed on a VG SIRA 10 mass spectrometer with a working standard independently calibrated against international reference standard materials of silicate, carbonate, grahphite and oil. $\delta^{18}O$ compositions of the quartz are quoted relative to SMOW (Standard Mean Ocean Water). Replicate analysis of inter-laboratory standard NBS # 28 produced an average $\delta^{18}O$ value of +9.6‰ (SMOW) with a precision of 0.13‰ (1σ).

3.4 ROTLIEGEND SANDSTONE

3.4.1 Geologic setting

The Rotliegend Sandstone is a sequence of Lower Permian continental clastic red beds that were deposited under semi-arid conditions in a rapidly subsiding intra-cratonic basin (Glennie, 1989). The study area is the Leman field (Figure 3.3), where gas production comes from the 225 m thick Rotliegend Sandstone. It is located in UK blocks 49/26 and 49/27, on the southern portion of the Sole Pit High, which is a major gas producing structure in the southern North Sea Basin (Figure 3.4).

Depositional environments included aeolian dune fields, sabkha flats, playa lakes, and wadi (fluvial) settings typical of a tropical desert region with internal drainage (Glennie, 1972). Within the Leman field, the Rotliegend has been further subdivided into lower, middle and upper units (Figure 3.5) on the basis of variations in the facies and environment of deposition (van Veen, 1975).

The lower unit consists of wadi (fluvial) and minor interbedded marginal dune deposits that were deposited unconformably on the Upper Carboniferous Coal Measures during rapid basin subsidence in Early Permian times. This basal unit varies in thickness between 15 to 61 m (50 to 200 ft), is commonly conglomeratic and very poorly sorted. The wadi deposits are generally poorly bedded and micaceous, often containing adhesion ripples, clay pebbles and interbeds of shale. Dune sediments, in this unit are weakly developed and the overall reservoir qualities are poor (Van Veen, 1975).

The middle unit represents a change from a marginal playa lake environment dominated by fluvial wadi deposits to one consisting entirely of aeolian dune deposits. It varies in thickness from 140 to 175 m (450 to 650 ft) and makes up the bulk of the Rotliegend Sandstone in the Leman field. These dune sequences are consistently well sorted and well rounded, fine to medium grained sandstones. Sedimentary structures are dominated primarily by steeply dipping planar dune foresets and less commonly, horizontally laminated bottom sets. Porosities of the middle unit vary from 6% to over 23% with an average value of approximately 15%. Alternating fine and coarse grained sandstone laminations are common within the steeply deeply dipping foresets and represent avalanche slope deposits formed by dune migration. Alternating coarse and fine grained laminations of the topsets have higher porosities than bottomsets due to the bimodal grain size and more abundant clay content of the bottomsets. Grains of both foresets and bottomsets are rounded to subrounded and compositionally mature, reflecting long periods of transport and reworking prior to final deposition.

The upper unit consists of aeolian sands that were reworked by

the Late Permian Zechstein marine transgression. This unit is variable in thickness, between 6 and 30 m (20 to 100 ft), and Van Veen (1975) suggests that this variation was caused by erosional relief at the top rather than at the base of the unit. The contact between the aeolian and reworked sediments is a planar erosional surface. Massive sands that display medium scale cross-laminations and slump structures occur above the contact and pass directly into the undeformed planar cross bedded sediments of aeolian origin.

3.4.2 Burial history

Following deposition, the Rotliegend Sandstone underwent continual burial until the Late Jurassic/Early Cretaceous, when the first of two episodes of uplift and erosion occurred on the Sole Pit High (Figure 3.6). As much as 1500 m (5000 ft) of overburden was removed during inversion in the Late Jurassic/Early Cretaceous (Marie, 1975; Glennie & Boegner, 1981; Cope, 1986; Bulat & Stoker, 1987). The amount of erosion is estimated both from the maturity of Upper Carboniferous coals (Cope, 1986) and from interval shale velocities from the Triassic Bunter Shale (Bulat & Stoker, 1987). The Rotliegend Sandstone in the Leman field was at its maximum burial of 3.5 km prior to this inversion. Some question exists concerning the timing of this uplift event. Examination of the stratigraphy of released well logs (49/27-3 & 49/27-4) indicates that sediments overlying the unconformity are of Early Cretaceous age (see Figure 3.4), suggesting that uplift occurred during the Late Jurassic to Early Cretaceous. Following renewed burial until the mid-Tertiary, a second period of uplift caused approximately 300 m (1000 ft) of erosion in the Leman region (Bulat & Stoker, 1987). The amount of uplift for this second period of erosion was estimated from interval shale velocities from Upper Cretaceous sediments deposited after the first phase of inversion. Present burial depth of the Rotliegend is about 2000 m (6700 ft) in the Leman field.

3.4.3 Detrital mineralogy

The Rotliegend sands are dominantly subarkoses of moderate maturity (Table 3.1; Appendix B.1). Quartz is the most abundant component of these rocks, forming over 90% of the detrital mineralogy in the samples examined. Both monocrystalline and polycrystalline quartz grains are present, with monocrystalline being the dominant type and comprising approximately 80% of the quartz. The strong undulose extinction and crenulated borders of crystallites contained within the polycrystalline quartz suggests that much of this quartz was derived initially from a metamorphic source. Feldspar is only a minor component of these sandstones and comprises 7 to 12% of the total composition of the samples. Untwinned orthoclase is the dominant type of feldspar in the Leman field. Microcline and plagioclase are also present, but in smaller amounts. Plagioclase and alkali feldspars both show signs of dissolution, with the plagioclase being the most extensively altered and dissolved. Rock fragments constitute approximately 7% of the total mineralogy, of which metamorphic rock fragments are the dominant type. These are mainly fragments of quartzite and schist and they are usually elongate grains with undulose extinction. Chert, consisting of microcrystalline aggregates, is present in most samples, and volcanic fragments have also been observed. Heavy minerals occur in trace amounts and include zircon, sphene, rutile and rare tourmaline.

3.4.4 Texture

The samples studied from the Rotliegend Sandstone are chiefly aeolian dune (high-angle cross-bedded) and interdune (flat-bedded) deposits. Thinly laminated dune cross-beds are grain-fall and wind ripple deposits, whereas centimetre thick cross-beds are probably avalanche deposits (Hunter, 1977). In general, the dune deposits and interdune deposits are extremely well sorted. Framework grains range from very

fine to coarse grained, with the dominant grain size being 200 to 300 μm. These sandstones are commonly bimodal with coarse to medium grained laminae alternating with finer grained laminae. Sorting and grain size distribution within individual laminae is, however, very uniform. Detrital grains display a high degree of rounding and sphericity. Coarser grains are commonly better rounded than fine grained material in these samples. The extreme rounding of grains reflects long periods of transport and reworking, typical of aeolian dune deposits.

The Rotliegend Sandstone has undergone considerable compaction. This is indicated by the occurrence of sutured grain contacts, although concavo-convex and long contacts are the most common types. Unstable grains, such as feldspar, which in some cases were partially dissolved prior to deep burial, have been crushed and broken due to mechanical compaction. The majority of the feldspar dissolution, however, occurred petrographically late, as no authigenic minerals fill secondary pores created by feldspar dissolution. Compaction has also significantly reduced the porosity in these sandstones. Minus cement porosities range from 15% (reworked dune deposits) to 30% (dune deposits), representing a reduction in porosity of approximately 15% from their original pre-compaction values of 40-45% porosity (Beard & Weyl 1973). The finer grained laminae are more compacted than the medium to coarse grained laminae, suggesting that preferential cementation of the latter, due to their higher permeability and porosity, may have helped prevent their compaction.

3.4.5 Diagenesis

The generalized sequence of diagenetic events in the Rotliegend Sandstone was compaction of framework grains, dissolution of unstable detrital components, precipitation of authigenic cements and formation of secondary porosity (Figure 3.7). The sequence of diagenetic events was determined using cement stratigraphy deduced from polarizing microscope, cathodoluminescence, SEM and microprobe studies. The

major diagenetic minerals present in the Rotliegend Sandstone in the Leman field are; (1) hematite and mixed layered illite/smectite, (2) dolomite (3) feldspar, (4) quartz, (5) chlorite, (6) illite, (7) ankerite, and (8) anhydrite. The general paragenetic sequence, observed in the Leman field, is the same for all seven wells examined.

3.4.5.1 *Early cements*

The first diagenetic minerals to form in the Rotliegend Sandstone were thin rims of tangentially orientated illite/iron oxide which coated detrital grains. The iron oxide rims give the Rotliegend its red colour, and reddening probably occurred very soon after deposition by intrastratal alteration of iron silicates by meteoric groundwater (Walker, 1976). Precipitation of early dolomite is interpreted to have been initiated by the influx of marine waters associated with the Zechstein transgression and the diffusion of ions from the Zechstein evaporites during shallow burial, although there also appears to be a Carboniferous component to the fluids at this time (Sullivan *et al.*, 1990). Dolomite is the first pore-filling cement and compactional textures within cemented zones also suggest it formed prior to significant burial and compaction. Three distinct morphologies of dolomite are observed in the Leman field; (1) micro-rhombic, (2) rhombic dolomite, and (3) coarse crystalline dolomite. Early authigenic K-feldspar is also present, as syntaxial overgrowths on detrital feldspar.

3.4.5.2 *Authigenic quartz*

Authigenic quartz is a pervasive cement in the Rotliegend Sandstone and, where it is an abundant authigenic phase, it significantly reduces porosity. The presence of well developed hematite-clay rims on detrital grains, which predate quartz cementation, made it possible to recognize secondary silica using the polarizing microscope, and in some

samples silica cement forms up to 30% of the total rock. Two generations of early diagenetic quartz are observed in the Leman field; (1) early individual prismatic crystals (Figure 3.8), and (2) early pore filling syntaxial overgrowths (Figure 3.9).

The earliest generation of quartz is represented by individual prismatic crystals which formed as "outgrowths" (McBride et al. 1987) on detrital quartz grains (Figure 3.8). These crystals range in size from 10 to 60 μm and are very euhedral. The precipitation of quartz "outgrowths" instead of overgrowths may have been due to grain coating clay cement which separates the authigenic quartz from the detrital cores. In several sandstones, clay coatings on detrital quartz grains are interpreted to have inhibited quartz cementation (Heald & Larese, 1974; McBride *et al.*, 1987). These studies suggest that outgrowths form at thin spots on the coatings, where nucleation is possible. Only a thin grain coating of hematite-clay separates the secondary quartz from the detrital cores, indicating that the quartz was an early diagenetic phase. Additional evidence for early formation include well developed rhombohedral crystal faces of outgrowths, suggesting that pores were relatively open during this phase of quartz precipitation.

Prismatic quartz was rapidly followed by the formation of syntaxial quartz overgrowths (Figure 3.9). Overgrowths commonly occlude pores, engulfing earlier prismatic quartz crystals (Figure 3.10). Intergrowth of pore-filling quartz and early authigenic feldspar indicate that this phase of quartz was also a relatively early diagenetic phase. Additional evidence for its early formation are loose grain packing and lack of pressure solution within well cemented zones, suggesting that it precipitated prior to significant compaction.

Multiple phases of early silica cement, in addition to the two generations recognized under the polarizing microscope, were observed using hot-stage cathodoluminescence studies (Figure 3.11). The blue luminescence of the authigenic quartz is much duller than that of the detrital grains that are thought to have been sourced from igneous rocks

formed at high temperatures. Overgrowths have a complex, polyphase internal structure, with most samples displaying between five and six zones. These vary from white-blue to medium blue to dark blue in colour and no recurrent zones are observed. These zones could have been produced either by variations in crystal growth rate or fluid chemistry or by discrete phases of cementation. Some zonations appear to have been produced by separate cementation events, but the complexity of zoning does not allow correlation between different samples. Other zones, however, probably reflect variations in pore fluid chemistry (Land *et al.* 1987; McBride, 1989) as luminescent zones in quartz are commonly are attributed to variations in Al and trace element concentrations (Sprunt, 1981; Matter & Ramseyer, 1985).

All phases of early quartz cement are best developed along coarser grained, aeolian cross-stratified laminae (Figure 3.12), suggesting a strong lithofacies control on their distribution (Table 3.1). The volume of quartz cement in this lithofacies is up to 30%, and in many samples quartz cement has completely occluded all available porosity. The centimetre thick cross-stratified deposits have dips ranging from 24° to 28° and represent sandflow avalanche deposits from the dune slip face (Hunter 1977). Sandflow cross-stratified sediments are extremely well sorted, medium grained sands. Separating individual sandflow cross-strata are millimetre to decimetre thick grainfall deposits. The associated grainfall deposits are generally much finer grained and have not been cemented by authigenic quartz. This indicates that the coarser grained beds of the dune slip face, which had higher depositional permeabilities, sequestered more dissolved silica from migrating porewaters than finer grained beds (McBride *et al.* 1987). Even medium to coarse grained bimodal bottom sets (2 to 5%) and coarse grained fluvial beds (5 to 7%) contain much less quartz cement than the cross-stratified slip face sandstones (Table 3.1), although this may have been due in part to earlier cementation by dolomite in these beds.

Case studies in the literature, however, suggest that twice as

many sandstones display textural selectivity of quartz cement for the finer grained beds as opposed to selectivity for the coarser grained beds (see McBride, 1989 Table V). Many workers attribute the selectivity of quartz cement to the finer grained beds to their greater abundance of nucleation sites (Heald & Renton, 1966; Füchtbauer, 1967; Stephan, 1970). In the Rotliegend though, the higher detrital clay content and more extensive development of hematite coatings on detrital grains in the finer grained beds may have inhibited quartz nucleation. By contrast, other studies have suggested that fluid flux is the most important factor controlling the distribution of quartz cement in sandstones (McBride, 1984; Mack 1984; Land, 1984; Haszeldine *et al.*, 1984; McBride *et al.*, 1987). The coarser grained beds in the Rotliegend Sandstone had the highest depositional permeabilities, and therefore would have permitted the largest fluid flux. These beds could therefore sequester more dissolved silica from migrating porewaters than finer grained beds and this is the most likely reason for the observed selectivity of quartz and feldspar cements in the Rotliegend Sandstone in the Leman field.

3.4.5.3 *Authigenic clays*

The main phase of illite precipitation was during late burial diagenesis. The cement consists of wispy illite flakes, formed by the merging and intergrowth of fibrous clay during continued precipitation. Plates of illite are oriented perpendicular to grain margins and have delicate, extremely fine grained wispy terminations. XRD analysis of illite indicates that it is nearly pure with only a very small amount of mixed layered smectite. Chlorite is only a minor authigenic cement, but it is observed in nearly all samples from the Rotliegend of the Leman field. It occurs as thin rims of pore-lining and pore-bridging plates which grew radially into pores from detrital grains. This type of texture can significantly reduce permeability, and has inhibited the precipitation of later authigenic minerals within these pores. The chlorite precipitated during deep burial, where it formed contemporaneously with the main

phase of illite growth.

3.4.5.4 *Late cements*

Ankerite, siderite and anhydrite were the last volumetrically important cements to precipitate. Ankerite formed as a partial replacement of earlier rhombic and poikilotopic dolomites, illustrating the late timing of ankerite precipitation. Ankerite is commonly in optical continuity with the partially dissolved dolomite onto which it has nucleated, and this texture suggests replacement, and subsequent overgrowth. Precipitation of late phase ankerite occurred from porewaters with a strong Carboniferous component (Sullivan *et al.*, 1990). Late siderite is volumetrically unimportant in the Leman field and only occurs in mineralized fractures associated with anhydrite. Anhydrite occurs as both intergranular poikilotopic and fracture-filling cements. Petrographic and isotopic evidence from samples of intergranular and fracture-filling anhydrite suggest they formed contemporaneously from Zechstein derived fluids (Sullivan *et al.* 1987). The lack of illite and chlorite cement coatings on ankerite and anhydrite crystals suggests that clay precipitation pre-dated their formation. Lastly, development of minor amounts of quartz and illite occurred associated with secondary porosity generation.

3.4.6 Oxygen isotope analysis

$\delta^{18}O$ compositions were measured for 10 samples of authigenic quartz from the Rotliegend Sandstone and vary from +19.7‰ to +22.3‰ (SMOW) (Table 3.3, Appendix D.3). This narrow range in oxygen isotope compositions of the quartz suggests that cementation was a relatively discrete event, but these values could have been produced by many possible combinations of temperature and water composition (Figure 3.13). These conditions, however, can be constrained by combining quartz oxygen isotope data with measured isotopic values of dolomite (pre-

quartz) and ankerite (post-quartz), and measured salinities/ homogenization temperatures for fluid inclusions in the quartz overgrowths.

Oxygen isotope data from early and late carbonates and fluid inclusion measurements in quartz overgrowths were used to restrict the temperature of quartz precipitation. Dolomite oxygen isotope compositions (+23.1+ to 27.2‰ SMOW) reflect precipitation temperatures of 35° to 60° C at depths of 400 m to 1.2 km and values of the later ankerite (+18.7‰ to +21‰ SMOW) suggest formation over a temperature interval of 105° to 125°C at a burial of 2 to 3 km (see section 2.8.1 and Figure 3.13). Since dolomite cementation pre-dates quartz and ankerite precipitation post-dates quartz, quartz cementation must have occurred at temperatures between 60° and 105°C. Homogenization temperatures for fluid inclusions in quartz overgrowths in the Rotliegend sandstone in the Vulcan field range from 72° to 97°C (McNeil *et al.*, 1990), and better constrain precipitation temperatures of authigenic quartz.

The original pore fluids were likely to have been Early Permian meteoric water derived from the semi-arid environment in which the Rotliegend was deposited. Carbon and strontium isotope data for early dolomite and late ankerite, however, indicate that these meteoric waters were flushed by Late Permian seawater during development of the Zechstein evaporites and that fluids derived from the underlying Carboniferous became increasingly important during burial diagenesis (Sullivan *et al.*, 1990). Recently published salinities for fluid inclusions in quartz overgrowths in the Rotliegend (Vulcan field) are as high 25 to 26 equivalent weight percent NaCl (McNeil *et al.*, 1990). The high salinities of the fluid inclusions and the isotopic data from the carbonates suggest that the quartz precipitated from a strongly evolved brine.

The $\delta^{18}O$ composition of the water was calculated using the temperatures of quartz precipitation derived from homogenization temperatures from fluid inclusions in the quartz, the measured $\delta^{18}O$ values for quartz cement and the oxygen-isotope fractionation equation

for quartz-water determined by Matsuhisa *et al.* 1979):

$$(\delta_{qtz} - \delta_w) = 3.34 \times 10^6 (T^{-2}) - 3.31$$

where δ_{qtz} =isotopic composition of quartz (relative to SMOW), δ_w = isotopic composition of the water from which the quartz precipitated (relative to SMOW) and T = the temperature of formation in degrees Kelvin. The water that would have precipitated the quartz cement with a $\delta^{18}O$ composition +19.7‰ to +22.3‰ at temperatures between 72° and 97°C would have had a $\delta^{18}O$ composition of approximately of -2‰ (SMOW), which is compatible with a highly modified meteoric water or a mixed meteoric/marine brine as suggested by the high salinities of the fluid inclusions and the isotopic data from the carbonates. These temperatures would have been attained at depths of approximately 1.5 to 2 km (4900 to 6500 ft), which would have occurred during the Late Triassic when the basin was under going extension and rapid burial (Figure 3.7).

3.4.7 Source of quartz cement

One of the largest problems in modelling the burial diagenesis of the Rotliegend Sandstone in the Leman field is locating the source or sources of the authigenic quartz. The Rotliegend Sandstone is approximately 250 m thick over an area of 4.8×10^8 m^2 in the Leman field. Quartz cement accounts for approximately 8 to 10% of the total rock (locally 30%), and therefore represents approximately 3×10^{16} g of quartz cement in the Leman field alone. Sufficient sources of silica within the Rotliegend Sandstone, however, have not been identified to account for the total volume of quartz cement present in Leman field.

Pressure solution: Pressure solution along stylolites and intergranular pressure solution are commonly suggested internal sources of silica (Pittman, 1972; Sibley & Blatt, 1976; Bjørlykke et al., 1979; Dutton, 1986; Dutton & Land, 1988), but in this case only a small amount of the

observed quartz cement can be attributed to these sources. Unlike quartz cemented sandstones of the northern North Sea and Gulf Coast (Bjørlykke *et al.*, 1979; Larese *et al.* 1984; 1986; Dutton & Diggs, 1990), there is little or no significant development of stylolites in the Rotliegend Sandstone in the Leman field to supply large quantities of silica. Development of intergranular pressure solution is also limited in these sandstones. Füchtbauer (1967) estimated that intergranular pressure solution in the Rotliegend, from the Dutch sector, began at depths of 1000 to 1200 m and attributed the observed quartz cement to pressure solution within the silty, finer grained beds. For these volumes to balance, it would require 30% of the silica in the silty inter-beds to be released by pressure solution to produce the volume of authigenic quartz in the adjacent strongly cemented beds or approximately 15% by volume of the detrital quartz grains to be dissolved by pressure solution throughout the Rotliegend Sandstone.

Examination of compactional textures in the cemented coarse grained beds and adjacent non-cemented silty, finer grained beds, suggests pressure solution was not capable of producing all of the observed quartz cement. In the strongly cemented laminae, most detrital grains have either floating, tangential or long grain contacts and minus cement porosities greater than 30% are common, suggesting little or no pressure solution had occurred in these beds. Waugh (1970) suggested that pressure solution had a minimal effect on quartz cementation of the Penrith Sandstone, which also has similar types of uncompacted grain contacts in strongly quartz cemented zones. Concavo-convex and sutured contacts are much more common in the adjacent uncemented, fine grained laminae and there is significant evidence of pressure solution at grain contacts (Figure 3.14) in these beds. Stylolites were only observed in one sample (Figure 3.15), but do not appear to be very common in the Leman field.

Estimating the actual volume of silica released by grain solution, however, is very difficult and at best can only be semi–quantitative. The method of Sibley and Blatt (1976) was use to determine the approximate volume of grain loss by pressure solution for fifteen of the Rotliegend

samples. Point count estimates of pressure solution were made using a standard petrographic microscope rather than a cathodoluminescence microscope as grain contacts in the Rotliegend Sandstone are easily identified in plane polarized light due the presence of clay rims on detrital grains. The maximum volume lost by grain pressure solution was approximately 10%, but the average volume lost appears to be approximately 4% (approximately half the total observed quartz cement; Figure 3.16, Table 3.4). Although, pressure solution appears capable of producing about half of the observed quartz cement, the question of timing of pressure solution relative to quartz cementation remains. Laminae in which pressure solution is best developed show no evidence of having ever been cemented during diagenesis, and though compaction of finer grained beds would have proceeded faster than that of the coarse grained beds, which had minus cement porosities of 30% at the time of cementation, it is unlikely that the observed pressure solution textures were produced at the depths inferred from isotopic and fluid inclusion evidence for quartz precipitation (1.5 to 2 km). In fact, it is likely that the observed pressure solution within the fine grained sandstones occurred after quartz cementation and that this internally derived silica has been moved out of the sandstone.

Feldspar dissolution: Another possible internal source of silica in the Rotliegend would have been the dissolution of detrital feldspar (Figure 3.17). Selective leaching of feldspar has contributed significantly to the porosity of the Rotliegend Sandstone in the Leman field. Feldspar dissolution can account for up to 20% of the total porosity in some samples, but only forms about 2% of the total rock (see Chapter 5). The time of major feldspar dissolution in the Rotliegend occurred after the main phase of quartz cementation (see Figure 3.7) and therefore could only have supplied silica to the small quantity of late quartz observed in secondary pores. Even if feldspar dissolution occurred earlier in the diagenetic history of the Rotliegend it could only have supplied at most 1% quartz cement.

Replacement of detrital grains by carbonate: A third possible source of silica from within the Rotliegend would have been the replacement of detrital quartz and feldspar grains by aggressive carbonate cements. Detrital silicate grains commonly display aggressive replacement by early dolomite, which pre-dates quartz cementation, as evidenced by embayed contacts where carbonate cements border detrital grains. This is especially evident in poikilotopic dolomite cement patches where significant corrosion of silt and very fine sand grains has occurred (Figure 3.18). Although carbonate grain replacement is a common feature of the Rotliegend Sandstone, it could only have supplied a very small amount of silica for quartz cementation, probably only a few percent of the observed authigenic quartz.

External silica sources: Even if the total volume of silica released by pressure solution, feldspar dissolution and detrital grain replacement is considered, irrespective of when these reactions were capable of releasing silica, only half of the quartz cement in the Rotliegend Sandstone can be accounted for from internal sources. The apparent lack of sufficient internal silica sources in the Rotliegend, therefore, suggests that additional volumes of silica were imported into the Rotliegend from external sources.

The most likely source of silica from outside the Rotliegend would have been pressure solution in the underlying thick sequence of Carboniferous shales and interbedded sandstones. Quartz grains in shales commonly display elongate, irregular shapes typical of those produced by pressure solution in siltstones and sandstones (Heald, 1955; Füchtbauer, 1967, 1978; Evans, 1989,1990) and concretions in shales often contain 10 to 50% more detrital quartz than host shale (Füchtbauer, 1978; Evans, 1989, 1990), indicating that quartz dissolution within shales is a potentially very important source of silica within sedimentary sequences. Most diagenetic reactions release silica at depths greater than the depth of quartz cementation (McBride, 1989). The Carboniferous shales beneath the Rotliegend in the Leman field are nearly a kilometre thick and therefore

would always have been at significantly higher temperatures and pressures. The temperatures of quartz precipitation (72° to 97°C) are also coincident with the temperatures (80° to 120°C) at which highly active chemical diagenesis due to the production of organic acids would have been occurring in the more deeply buried Carboniferous shales (Surdam *et al.*, 1989), where silica is likely to be released by pressure solution and clay transformations. Direct evidence for export of silica is suggested by Füchtbauer (1974) from the Upper Carboniferous of Germany. He accounted for quartz cement in overlying Lower Permian sandstones by silica released by pressure solution in the underlying Carboniferous sediments. This conclusion was reached from petrographic analysis of the Upper Carboniferous sediments which indicates that a significant amount of pressure solution has occurred, but only a small amount of this silica can be accounted for in these sediments. In contrast, the overlying Lower Permian rocks are strongly cemented by quartz but display little pressure solution.

3.4.8 Palaeohydrology

The lack of sufficient internal sources of silica strongly suggests that much of the silica cement in the Rotliegend was derived from an external source, with the most likely source being the underlying Carboniferous shales. The silica therefore must have been introduced either by diffusion or by advection of silica-supersaturated waters and four general mechanisms have been suggested to explain the occurrence of quartz cement in the Rotliegend Sandstone.

3.4.8.1 *Diffusion*

The difficulty of cementing thick sandstones with silica supplied by difussion from adjacent shales has been raised by several authors (Wood & Hewett, 1982; Land, 1984; McBride,1989; Mullis, 1991). Diffusion has been suggested to be a significant transport mechanism on the order of

a few metres (Wood & Hewett, 1982), but it is not thought that diffusion could have transported sufficient silica from adjacent pressure dissolved beds within the Rotliegend and from underlying Carboniferous shales to cement 250 m of laterally extensive sandstone (Mullis, 1991). Introduction of the silica by diffusion from the underlying shales into the Rotliegend might also be expected to have produced more pervasive cementation at the base of the Rotliegend due to its proximity to the source (Füchtbauer, 1967; Wood & Surdam, 1979; Sullivan & McBride, 1991; Mullis, 1991), but no such occurrence is observed. The amount of silica in the coarse grained laminae (20 to 30%) greatly exceeds the volume of pressure solution in adjacent fine grained beds and therefore also does not reflect internal redistribution of silica by diffusion. Further, if the silica had been supplied by diffusion, cementation of both fine and coarse grained beds would be expected. The strong dominance of authigenic quartz in the coarser grained, well sorted beds with higher pre-cement permeabilities and porosities suggests, however, that diffusion was not the mechanism of silica transport in the Rotliegend. Instead, the preferential development of authigenic quartz in the more permeable beds (Figure 3.12) suggest cementation occurred in the sandstones which transmitted the largest volumes of mineralizing fluids.

3.4.8.2 *Advection*

Petrographic data (see section 3.4.5.2), including cathodoluminescence petrography, and textures observed in core, support the theory of movement and importation of silica by migrating fluids. Two distinct generations of early quartz cement are observed; (1) prismatic outgrowths, and (2) pore-filling syntaxial overgrowths which commonly enclose outgrowths (Figure 3.10). These multiple generations of authigenic quartz suggest cementation took place episodically, possibly in response to pulses of silica-rich water entering or circulating within the Rotliegend. Additional evidence for cementation occurring by advecting

waters are the luminescence zones observed in the quartz cement using hot cathodoluminescence (Figure 3.11). Luminescent zones in quartz are commonly attributed to variations in Al and trace element concentrations (Sprunt, 1981; Matter & Ramseyer, 1985) and also suggest that cementation proceeded episodically from formation waters of variable composition, (Land *et al.* 1987; McBride, 1989). The dominance of quartz cement in the high permeability beds compared to low permeability beds is further evidence that the silica was emplaced by the flow of silica-rich fluids, rather than diffusion. Finally, quartz mineralized fractures, which may have acted as conduits for ascending fluids, are observed cross-cutting beds strongly cemented by quartz (Figure 3.19). Although the relationship between these fractures and quartz cementation in the Rotliegend is still unclear, their occurrence in or near silica cemented zones strongly suggests there may be a link.

Textural selectivity of authigenic quartz distribution and thin-section petrography therefore suggest that the silica was transported by advection, rather than diffusion. Temperature appears to be a strong control on silica solubility (Porter & James, 1986), such that quartz would be more soluble at high temperatures and would precipitate as silica-rich waters rose and began to cool, becoming oversaturated. The amount of rising, cooling silica-supersaturated water required to introduce sufficient silica for quartz cementation has been calculated for several sandstones (Land & Dutton, 1978, 1979; Bjørlykke 1979a, 1979b, 1983; Haszeldine *et al.*, 1984) and most calculations suggest that between 10^4 to 10^5 cm^3 of water are required to cement each cm^3 of of rock.

The importance of organic compounds on silica solubility has also been raised by several authors (Moncure *et al.*, 1984; Surdam *et al.*, 1984; Bennett & Siegel, 1987; Bennett *et al.*, 1988) A recent study of an oil contaminated ground water has shown that dissolved silica concentrations correlate with concentrations of dissolved organic carbon (Bennet & Siegel, 1987). The quartz grains in these groundwaters are being strongly etched at near neutral pH and dissolved silica concentrations are

15 to 20 times that expected for the pH and temperature conditions present. This study by Bennet and Siegel (1987) and additional experimental work on dissolution of quartz in dilute solutions of organic acids at 25°C (Bennet *et al.*, 1988), suggest that silica is being complexed by by organic compounds which lower the activity of silicic acid, thereby accelerating the dissolution quartz at near neutral pH. High concentrations of organic acids are reported to occur in many oil and gas fields (Carothers & Kharaka, 1978; Surdam *et al.*, 1984) and organic acid complexing of silica may therefore be an important mechanism for mobilizing and transporting silica during diagenesis, especially in environments of high organic contents such as organic rich source rocks like the Upper Carboniferous shales underneath the Rotliegend Sandstone in the Leman field. If organic acids can increase the the solubility of silica by 15 to 20 times those expected at given pH and temperature conditions as suggested by Bennett and Siegel (1987) and Bennet *et al.*, (1988), then the volume of water required to transport silica in solution would be greatly reduced and volumes on the order of only 10^3 to 10^4 cm^3 would be required to introduce 10% silica into each cm^3 of rock. It must be stressed, however, that even these reduced volumes of water required for introduction of 10% quartz cement into each cm^3 of a 100 m thick sandstone are still extremely large.

Compactional Dewatering: Although up to half of the quartz cement in the Rotliegend may have been derived internally, extremely large volumes of water are still required to import the the remainder of the observed cement and also to redistribute internally derived silica to sites of cementation. Dewatering of shales undergoing compaction and clay diagenesis has been suggested as a major source of silica saturated fluid during burial diagenesis (Heald, 1955; Füchtbauer, 1967, 1978; Land & Dutton, 1978; Boles & Franks, 1979). Compactional dewatering of the Carboniferous shales would have produced 0.15 cm^3 of water for each cm^3 of shale compacted by 15% during compaction from 1 to 4 km of burial. This would have produce an upward flux of 6.6×10^{16} cm^3 of water from

the Upper Carboniferous shales for the transportation of silica into the Rotliegend. Even utilizing the maximum inferred solubilities of silica that could have been produced by effects of temperature and organic acids (i.e. 2000 ppm), it would have required an upward flow of at least 1.32 x 10^{18} cm^3 of water, which is about 20 times the volume of water available from the shales. Possible dewatering of more deeply buried units such Lower Carboniferous limestones and pre-Carboniferous rocks could have contributed additional water, but a very large discrepancy would still remain.

Meteoric Recharge: Another possible source of the fluids required for silica importation could have been deep circulation of meteoric water. Gravity-induced cross-formational flow of meteoric water to depths exceeding 1.5 km has been reported for several deep sedimentary basins (Toth, 1978; Fisher, 1982; Galloway, 1984; Harrison & Bethke, 1986; Dutton & Land, 1988; Dutton & Diggs, 1990) and the palaeogeographic setting of the southern North Sea Basin during the Triassic should have permitted deep circulation of meteoric water through the Carboniferous and Pre-Carboniferous rocks which underlie the Rotliegend (Figure 3.20) The proto-Pennine High and London-Brabant Massif both remained exposed highs during the entire Triassic period (Zeigler, 1982) and therefore could have been recharge zones for a regional meteoric flow system. The water which precipitated the quartz cement was probably part of an ascending limb of a regional meteoric water circulating system, such that as the water was circulated to deeper, hotter zones it became saturated with respect to quartz and then precipitated quartz cement as it rose, cooled and became oversatuated.

The water from which the quartz cement precipitated must have interacted considerably with the rocks through which it passed, because the $\delta^{18}O$ composition and salinity of the water is significantly modified from that of meteoric water. Meteoric water during the Permian and Triassic probably had an isotopic composition of -5‰ (SMOW) (Craig, 1961), but the interpreted $\delta^{18}O$ composition of the water from which the quartz precipitated was approximately -2‰ (SMOW). As the fluids

recharged the basin, the $\delta^{18}O$ of the water must have become progressively heavier and the salinity gradually increased because of interaction with the rocks through which it passed (Clayton *et al.*, 1966). Many deeply circulated formation brines of meteoric origin progressively become enriched in ^{18}O and total dissolved solids with increasing depth and evolved meteoric brines commonly have $\delta^{18}O$ compositions as heavy as –2‰ (SMOW) and extremely high salinities due to water rock interaction (Clayton *et al.*, 1966; Hitchon & Friedman, 1969; Dutton & Land, 1985; Egeberg & Aagaard, 1989; Fisher & Boles, 1990). Ascending meteoric water could have also been modified as it entered the Rotliegend by the influx of fluids and/or diffusion of ions from the Zechstein evaporites which were an important source of fluids and ions through much of the diagenesis of the Rotliegend (Sullivan *et al.*, 1990).

3.5 PENRITH SANDSTONE

3.5.1 Geologic setting

The Lower Permian Penrith Sandstone consists of continental, aeolian sandstones deposited in a structurally controlled, elongate basin (Waugh, 1970). This basin extended some 50 km from Armathwaite in the north to Kirby Stephen in the south, roughly conforming to the present day Vale of Eden (Figure 3.21). This study examined the Lower Permian sandstones from the northern portion of the basin in the area between Armathwaite and Lazonby (Figure 3.22). This part of the basin contains numerous faults, with the dominant structures being northwest-southeast trending, such as the Abbott Moss Fault, and smaller faults trending perpendicular to these in a northeast-southwest direction (Figure 3.22). The Penrith Sandstone reaches a maximum thickness of 300 m in this region (Figure 3.23). These sands unconformably overlie a thick sequence of Lower Carboniferous shales and are overlain in turn by the Eden Shales, which are thinly bedded sandstones, shales and evaporites of

mixed marine and sabkha origin (Arthurton & Wadge, 1981). The Penrith Sandstone was deposited as barchan sand dunes in a hot, arid desert environment (Waugh, 1970) and the lithologies are very similar to those of the Rotliegend Sandstone in the southern North Sea. The basin fill is comprised almost exclusively of aeolian sands, with minor fluvial and wadi deposits occurring at the basin margins (Arthurton & Wadge, 1981). In the study area, the Penrith Sandstone consists entirely of reddish-brown, cross-bedded aeolian dune sands, closely resembling the aeolian sands of the middle unit of the Rotliegend Sandstone (Figure 3.24). Aeolian cross-bedding is particularly well developed in the Penrith, consisting of massive units of high angle, trough cross-strata. Dune deposits are very well sorted and rounded, medium to coarse grained sandstones.

3.5.2 Petrography

3.5.2.1 *Detrital mineralogy*

Petrographically the Penrith sandstones are subarkoses (Appendix B.1). In all samples, monocrystalline quartz is the most abundant type of detrital grain, generally showing unstrained extinction, while polycrystalline quartz is less common. Together, mono and polycrystalline quartz account for 90 to 95% of the whole rock. Undulose extinction and crenulated borders of crystallites suggest a metamorphic origin for much of the quartz. Feldspar comprises 5 to 8% of the rock , the majority being extensively weathered. Rock fragments vary from 2 to 5 %, and are predominantly of metamorphic origin, with subordinate amounts of volcanic and sedimentary clasts.

3.5.2.2 *Diagenesis*

Diagenetic fabrics, authigenic mineral types and timing of

cementation events in the Penrith Sandstone closely resemble those of the Rotliegend Sandstone (Figure 3.25). As in the Rotliegend, the first authigenic cements to precipitate were clay/hematite coatings on detrital grains. This was followed by precipitation of dolomite. Dolomite is only a very minor cement and often the only evidence of its precipitation are empty molds and occasional quartz pseudomorphs after dolomite (Waugh, 1970). Authigenic K-feldspar also forms as an early cement, occuring as overgrowths on detrital feldspars.

Quartz cementation occurred next and is volumetrically the most important cement in the Penrith Sandstone, occupying approximately 70% of the depositional porosity. Within the study area, the entire section of Penrith Sandstone appears to be extremely well silicified and in places contains near vertical silicified "veins" (Figure 3.26). Authigenic quartz occurs as syntaxial overgrowths (Figure 3.27) forming up to 28% of the total volume in many samples. Overgrowths are separated from detrital grains by dust rims of mixed clay and hematite, but these clay coatings are not as well developed as those in the Rotliegend. Outgrowths do not occur in the Penrith Sandstone and this may reflect less extensive development of clay rims on detrital grains. Early formation of authigenic quartz is reflected by the extremely euhedral shape of large overgrowths, which must have had sufficient space to develop their prismatic form. Further evidence for its early origin is loose grain packing and lack of pressure solution within well cemented zones, which are similar to compaction textures in the Rotliegend and suggest cementation occurred prior to significant burial.

3.5.3 Oxygen isotope results

Three samples of authigenic quartz from the Penrith Sandstone were analyzed for $\delta^{18}O$. The samples that were analyzed were collected from Nunnery Walks [5275 4265], in the vicinity of the Nunnery Walks Fault (Figure 3.22). Sample NW #3 was taken five metres from the fault,

NW #2 three metres from the fault, and NW #1 one metre from the fault. $\delta^{18}O$ values range from +21.5‰ to +22.9‰ (SMOW) (Table 3.3) and no recognizable trends in oxygen isotope compositions are observed over the sampling interval with respect to the Nunnery Walks Fault. Significantly though, these $\delta^{18}O$ values are almost identical to oxygen isotope values of quartz overgrowths from the Rotliegend Sandstone (+19.7 to +22.3‰ SMOW). Homogenisation temperatures measured in fluid inclusions in quartz overgrowths indicate precipitation temperatures of approximately 105°C (Anderson, 1987), which are also very similar to those from quartz overgrowths in the Rotliegend (72° to 97°C). The $\delta^{18}O$ of the water that precipitated quartz cement at temperatures of approximately 105°C would have been about –1‰ (SMOW), which is almost identical to oxygen isotope composition of the waters from which the quartz in the Rotliegend precipitated. We conclude from this data that fluid and temperature conditions under which quartz precipitated were very similar for both the Rotliegend and Penrith sandstones.

3.5.4 Silica source

As with the Rotliegend Sandstone, the volume of quartz cement in the Penrith Sandstone cannot be attributed entirely to internally available silica sources. Petrographic analyses show that pressure solution has had only a minimal effect on these sands and was totally insufficient to supply the required volumes of silica, in fact much more so than in the Rotliegend Sandstone. Most detrital grains have either floating, tangential or long grain contacts in the Penrith Sandstone and show little or no evidence of pressure solution. Even the fine grained laminae show little evidence of pressure solution. Therefore, pressure solution in these sands could not have produced more than a few percent of the observed quartz cement.

Detrital feldspars in the Penrith Sandstone have been significantly altered and feldspar dissolution would have been another internal source of silica. Today feldspar comprises about 5% of these

sands, but it may have been more abundant at the time of deposition (possibly 10%). Even if 5 to 10% feldspar had been dissolved it would have only supplied a minor amount of the observed quartz cement. Since feldspar dissolution appears to have occurred after the main phase of quartz precipitation, this silica could have only been supplied to any late generation quartz cement.

There also is no petrographic evidence for dissolution of silt-sized quartz, or of biogenic quartz within the Penrith Sandstone. Waugh (1970) suggested that the quartz cement in the Penrith was supplied by preferential dissolution of quartz dust derived from grain abrasion during deposition. This would require dissolution of enormous volumes of quartz dust to produce 20% of silica cement observed throughout the northern portion of the Solway basin. It is unlikely that such large volumes of quartz could have been supplied by dissolution of dust in desert groundwaters and the high temperatures of precipitation suggested by fluid inclusions in quartz overgrowths (Anderson, 1987) and oxygen isotope data for the overgrowths are also not consistent with early precipitation from desert groundwaters.

Preferential development of quartz cement in high permeability sandstones compared to low permeability sandstones suggests that the flow of silica-saturated fluids, rather than diffusion, was the dominant method of importing silica. This is also supported by the recognition of growth zones in quartz overgrowths from hot-stage cathodoluminescence studies (Figure 3.28). Authigenic quartz has a dull blue luminescence very similar that that of the quartz cement in the Rotliegend Sandstone. Overgrowths in the Penrith also display complex, polyphase internal structures, and samples generally have between three and four zones. These growth zones closely resemble those in Rotliegend quartz cement and indicate that quartz precipitation occurred episodically from formation waters of variable composition (Land *et al.*, 1987; McBride, 1989), possibly reflecting pulses of silica-bearing fluids entering the Penrith Sandstone. In addition, samples collected near faults often contain

fractured and broken grains cemented by authigenic quartz (Figure 3.29). This cement has the similar CL colours and is petrographically the same as quartz cement from samples collected tens of metres from mapped faults. This suggests quartz cementation throughout the region occurred at the same time as tectonism with faults acting as conduits for fluids during burial diagenesis. The occurrence of silicified veins within strongly quartz cemented sands, similar to those described from Rotliegend core (Figure 3.26), also supports this relationship between faults, importation of silica-bearing diagenetic fluids and quartz cementation.

3.6 CONCLUSIONS: MODEL FOR QUARTZ CEMENTATION IN THE ROTLIEGEND AND PENRITH SANDSTONES

Existing petrographic, isotopic and fluid inclusion data all suggest that quartz cementation in the Rotliegend and Penrith sandstones occurred under similar temperature and fluid conditions, and therefore a single schematic model for silica diagenesis is proposed (Figure 3.30). The extremely high salinities measured for fluid inclusions in quartz overgrowths and isotope data(C & Sr) for carbonate cements indicate that during quartz precipitation the porewaters had a large, if not dominant, marine component. The greatest volume of quartz is interpreted as having precipitated relatively early in the burial history at temperatures between 72° and 105°C (1.5 to 2 km) from evolved meteoric brines (-2‰ to 0‰ SMOW). Examination of the burial curve for the Leman field suggests this would have occurred during the Late Triassic when the basin was undergoing rifting and rapid burial (see Figure 3.6). Internal silica sources, such as pressure solution and feldspar dissolution, do not appear to have been sufficient to supply the total volume of quartz cement present in the Rotliegend and Penrith sandstones and therefore suggests silica import. Selective cementation of higher permeability beds by quartz suggests that silica was transported by migrating fluids, rather than diffusion. The temperatures of quartz precipitation (72° to 105°C) are

coincident with the temperatures at which maximum silicate diagenetic reactions, 80° to 120°C, (Surdam & Crossey, 1989) would have been occurring in the deeper buried Carboniferous shales. Compactional dewatering of the shales would not have supplied sufficient water for importing the silica into the Rotliegend so it is thought that deep circulation of meteoric waters was responsible, These waters were considerably modified by interaction with the rocks through which they passed. The water which precipitated the quartz cement was probably part of an ascending limb of a regional meteoric water circulating system, such that as the water was circulated to deeper, hotter zones it became saturated with respect to quartz and then precipitated quartz cement as it rose, cooled and became oversaturated. The common occurrence of silicified veins in strongly quartz cemented sands suggests that faults may have acted as conduits for ascending meteoric fluids.

3.7 ACKNOWLEDGEMENTS

Supported by funds from Amoco (UK) Exploration and Shell/Esso U.K. Exploration and Production. This research was carried out at the Department of Geology and Applied Geology, University of Glasgow, and the Isotope Geology Unit, Scottish Universities Research and Reactor Centre (SURRC). Core was supplied by the British Geological Survey and by Shell/Esso. The authors thank Graeme Walker and Eric Lanacke of University of Manachester Instsitute of Science and Technology for the use of cathodoluminescence facilities. The authors also thank Douglas Maclean (Glasgow University) for his assistance with the production of photographic plates. The SURRC is supported by Natural Environment Research Council of Britain and the Scottish Universities.

3.8 REFERENCES CITED

Anderson, S.H., 1987. A diagenetic study of the Penrith Sandstone (Lower Permian) of North West England. 4th year applied project thesis, University of Strathclyde, Glasgow, Scotland, 34p.

Arthurton, R.S., and Wadge, A.J., 1981. Geology of the country around Penrith. Mem. *Geol. Surv. Great Britain*, **Sheet 24**, 68-82.

Beard, D.C. and Weyl, P.K. 1973. Influence of texture on porosity and permeability of unconsolidated sand. *Bull. Amer. Assoc. Petrol. Geol.*, **57**, 334-369.

Bennet, P.C. and Siegel, D.I., 1987. Increased solubility of quartz in water due to complexing by dissolved organic compounds. *Nature*, **326**, 684-687.

Bennet, P.C., Melcer, M.E., Siegel, D.I. and Hasset, J.P., 1988. The dissolution of quartz in dilute aqueous solutions of organic acids at 25°C. *Geochim. Cosmochim. Acta*, **52**, 1521-1530.

Bjørlykke, K. 1979a. Cementation of sandstones-a discussion. *Jour. Sediment. Petrol.*, **49**, 1358-1359.

Bjørlykke, K., Elverhøi, A., and Malm, A.O., 1979b. Diagenesis in Mesozoic Sandstones from Spitsbergen and North Sea - a comparison. *Geol. Rundsch.*, **68**, 1152-1171.

Boles, J.R., and Franks, S.G., 1979. Clay diagenesis in Wilcox sandstones of southwest Texas: implications of smectite diagenesis on sandstone cementation. *Jour. Sediment. Petrol.*, **49**, 55-70.

Borthwick, J., and Harown, 1982. A note regarding ClF_3 as an alternative to BrF_5 for oxygen isotope analysis. *Geochim. Cosmochim. Acta*, **46**, 1665-1668.

Bulat, J. and Stoker, S.J. 1987. Uplift determination from interval velocity studies, UK, southern North Sea. *Petroleum Geology of North West Europe*. Brooks, J. and Glennie, K.W. (eds). Graham and Trotman, London, 293-306.

Carothers, W.W. and Kharaka, Y.K., 1978. Aliphatic acid ions in oil-field

waters—implications for origin of natural gas. *Bull. Am. Ass. Petrol. Geol.* **62**, 2441-2453.

Clayton, R.N., and Mayeda, 1963. The use of bromine penta-fluoride in the extraction of oxygen from oxides and silicates for isotopic analysis. *Geochim. Cosmochim. Acta*, **27**, 43-52.

Clayton, R.N., Friedman, I., Graf, Mayeda, T.K., Meents, W.F. and Shimp, M.F., 1966. The origin of formations-I. Isotopic composition. *Jour. Geophs. Res.*, **71**, 3869-3882.

Cope, M.J. 1986. An interpretation of vitrinite reflectance data from the southern North Sea Basin. *Habitat of Palaeozoic Gas in N.W. Europe*. Brooks, J., Goff, J. and van Hoorne, B. (eds). Spec. Publs Geol. Soc. 23, Scottish Academic Press, London, 85-101.

Craig, H. 1961. Isotopic variations in meteoric waters. *Science*, **133**, 1702-1703.

Dutton, S.P., 1986. Diagenesis and burial history of the Lower Cretaceous Travis Peak Formation, East Texas. Ph.D. diss., University of Texas, Austin, Texas, 165 pp.

Dutton, S.P., and Land, L.S. 1985. Meteoric burial diagenesis of Pennsylvanian Arkosic sandstones, Southwestern Anadarko Basin, Texas. *Bull. Amer. Assoc. Petrol. Geol.*, **69**, 22-38.

Dutton, S.P. and Land, L.S. 1988. Cementation and burial history of a low permeability quartzarenite, Lower Cretaceous Travis Peak Formation, East Texas. *Geol. Soc. Amer. Bull.*, **100**, 1271-1282.

Dutton, S.P., and Diggs, T.N., 1990. History of quartz cementation in the Lower Cretaceous Travis Peak Formation, East Texas. *Jour. Sediment. Petrol.*, **60**, 191-202.

Egeberg, P. K. and Aagaard, P., 1989. Origin and evolution of formation waters from oil fields on the Norwegian shelf. *Appl. Geoch.*,**4**, 131-142.

Evans, I.J., 1989. Geochemical fluxes during diagenesis: an example from the Ordovician of Morocco. In: *Water-rock Interactions VI*, Miles, D.L. (ed), Balkema, Rotterdam, 219-222.

Evans, I.J., 1990. Quartz dissolution during shale diagenesis-implications for quartz cementation in sandstones. Abstracts of *IAS* meeting, Nottingham.

Fisher, J.B. and Boles, J.R., 1990. Water-rock interaction in Tertiary sandstones, San Joaquin basin, California, U.S.A.: diagenetic controls on water composition. *Chem. Geol.*, **82**, 83-101.

Fisher, R.S., 1982. Diagenetic history of Eocene Wilcox sandstones and associated formation waters, South-Central Texas. Ph.D. diss., University of Texas, Austin, Texas, 165 pp.

Füchtbauer, H., 1967. Influence of different types of diagenesis on sandstone porosity. *7th World Petrol. Congr.*, **2**, 353-369.

Füchtbauer, H., 1974. *Sediments and Sedimentary Rocks.* Wiley, New York, 464 pp.

Füchtbauer, H., 1978. Zur Herkunft des Quarzzements. Abschätzung der Quartzauflösung in Silt und Sandsteinen. *Geol. Rundsch.*, **67**, 991-1008.

Galloway, W.E., 1984. Hydrologic regimes of sandstone diagenesis. In: *Clastic Diagenesis,* McDonald, D.A. and Surdam, R.C. (eds). *Am. Ass. Petrol. Geol. Mem.*, **37**, 3-14.

Glennie, K.W. 1972. Permian Rotliegendes of Northwest Europe interpreted in light of modern desert sedimentation studies. *Bull Amer. Assoc. Petrol. Geol.*, **56**, 1048-1071.

Glennie, K.W. 1989. Lower Permian—Rotliegend. In: *Introduction to the Petroleum Geology of the North Sea* (3rd edition). Glennie, K.W. (ed), Blackwell Scientific Publications, Oxford, 120-152.

Glennie, K.W., Mudd, G.C., and Nagtegaal, P.J.C., 1978, Depositional environment and diagenesis of Permian Rotliegendes sandstones in Leman Bank and Sole Pit areas of the U.K. southern North Sea: *Jour. Geol. Soc. London*, **135**, p. 25-34.

Glennie, K.W. and Boegner, P.L.E. 1981. Sole pit inversion tectonics. In:

Petroleum Geology of the Continental Shelf of North-West Europe, Illing, L.V., and Hobson, G.D. (eds), Heyden, London, 110-120.

Harrison, W.J., and Bethke, C.M., 1986. Paleohydrologic analysis of interacting meteoric and compactional flow regimes in the U.S. *Gulf Coast. Geol. Soc. Amer. Abs.*, **18**, 630.

Haszeldine, R.S., and Samson, I.M., 1984. Quartz diagenesis and convective fluid movement: Beatrice oilfield, UK North Sea. *Clay Minerals*, **19**, 391-402.

Heald, M.T., 1955. Stylolites in sandstones. *Jour. Geol.*,**63**, 101-114.

Heald, M.T. and Renton, J.J., 1966. Experimental study of sandstone cementation. *Jour. Sediment. Petrol.*,**36**, 972-991.

Heald, M.T., and Larese, 1974. Influence of coatings on quartz cementation. *Jour. Sediment. Petrol.*, **44**, 1269-1274.

Hitchon, B and Friedman, I., 1969. Geochemistry and origin of formation waters in the western Canada sedimentary basin I. Stable isotopes of hydrogen and oxygen. *Geochim. Cosmochim. Acta*, **35**, 567-598.

Hunter, R.E., 1977. Basic types of stratification in small eolian dunes. *Sedimentology*, **24**, 361-387.

Land, L.S., 1984. Frio sandstone diagenesis, Texas Gulf Coast. A regional isotopic study. In: D.A. McDonald and R.C. Surdam (eds), Clastic Diagenesis. *Amer. Assoc. Petrol. Geol. Mem.*, **37**, 47-62.

Land, L.S., and Dutton, S.P., 1978. Cementation of a Pennsylvanian deltaic sandstone: isotopic data. *Jour. Sediment. Petrol.*, **48**, 1167-1176.

Land, L.S., and Dutton, S.P., 1979. Cementation of sandstone-a reply. *Jour. Sediment. Petrol.*, **49**, 1359-1361.

Land, L.S., Milliken, K.L. and McBride, E.F.,1987. Diagenetic evolution of Cenozoic sandstones, Gulf Coast of Mexico sedimentary basin. *Sediment. Petrol.*, **50**, 195-225.

Larese, R.E., Pittman, E.D. and Heald, M.T., 1984. Effect of diagenesis on porosity development, Tuscaloosa sandstone, Louisiana (Abstr.) *Bull. Amer. Assoc. Petrol. Geol.*, **68**, 498.

Lee, M., 1984. Diagenesis of the Permian Rotliegendes Sandstone, North Sea: K/Ar, O^{18}/O^{16}, and petrological evidence. Ph.D. thesis, Case Western University, Cleveland, Ohio, 346p.

Lee, M., and Savin, S.M., 1985. Isolation of diagenetic overgrowths on quartz sand grains for oxygen isotopic analysis. *Geochim. Cosmochim. Acta*, **49**, 497-501.

Mack, L.E., 1984. Petrography and diagenesis of a submarine fan sandstone, Cisco Group (Pennsylvanian), Nolan Country, Texas. M.Sc. thesis, University of Texas, Austin, Texas, 254 pp.

Marie, J.P.P. 1975. Rotliegendes stratigraphy and diagenesis. In: *Petroleum and the Continental Shelf of North West Europe*, Woodland, A.W. (ed.). *Applied Science Publ.*, London, 205-211.

Matter, A., and Ramseyer, K., 1985. Cathodoluminescence microscopy as a tool for provenance studies of sandstones. In: G.G. Zuffa (ed), *Provenance of Arenites. Reidel, Dordrecht*, 191-211.

McBride, E.F., 1984. Rules of sandstone diagenesis related to reservoir quality (expanded abstr.) *Gulf Coast Assoc. Geol. Soc. Trans.*, **34**, 137-139.

McBride, E.F., 1989. Quartz cement in sandstones: a review. *Earth-Science Reviews*, **26**, 69-112.

McBride, E.F., Land, L.S. and Mack, L.E. 1987. Diagenesis of eolian and fluvial feldspathic sandstones, Norphlet Formation (Upper Jurassic), Rankin County, Mississippi, and Mobile County, Alabama. *Bull. Am. Ass. Petrol. Geol.*, **79**, 1019-1034.

McNeil, B., Rankin, A.H., Shaw, H.F., and Cubitt, J., 1990. A fluid inclusion study of the Rotliegend cements of the Vulcan gas field, southern North Sea: *Third Biennal Pan-American Conference on Research on Fluid Inclusions, Pacrofi III.* Abstracts, **3**, 59.

Moncure, G.K., Lahann, R.W. and Siebert, R.M., 1984. Origin of secondary porosity and cement distribution in a sandstone/shale sequence from the Frio Formation (Oligocene). In: D.A. McDonald and R.C. Surdam (eds), Clastic Diagenesis. *Amer. Assoc. Petrol.*

Geol. Mem., **37**, 151-162.

Mullis, A., 1991. A numerical model for porosity modification at a sand/mud boundary by quartz pressure solution and diffusive mass transfer. *Submitted to Sedimentology.*

Oxburgh, E.R. and Andrews-Speed, C.P. 1981. Temperature, thermal gradients and heat flow in the Southwestern North Sea. In: *Petroleum Geology of the Continental Shelf of North West* Europe, Illing, L.V. and Hobson, G.D. (eds). Heyden, London, 141-151.

Pittman, E.D., 1972. Diagenesis of quartz in sandstones as revealed by scanning electron microscopy. *Jour. Sediment. Petrol.*, **42**, 507-519.

Porter, E.W. and James, W.C., 1986. Influence of pressure solution, salinity, temperature and grain size on silica diagenesis in quartzose sandstones. *Chem. Geol.*, **52**, 259-269.

Sibley, D.F. and Blatt, H., 1976. Intergranular pressure solution and cementation of the Tuscarora orthoquartzite. *Jour. Sediment. Petrol.*,**46**, 881-896.

Skipsey, E., 1989. Geological excursion guide 6: The Eden Valley, Cumbria. *Geol. Today*, **5**, 175-178.

Sprunt, E.S., 1981. Causes of quartz cathodoluminescence colors. *Scanning Electron Microscopy*, **Part 1**, 525-535.

Stephan, H.J., 1970. Diagenesis of the Middle Buntsandstein in South Oldenburg, Lower Saxony. *Meyniana*, **20**, 39-82.

Sullivan, K.B. and McBride, E.F., 1991. Diagenesis of sandstones at shale contacts and diagenetic heterogeneity, Frio Formation, Texas. *Bull. Am. Ass. Petrol. Geol.*, **75**, 121-138.

Sullivan, M.D., Haszeldine, R.S., Hamilton, P.J., and Fallick, A.E., 1987, Integrated petrographic and isotopic study of the diagenesis of the Rotliegendes Sandstone in the Leman gas field: British Sedimentological Research Group Abstracts, **v. 6** p. 133.

Sullivan, M.D., Haszeldine, R.S., and Fallick, A.E., 1990, Linear coupling of

carbon and strontium isotopes in Rotliegend Sandstone, North Sea: Evidence for cross-formational fluid flow: *Geology*, **18**, 1215-1218.

Surdam, R.C., Boese, S.W. and Crossey, L.J. 1984. The chemistry of secondary porosity. In: *Clastic Diagenesis*, McDonald, D.A. and Surdam, R.C. (eds). *Am. Ass. Petrol. Geol Mem.*, **37**, 127-150.

Surdam, R.C., Crossey, L.J., Hagen, E.S., and Heasler, H.P.,1989. Organic-inorganic interactions and sandstone diagenesis. *Bull. Am. Ass. Petrol. Geol.*, **73**, 1-23.

Toth, J., 1978. Gravity-induced cross-formational flow of formational fluids, Red Earth region, Alberta, Canada. Analysis, patterns and evolution. *Water Resour. Res.*, **32**, 805-843.

van Veen, F.R. 1975. Geology of the Leman gas field. In: *Petroleum and the Continental Shelf of North West Europe*, Woodland, A.W. (ed.). Applied Science Publ., London, 223-231.

Walker, T.R. 1976. Diagenetic origin of continential red beds. In: *The Continental Permian in West, Central and South Europe*, Falke, H. (ed). Reidel Publ. Co., Dordrecht, Holland, 352.

Waugh, B. 1978. Authigenic K-feldspar in British Permo-Triassic sandstones. *Jour. Geol. Soc. London*, **135**, 51-56.

Wood, J.R. and Hewett, T.A., 1982. Fluid convection and mass transfer in porous sandstone - a theoretical model. *Geochim. Cosmochim. Acta,*, **46**, 1707-1713.

Wood, J.R. and Surdam, R.C., 1979. Application of convective-diffusion model to diagenetic processes. In: *Aspects of Diagenesis*, Scholle, P.A. and Schluger, P.R. (eds). *Soc. Econ. Paleontol. Miner. Spec. Publ.*, **26**, 243-250.

Zeigler, P.A. 1982. Geological Atlas of Western and Central Europe. Shell International Petroleum Maatschappij, Enclosure **#13**.

3.9 TABLES

TABLE 3.1 Modal analyses of selected samples of the Rotliegend Sandstone in the Leman field, Quadrant 49, based on 500 point counts per sample.

WELL	26-5	26-26	26-26	27-2	27-2
DEPTH (in feet)	6566'	6395'	6754'	6418'	6910'
Detrital					
mono x-tal quartz	49.3	47.2	45.2	47.7	49.7
poly x-tal quartz	13.7	12.6	11.5	11.5	12.0
k-spar	6.3	5.5	6.4	5.4	2.9
plagioclase	1.1	0.8	2.1	2.1	Tr
rock fragments	5.0	7.5	4.5	6.5	8.2
heavy minerals	Tr-z	Tr-z	– –	Tr	Tr-s
Authigenic					
dolomite	3.0	Tr	1.2	3.3	5.2
ankerite	4.1	2.8	Tr	1.2	– –
anhydrite	4.5	– –	5.5	0.8	– –
quartz	1.2	15.1	8.5	11.5	1.4
k-spar	0.7	1,1	1.2	1.2	0.3
clay	1.2	0.7	0.5	1.4	2.3
porosity	9.5	7.2	12.4	8.4	18.0

(Tr - trace, z - zircon, s - sphene)

Table 3.2 Distribution of quartz cement by lithofacies.

	Mean (%)	Standard Deviation	Number samples
Sand flow (coarse grained)	17.2	5.8	21
Sandflow/grain fall (fine grained)	2.5	1.9	18
Wind ripple	4.8	3.2	11
Fluvial	5.6	2.4	6
marine reworked	3.1	1.5	6

Table 3.3 Summary of isotopic analyses of quartz cement in the Rotliegend and Penrith sandstones.

well no.	depth (ft)	$\delta^{18}O$ total quartz	$\delta^{18}O$ authigenic quartz	% quartz cement
Rotliegend Sandstone				
49/26-B240	6933	18.6	20.7	73
49/26-B240	6945	19.0	21.8	75
49/26-B240	6988	19.6	20.5	89
49/26-5	6459	17.2	22.0	49
49/26-26	6395	17.8	22.3	55
49/26-26	6458	18.9	20.1	85
49/26-26	6467	18.2	21.0	66
49/27-2	6418	18.3	19.7	80
49/26-2	6463	17.9	21.8	55
49/27-3	6535	18.8	19.9	91
Penrith Sandstone				
Nunnery Walks #1	[5275 4265]	21.1	21.5	96
Nunnery Walks #2	[5275 4265]	20.9	22.9	81
Nunnery Walks #3	[5275 4265]	20.5	21.9	95
Detrital Quartz (Rotliegend)		13.0		

Note: the % quartz cement (purity) for each sample was determined by examination of samples under cathodoluminescence. Detrital quartz from the Penrith Sandstone was not measured and therefore has been assumed to have the same $\delta^{18}O$ composition as detrital quartz from the Rotliegend Sandstone.

Table 3.4 Data for percentage quartz cement vs. volume of detrital grains lost by pressure solution. Letters A to O refer to plot of volume lost by pressure solution vs. quartz cement shown in Figure 3.16.

	well no.	depth (ft)	% quartz cement	% pressure solution
A	49/26-26	6391	19.6	1.6
B	49/26-26	6395	15.1	0.8
C	49/26-26	6410	9.5	2.1
D	49/26-26	6441	2.1	1.9
E	49/26-26	6512	5.1	2.9
F	49/26-26	6534	1.6	3.5
G	49/26-26	6585	1.1	9.9
H	49/26-26	6624	12.0	0.5
I	49/26-26	6631	1.1	3.2
J	49/26-26	6658	8.3	2.2
K	49/26-26	6667	6.1	1.8
L	49/26-26	6751	0.5	4.1
M	49/26-26	6756	15.3	0.5
N	49/26-26	6913	17.8	1.6
O	49/26-26	6982	0.4	5.1

3.10 FIGURES AND FIGURE CAPTIONS

Figure 3.1 Early Permian rift basins (from Ziegler, 1982).

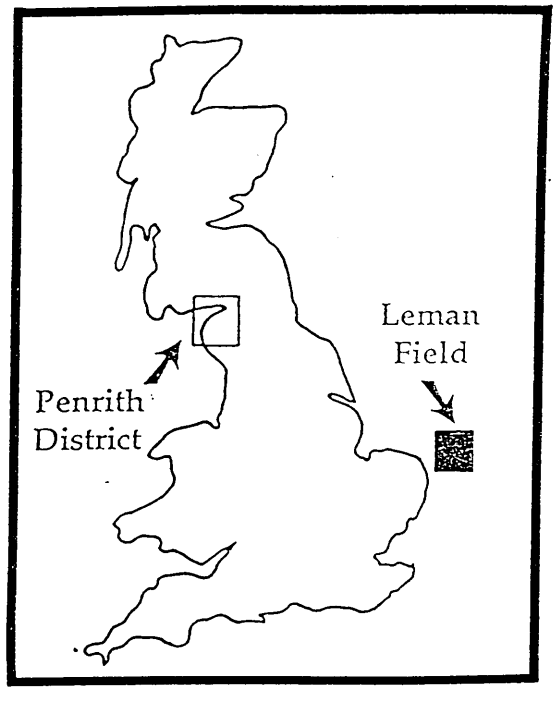

Figure 3.2 Location map showing the Leman field and Penrith District.

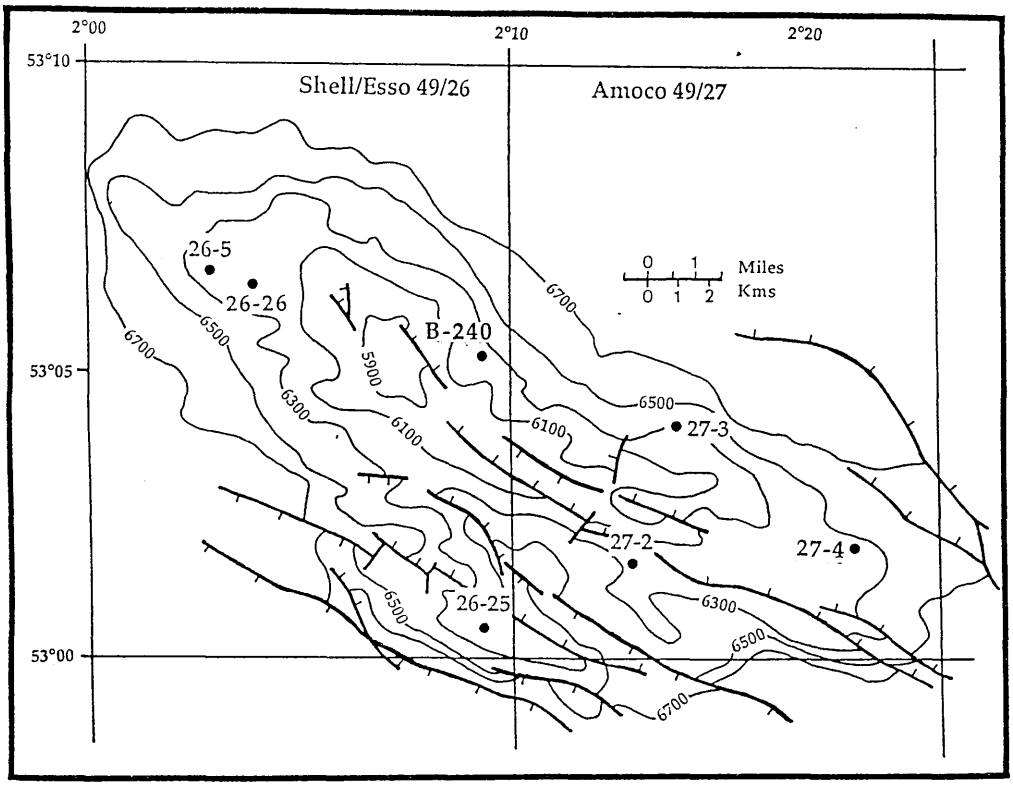

Figure 3.3 Present interpretation of Leman field, showing contours of the top of the Rotliegend in feet below sea level and locations of wells used in this study (from van Veen, 1975).

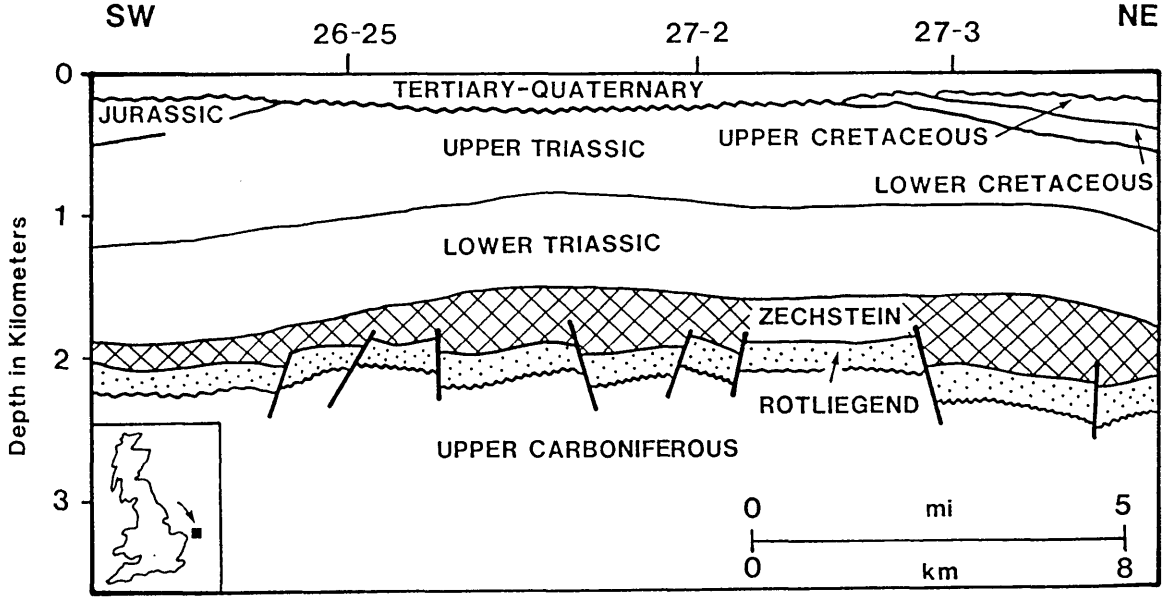

Figure 3.4 Location of Leman gas field (North Sea) and geologic cross section for the Leman region (after Glennie 1990).

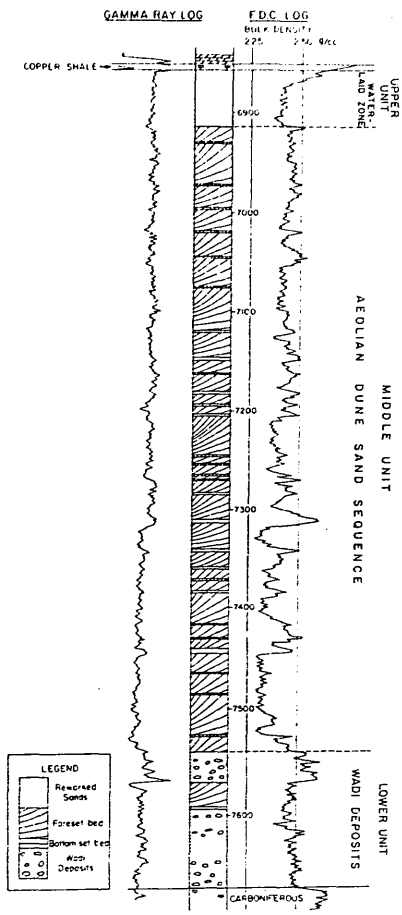

Figure 3.5 Type log of the Rotliegend in the Leman field (from van Veen, 1975).

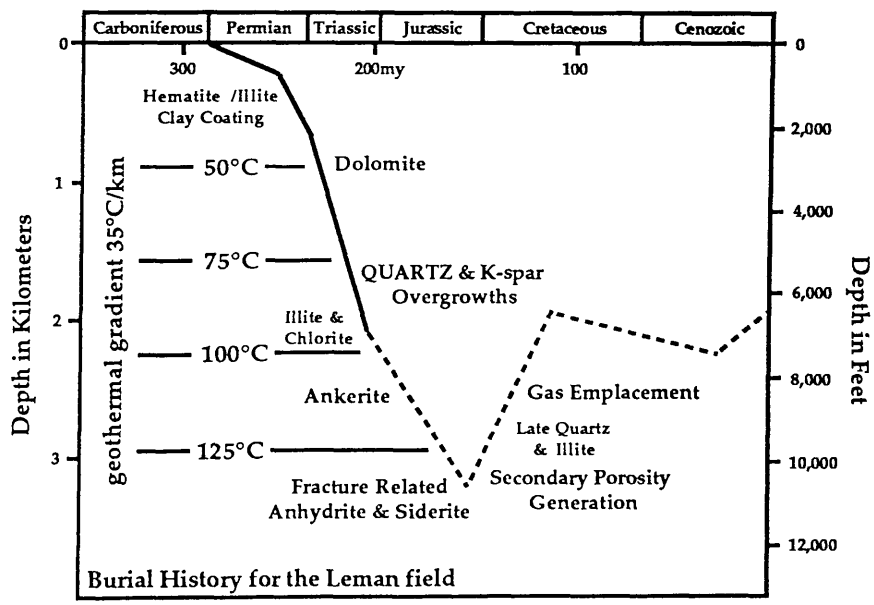

Figure 3.6 Burial curve for the Rotliegend Sandstone in the Leman field showing time and temperature of quartz precipitation and other major diagenetic events. The reconstructed burial curve is based on well logs 49/27-3 & 49/27-4, interval velocity data from Marie (1975), Glennie et al. (1978) and Bulat & Stoker (1987), and vitrinite reflectance data from Cope (1986).

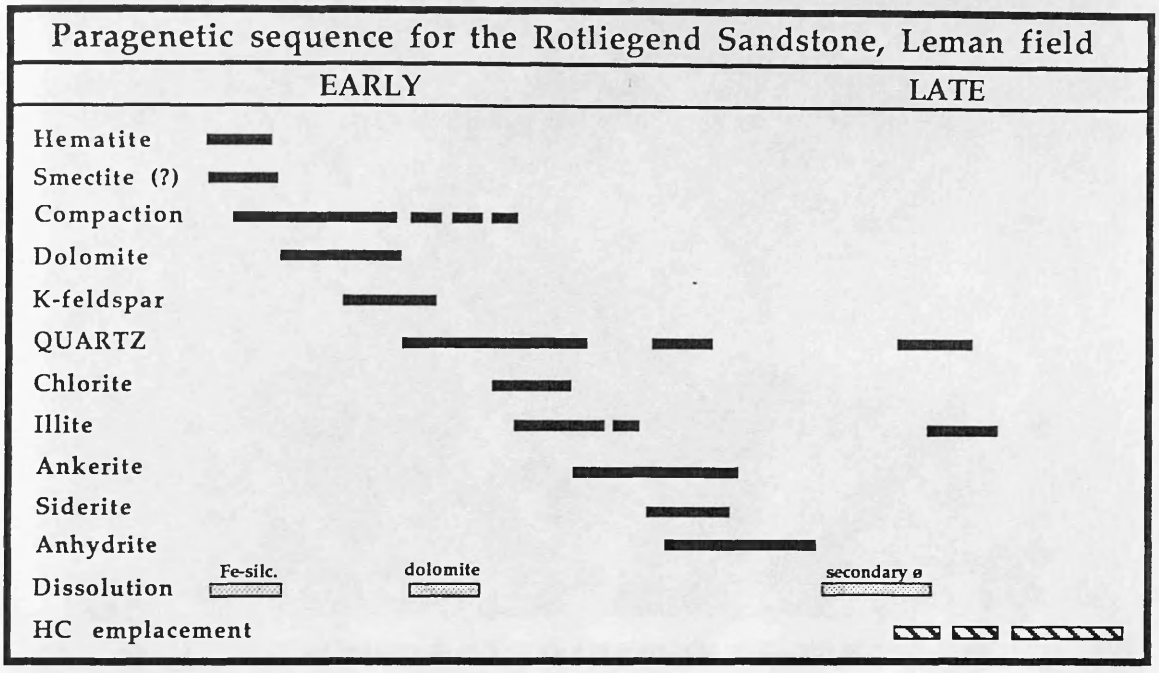

Figure 3.7 Paragenetic sequence showing timing of major diagenetic events in the Rotliegend Sandstone in the Leman gas field.

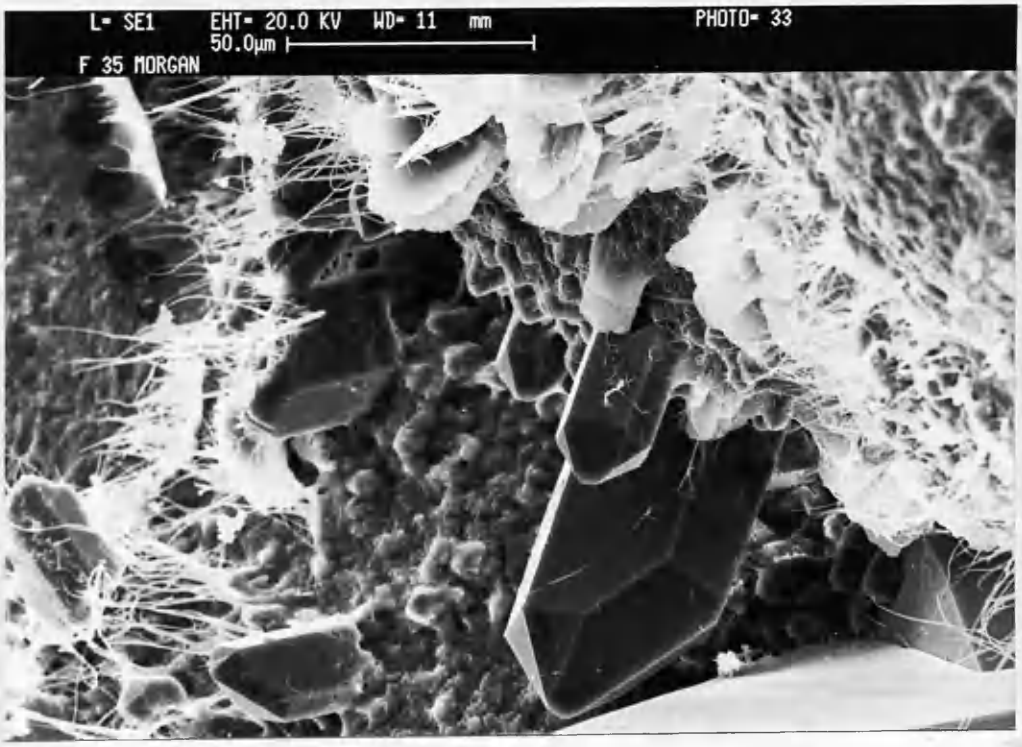

Figure 3.8 SEM photomicrograph showing prismatic outgrowths of quartz cement on detrital grain. 49/26-26, 6913'.

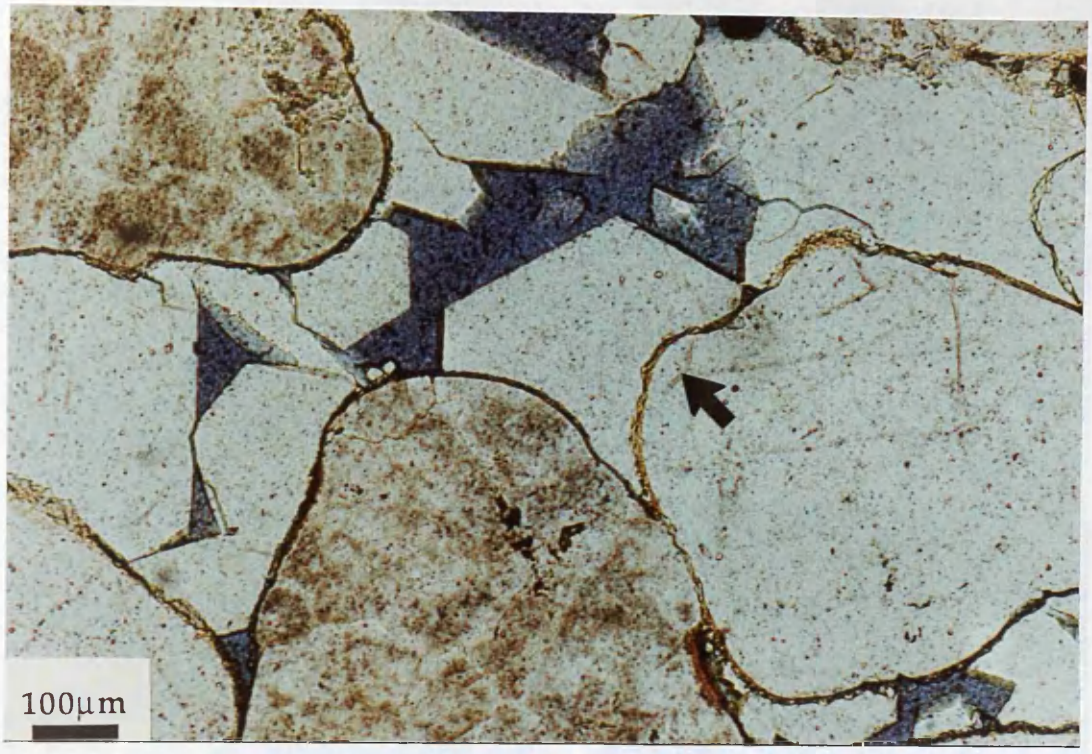

Figure 3.9 Photomicrograph of blocky overgrowths of quartz cement, note presence of well developed hematite/clay cement on nearly all detrital grains (arrow). 49/26-26, 6913'.

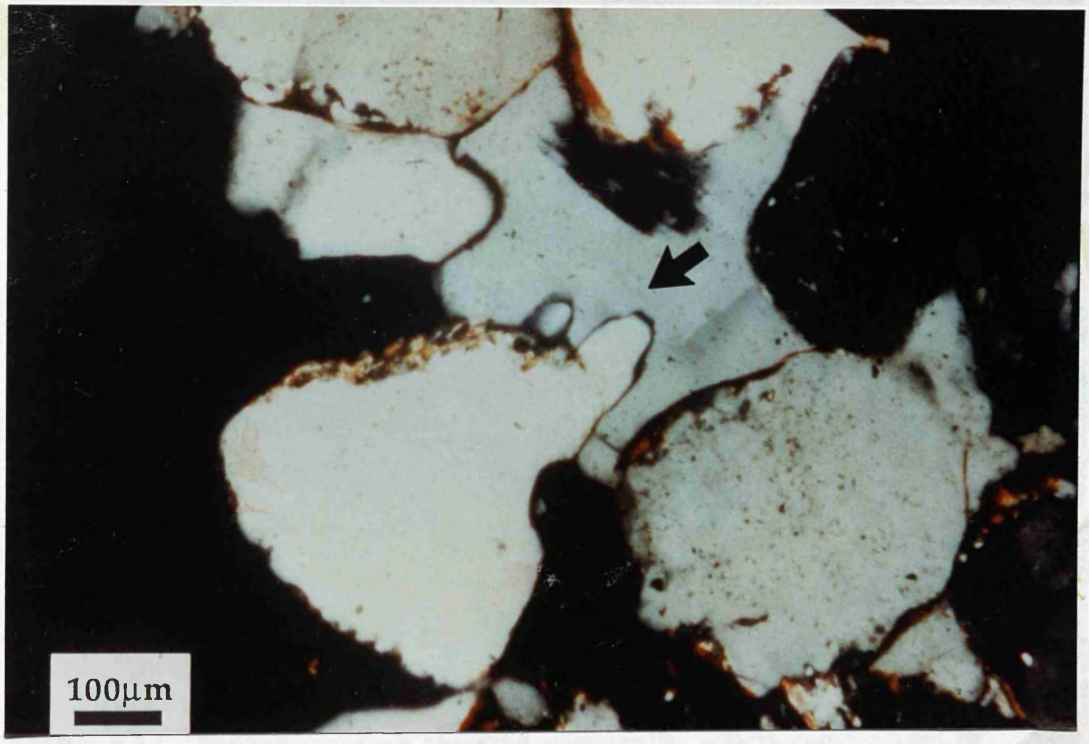

Figure 3.10 Photomicrograph of small prismatic quartz outgrowths (arrow) which precipitated on detrital grains and were subsequently engulfed by later pore-filling quartz. 49/27-3, 6463'.

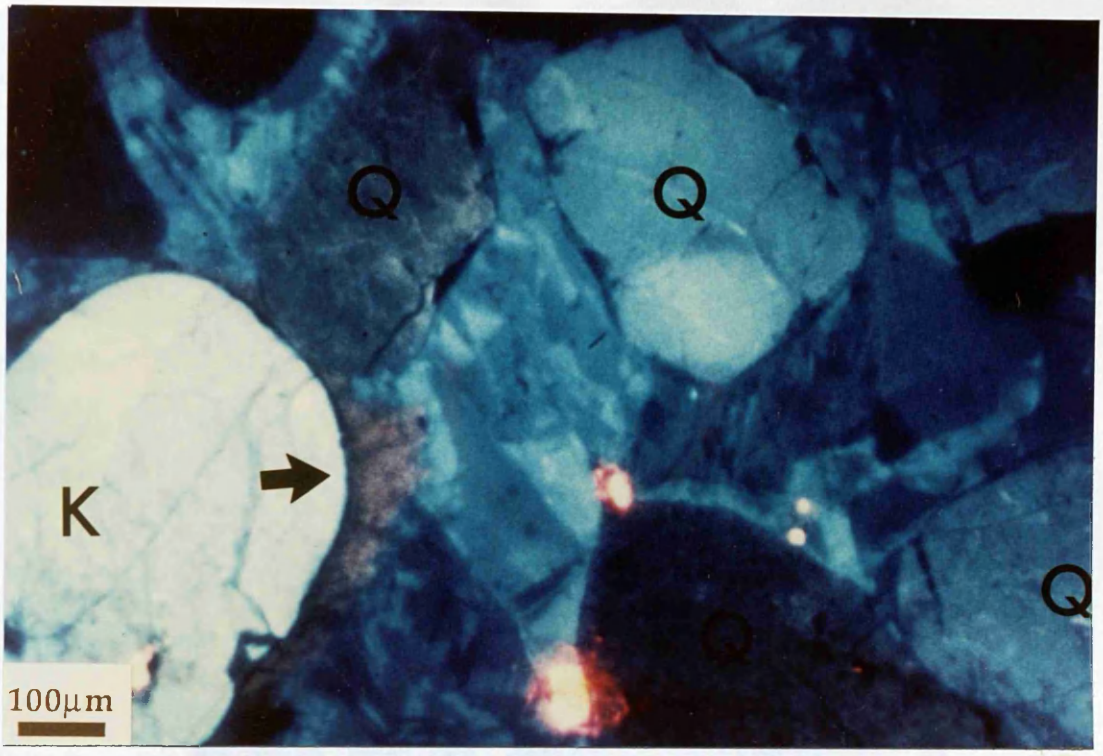

Figure 3.11 Hot-stage cathodoluminescence photomicrograph of complicated zoning in pore-filling quartz cement which is intergrown with authigenic k-spar (arrow), detrital quartz grains are labelled Q and feldspar grains K. Zoning such as this in quartz is interpreted to reflect precipitation from waters of variable composition. 49/26-26, 6458'.

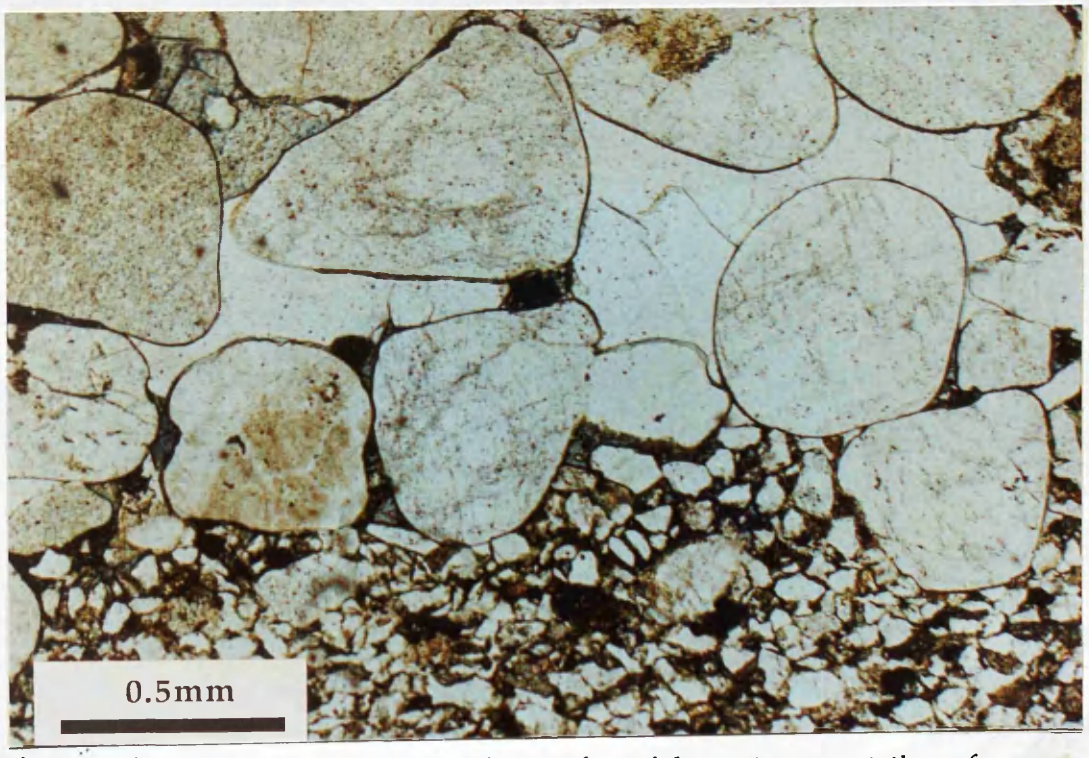

Figure 3.12 Photomicrograph showing preferential quartz cementation of coarser grained, high permeability sands rather than the adjacent finer grained lower permeability sands. 49/26-6, 6913'.

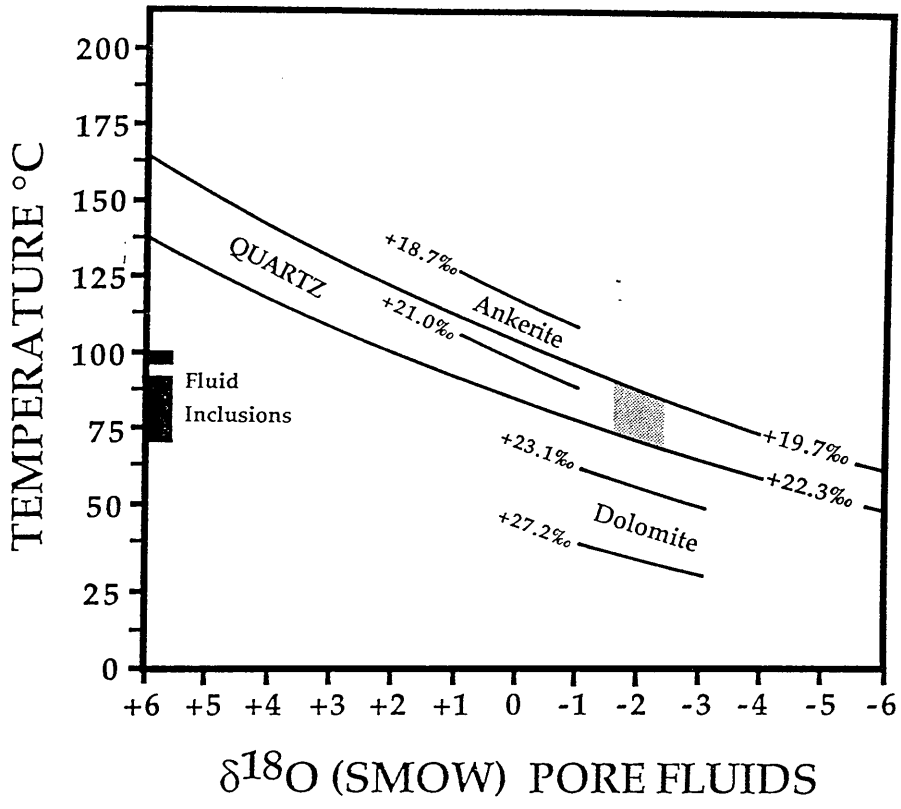

Figure 3.13 Equilibrium relationship between $\delta^{18}O$ of water, $\delta^{18}O$ of quartz and temperature. Quartz cementation is inferred to have occurred at temperatures between 72° to 97°C (McNeil et al., 1990) from an evolved brine with an oxygen isotope composition of -2‰ (SMOW). See section 2.8.1 for oxygen isotope data for carbonates.

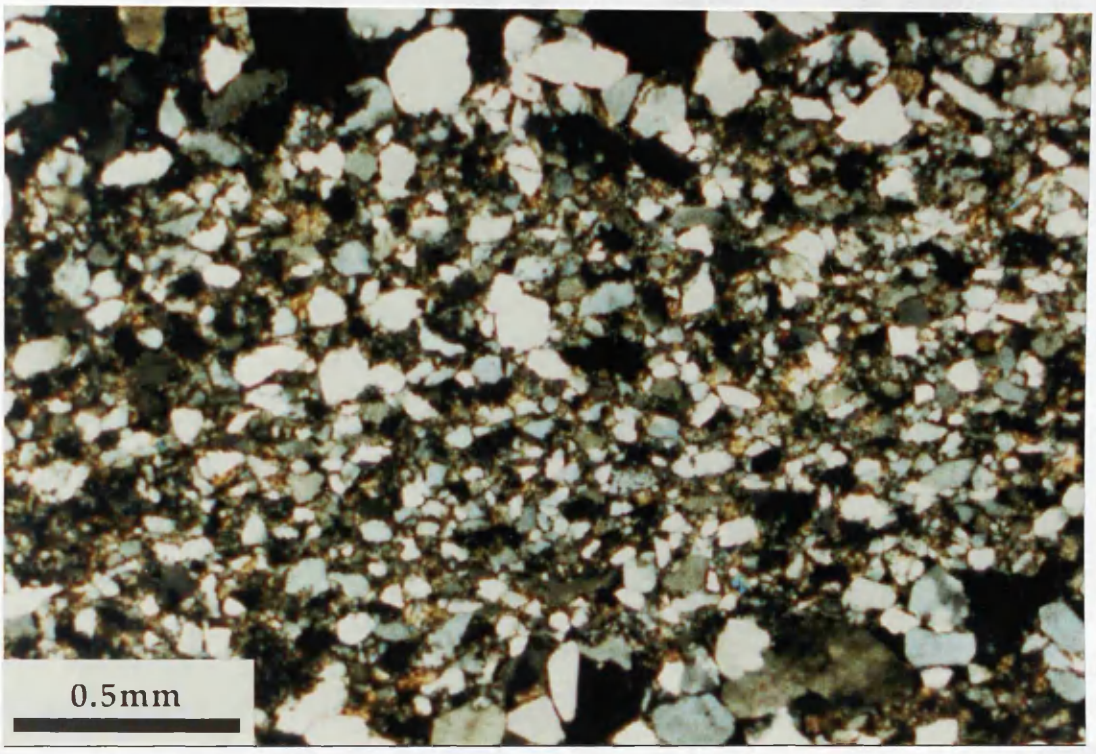

Figure 3.14 Photomicrograph showing pressure solution within highly compacted fine grained bed which has not been cemented by quartz. 49/26-6, 6754'.

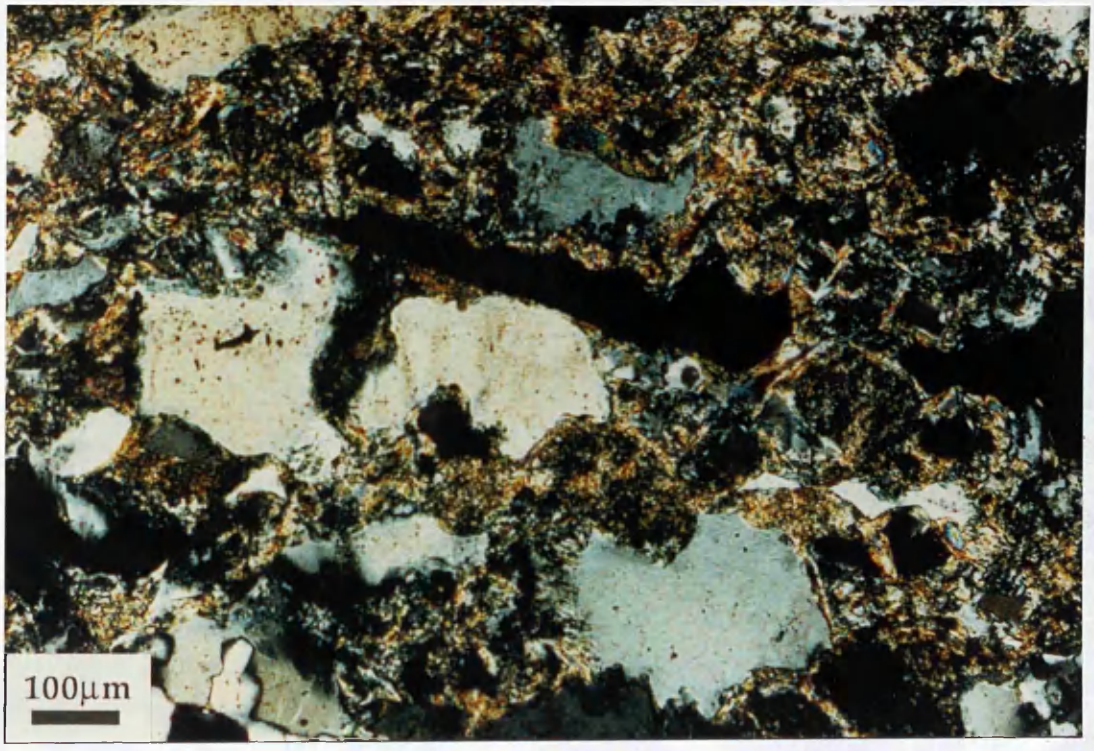

Figure 3.15 Photomicrograph showing stylolite development in clay rich horizon. Note elongate and irregular shapes of detrital grains which indicate significant quartz dissolution by pressure solution. 49/26-6, 6585'.

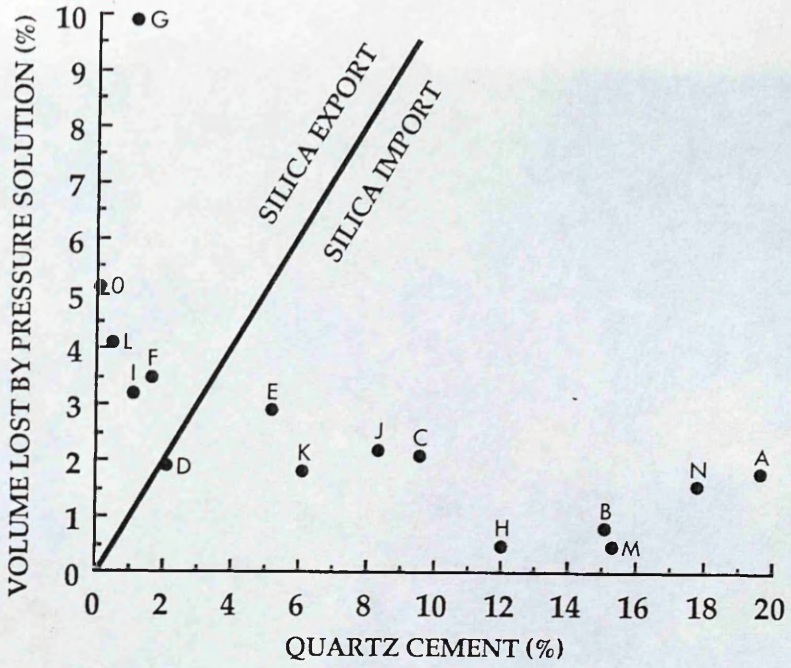

Figure 3.16 Crossplot of quartz cement versus volume of detrital grains lost by pressure solution. The line divides the samples for which volume lost by pressure solution exceeds volume quartz cement (net silica exported), from samples for which volume of quartz cement exceeds volume lost by pressure solution (net silica import). Letters A to O refer to samples listed in Table 3.4.

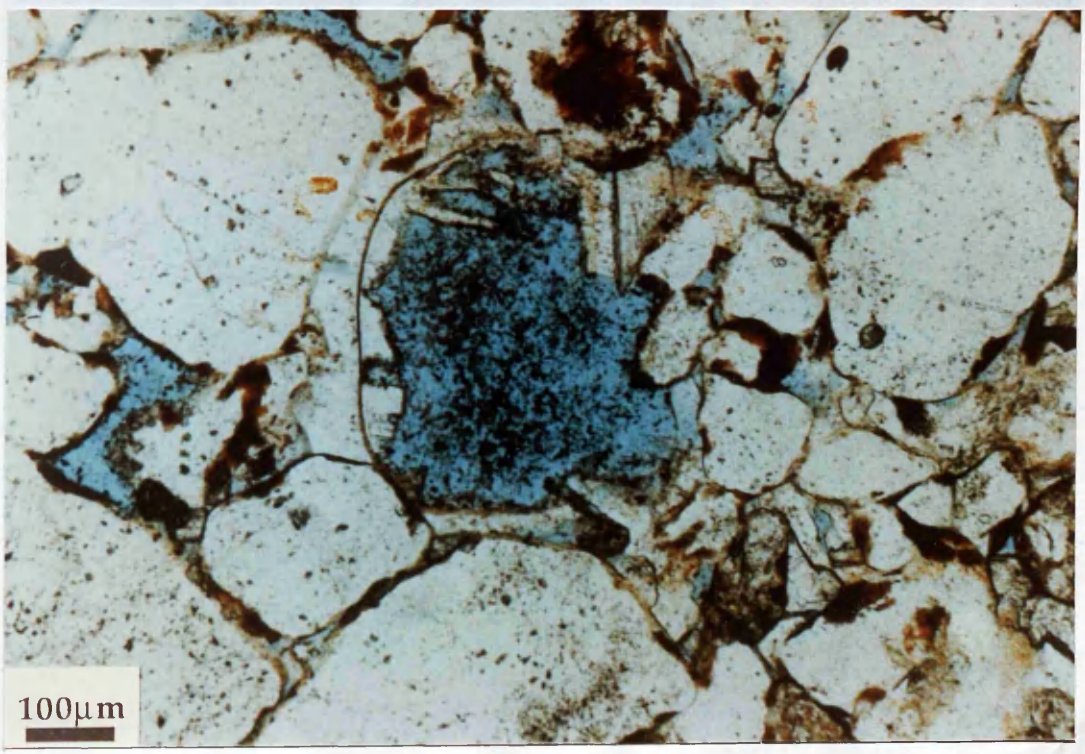

Figure 3.17 Photomicrograph of macropore produced by the near complete dissolution of a detrital plagioclase (arrow). 49/27-2, 6515'.

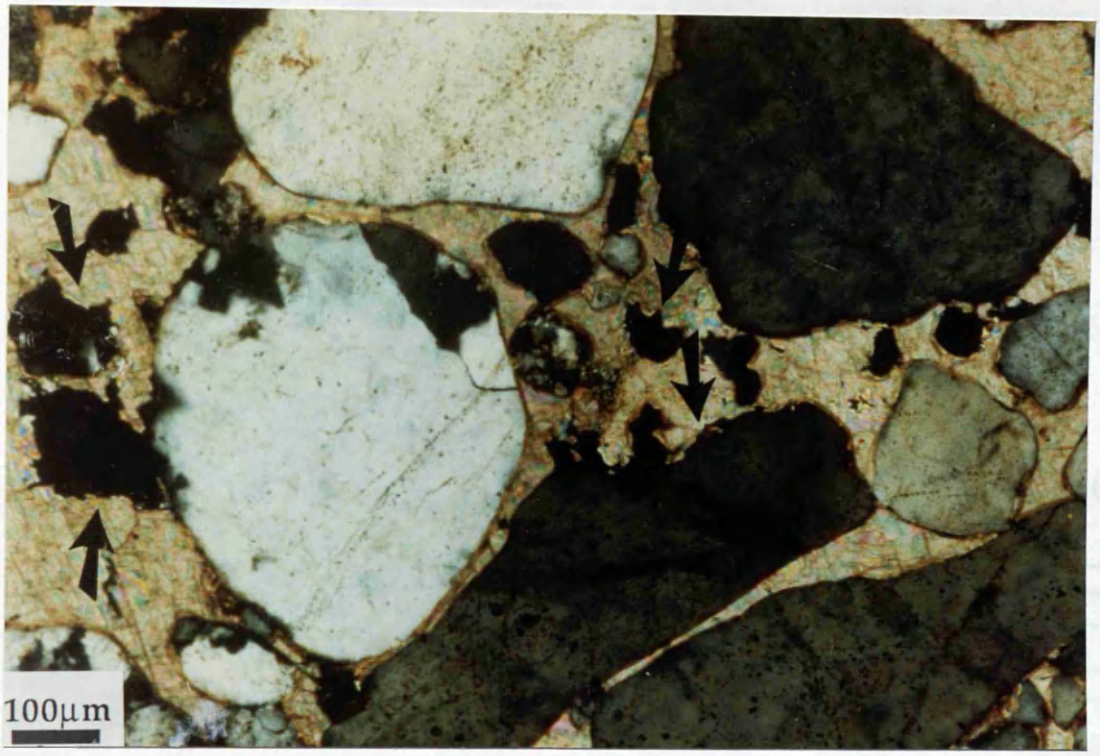

Figure 3.18 Photomicrograph showing aggressive replacement of detrital grains, especially of silt size material (arrows), by early dolomite cement. 49/26-5, 6854'.

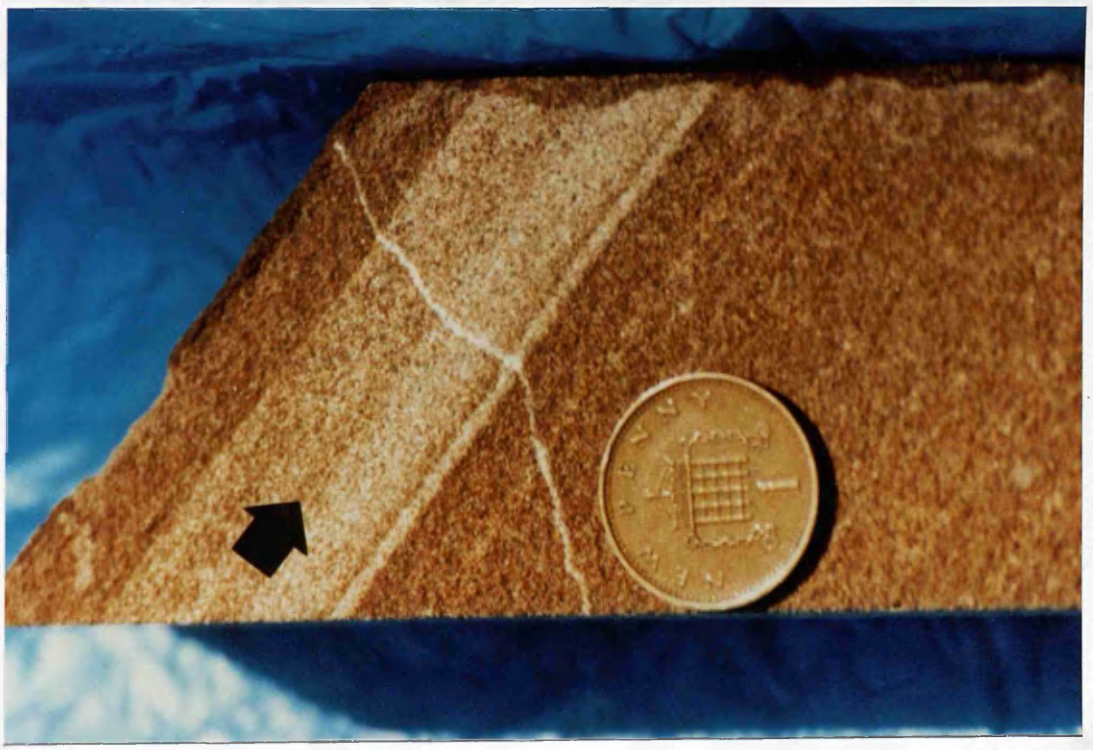

Figure 3.19 Rotliegend core photo showing selective quartz cementation along coarser grained beds (arrow). Cross-cutting this strongly silica cemented bed is a quartz mineralized fracture, suggesting faults and microfractures may have acted as conduits for silica-bearing fluids. 49/26-B240, 6933'.

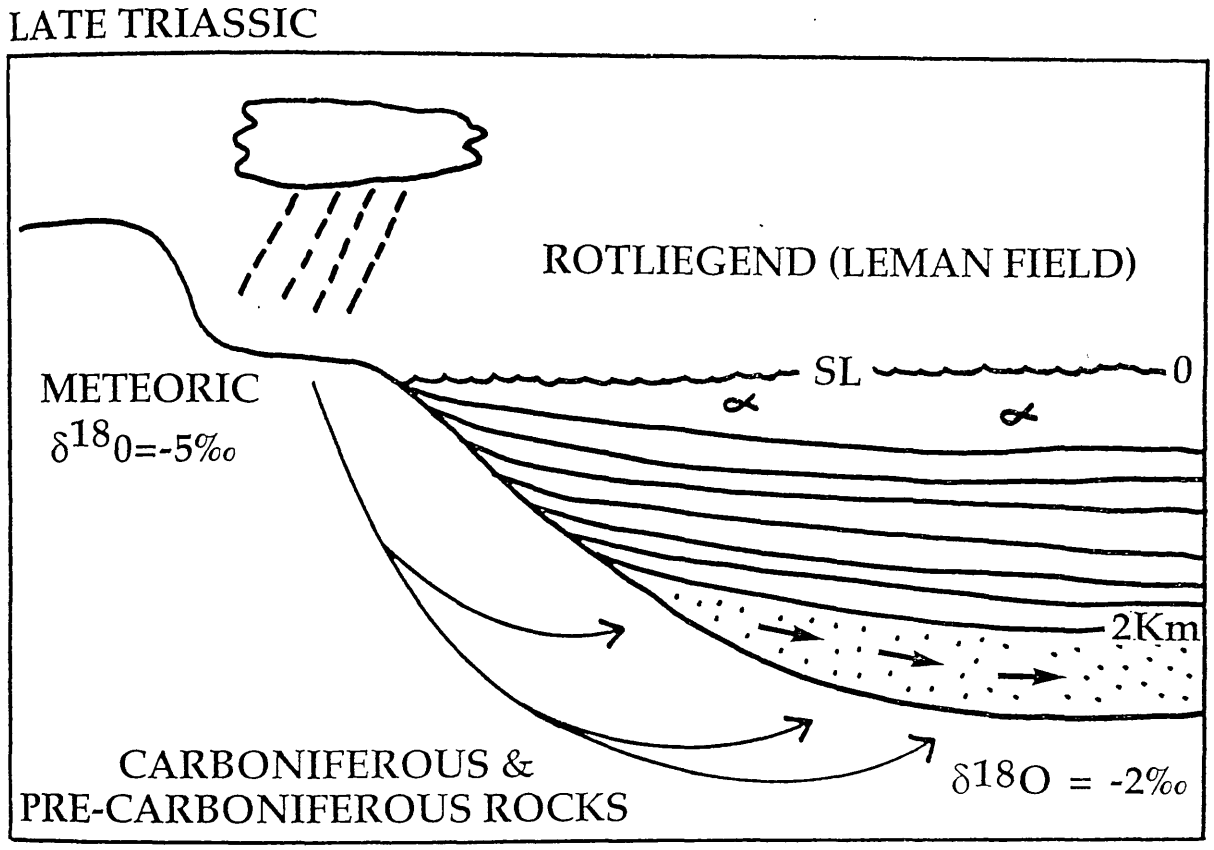

Figure 3.20 Model for flow of meteoric water into the Rotliegend by deep circulation through underlying Carboniferous and Pre-Carboniferous rocks. The water which precipitated the quartz cement was probably part of an ascending limb of a regional meteoric water circulating system, such that as the water was circulated to deeper, hotter zones it became saturated with respect to quartz and then precipitated quartz cement as it rose, cooled and became oversaturated.

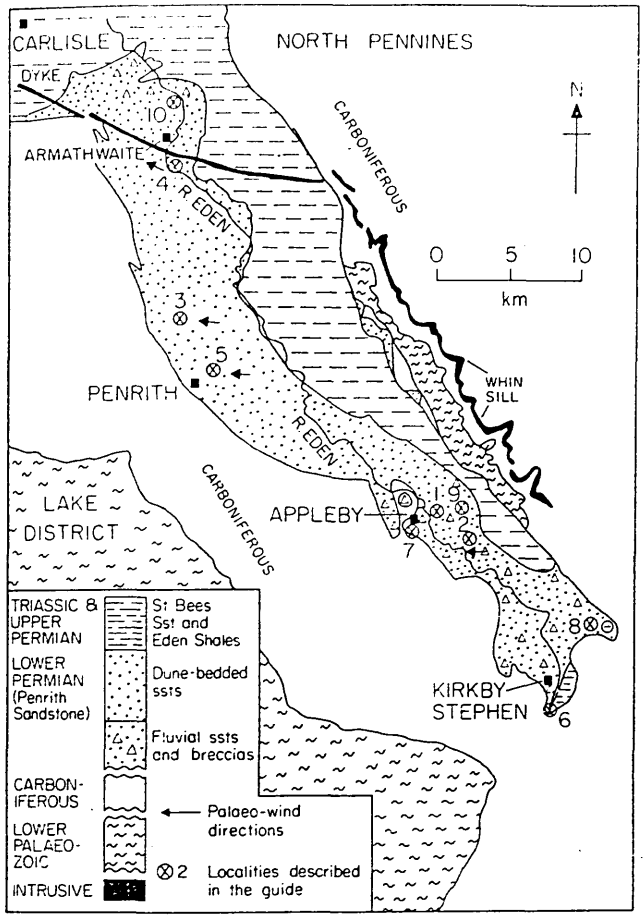

Figure 3.21 General setting of the Penrith Sandstone and Triassic rocks in NW England (Skipsey, 1989).

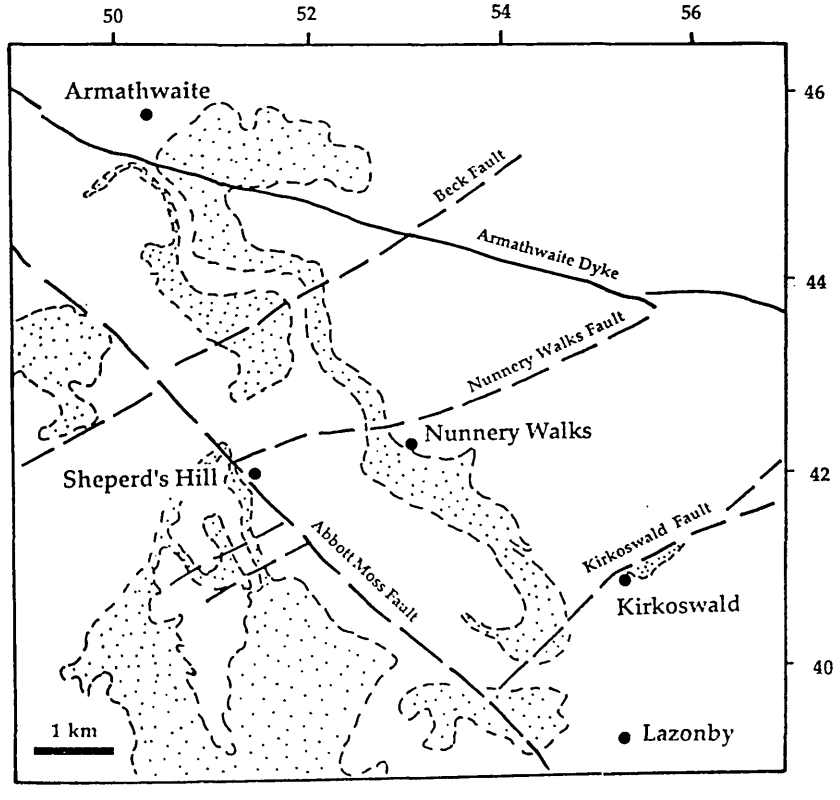

Figure 3.22 Location of field study area and major faults.

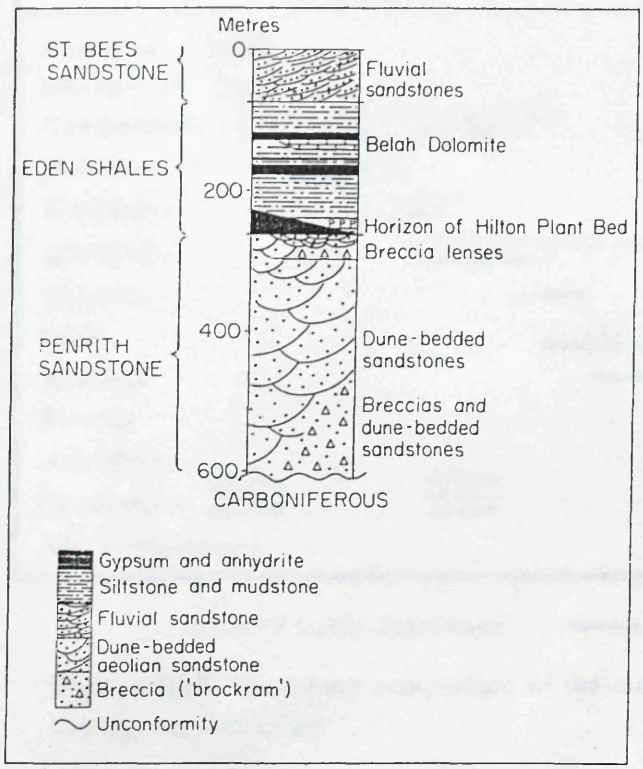

Figure 3.23 Lithostratigraphical units of the Permo-Triassic succession in the vale of Eden (from Skipsey, 1989).

Figure 3.24 Dune cross-bedding in the Penrith Sandstone, Nunnery Walks, Penrith [5275 4265].

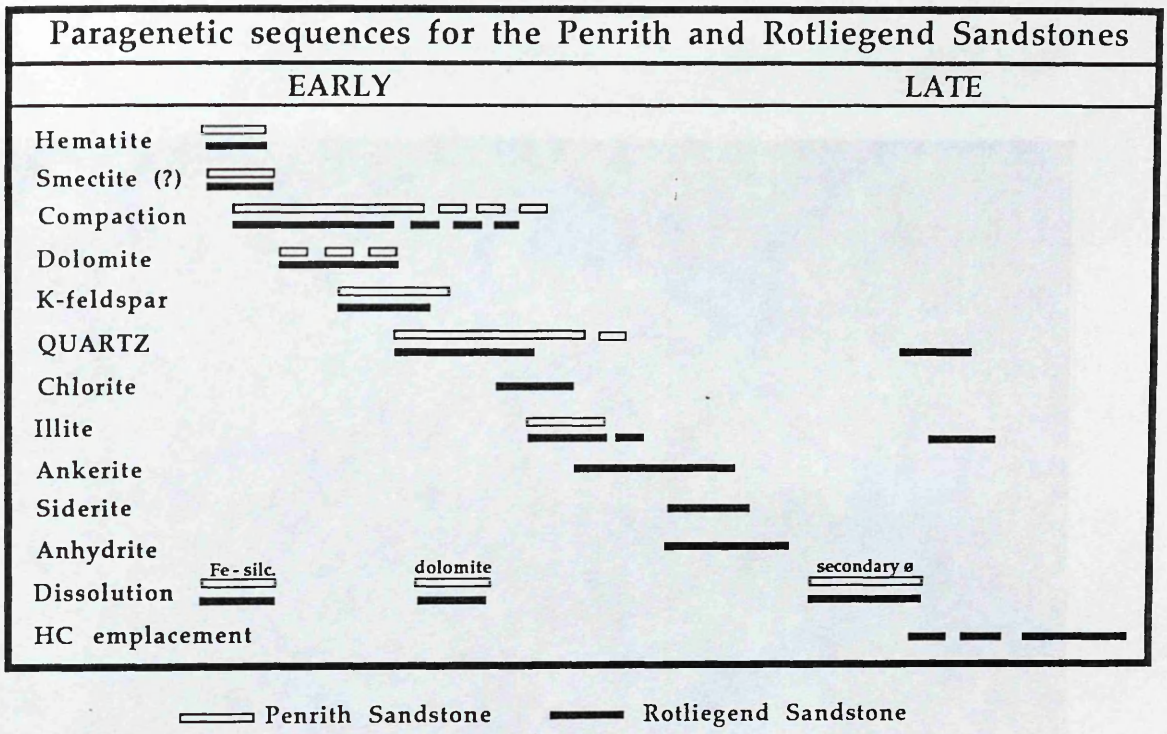

Figure 3.25 Summary comparison of the major diagenetic events in the Penrith and Rotliegend sandstones.

Figure 3.26 Strongly silica cemented dune cross-bedded sands in the Penrith with near vertical silica-filled fractures (arrow), Nunnery Walks [5235 4330].

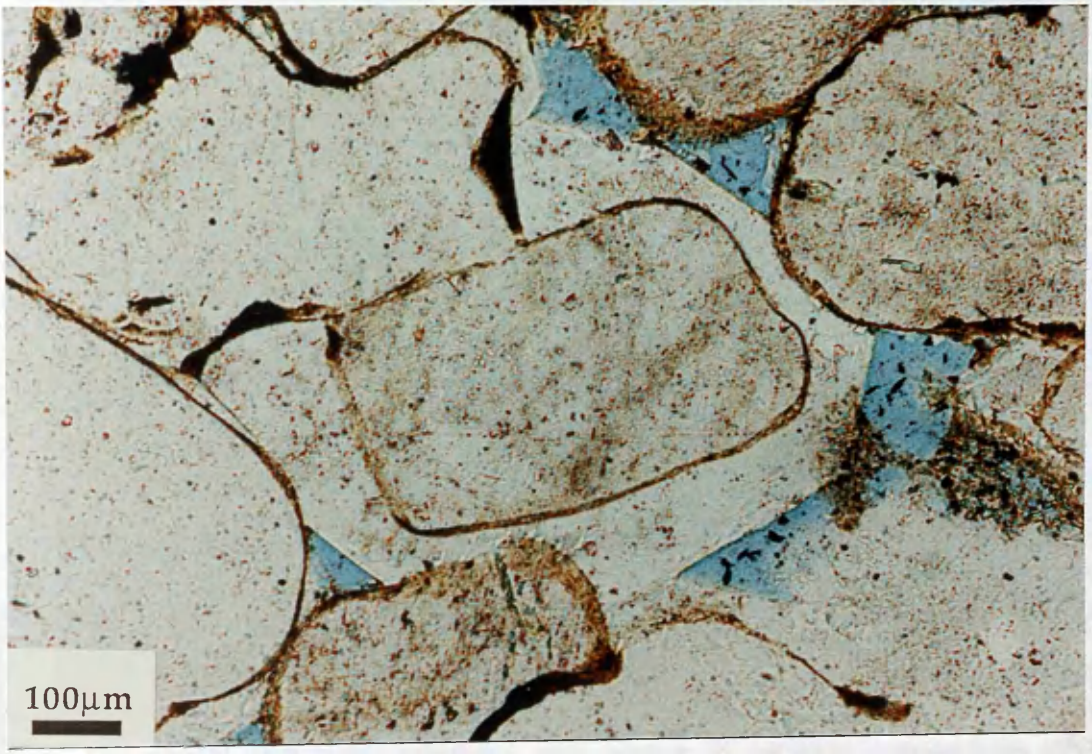

Figure 3.27 Photomicrograph of well developed quartz overgrowths. NW #5.

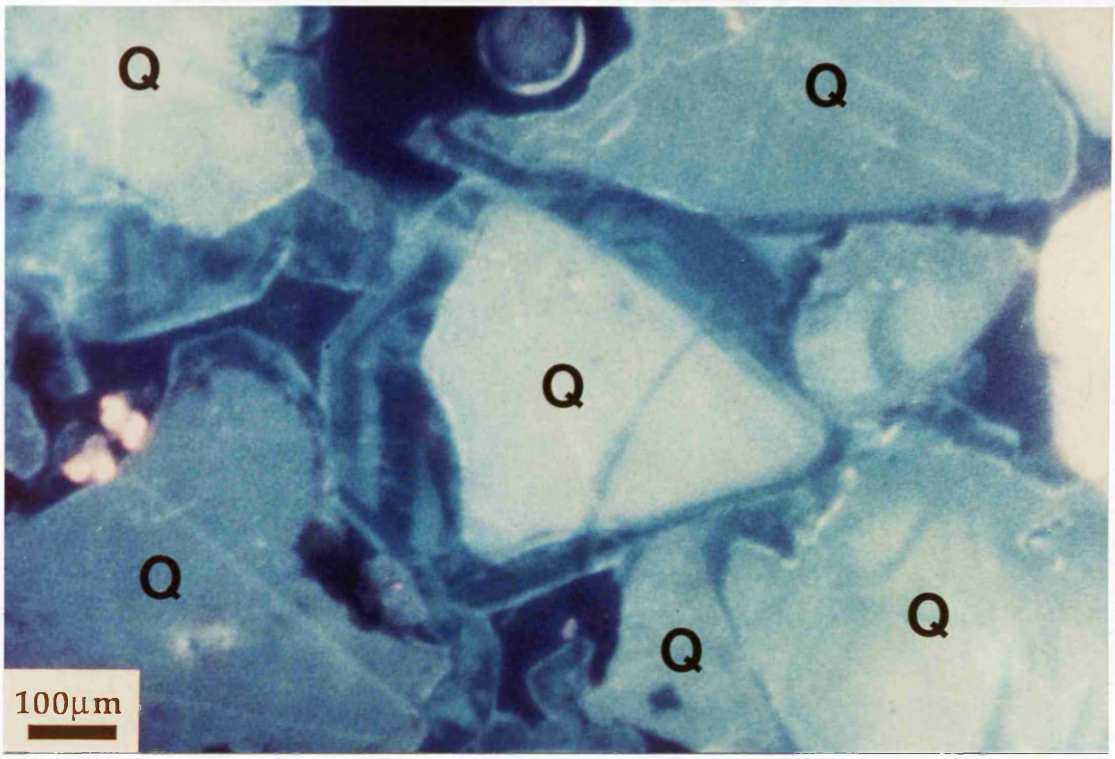

Figure 3.28 Hot-stage cathodoluminescence photomicrograph of zoned quartz cement. This zoning is similar to that observed in authigenic quartz in the Rotliegend and is thought to reflect precipitation from waters of variable composition. NW #5 approximately 30 m from Nunnery Walks Fault [5275 4260].

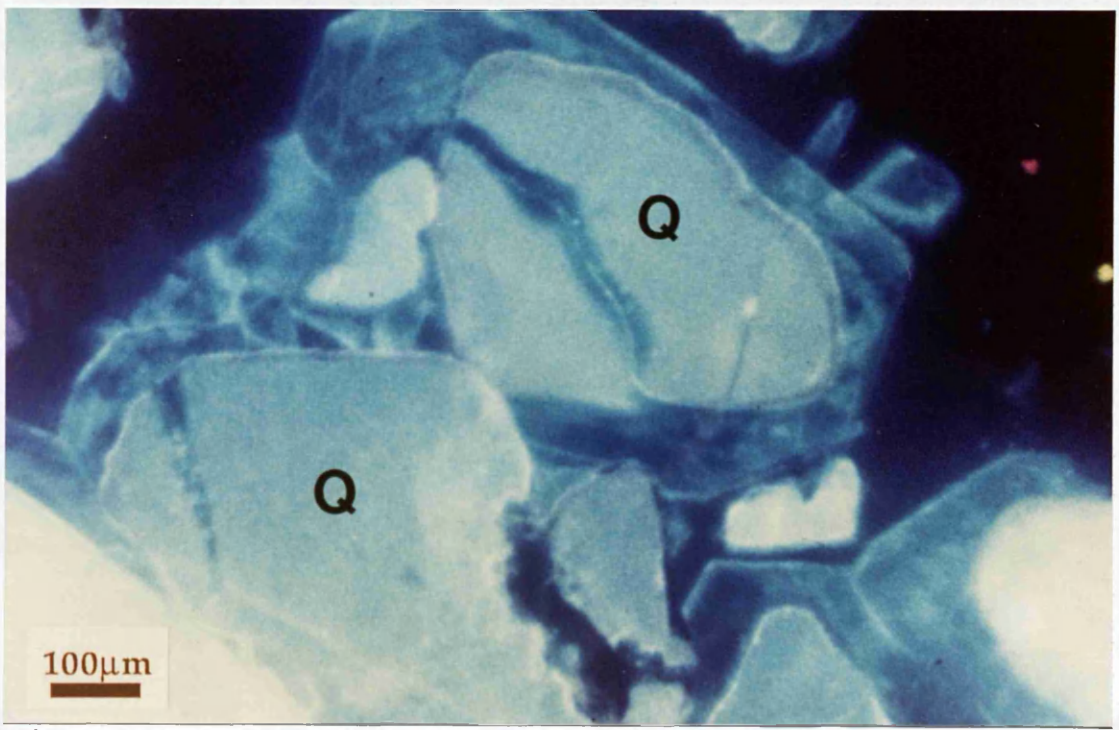

Figure 3.29 Hot-stage cathodoluminescence photomicrograph of sample grains have been cemented by quartz cement with the same luminescence colours and appearance as cement tens of metres from the fault. This suggests that faults may have acted conduits from transporting mineralizing fluids. NW #1 - 1 m from Nunnery Walks Fault [5275 4265].

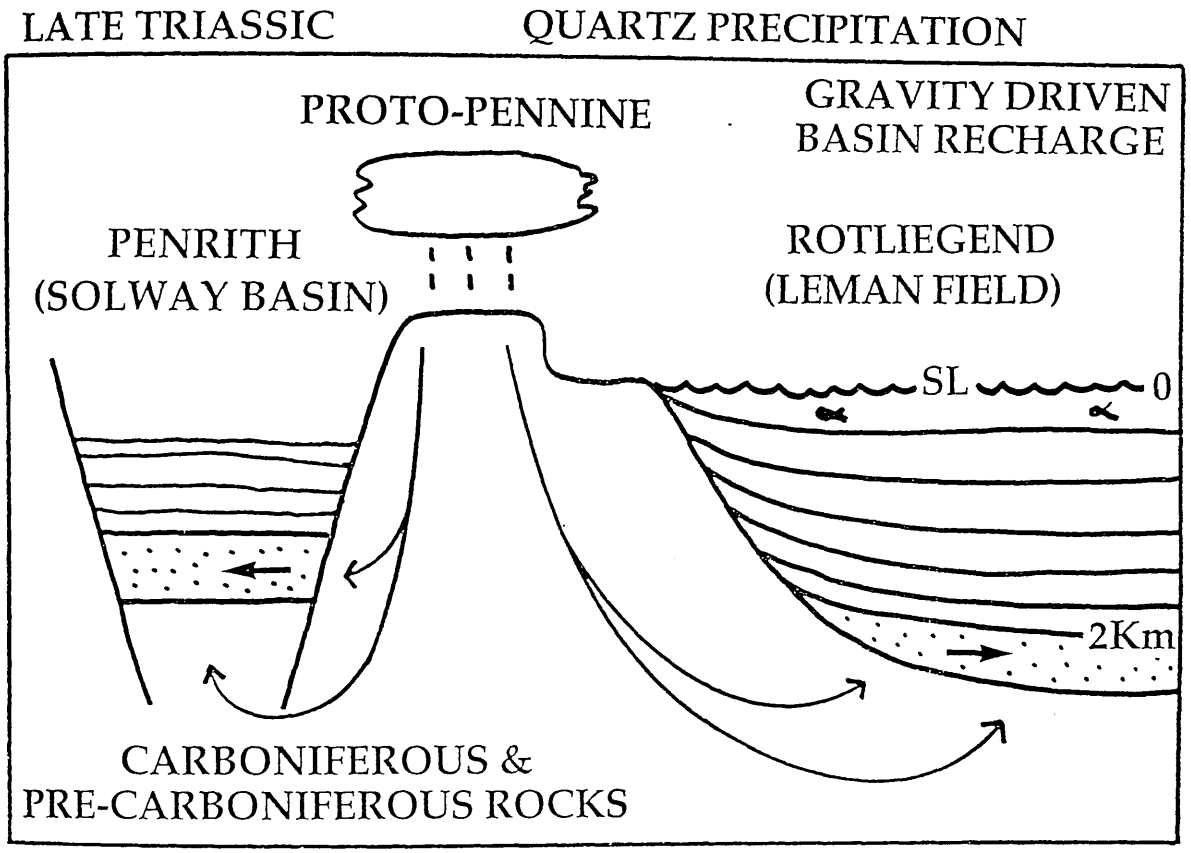

Figure 3.30 Schematic model for silica diagenesis in the Rotliegend and Penrith sandstones. Silica was imported into the Rotliegend by deep circulation of meteoric water through underlying Carboniferous and Pre-Carboniferous rocks. The water which precipitated the quartz cement was probably part of an ascending limb of a regional meteoric water circulating system, such that as the water was circulated to deeper, hotter zones it became saturated with respect to quartz and then precipitated quartz cement as it rose, cooled and became oversaturated. Fluids probably exited the basin by deep gravity driven flow and compactionally driven flow.

CHAPTER 4

ISOTOPIC EVIDENCE FOR THE ORIGIN OF LATE ANHYDRITE CEMENT IN THE ROTLIEGEND SANDSTONE, LEMAN GAS FIELD, SOUTHERN NORTH SEA

Morgan Sullivan, R. Stuart Haszeldine
Department of Geology and Applied Geology, University of Glasgow,
Glasgow G12 8QQ, Scotland

Adrian J. Boyce, Graeme Rogers, Anthony E. Fallick
Isotope Geology Unit, Scottish Universities Research and Reactor Centre,
East Kilbride, Glasgow G75 0QU, Scotland

4.1 ABSTRACT

Authigenic anhydrite is a pervasive late cement in the Rotliegend Sandstone in the Leman field, where it occurs as both intergranular poikilotopic and fracture-filling cements. Poikilotopic anhydrite is best developed along coarser grained laminae suggesting that their high porosities and permeabilities influenced its precipitation. Steeply dipping fractures filled with anhydrite are randomly distributed throughout the stratigraphic section. Both morphologies of anhydrite are interpreted as representing the same generation of cement.

$\delta^{34}S$ values for both intergranular and fracture-filling anhydrite in the Rotliegend from the Leman field are approximately +10‰, which coincides exactly with the $\delta^{34}S$ values of Late Permian Zechstein marine sulphate. The coincidence between the sulphur isotope compositions of the anhydrite in the Rotliegend and that of the Zechstein indicates that the source of the sulphate in the Rotliegend was the stratigraphically overlying Zechstein evaporites. The $^{87}Sr/^{86}Sr$ ratios of the anhydrite (0.7093 to 0.7112), however, were not derived solely from the overlying evaporites (0.7068 to 0.7070). Instead, they suggest variable mixing of more radiogenic strontium derived from diagenetic reactions in the underlying Carboniferous shales with strontium sourced from the overlying Zechstein evaporites. The oxygen isotope compositions of anhydrite cements reflect precipitation temperatures between 125° and 140°C, which are the highest possible burial temperatures for the Rotliegend Sandstone in the Leman field and would have occurred during the maximum burial depths of between 3.5 and 4 km (11,500 to 13,100 ft).

4.2 INTRODUCTION

The Lower Permian Rotliegend Sandstone consists of a sequence of continental clastic red beds that were deposited in a variety of environments including aeolian dune fields, sabkha flats, playa lakes, and

wadi (fluvial) settings typical of a tropical desert with an internal drainage system (Glennie, 1972). The Rotliegend Sandstone in the economically important Leman gas field is predominantly composed of aeolian sandstones, with only minor marine reworked and fluvial sandstones. These sandstones overlie Late Carboniferous (Westphalian) mudstones with angular unconformity, and are in turn overlain by Late Permian Zechstein anhydrite, dolomite and halite evaporites (Figure 4.1). The Leman gas field is located in UK blocks 49/26 and 49/27 (Figure 4.2), on the southern portion of the Sole Pit High, which is a major gas producing structure in the southern North Sea Basin. The petrology and diagenetic history of the Rotliegend Sandstone in the Leman field has been described by van Veen (1975), Glennie *et al.* (1978) and Arthur *et al.* (1986). The dominant reservoir sands are fine- to medium-grained subarkoses with porosities ranging from 5% to 25% (average 15%). The main diagenetic events, summarized in Figure 4.3, are dominated by compaction of sediments, precipitation of dolomite, quartz, chlorite, illite, ankerite and anhydrite cements, and development of secondary porosity. Anhydrite cementation in the Rotliegend Sandstone was studied using conventional petrography in conjunction with stable and radiogenic isotope geochemistry. This integrated approach was used to examine the controls and timing of the anhydrite cementation, and to determine whether the anhydrite was derived from remobilization of non-marine sulphate from evaporite sequences within the Rotliegend, or from marine sulphate sourced from the underlying Late Carboniferous evaporites or overlying Late Permian Zechstein evaporites.

4.3 METHODS

Preparation of sulphate samples for sulphur isotopic analysis was accomplished following the method described by Coleman and Moore (1978), in which the sulphate is directly reduced to SO_2. 10 to 15 mg of sulphate were mixed with 200 mg of Cu_2O and 600 mg of silica in an agate

mortar, powdered and placed in a silica tube with silica wool at either end to retain the sample. The silica tube containing the sample was then placed in a vacuum furnace at 1120°C and allowed to react with the Cu_2O for 30 minutes. This reaction produced both SO_2 gas and SO_3 gas, which fractionates the original $\delta^{34}S$ of the sulphate. These gases, therefore, were passed through copper gauze placed at the end of the furnace, and a copper furnace at 680°C to reduce all the SO_3 to SO_2. The SO_2 gas was purified in an extraction line to remove H_2O, CO_2 and non-condensible gases, using dry-ice/acetone, n-pentane traps and liquid nitrogen traps respectively. The yield of purified SO_2 was measured on a capacitance manometer. The gas was frozen into a sample tube and attached to a mass spectrometer manifold.

The SO_2 gas was analyzed on an ISOSPEC 64 mass spectrometer. All $\delta^{34}S$ values are reported relative to the Cannon Diablo meteorite troilite standard (CDT). Repeat analyses of inter-laboratory standards NBS123 and NZ-1 yielded mean $\delta^{34}S$ values of +17.1‰ and -0.1‰ respectively with a standard deviation (1σ) of 0.2‰.

Strontium concentrations and $^{87}Sr/^{86}Sr$ ratios were determined on powdered samples weighing 3 to 11 mg using isotope dilution techniques. Strontium was separated using standard cation-exchange chromatography, and analysed on a VG-Isomass 54E thermal ionization mass spectrometer. $^{87}Sr/^{86}Sr$ results were corrected for mass fractionation using $^{87}Sr/^{86}Sr = 0.1194$. Replicate analyses of NBS987 gave $^{87}Sr/^{86}Sr$ values of 0.71028 ±2(2σ); all data are reported relative to NBS987 $^{87}Sr/^{86}Sr = 0.71022$. Rubidium concentrations were also determined on the anhydrite in order to correct the measured $^{87}Sr/^{86}Sr$ ratios for radioactive decay since the Permian. However, in most cases the rubidium content was zero, and in others the $^{87}Rb/^{86}Sr$ ratio was so low ($<2 \times 10^{-3}$) that there was no change in the measured $^{87}Sr/^{86}Sr$ ratio with age correction. Therefore, the measured $^{87}Sr/^{86}Sr$ ratios represent the values at the time of anhydrite precipitation.

The method used for sulphate oxygen isotope extractions was

that described by Lloyd (1968). Lloyd found that in order to obtain good yields and isotopically reproducible results, sulphates had to be in the form of barium sulphate. Therefore anhydrite from the Rotliegend Sandstone was reprecipitated as barite prior to oxygen isotope extractions. Anhydrite was first dissolved in 2.5M HCl at room temperature overnight. The SO_4^{2-} ion was separated from other ions, such as Ca^{2+} and Mg^{2+}, using standard cation-exchange chromatography because enrichment of these ions can inhibit $BaSO_4$ precipitation (Sakai, 1977). $BaSO_4$ was then precipitated from a boiling solution by adding excess 0.5M $BaCl_2$, and the precipitate was filtrated off.

The oxygen of the reprecipitated sulphates was converted to CO_2 using the carbon combustion method described by Clayton and Epstein (1958) as modified by Lloyd (1968). Approximately 10 mg of reprecipitated sulphate was mixed with 10 mg of spectrographic pure graphite (1:1 weight ratio) in an agate mortar and placed in a platinum crucible. The platinum crucible containing the sample was then placed in an evacuated system, heated to 500°C for 30 minutes for degassing of sample and then gradually heated to 1000°C. Both CO_2 and CO were produced by this reaction, which fractionates the original $\delta^{18}O$ of the sulphate. CO was therefore converted to CO_2 and carbon in a platinum-electrode, high voltage (2kV) discharge vessel held at liquid nitrogen temperature. After each sample was fully reacted the CO_2 gas was passed through a dry ice-acetone trap to removed any water vapor. The CO_2 was then frozen down, using liquid nitrogen, and any non-condensible gases were pumped away. The yield of CO_2 was measured on a capacitance manometer and the purified CO_2 gas was then transferred to a sample tube and attached to the mass spectrometer manifold.

The CO_2 gas was analysed on a VG SIRA 10 mass spectrometer. $\delta^{18}O$ compositions of the anhydrite are quoted relative to SMOW (Standard Mean Ocean Water). Replicate analyses of inter-laboratory standards gave the following results: OGS-1 = +9.46±0.04‰ (1σ=3); NBS127 = +9.20±0.18‰ (1σ=3).

4.4 ANHYDRITE PETROGRAPHY

Anhydrite occurs as both intergranular poikilotopic and fracture-filling cements. It is a common late authigenic cement and ranges from 1 to 12% in abundance. Poikilotopic anhydrite is best developed along medium-grained laminae suggesting that higher porosities influenced its precipitation. Petrographic observations, such as intergranular anhydrite enclosing late authigenic ankerite and pressure-solved cemented grains (Figures 4.4 & 4.5), suggest that anhydrite formed late in the diagenetic history of the Rotliegend Sandstone. Anhydrite cemented laminae commonly display "apparent" open compactional textures, but since petrographic evidence indicates that the anhydrite is a late diagenetic phase, these open textures must result from dissolution and replacement of detrital grains and earlier cements.

Anhydrite also occurs in steeply dipping mineralized fractures. There is no concentration of fractures within one particular stratigraphic horizon and they appear to be randomly distributed throughout the Rotliegend Sandstone. Mineralized fractures are up to 0.5 cm in width, 0.5 m in length (Figure 4.6) and are filled with bladed anhydrite which has grown sub-parallel to the fracture walls (Figure 4.7). Fracture-filling anhydrite all appears to be of a single generation, suggesting that these fractures were open during mineralization, possibly due to high fluid pressure within them. If the fractures had been opened by incremental mineral growth, it would be expected that the anhydrite would have grown perpendicular to the fracture walls, and that more than one phase of growth would be observed. The fracture fill is dominated by anhydrite with only minor euhedral siderite having formed along the walls. Coarse grained laminae completely cemented by anhydrite are observed intersecting the mineralized fractures which suggests that fluids moved from the fractures into high permeability zones within the sandstones (Figure 4.8). This textural evidence suggests that the intergranular and fracture-filling anhydrite represent the same generation of cementation.

4.5 ISOTOPE GEOCHEMISTRY

4.5.1 Sulphur

$\delta^{34}S$ values were measured for twenty-two samples of intergranular and fracture-filling anhydrite from the aeolian facies of the Rotliegend Sandstone in order to investigate the source of this sulphate (Table 4.1). Several possible sources of sulphate in the Rotliegend are modelled (Figure 4.9): the dissolution of Carboniferous evaporites with a $\delta^{34}S$ value between +15 to +25‰ (Claypool *et al.*, 1980), oxidation of sulphides from shales, hydrothermal veins and igneous rocks $\delta^{34}S$ = –40 to +5‰ (Kaplan, 1984), remobilization of non-marine sulphate from evaporites within the Rotliegend Sandstone +4 to 10‰ (Holser, 1979), and hydrothermally and volcanically derived sulphur δ^{34} = –10 to –15‰ (Holser and Kaplan, 1966), and remobilization of Late Permian Zechstein marine sulphate $\delta^{34}S$ = +10‰ (Claypool *et al.*, 1980; Taylor, 1983). Glennie *et al.* (1978) suggested that the anhydrite in the Rotliegend was derived from fluids moving along faults and zones of high permeability from the Zechstein evaporites during basin inversion in the Cretaceous. If this is so, then the sulphur isotope values of the Rotliegend anhydrite should be similar to the isotopic composition of the Late Permian seas, (i.e. +10‰; Claypool *et al.*, 1980).

$\delta^{34}S$ results ranged from +9.10 to 11.0.‰ (CDT), with an average value of +10.3‰, for both occurrences of anhydrite in the Rotliegend Sandstone (see Table 4.1). This narrow range of isotopic compositions strongly suggests that both the intergranular and fracture-filling anhydrite had the same homogeneous source of sulphate. The sulphur isotopic values of the anhydrite in the Leman field are identical to those of Late Permian marine sulphate which are between +10‰ (Claypool *et al.*, 1980) and +10.5‰ (Taylor, 1983). If the sulphate in the Rotliegend had been derived from continental waters then the $\delta^{34}S$ values would have reflected dissolution of Late Carboniferous marine sulphate (+15 to

+25‰), the oxidation of earlier sulphides from exposed shales (average value = –12‰), or possibly a mixture of the two.

Holser (1979) reported $\delta^{34}S$ compositions for anhydrite from evaporites associated with the playa lake deposits in Lower Permian Rotliegend Sandstone of +6.9‰ (15 samples from Germany) and +7.8±3.4‰ (84 samples from the Netherlands). These values are well below Lower Permian age marine sulphate sulphur isotopic compositions ($\delta^{34}S$ = +12‰) reported by Claypool *et al.* (1980). The sulphur isotope compositions for the anhydrite from the evaporites associated with the playa lake deposits have, therefore, been interpreted to be of non-marine origin, resulting from the mixing of isotopically heavy sulphate from the dissolution of older marine evaporites and isotopically light sulphate from the weathering and oxidation of sulphides in exposed shales (Holser, 1979). This indicates that non-marine waters in the playa lake environment within the Rotliegend basin, which precipitated the early anhydrite in Germany and the Netherlands, had more depleted sulphur isotopic compositions than the fluids from which the late anhydrite (+10.3‰) in the aeolian Rotliegend Sandstone in the Leman field precipitated, and could not have been the source of sulphate in the Leman field.

The correlation between the sulphur isotopic composition of the intergranular and fracture-filling anhydrite in the Rotliegend, and that of the Zechstein marine sulphate is excellent, all with $\delta^{34}S$ compositions of approximately +10‰. This, therefore, strongly implies that the source of the sulphate in the Rotliegend Sandstone in the Leman field was the overlying Late Permian Zechstein evaporites, and that access for fluid movement was possible via faults and zones of high permeability related to tectonic activity.

4.5.2 Strontium

The strontium isotopic compositions of four samples of

intergranular anhydrite and two of fracture-filling anhydrite (Figure 4.1) are comparable to those reported by Sullivan *et al.* (1990) for the late phase ankerite (0.7089 to 0.7110), but higher than the early dolomite (0.7077 to 0.7087) from the Rotliegend Sandstone (Figure 4.10). Strontium isotope ratios for the intergranular anhydrite range from 0.7093 to 0.7098 with strontium concentrations between 1000 and 1559 ppm, and those of the two fracture-filling anhydrite samples are 0.7111 and 0.7112 with concentrations of 2235 ppm and 2148 ppm respectively (Table 4.1). The strontium isotopic compositions of the fracture-filling phase of anhydrite are significantly more radiogenic than those of the intergranular anhydrite, suggesting that anhydrite in the fractures was precipitated from a fluid with a larger component of radiogenic strontium. The strontium concentrations of the fracture-filling anhydrite are also significantly higher, almost double in some cases, than those of the non-fracture anhydrite. This indicates that strontium concentrations of the fluids in the fractures were much higher than in the Rotliegend porewaters, possibly due to the larger input of radiogenic strontium.

Strontium isotope ratios for the both intergranular and fracture-filling anhydrite are much higher than Late Permian seawater ($^{87}Sr/^{86}Sr$ = 0.7068 to 0.7070; Burke *et al.*, 1982), so this can not be the sole source of the strontium in the anhydrite. Nor can the strontium be derived exclusively from unmodified fluids expelled from the underlying shales as these would reflect Late Carboniferous seawater ($^{87}Sr/^{86}Sr$ = 0.7085; Burke *et al.*, 1982). The strontium isotope values of both occurrences of anhydrite therefore reflect an input of radiogenic strontium, together marine-derived strontium. Dissolution of detrital silicates (feldspar, mica), which typically have $^{87}Sr/^{86}Sr$ ratios of 0.720 (Faure, 1986), would have been a source of enriched radiogenic strontium. Although there is a recognized phase of feldspar dissolution in the Rotliegend, it post-dates anhydrite precipitation (Figure 4.3) and is therefore unlikely to have supplied strontium to anhydrite. Also, the Rotliegend is a well-sorted wind-blown deposit containing very little muscovite or biotite. The

minor amount of mica it does contain is very fresh and shows no sign of dissolution. Therefore, the high radiogenic strontium component of the anhydrite was not supplied by diagenetic reactions within the Rotliegend, but instead was most likely derived from the underlying Carboniferous shales. It is also possible that the low $^{87}Sr/^{86}Sr$ component could have been derived from the underlying Upper Carboniferous sediments (0.7085) though the interpretation of carbon and strontium isotope data from dolomite and ankerite cements suggests that the remobilization Late Permian seawater-derived strontium privided the main low $^{87}Sr/^{86}Sr$ component (Sullivan *et. al.*, 1990). As it is thought that ankerite and anhydrite formed penecontemporaneously (Figure 4.3) it is reasonable to assume that Late Permian seawater was also the main source of low $^{87}Sr/^{86}Sr$ for the anhydrite.

4.5.3 Oxygen

Anhydrite cementation was one of the last important diagenetic events to affect the Rotliegend Sandstone in the Leman field. The oxygen isotopic composition of ten samples of intergranular and fracture-filling anhydrite was measured in order to understand more precisely the late diagenetic conditions in the Rotliegend Sandstone. The $\delta^{18}O$ values of the intergranular and fracture-filling anhydrites range from +14.04 to 15.99‰ (SMOW) (Table 4.1). Since petrographic evidence suggests that ankerite and anhydrite cements in the Rotliegend formed penecontemporaneously (Figure 4.3), and Sr isotopic compositions for both minerals are similar, the waters from which the anhydrite precipitated are assumed to have had an oxygen isotopic composition similar to that of the waters which precipitated the late phase ankerite (approximately 0‰ SMOW, see section 2.8.1).

The temperatures of anhydrite precipitation were calculated from the following oxygen-isotope fractionation equation for anhydrite-water:

$$(\delta_a - \delta_w) = 3.21 \times 10^6(T^{-2}) - 4.72 \quad \text{(Chiba } et\ al.\text{, 1981)}$$

where δ_a = oxygen isotope composition of the anhydrite (relative to SMOW), δ_w = oxygen isotope composition of the water from which the anhydrite precipitated (relative to SMOW) and T = the temperature of formation in degrees Kelvin. Assuming the anhydrite did precipitate in equilibrium with water with an oxygen isotopic composition of approximately 0‰ (SMOW), then the isotope equilibration temperatures for anhydrite precipitation would have ranged from 125° to 140°C (Figure 4.11). These temperatures would have been attained at burial depths of approximately 3.5 to 4 km (11,500 to 13,100 ft), which correspond to the maximum burial depths estimated by Marie (1975), Glennie *et al.*, (1978), Cope (1986), and Bulat and Stoker (1987) for the Rotliegend Sandstone in the Leman field (Figure 4.12).

4.6 CONCLUSIONS

Intergranular and fracture-filling anhydrites are late authigenic cements that were precipitated from similar diagenetic fluids. $\delta^{34}S$ values for both intergranular and fracture-filling anhydrite in the Rotliegend Sandstone from the Leman field are approximately +10‰ and indicate that the source of the sulphate was the stratigraphically overlying Zechstein marine evaporites, and not remobilization of sulphate from evaporites either within the Rotliegend or from the Carboniferous beneath. The strontium isotopic compositions of the anhydrite (0.7093 to 0.7112), however, were not derived solely from the overlying evaporites and instead suggest a mixing of radiogenic strontium from the underlying Carboniferous ($^{87}Sr/^{86}Sr$ = 0.720) with strontium derived from the Zechstein evaporites ($^{87}Sr/^{86}Sr$ = 0.7070). The oxygen isotope compositions of anhydrite cements reflect precipitation temperatures between 120° and 140°C, which occurred in the Leman field during maximum burial of the Rotliegend at depths of between 3.5 and 4 km (11,500 to 13,100 ft).

4.7 ACKNOWLEDGEMENTS

Supported by funds from Amoco (UK) Exploration and Shell/Esso U.K. Exploration and Production. This research was carried out at the Department of Geology and Applied Geology, University of Glasgow, and the Isotope Geology Unit, Scottish Universities Research and Reactor Centre (SURRC). Core was supplied by the British Geological Survey and by Shell/Esso. The authors thank Douglas Maclean (Glasgow University) for his assistance with the production of photographic plates. The SURRC is supported by Natural Environment Research Council of Britain and the Scottish Universities.

4.8 REFERENCES CITED

Arthur, T.J., Pilling, D., Bush, D., and Macchi, L., 1986, The Leman Sandstone Formation in U.K. block 49/28: Sedimentation, diagenesis and burial history. In: *Habitat of Palaeozoic Gas in N.W. Europe*. Brooks, J., Goff, J. and van Hoorne, B. (eds). *Spec. Publs. Geol. Soc.* **23,** Scottish Academic Press, London, 251-266.

Burke, W.M., Denison, R.E, Hetherington, E.A., Koepnick, R.B., Nelson, M.F. and Otto, J.B., 1982. Variation of sea-water $^{87}Sr/^{86}Sr$ throughout Phanerozoic time. *Geology,* **10,** 516-519.

Bulat, J. and Stoker, S.J., 1987. Uplift determination from interval velocity studies, UK, southern North Sea. *Petroleum Geology of North West Europe*. Brooks, J. and Glennie, K.W. (eds). Graham and Trotman, London, 293-306.

Chiba, H., Kusakabe, M., Hirano, S., Matsuo, S., and Somiya, S., 1981. Oxygen isotope fractionation factors between anhydrite and water from 100°C to 550°C. *Earth and Planet. Sci. Lett.*, **53,** 55-62.

Claypool, G.E. , Holser, W.T., Kaplan, I.R. , Sakai, H. and Zak, I. 1980. The age curve of sulphur and oxygen isotopes in marine sulphate and their mutual interpretation. *Chem. Geol.*, **50,** 1594-159.

Clayton, R.N. and Epstein, S., 1958. The relationship between O^{18}/O^{16} ratios in coexisting quartz, carbonate and iron oxides from various geological deposits. *Geology,* **66,** 352-371.

Coleman, M.L. and Moore, M.P. 1978. Direct reduction of sulphates to sulphur dioxide for isotopic analysis. *Anal. Chem.*, **28,** 199-260.

Cope, M.J. 1986. An interpretation of vitrinite reflectance data from the southern North Sea Basin. In: *Habitat of Palaeozoic Gas in N.W. Europe*. Brooks, J., Goff, J. and van Hoorne, B. (eds). *Spec. Publs Geol. Soc.*, **23,** Scottish Academic Press, 85-101.

Glennie, K.W. 1972. Permian Rotliegendes of Northwest Europe interpreted in light of modern desert sedimentation studies. *Bull. Am. Ass. Petrol. Geol.*, **56,** 1048-1071.

Glennie, K.W., 1990. Lower Permian—Rotliegend. In: *Introduction to the Petroleum Geology of the North Sea* (3rd edition). Glennie, K.W. (ed.), Blackwell Scientific Publications, Oxford, 120-152.

Glennie, K.W., Mudd, G.C. and Nagtegaal, P.J.C. 1978. Depositional environment and diagenesis of Permian Rotliegendes sandstones in Leman Bank and Sole Pit areas of the U.K. Southern North Sea. *Jour. Geol. Soc. London,* **135**, 25-34.

Holser, W.T., 1979. Rotliegend evaporites, Lower Permian Northwestern Europe. *Petrochemie vereinigt mit Brennstoff-Chemie,* **34**, 159-162.

Holser, W.T. and Kaplan, I.R., 1966. Isotope geochemistry of sedimentary sulphates. *Chem. Geol.,* **1**, 93-135.

Lloyd, R.M., 1968. Oxygen isotope behavior in the sulphate-water system. *Jour. of Geophys.Res.,* **73**, 6099-6110.

Marie, J.P.P. 1975. Rotliegendes stratigraphy and diagenesis. In: *Petroleum and the Continental Shelf of North West Europe,* Woodland, A.W. (ed.). *Appl. Sci. Publ.,* London, 205-211.

Sakai, H., 1977. Sulfate-water isotope thermometry applied to geothermal systems. *Geothermics,* **5**, 67-74.

Sullivan, M.D., Haszeldine, R.S., and Fallick, A.E., 1990, Linear coupling of carbon and strontium isotopes in Rotliegend Sandstone, North Sea: Evidence for cross-formational fluid flow. *Geology,* **18**, 1215-1218.

Taylor, S.R. 1983. A stable isotope study of the Mercia Mudstones (Keuper Marl) and associated sulphate horizons in the English Midlands. *Sedimentology,* **30**, 11-31.

van Veen, F.R. 1975. Geology of the Leman gas field. In: *Petroleum and the Continental Shelf of North West Europe,* Woodland, A.W. (ed.). *Appl. Sci. Publ.,* London, 223-231.

Veizer, J., Holser, W.T., and Wilgus, C.K., 1980. Correlation of $^{13}C/^{12}C$ and $^{34}S/^{32}S$ secular variations. *Geochim. Cosmochim. Acta,* **44**, 579-587.

4.9 TABLES

Table 4.1 Summary of data on anhydrite cement and fracture fill from the Rotliegend Sandstone, Leman gas field, Quadrant 49.

Well no.	Depth (feet)	$\delta^{34}S$ (‰ CDT)	$\delta^{18}O$ (‰ SMOW)	Sr (ppm)	$^{87}Sr/^{86}Sr$ $\pm 2(2\sigma)$	Type of anhydrite
26-5	6565.5	+10.2				cement
26-5	6565.5	+10.0	+14.86	2235	0.7111	fracture
26-25	6471	+10.7				cement
26-25	6854	+9.8				cement
26-26	6395	+9.5	+15.99	1000	0.7094	cement
26-26	6463	+10.2	+14.97			cement
26-26	6606	+10.4	+14.27	2149	0.7112	fracture
26-26	6677	+9.8	+15.13			cement
26-26	6982	+10.8	+14.99	1559	0.7095	cement
26-26	6996	+9.9	+14.04			cement
26-26	7066	+11.0	+15.24	1518	0.7098	cement
27-2	6305	+9.8	+15.62	1207	0.7093	cement
27-2	6737	+10.0				cement
27-2	6922	+10.1				cement
27-2	6922	+10.6				fracture
27-3	6286	+9.1	+14.98			cement
27-3	6463	+10.56				cement
27-4	6670	+9.84				cement
27-4	6778	+10.10				cement
27-4	6851	+10.39				cement
27-4	6881	+10.25				cement

4.10 FIGURES AND FIGURE CAPTIONS

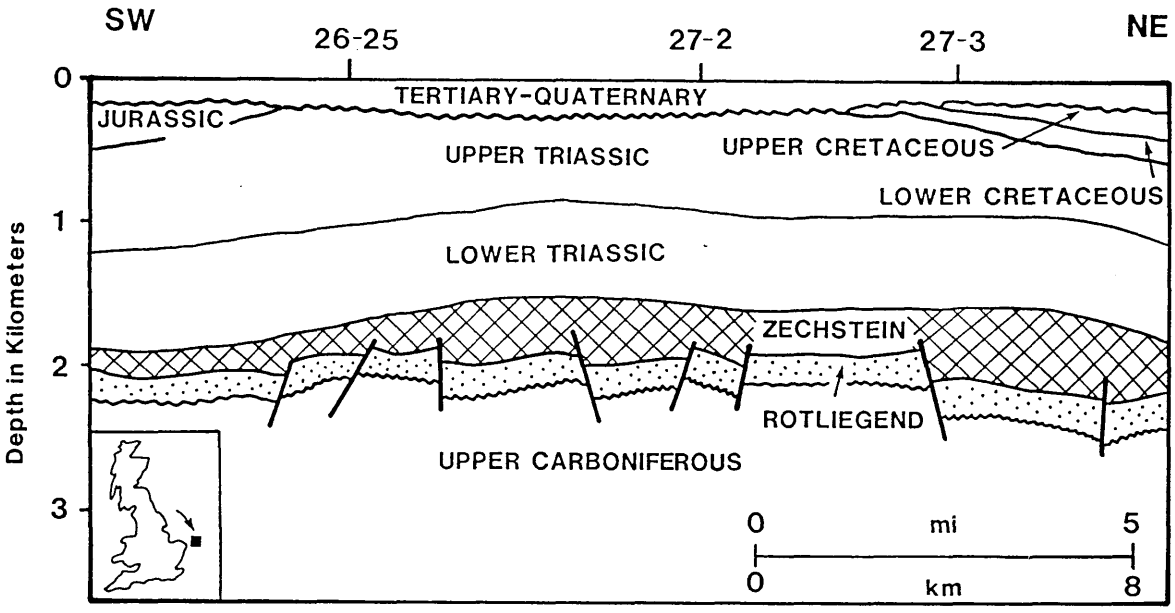

Figure 4.1 Location of Leman gas field (North Sea) and geologic cross section for the Leman region (after Glennie 1990).

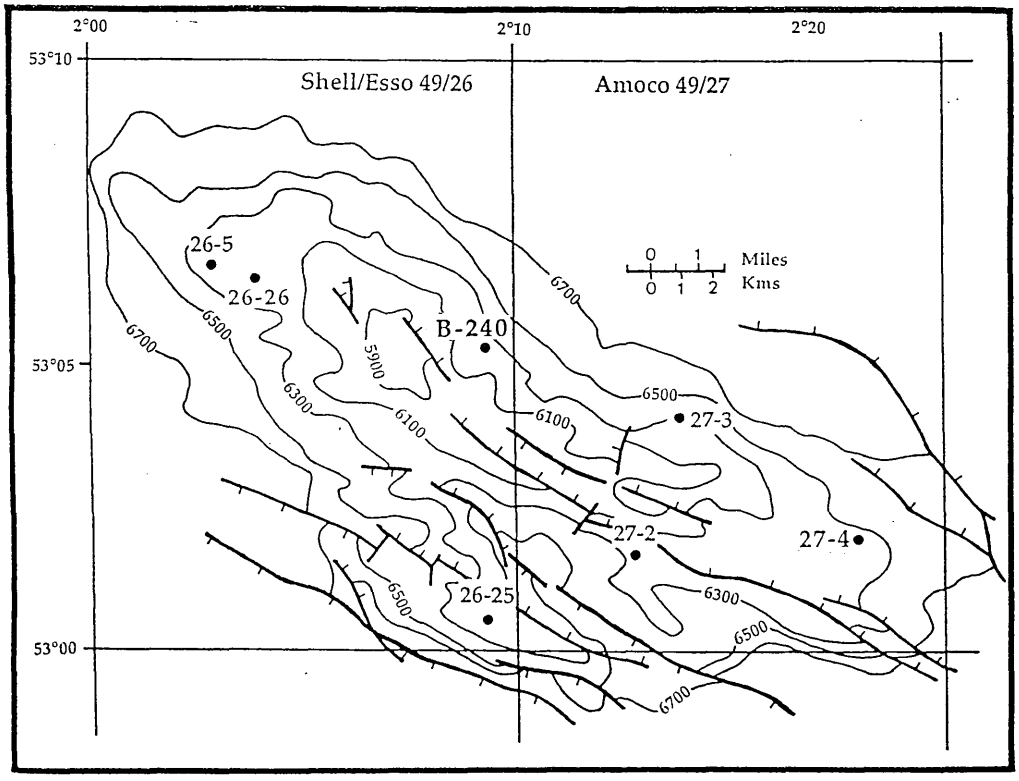

Figure 4.2 Present interpretation of Leman field, showing contours of the the top of the Rotliegend in feet below sea level and locations of wells used in this study (from van Veen, 1975).

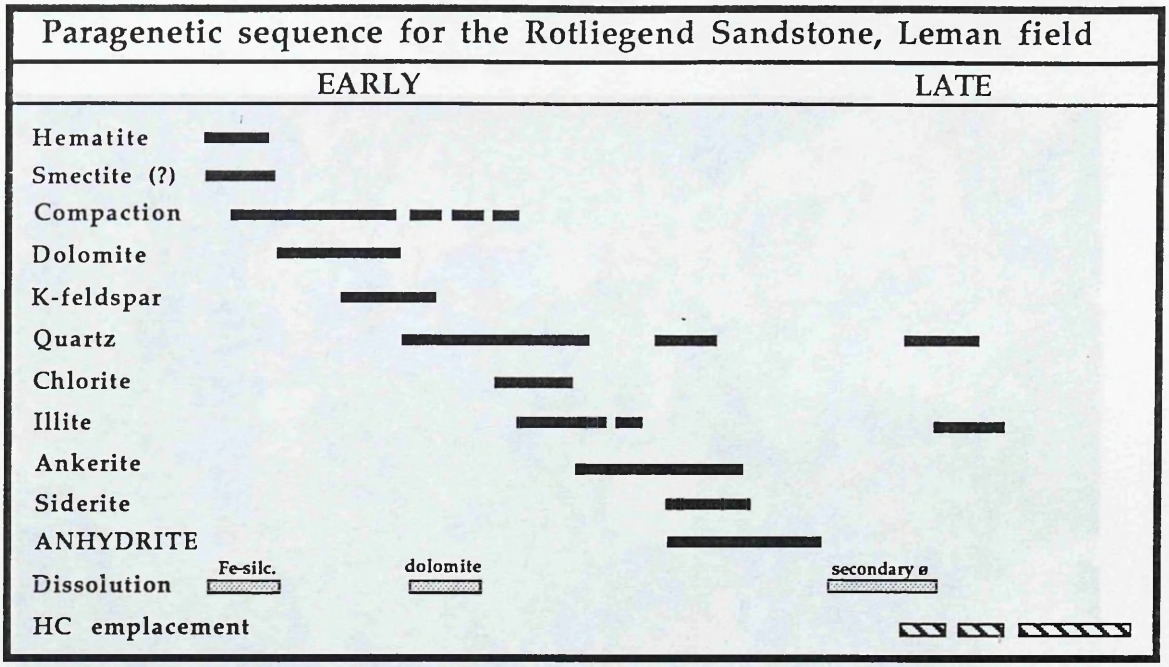

Figure 4.3 Paragenetic sequence showing timing of major diagenetic events in the Lower Permian Rotliegend Sandstone in the Leman gas field.

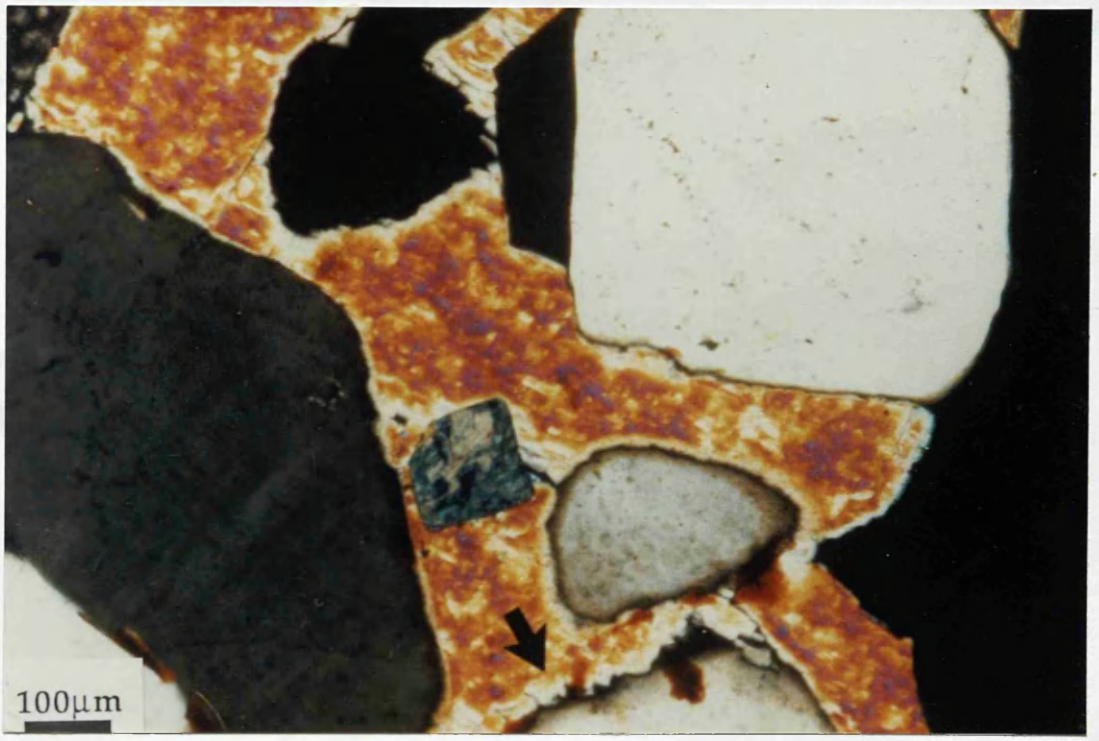

Figure 4.4 Photomicrograph of poikilotopic anhydrite enclosing late ankerite (stained blue). Note aggressive replacement of detrital quartz grains by anhydrite (arrow). Well 49/27–2, 6910'.

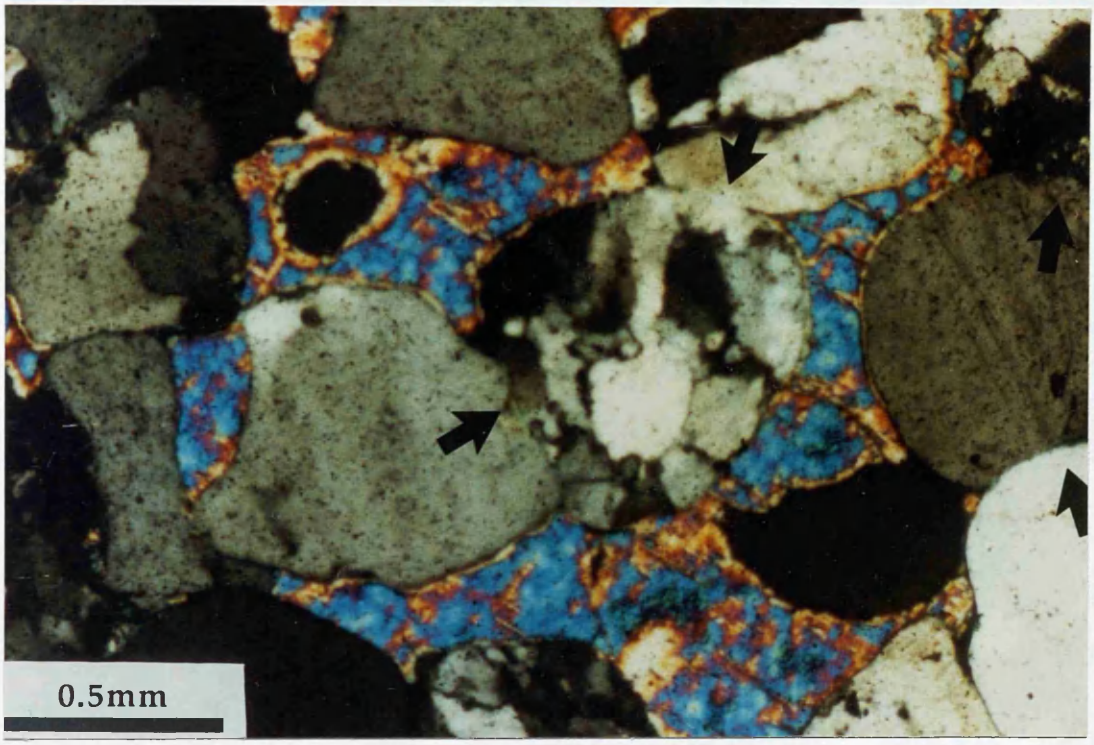

Figure 4.5 Photomicrograph of poikilotopic anhydrite with cemented framework grains displaying evidence of pressure solution and grain suturing (arrows). Well 49/27-2, 6305'.

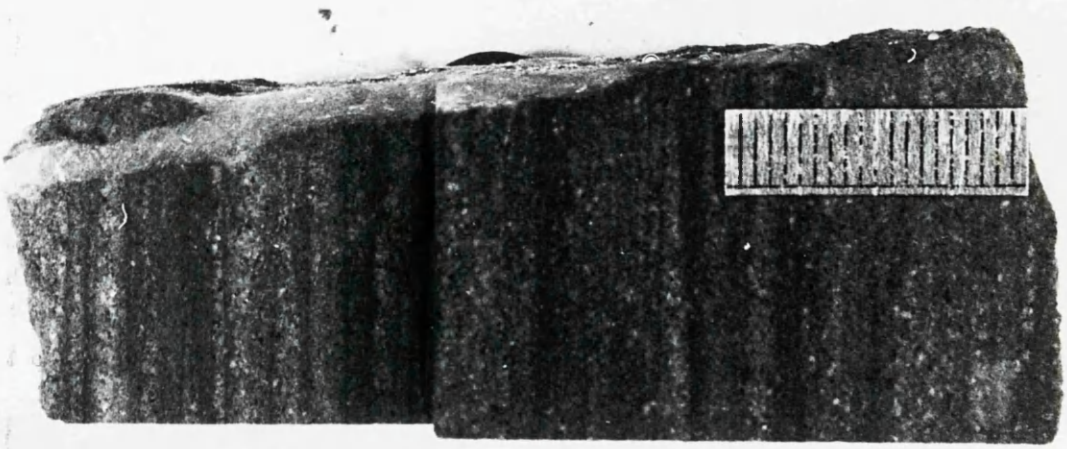

Figure 4.6 Photo of large mineralized fracture filled with siderite and bladed anhydrite. Scale bar 2 cm. Well 49/26-5, 6565.5'.

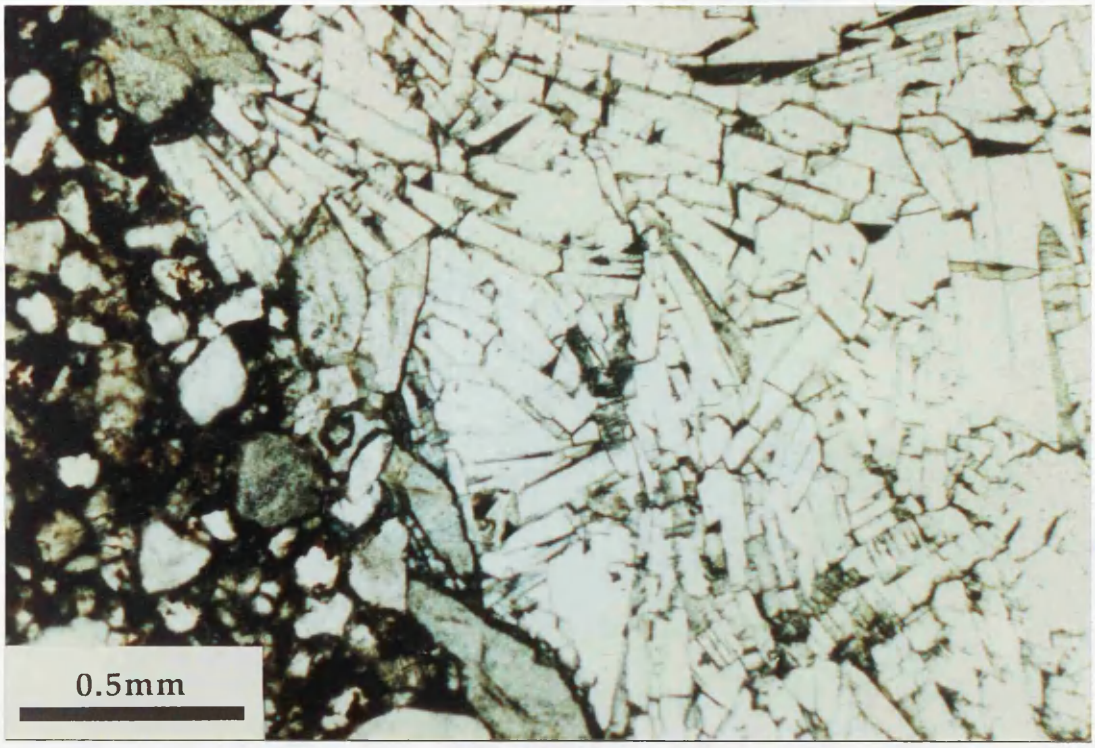

Figure 4.7 Photomicrograph of mineralized fracture filled with bladed anhydrite which has grown sub-parallel to the fracture walls. Well 49/26–5, 6565.5'.

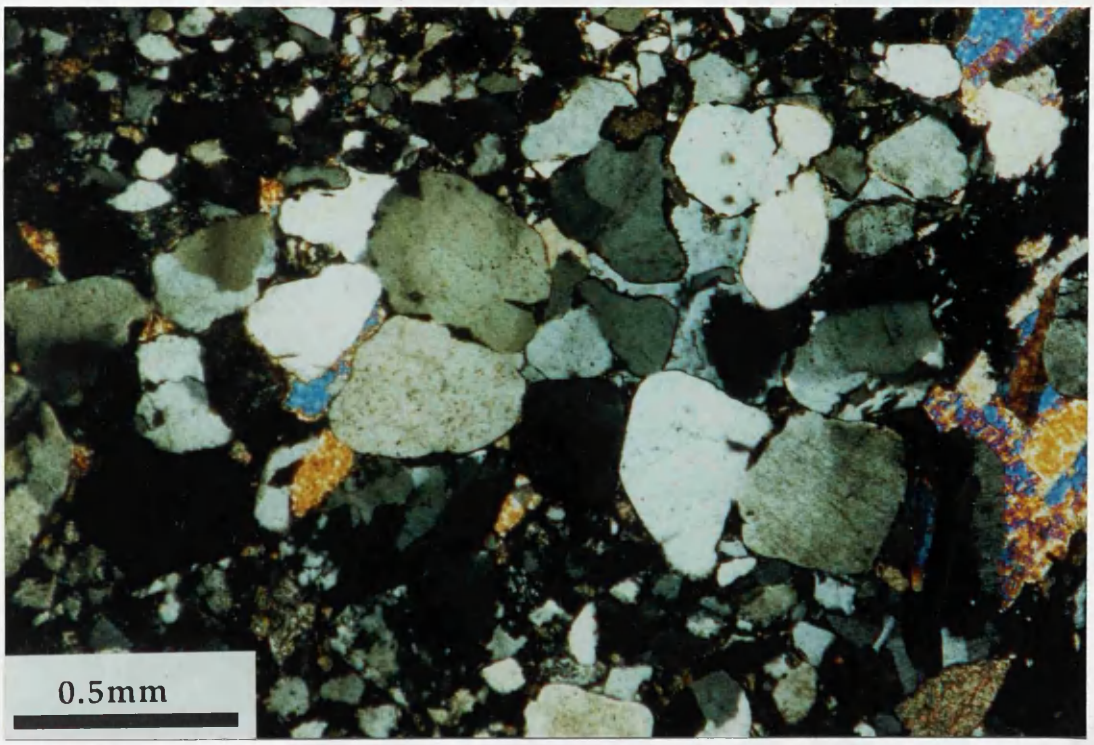

Figure 4.8 Photomicrograph of anhydrite cemented coarse-grained laminae adjacent to vertical anhydrite-filled fracture at the right. Well 49/26-5, 6556.5'.

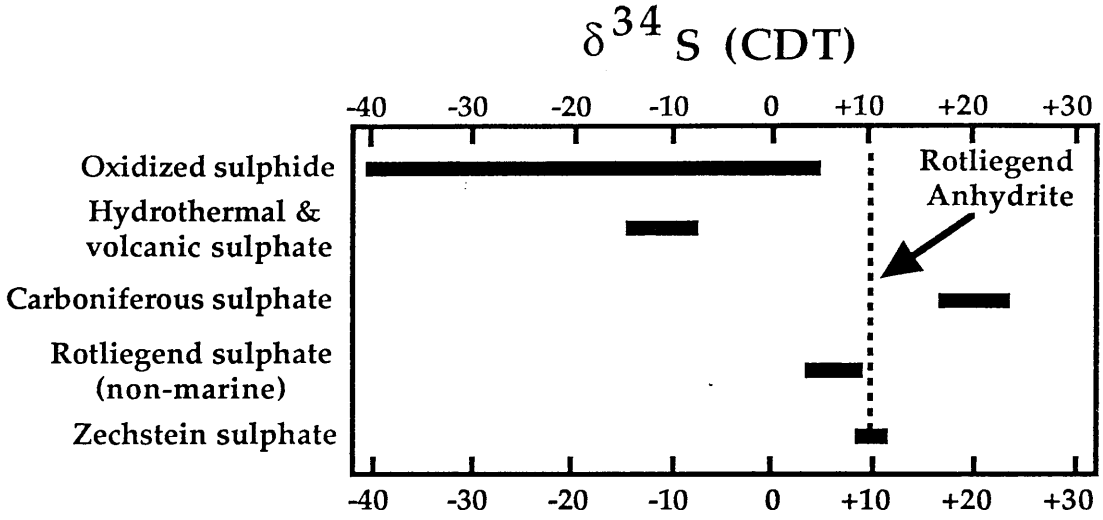

Figure 4.9 Schematic diagram for the possible sources of sulphate for the late anhydrite cement in the Rotliegend sandstone in the Leman field. See text for references.

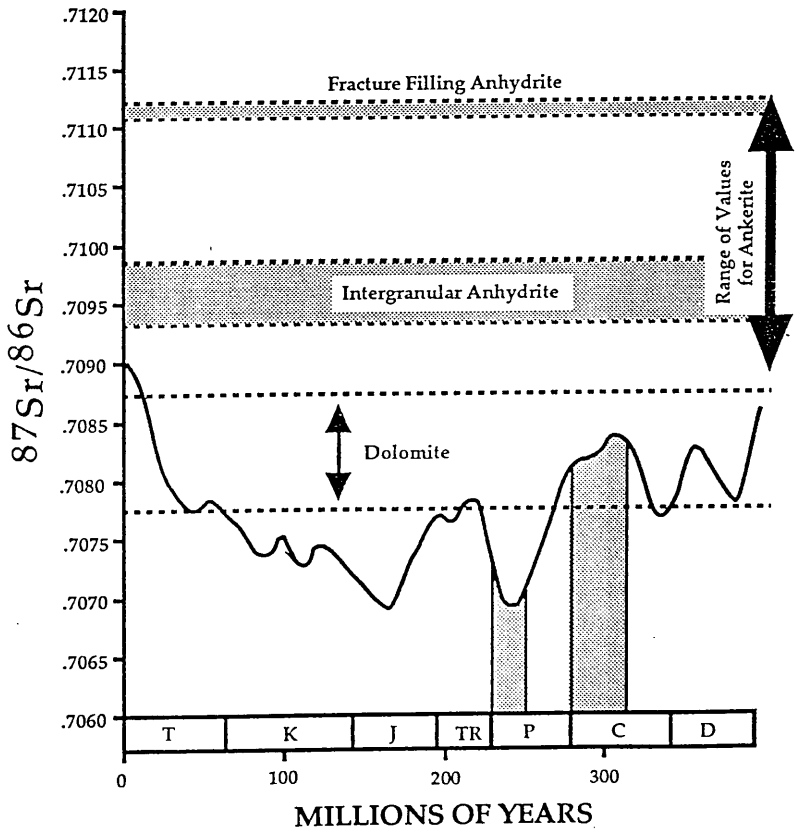

Figure 4.10 Plot of $^{87}Sr/^{86}Sr$ values of intergranular and fracture-filling anhydrite cements vs $^{87}Sr/^{86}Sr$ values of seawater and carbonate cements in the Rotliegend Sandstone. Isotope values for seawater are from Veizer *et al.* (1980) and Burke *et al.* (1982), values for dolomite and ankerite are from Sullivan *et al.*, 1990.

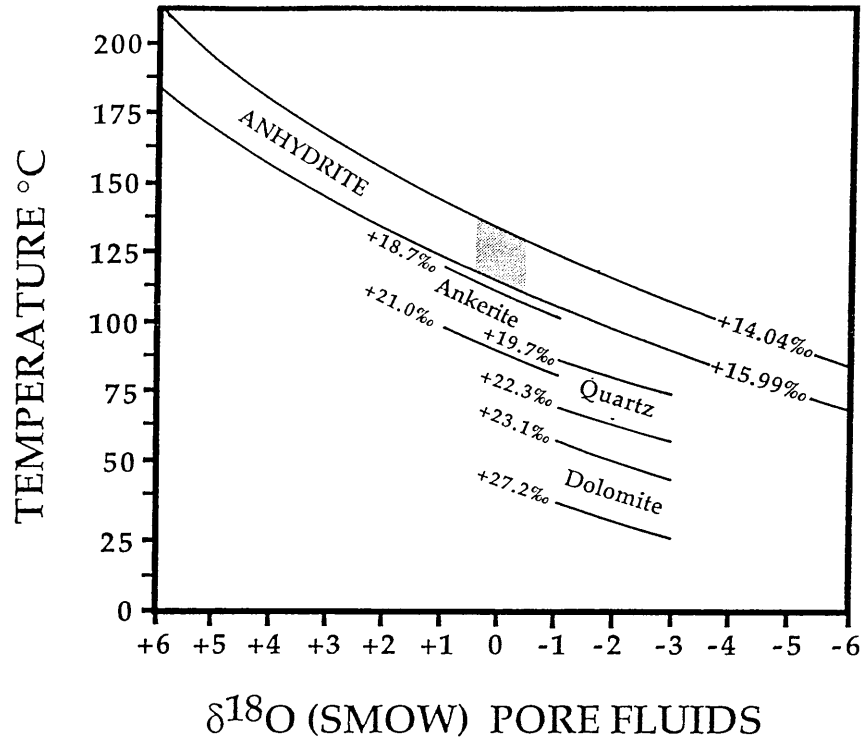

Figure 4.11 Equilibrium relationship between $\delta^{18}O$ of water, $\delta^{18}O$ of anhydrite and temperature. Anhydrite cementation is inferred to have occurred at temperatures between 120° to 140°C from an evolved brine with an oxygen isotope composition of approximately 0‰ (SMOW). See section 2.8 for oxygen isotope data for carbonates and section 3.9 for oxygen isotope data for quartz.

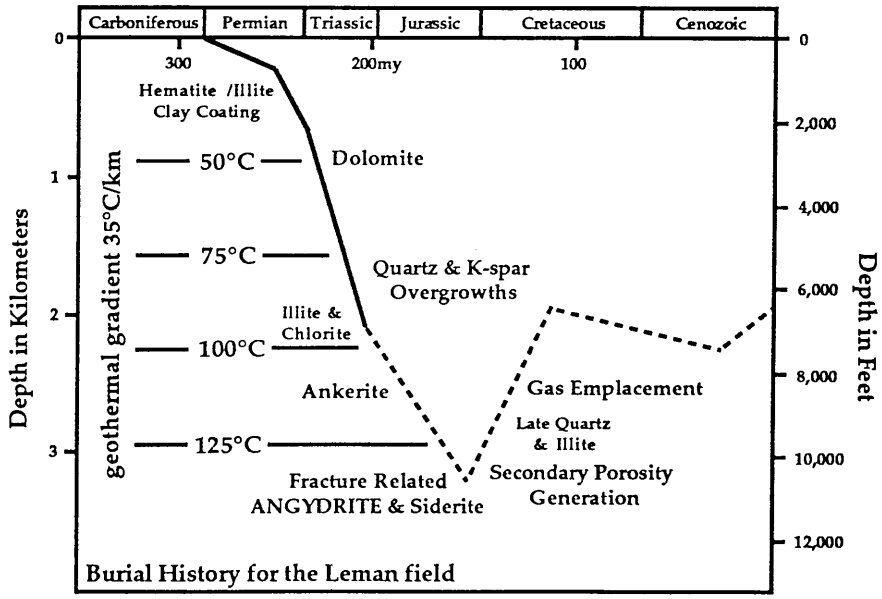

Figure 4.12 Burial curve for the Rotliegend Sandstone in the Leman field showing time and temperature of anhydrite precipitation and other major diagenetic events. The reconstructed burial curve is based on well logs 49/27-3 & 49/27–4, interval velocity data from Marie (1975), Glennie et al. (1978) and Bulat & Stoker (1987), and vitrinite reflectance data from Cope (1986).

CHAPTER 5

SECONDARY POROSITY DEVELOPMENT IN THE ROTLIEGEND SANDSTONE, LEMAN GAS FIELD, SOUTHERN NORTH SEA

Morgan D. Sullivan, R.Stuart Haszeldine
Department of Geology & Applied Geology, Glasgow University,
Glasgow G12 8QQ, Scotland

Anthony E. Fallick
Isotope Geology Unit, Scottish Universities Research and Reactor Centre,
East Kilbride, Glasgow G75 0QU, Scotland

5.1 ABSTRACT

Petrographic analysis of selected cores from the Rotliegend Sandstone in the Leman field suggests that a significant portion of the porosity was formed as a result of detrital and authigenic mineral dissolution, especially framework-supporting carbonate and sulphate cements. Textural evidence for mineral dissolution includes oversized and elongate pores, floating grains, corroded grain margins and partially dissolved detrital grains and authigenic cements. The fabrics and pore geometries produced by mineral dissolution suggest that secondary porosity generation was a late event created by post-depositional dissolution due to undersaturated or aggressive fluids. The two currently favoured mechanisms for post-depositional dissolution are: (1) meteoric ground waters recharging the basin being driven by an elevated water table and (2) acid pore-fluids generated by the maturation of organic matter and decarboxylation of organic acids in source rocks. Dissolution by meteoric ground waters was probably not important in the generation of secondary porosity, due to the long distance these fluids would have had to travel because of the deep burial of the Rotliegend Sandstone in the Leman field at the time of secondary porosity generation. Meteorically derived fluids would have likely attained equilibrium with respect to reactive minerals along the initial portion of their flow path. It is therefore suggested that the observed secondary porosity in the Rotliegend was generated by acid fluids produced during thermal maturation of the underlying Carboniferous Coal Measures. Mass balance calculations indicate that CO_2 generated by decarboxylation of the Westphalian source rocks can account for 12% secondary porosity, yet an average of only 5% secondary porosity is observed in the Rotliegend. Therefore the observed secondary porosity in the Rotliegend could have been generated via CO_2 migration during maturation of the underlying Westphalian Coal Measures.

5.2 INTRODUCTION

The Lower Permian aeolian and wadi subarkoses of the Rotliegend Sandstone, southern North Sea are up to 275 m (900 ft) thick and form the reservoir for the Leman gas field (Fig. 5.1). These sands overlie 915 m (3000 ft) of Upper Carboniferous (Westphalian) mudstones with angular unconformity, and are in turn overlain by 550 m (1800 ft) of Upper Permian Zechstein anhydrite and halite evaporites. The petrology and diagenetic history of the Rotliegend Sandstone in the Leman gas field has been described by Van Veen (1975), Glennie *et al.* (1978) and Arthur *et al.* (1986). The main diagenetic events in the Rotliegend from wells 49/26-5, 49/26-25, 49/26-26, 49/26-B240, 49/27-2, 49/27-3, and 49/27-4 of the Leman gas field (Figure 5.2) are summarized in Figure 5.3.

Petrographic examination of the porosity in the Rotliegend Sandstone in the Leman field suggests that much of the porosity was formed as the result of detrital and authigenic mineral dissolution, based on the textural criteria for the recognition of secondary porosity outlined by Schmidt & McDonald (1979b) and Burley & Kantorowicz (1986). The term secondary porosity is used here to describe porosity produced by post-depositional dissolution of soluble detrital and authigenic components in sedimentary rocks. Pore geometries and textures in the Rotliegend Sandstone suggestive of secondary origin due to mineral dissolution are oversized and elongate pores, floating grains, corroded grain margins and partially dissolved detrital grains and authigenic cements. Sixty thin sections were initially examined, and twenty tof these were selected for detailed petrographic analysis of porosity types in order to ascertain the origin and extent of secondary porosity development (Table 5.1; Figure 5.4). Minerals that underwent dissolution included many of the detrital plagioclase grains and the cement minerals dolomite, ankerite, and anhydrite.

5.3 CARBONATE AND SULPHATE CEMENT DISSOLUTION

Carbonate and sulphate dissolution are volumetrically the most important sources of secondary porosity in the samples examined. Dissolution of carbonate and sulphate cements has been observed in nearly all of the thin sections studied, and in many samples it may account for as much as 50% of the total porosity (Table 5.1, Figure 5.4). Typically cement dissolution forms about a third of the total porosity. Estimating the actual amount of cement dissolution is problematic as some pores which appear to be primary may have resulted from the complete removal of pore filling cement, and pores which seem to be entirely of secondary origin may have been only partially filled prior to cement dissolution. Such discrepancies in distinguishing primary and secondary porosity add uncertainties to secondary porosity measurements. Cement dissolution, however, is thought to account for a significant amount of the porosity in the Rotliegend Sandstone.

Dissolution textures and pore geometries observed in the Rotliegend are characteristic of secondary pores formed by the dissolution of pervasive pore filling cements, which formerly provided support for framework grains, and also cements which had extensively replaced detrital grains. For example, in extremely porous portions of laminae there is commonly no framework-supporting cement, but further along the same lamina, or in adjacent laminae within the same thin-section, framework-supporting cements often are present. Both cement-free and cemented regions of these laminae display similar compactional textures (Figure 5.5). This suggests that the dissolution of pervasive cements, such as dolomite, ankerite and anhydrite, which prevented compaction and enhanced potential porosity through grain replacement, resulted in a significant portion of the observed porosity in the highly porous zones.

Additional textural evidence was observed which is consistent with the dissolution of pervasive pore filling cement. Oversized pores, with diameters larger than those of adjacent framework grains, are

common in highly porous regions and are interpreted to have formed by the dissolution of both pore filling cements, and aggressive carbonate and sulphate minerals which corroded detrital grains prior to secondary porosity development (Figure 5.6). Evidence for partial mineral replacement followed by dissolution is also indicated by floating grain textures and corroded grain margins (Figure 5.6). Other important evidence of secondary porosity development is the presence of patches of partially dissolved cement (both carbonate and sulphate) adjacent to pores that were probably filled with cement prior to dissolution (Figure 5.7). Elongate secondary pores are also observed and could have been formed by replacement along framework grain boundaries by carbonate and sulphate minerals, which were later dissolved (Figure 5.8).

In terms of timing, the secondary porosity produced by the dissolution of carbonate and sulphate minerals appears to have been generated during the later stages of diagenesis (Figure 5.3). Petrographic evidence used to construct the paragenetic sequence, such as compactional textures of cemented grains and the cement fabrics, and isotopic data, indicate that ankerite and anhydrite precipitated after significant burial (see Chapters 2 & 4). Dissolution of these minerals must, therefore, have occurred late in the diagenetic history of the Rotliegend. Preservation of the extremely open pore geometries created by dissolution of framework-supporting carbonate and sulphate cements (i.e. elongate pores, oversized pores, and floating grains) also suggests that this was a late event, as these features would not survive significant compaction.

5.4 DETRITAL FELDSPAR DISSOLUTION

Selective dissolution of detrital feldspar has also contributed to the porosity of the Rotliegend Sandstone. Feldspar dissolution accounts for up to 20% of the total porosity in some samples, though it typically forms only 10%. Dissolution of feldspar has resulted in the development of both micro and macroporosity, depending on the degree of dissolution.

Plagioclase feldspar has been most affected by dissolution.

Detrital potassium feldspar generally appears fresh, and displays little evidence of alteration, although in other regions of the southern North Sea it has been extensively leached (Lee, 1984; Goodchild & Whitaker, 1986). Potassium feldspar overgrowths occur on both detrital plagioclase and potassium feldspar and these overgrowths display little evidence of dissolution. Even where selective dissolution of plagioclase grain cores has occurred, the potassium feldspar overgrowths are generally unaltered (Figure 5.9).

Secondary pores produced by the plagioclase dissolution range from micropores to large moldic pores. Microporosity has been created by the partial dissolution of plagioclase and appears to have been controlled by the crystallographic structure of grains, with dissolution being concentrated along cleavage planes (Figure 5.10). This partial dissolution has produced numerous micropores, which has created a honeycomb texture in affected grains. Volumetrically more important are the macropores created by the complete or near complete dissolution of plagioclase grains. The selective dissolution of plagioclase is largely restricted to the interiors of grains, and where dissolution has been extensive, the only remnants of leached grains are authigenic overgrowths of potassium feldspar (Figure 5.9). Moldic secondary porosity also appears to have been controlled by the crystal structure of plagioclase grains, suggesting that large macropores simply represent more complete dissolution of plagioclase grains than micropores do.

In terms of timing, dissolution of plagioclase, like that of carbonate and sulphate minerals, took place relatively late in the diagenetic history of the Rotliegend. This is suggested by the absence of late carbonate and sulphate cements in secondary voids created by feldspar dissolution, indicating that dissolution occurred after precipitation of these late cements. Additional evidence for late stage dissolution of plagioclase is the delicate textures displayed by many of the altered grains. The rigidity of these leached grains is greatly reduced and dissolution must have taken place after the main phase of compaction because these delicate

grains would not have survived significant compaction.

5.5 ORIGIN OF SECONDARY POROSITY

5.5.1 Source of aggressive fluids

The fabrics and pore geometries produced by mineral dissolution suggest that secondary porosity generation was a late diagenetic event (Figure 5.3) created by post-depositional dissolution by aggressive or undersaturated fluids. Secondary porosity is interpreted to have occurred following deepest burial of the Rotliegend (3.5 to 4 km prior to basin inversion; Figure 5.11) and temperatures for its formation are thought to have been between 140°C, the highest inferred temperatures from oxygen isotope data, see section 4.7, and 70°C, the present day formation temperatures (Figure 5.11). The source of the aggressive fluids, however, is unknown. The two mechanisms currently favoured for post depositional dissolution are; (1) meteoric ground waters recharging the basin being driven by an elevated water table (Bjørlykke, 1983; 1984), and (2) acid pore-fluids generated by the maturation of organic matter in sources rocks (Schmidt & McDonald, 1979a; Al-Shabieb & Shelton, 1981; Surdam *et al.*, 1984, 1985, 1989). Dissolution caused by meteoric ground water generally occurs relatively early, at burial depths of less than 1000 m (Bjørlykke, 1984), whereas dissolution due to the generation of CO_2 and/or organic acids during the thermal maturation of organic matter occurs during the later stages of burial, between 2 and 4 km (Schmidt & McDonald, 1979a).

Meteoric water: Secondary porosity generation occurred late in the diagenetic history of the Rotliegend when it was deeply buried (between 2 and 4 km; Figure 5.11). The dissolution capability of meteoric water depends on the initial saturation of the water, and the reactions that occur along its flow path (Giles & Marshall, 1986). Meteoric fluids would have most probably attained equilibrium, with respect to reactive minerals

along the initial portion of their flow path, due to the long distances these waters would have had to travel to reach the deeply buried Rotliegend in the Leman field. Therefore, meteoric waters would have been unlikely to have been important in the generation of secondary porosity.

Acid waters: Since meteoric waters do not appear to have been important in the generation of secondary porosity, it is suggested that the observed dissolution porosity in the Rotliegend was produced by the generation of acid waters at depth, as proposed by Goodchild & Whitaker (1986) for dissolution porosity in the Rotliegend Sandstone in the Rough field. Strong evidence supporting the generation of the observed secondary porosity in the Leman field by acid waters produced at depth are the numerous bleached fractures (Figures 5.12 & 5.13) which occur throughout the Rotliegend Sandstone. These fractures commonly are found in regions of abundant secondary porosity and are thought to have been pathways for aggressive fluids. Other evidence for the generation of acid waters is the common whitened zones which occur at the base of the Rotliegend Sandstone (such as well 49/26-5). Glennie *et al.* (1978) have suggested that this was due to acidic fluids being released from the underlying Carboniferous during coalification and maturation of organic matter.

A frequently invoked mechanism for producing the acid waters required for secondary porosity generation is the thermal maturation of organic matter in source rocks which releases CO_2 by decarboxylation of carboxylic acids (Schmidt and McDonald, 1979a; Al-Shabieb & Shelton, 1981; Surdam *et al.*, 1984, 1985, 1989). It has been argued, however, that insufficient quantities of CO_2 are generated during maturation of organic matter to produce the amounts of secondary porosity observed in reservoir sandstones (Bjørlykke, 1983 and 1984; Lundegard *et. al.*, 1984; Giles and Marshall, 1986; Giles, 1987). Although this may be true for many hydrocarbon reservoirs, the Westphalian humic source rocks beneath the Rotliegend in the Leman field may have been capable of generating the necessary volumes of CO_2 required to form the observed secondary porosity. A simplistic mass balance calculation (below) illustrates this

concept.

5.5.2 Mass balance considerations for CO_2 generation

A source rock/CO_2 mass balance was calculated for the secondary porosity in the Rotliegend Sandstone in the Leman field (Table 5.2). This enables the evaluation of the potential to generate sufficient CO_2 to account for the observed mineral dissolution (Table 5.1; Figure 5.4). The source of CO_2 is taken to be the 915 m (3000 ft) of Westphalian A/B Coal Measures which directly underlie the Rotliegend Sandstone in the Leman field (Eames, 1975; van Wijhe, 1980). These organic rich sediments are also interpreted to have been the source for the southern North Sea gas. Significantly, all major gas fields in the southern North Sea Basin overlie, or are close to, the subcrop of the Westphalian Coal Measures (Eames, 1975). This suggests that the proximity of the source rocks not only controlled the accumulation of hydrocarbons in the basin, but may have also controlled the secondary porosity potential of the overlying reservoir rocks.

The Carboniferous Coal Measures, in the vicinity of the Leman field, are dominated by carbonaceous shales and coals (Cornford, 1989). The Coal Measures are rich in organic carbon, and total organic carbon (TOC) contents of greater than 50% have been reported for non-marine Carboniferous shales onshore (Spears & Sezgin, 1985). The average organic carbon content of the Westphalian A/B, however, is not known. Spears and Sezgin (1985) reported TOC values ranging from 2.4 to 15.1% (average 7.7% TOC) for marine shales and TOC values of 3.7 to 6.0% (average 4.8% TOC) for non-marine shales from the base of the Westphalian A in South Yorkshire. Namurian marine and non-marine shales in South Yorkshire, which directly underlie the Westphalian A, have similar TOC values to those reported for the Westphalian, with average TOC values of 5.3% and 3.0% respectively (Spears & Amin, 1981). Marine shales are common in the Westphalian and form approximately

20% of the total thickness of the section (Kettel, 1989). A TOC content of between 3 and 4% has therefore been assumed for the carbonaceous shales, siltstones and sandstones in the Westphalian, which has a shale to sandstone ratio of approximately 4 to 1 in the Leman region (Goodchild & Whitaker, 1986). The Westphalian A/B sequences also have the greatest development of coaly intervals, averaging 3% of the total Carboniferous sequence (Lutz, 1975). The Westphalian coals underlying the Leman field are semi-anthracite rank according to Tissot & Welte (1978) and they reported German Carboniferous coals of the semi-anthracite rank with TOC contents of approximately 92%.

The amount of CO_2 generated during thermal maturation is dependent on both the type and maturity of the kerogen. Organic matter in carbonaceous shales and coal seams of the Westphalian sequence is dominantly humic, Type III kerogen, which is the type most likely to yield CO_2 during thermal maturation (Tissot and Welte, 1978). Maturity estimates derived from vitrinite reflectance measurements indicate that this organic matter is extremely mature for methane generation, with reflectance values greater than 2.0% beneath Leman (Barnard & Cooper, 1983) indicating that it has attained semi-anthracite to anthracite maturity. Karweil (1969) has shown from experimental work that up to 75 liters of CO_2 can be released per kg of coal by the maturation of lignite to semi-anthracite.

The calculated volume of thermally mature shale, siltstone and coal in the Westphalian A/B Coal Measures of the Leman field is 4.5×10^{11} m^3 utilizing an area of 4.8×10^8 m^2 for the Leman field. If an average bulk density for the Westphalian A/B Coal Measures of 2.6 g/cm^3 is assumed, then the weight of organic rich shale and siltstone is 1.20×10^{15} kg. Using a TOC content of 3.5% for the Westphalian, this weight of shale and siltstone contains 4.2×10^{13} kg of kerogen. The volume of semi-anthracite grade coal underlying the Rotliegend in the Leman field is 1.65×10^{10} m^3, assuming that coaly intervals form 3% of the sequence. If an organic carbon content of 92% and a density of $1.5 g/cm^3$ is utilized for the

Westphalian coal, then this volume of coal contains 2.3×10^{13} kg of kerogen. The total estimated weight of kerogen in the Westphalian Coal Measures beneath the Leman field is, therefore, 6.5×10^{13} kg.

The volume of Rotliegend Sandstone in the Leman field is 1.0×10^{11} m^3, assuming an average sandstone thickness of 225 m (750 ft) and an area of 4.8×10^8 m^2 for the Leman field. The observed secondary porosity in the field due to detrital and authigenic mineral dissolution is approximately 5% (5.0×10^9 m^3). If dissolution occurred by the reactions

$$CaCO_3 + H_2O + CO_2 \rightarrow Ca^{++} + 2HCO_3^-$$

and by

$$2KAlSi_3O_8 + 2CO_2 + 11H_2O \rightarrow$$
$$Al_2Si_2O_5(OH) + 2K^+ + 4H_4SiO_4 + 2HCO_3^-$$

then the number of moles of CO_2 required is equal to the number of moles of carbonate and feldspar dissolved. The maturation of 6.5×10^{13} kg of Type III humic kerogen to semi-anthracite grade would produce 2.25×10^{14} moles of CO_2. This volume of CO_2 would have been capable of dissolving 2.4×10^{16} g of carbonate or 8.4×10^{16} g of feldspar. Since 2/3 of the secondary porosity was formed by carbonate and sulphate dissolution and 1/3 by detrital feldspar dissolution, 2.25×10^{14} moles of CO_2 could have dissolved 12.0×10^9 m^3 of sandstone or approximately 12% pore space, assuming none of the CO_2 was neutralized by reactions occurring in the Westphalian Coal Measures during CO_2 generation.

5.5.3 Timing of decarboxylation and migration of CO_2

Its appears from mass balance considerations that sufficient CO_2 was generated by the source rocks, but it is also important to consider the timing of secondary porosity development relative to production of CO_2 by decarboxylation of carboxylic acids. The best estimate of the

temperature of secondary porosity development in the Rotliegend Sandstone in the Leman field is between 140°C (maximum burial temperature from isotopic constraints on late anhydrite, see Figure 5.11 & section 4.7) and 70°C (present day burial temperatures). According to Hunt (1979) the origin of CO_2 from the maturation of organic matter is primarily by the decomposition of carboxyl (C=O) oxygen group. Carothers and Kharaka (1978) have shown that carboxylic acids are most abundant in oil and gas field waters in the 80 to 140°C temperature range. They explain the dominance of organic acids in the 80° to 140°C range as a consequence of bacteria consuming the organic acids at temperatures below 60 to 80°C producing HCO_3^-. Above 140°C thermal decarboxylation destroys carboxylic acid anions and also produces HCO_3^- (Figure 5.14). Therefore CO_2 is produced both early in the burial history (<80°C) by bacterial decomposition of organic acids and extremely late (>140°C) by thermal decarboxylation of organic acids. This is also supported by the trend of increasing CO_2 content of produced gases with depth in the Gulf Coast described by Franks and Forester (1984) which suggests that only a small amount of the organic acids are converted to CO_2 at shallow depth and that the progressive decarboxylation of organic acids, with corresponding increases in partial pressure CO_2, occurs at temperatures greater than 120°C (Figure 5.15). Although some of the carboxylic acids would have been destroyed by bacteria during early burial (<80°C), the maximum production of CO_2 by thermal decarboxylation of organic acids is in the same range as the temperatures inferred for main secondary porosity event in the Rotliegend Sandstone in the Leman field.

The efficiency of migration of the CO_2 into the reservoir and the reaction of CO_2 with carbonate in the shales must also be considered. The migration of CO_2 from the source rocks to the overlying Rotliegend Sandstone is assumed to have occurred along microfractures produced by abnormal pore pressures resulting from hydrocarbon and CO_2 generation (Meissner, 1980; Momper, 1980; Al-Shaieb and Shelton, 1981) and along faults and fractures created by basin inversion during the Late Jurassic-

Early Cretaceous. As the CO_2 moved along the open fractures it possibly reacted with reactive minerals in the source rock. If the source rock contained abundant carbonate minerals (>20%) it would be capable of neutralizing the majority of the CO_2 released from the kerogen in the source rocks (Giles & Marshall, 1986). This of course depends on the frequency of microfractures, as low permeabilities in shales would inhibit the interaction of fluids with the source rocks, and, hence, the volume of carbonate the CO_2 contacted during migration. Bulk XRD analysis of the Westphalian Coal Measures indicates that carbonate minerals are not an abundant constituent of the shales and account for less than 1% of the bulk volume (Draxler and Edwards, 1986). The amount of feldspar and carbonate in the siltstones is certainly higher, but these rocks constitute less than 20% of the total Westphalian sequence (Goodchild & Whitaker, 1986). Although some of the CO_2 could have been neutralized in the Coal Measures, the majority appears to have been capable of migrating into the Rotliegend.

Thus, there is a strong potential for organic reactions in the Carboniferous to produce acidic fluids by the decarboxylation of carboxylic acids and for the migration of these fluids upwards into the Rotliegend to generate the observed secondary porosity.

5.6 CONCLUSIONS

The main phase of mineral dissolution and generation of secondary porosity occurred after the precipitation of late carbonate and sulphate cements and is therefore thought to have been associated with, or following the deepest burial of the Rotliegend Sandstone in the Leman field. Secondary porosity, which makes up approximately a third of the present porosity, formed by the dissolution of plagioclase, dolomite, ankerite and anhydrite. Textural evidence for mineral dissolution includes oversized and elongate pores, floating grains, corroded grain margins and authigenic cements. The fabrics and pore geometries

produced by mineral dissolution suggest that secondary porosity was created by post-depositional leaching at depth by aggressive or undersaturated fluids. The source of the acid waters responsible for secondary porosity generation is thought to have been the maturation of the underlying Westphalian source rocks which resulted in the release of large volumes of CO_2. Mass balance calculations indicate that CO_2 generated by decarboxylation of the Westphalian source rocks can account for 12% secondary porosity in sandstones, yet an average of only 5% secondary porosity is observed in the Rotliegend. Therefore the observed secondary porosity in the Rotliegend could have been generated via CO_2 migration during maturation of the underlying Westphalian Coal Measures.

5.7 ACKNOWLEDGEMENTS

Supported by funds from Amoco (UK) Exploration and Shell/Esso U.K. Exploration and Production. This research was carried out at the Department of Geology and Applied Geology, University of Glasgow, and the Isotope Geology Unit, Scottish Universities Research and Reactor Centre (SURRC). Core was supplied by the British Geological Survey and by Shell/Esso. The authors thank Douglas Maclean (Glasgow University) for his assistance with the production of photographic plates. The SURRC is supported by Natural Environment Research Council of Britain and the Scottish Universities.

5.8 REFERENCES CITED

Al-Shaieb, Z. and Shelton, J.W. 1981. Migration of hydrocarbons and secondary porosity in sandstones. *Bull. Am. Ass. Petrol. Geol.***65**, 2433-2436.

Arthur, T.J., Pilling, D., Bush, D., and Macchi, L., 1986, The Leman Sandstone Formation in U.K. block 49/28: Sedimentation, diagenesis and burial history. In: *Habitat of Palaeozoic Gas in N.W. Europe*. Brooks, J., Goff, J. and van Hoorne, B. (eds). *Spec. Publs Geol. Soc.* **23,** Scottish Academic Press, London, 251-266.

Barnard, P.C.and Cooper, B.S. 1983. A review of geochemical data related to the North-west gas province. In: *Petroleum Geochemistry and Exploration of Europe,* Brooks, J. (ed). Blackwell Scientific Publications, 271-282.

Bjørlykke, K. 1983. Diagenetic reactions in sandstones. In: *Sediment Diagenesis,* Parker, A. and Sellwood, B.W. (eds), NATO ASI Series, 169-213.

Bjørlykke, K. 1984. Formation of secondary porosity: how important is it? In: *Clastic Diagenesis,* McDonald, D.A. and Surdam, R.C. (eds). *Am. Ass. Petrol. Geol. Mem.* .**37**, 277-286.

Bulat, J. and Stoker, S.J. 1987. Uplift determination from interval velocity studies, UK, southern North Sea. *Petroleum Geology of North West Europe.* Brooks, J. and Glennie, K.W. (eds). Graham and Trotman, London, 293-306.

Burley, S.D. and Kantorowicz, J.D. 1986. Thin section and S.E.M. textural criteria for the recognition of cement-dissolution porosity in sandstones. *Sedimentology* **33**, 587-604.

Carothers, W.W. and Kharaka, Y.K., 1978. Aliphatic acid ions in oil-field waters—implications for origin of natural gas. *Bull. Am. Ass. Petrol. Geol.* **62**, 2441-2453.

Cope, M.J. 1986. An interpretation of vitrinite reflectance data from the southern North Sea Basin. *Habitat of Palaeozoic Gas in N.W. Europe*. Brooks, J., Goff, J. and van Hoorne, B. (eds). *Spec. Publs Geol. Soc.* **23,** Scottish Academic Press, London, 85-101.

Cornford, C., 1989. Source rocks and hydrocarbons of the North Sea. In: *Introduction to the Petroleum Geology of the North Sea* (3rd edition). Glennie, K.W. (ed), Blackwell Scientific Publications,

Oxford, 294-363.

Draxler, J.K. and Edwards, D.P. 1986. Evaluation procedures in the Carboniferous of Nothern Europe. *Habitat of Palaeozoic Gas in N.W. Europe*. Brooks, J., Goff, J. and van Hoorne, B. (eds). *Spec. Publs Geol. Soc.* **23**, Scottish Academic Press, London, 151-168.

Eames, T.D. 1975. Coal rank and gas source relationships-Rotliegendes reservoirs. In: *Petroleum and the Continental Shelf of North West Europe*, Woodland, A.W. (ed.). *Applied Science Publ.*, London, 191-204.

Franks, S. and Forester, R., 1984. Relationship among secondary porosity, pore-fluid chemistry and carbon dioxide, Texas Gulf Coast. In: *Clastic Diagenesis*, McDonald, D.A. and Surdam, R.C. (eds). *Am. Ass. Petrol. Geol. Mem.* , **37**, 63-80.

Giles, M.R. 1987. Mass transfer and problems of secondary porosity creation in deeply buried hydrocarbon reservoirs. *Marine and Petrol. Geol.*, **4**, 188-204.

Giles, M.R. and Marshall, J.D. 1986. Constraints on the development of secondary porosity in the subsurface: re-evaluation of processes. *Marine and Petrol. Geol.*, **3**, 243-255.

Glennie, K.W., Mudd, G.C. and Nagtegaal, P.J.C. 1978. Depositional environment and diagenesis of Permian Rotliegendes sandstones in Leman Bank and Sole Pit areas of the U.K. Southern North Sea. *Jour. Geol. Soc. Lond.*, **135**, 25-34.

Glennie, K.W. 1989. Lower Permian—Rotliegend. In: *Introduction to the Petroleum Geology of the North Sea* (3rd edition). Glennie, K.W. (ed), Blackwell Scientific Publications, Oxford, 120-152.

Goodchild, M.W. and Whitaker, J. McD. 1986. A petrographic study of the Rotliegendes Sandstone reservoir (Lower Permian) in the Rough gas field. *Clay Minerals*, **21**, 459-477.

Hunt, J.M. 1979. *Petroleum Geochemistry and Geology*. San Francisco, W. H. Freeman & Co., 716p.

Karweil, J., 1969. Aketuelle Probleme der Geochemie der Kohle. In: *Advances in Organic Geochemistry 1968*.Schenck, P.A., Havenaer, I. (eds.). Oxford: Pergamon Press, 59-84.

Kettel, D., 1989. Upper Carboniferous source rocks north and south of the Variscan Front (NW and Central Europe). *Marine and*

Petrol. Geol., **6**, 170-181.

Lee, M. 1984. Diagenesis of the Permian Rotliegendes Sandstone, North Sea : K/Ar, O^{18}/O^{16}, and petrological evidence. Ph. D. thesis, Case Western University, Cleveland, Ohio, 346pp.

Lundegard, P.D., Land, L.S. and Galloway, W.E. 1984. Problem of secondary porosity: Frio Formation (Oligocene), Texas Gulf Coast. *Geology* **12**, 399-402.

Lutz, M.,Kaasschieter, J.P.H. and van Wijke. D.H. 1975. Geological factors controlling Rotliegend gas accumulations in the mid-European basin. *Proceedings of 9th World Petroleum Congress*. Applied Science, 93-103.

Marie, J.P.P. 1975. Rotliegendes stratigraphy and diagenesis. In: *Petroleum and the Continental Shelf of North West Europe*, Woodland, A.W. (ed.). *Applied science Publ.*, London, 205-211.

Meissner, F.F. 1980. Examples of abnormal fluid pressure produced by hydrocarbon generation (abs): *Bull. Am. Ass. Petrol. Geol.* **64**, 749.

Momper, J.A. 1980. Generation of abnormal pressures through organic matter transformation (abs): *Bull. Am. Ass. Petrol. Geol.*, **64**, 753.

Schmidt, V. and McDonald, D.A. 1979a. The role of secondary porosity in the course of sandstone diagenesis. In: *Aspects of Diagenesis*, Scholle, P.A. and Schluger, P.R. (eds). *S.E.P.M. Spec. Publ., Tulsa, Oklahoma*, **26**, 175-208.

Schmidt, V. and McDonald, D.A. 1979b. Texture and recognition of secondary porosity in sandstones. In: *Aspects of Diagenesis*, Scholle, P.A. and Schluger, P.R. (eds). *S.E.P.M. Spec. Publ., Tulsa, Oklahoma*, **26**, 209-225.

Spears, D.A. and Amin, M.A., 1981. Geochemistry and mineralogy of marine and non-marine Namurian black shales from the Tansley Borehole, Derbyshire. *Sedimentology*, **28**, 408-417.

Spears, D.A. and Sezgin, H.I., 1985. Mineralogy and geochemistry of the Subcrenatum Marine Band and associated coal bearing sediments, Langsett, South Yorkshire. *Jour. Sed. Petrol.*,**55**, 570-578.

Surdam, R.C., Boese, S.W. and Crossey, L.J. 1984. The chemistry of

secondary porosity. In: *Clastic Diagenesis,* McDonald, D.A. and Surdam, R.C. (eds). *Am. Ass. Petrol. Geol. Mem.*, **37**, 127-150.

Surdam, R.C., and Crossey, L.J., 1985. Organic-inorganic reactions during progressive burial: key to porosity and permeability enhancement and preservation. *Phil. Trans. Roy. Soc. London, Series A.* **315**. 135-156.

Surdam, R.C., Crossey, L.J., Hagen, E.S., and Heasler, H.P.,1989. Organic-inorganic interactions and sandstone diagenesis. *Bull. Am. Ass. Petrol. Geol.*, **73**, 1-23.

Tissot, B.P. and Welte, D.H. 1978. *Petroleum Formation and Occurrence.* Springer Verlag, Berlin. 538 p.

van Veen, F.R. 1975. Geology of the Leman gas field. In: *Petroleum and the Continental Shelf of North West Europe,* Woodland, A.W. (ed.). *Applied Sci. Publ.*, London, 223-231.

Van Wijhe, D.H., Lutz, M. and Kaasschieter, J.P.H. 1980. The Rotliegend in the Netherlands and its gas accumulations. *Geol. Mijnbouw* **59**, 3-24.

5.9 TABLES

Table 5.1 Summary of porosity analysis from thin sections, based on 500 point counts per sample.

Sample (Well)	Total Porosity(%)	Secondary Porosity (%)		
		Cement Ø /	Feldspar Ø /	Total
6305' (27-2)	12.3%	2.7%	0.8%	3.5%
6396' (27-2)	12.1%	4.3%	2.1%	6.4%
6418' (27-2)	11.4%	1.7%	1.3%	3.0%
6466' (26-5)	9.0%	1.8%	1.1%	2.9%
6560' (27-3)	5.6%	0.8%	0.3%	1.1%
6581' (26-25)	21.7%	7.5%	2.5%	10%
6585' (26-25)	23%	12%	2.8%	14.8%
6623' (27-2)	22%	10%	3.5%	13.5%
6670' (27-4)	7.9%	1.3%	0.5%	1.8%
6670' (26-5)	12.5%	5.8%	2.1%	7.9%
6697' (27-2)	9.3%	3.2%	1.5%	4.7%
6700' (26-25)	17%	7.0%	2.5%	9.5%
6717' (27-3)	2.6%	0.4%	0	0.4%
6737' (27-2)	5.1%	1.1%	0.4%	1.5%
6851' (27-4)	4.2%	0.6%	0.3%	.9%
6892' (27-2)	13.1%	2.0%	1.5%	3.5%
6910' (27-2)	18%	8.0%	2.0%	10%
6925' (26-5)	16.6%	5.4%	2.3%	7.7%
6934' (27-4)	18.1%	6.4%	2.1%	8.5%
7040' (26-5)	8.3%	1.1%	0.6%	1.7%

Table 5.2 Calculated CO_2 production and leaching capacity of Westphalian source rocks associated with the Rotliegend Sandstone in the Leman field.

Thickness of sandstone:	225 m
Thickness of Westphalian:	915 m
Area for Leman field:	4.8×10^8 m^2
Rotliegend Sandstone volume:	1.0×10^{11} m^3
Thermally mature shale volume:	5×10^{11} m^3
Total organic carbon in shale:	3.5% (humic - type III)
Coal (anthracite) volume:	1.65×10^{10} m^3
Total kerogen in source rocks:	6.5×10^{13} kg
Observed secondary porosity:	5.0×10^9 m^3 (5%)

Approach

Assuming a yield of **75 liters of CO_2 per kg** of thermally mature humic Type III kerogen (Karweil, 1969), then **6.5×10^{13} kg** of mature kerogen will generate 5.0×10^{15} liters of CO_2 or **2.25×10^{14} moles of CO_2**. This volume of CO_2 would have been capable of dissolving 2.4×10^{16} g of carbonate or 8.4×10^{16} g of feldspar. Since 2/3 of the secondary porosity was formed by carbonate and sulphate dissolution and 1/3 by detrital feldspar dissolution, 2.25×10^{14} moles of CO_2 could have dissolved 12.0×10^9 m^3 of sandstone or approximately **12% porosity**. Therefore the observed secondary porosity could have been generated by CO_2 generated in the Westphalian source rocks.

5.10 FIGURES AND FIGURE CAPTIONS

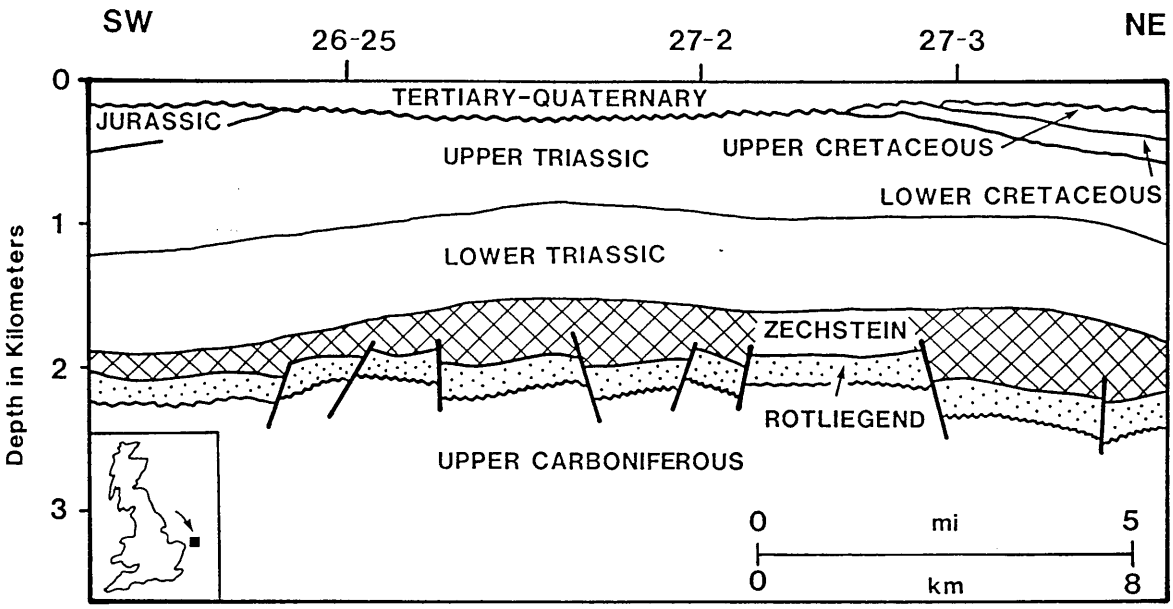

Figure 5.1 Location of Leman gas field (North Sea) and geologic cross section for the Leman region (after Glennie 1990).

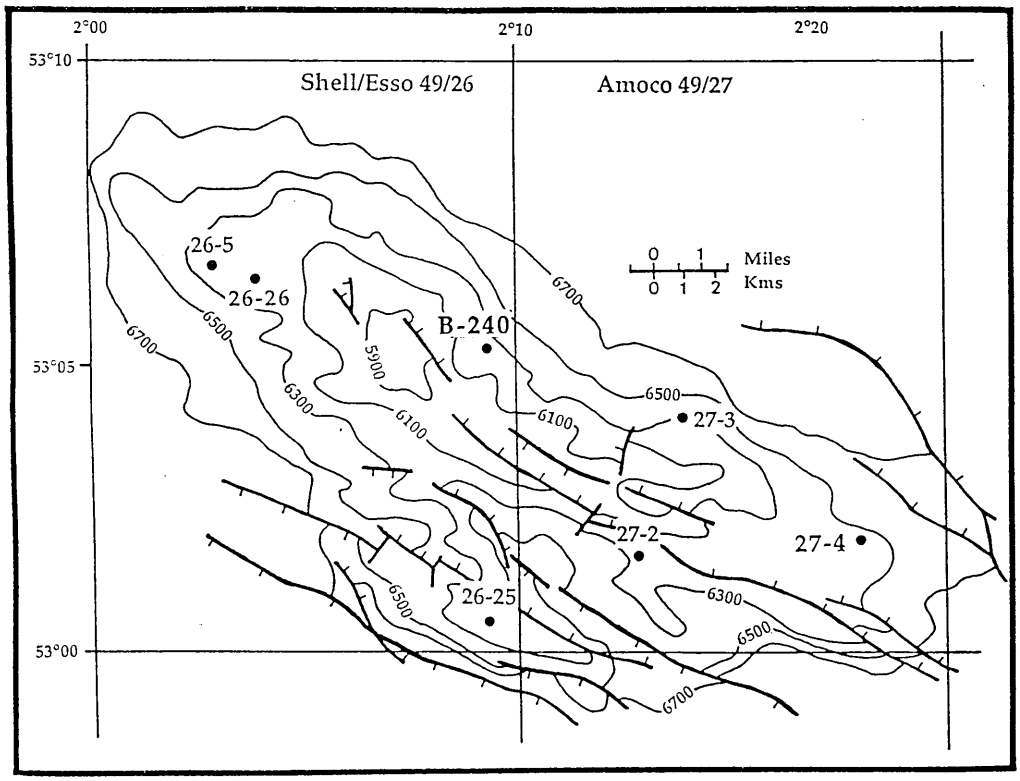

Figure 5.2 Present interpretation of Leman field, showing contours of the the top of the Rotliegend in feet below sea level and locations of wells used in this study (from van Veen, 1975).

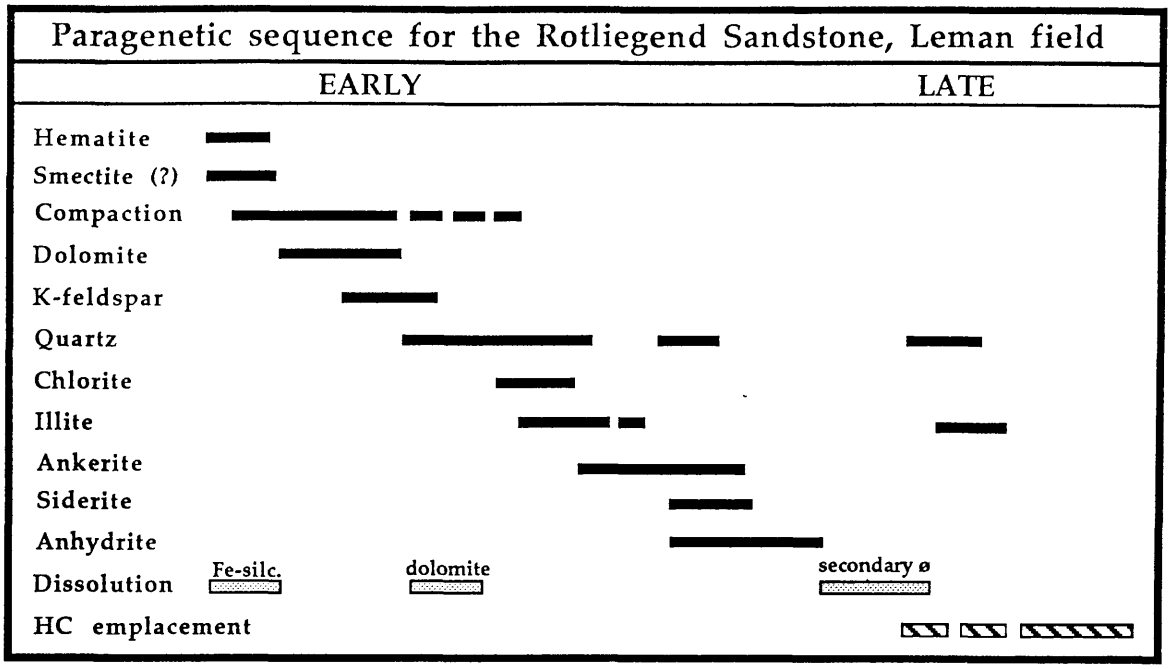

Figure 5.3 Paragenetic sequence showing timing of major diagenetic events in the Lower Permian Rotliegend Sandstone in the Leman gas field.

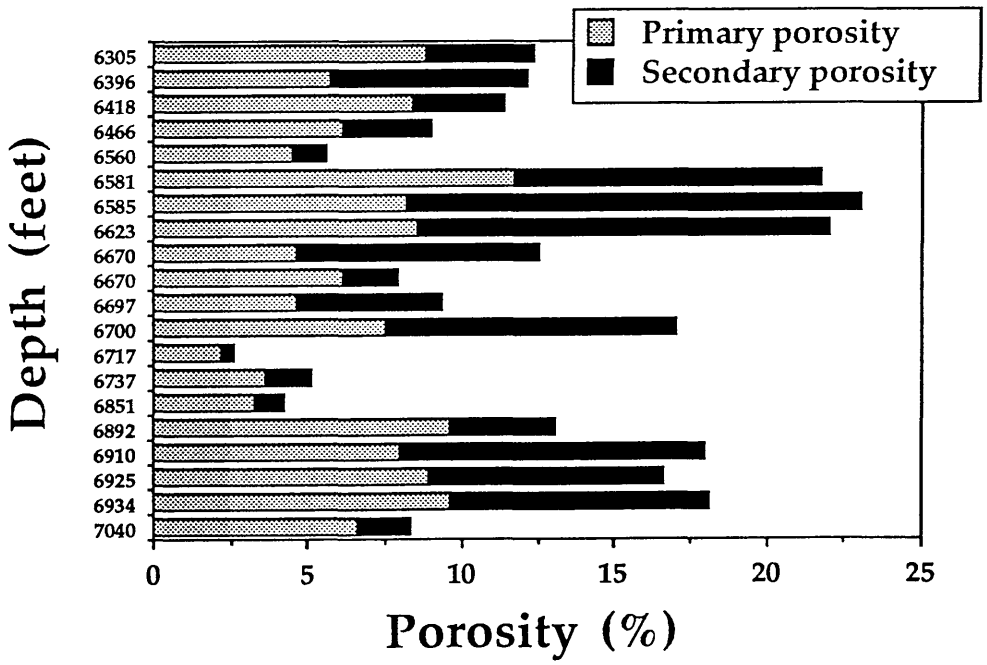

Figure 5.4 Porosity distribution (primary vs. secondary) for the Rotliegend Sandstone in the Leman field.

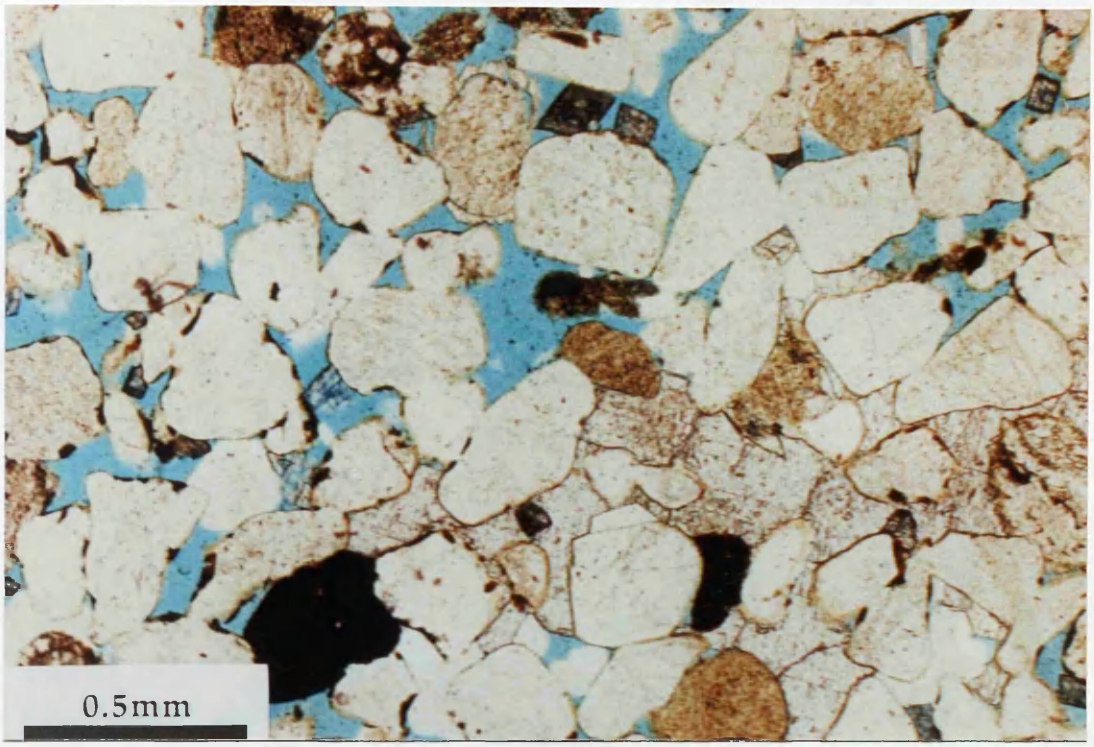

Figure 5.5 Photomicrograph of secondary porosity created by the dissolution of pervasive framework-supporting cement. Porosity = light blue, anhydrite = white cement and dark blue rhombs (stained) are ankerite. Note both cemented and cement free zones display similar compactional textures. Well 49/27-2, 6396'.

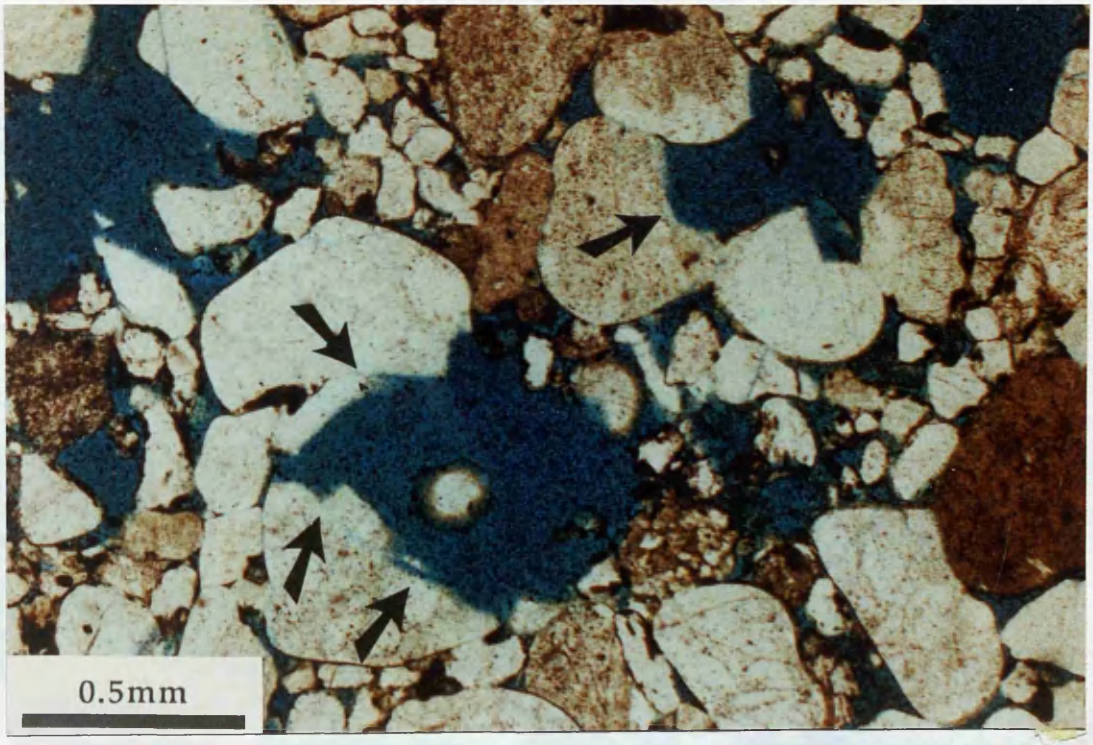

Figure 5.6. Photomicrograph of secondary pores (light blue) generated by the dissolution of aggressive framework-supporting minerals which corroded detrital grain margins (arrows) prior to secondary porosity creation. Well 49/27-2. 6623'.

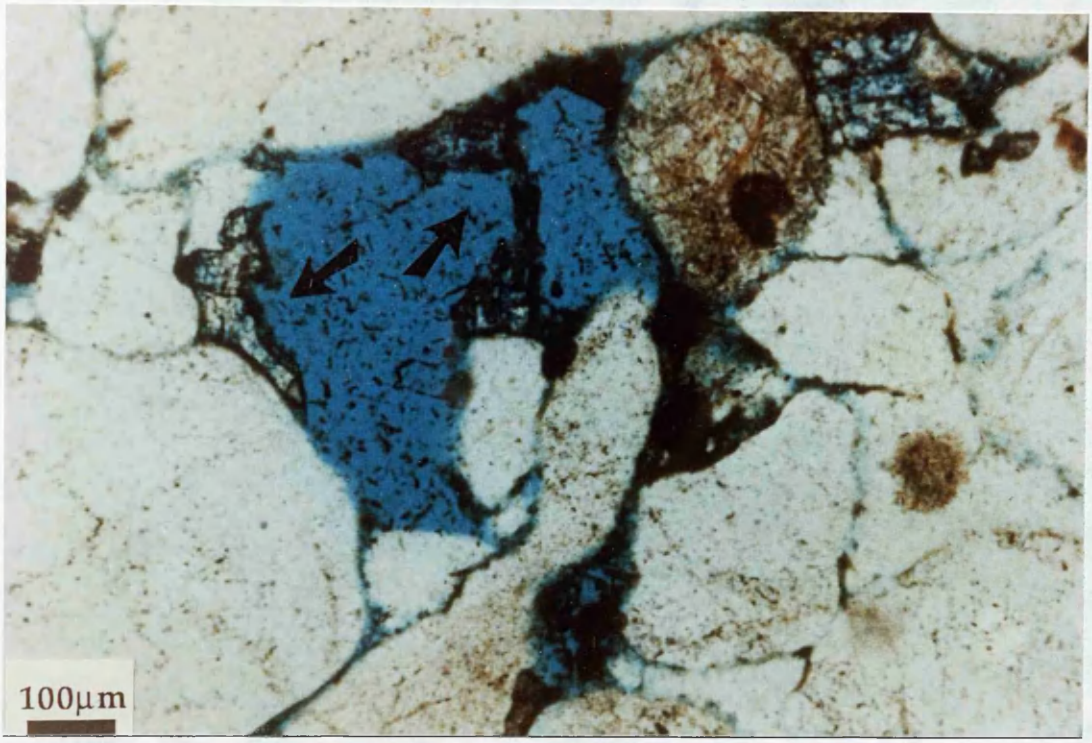

Figure 5.7 Photomicrograph of secondary porosity produced by partially dissolution of ankerite cement (stained blue-arrows). Well 49/26-5, 6670'.

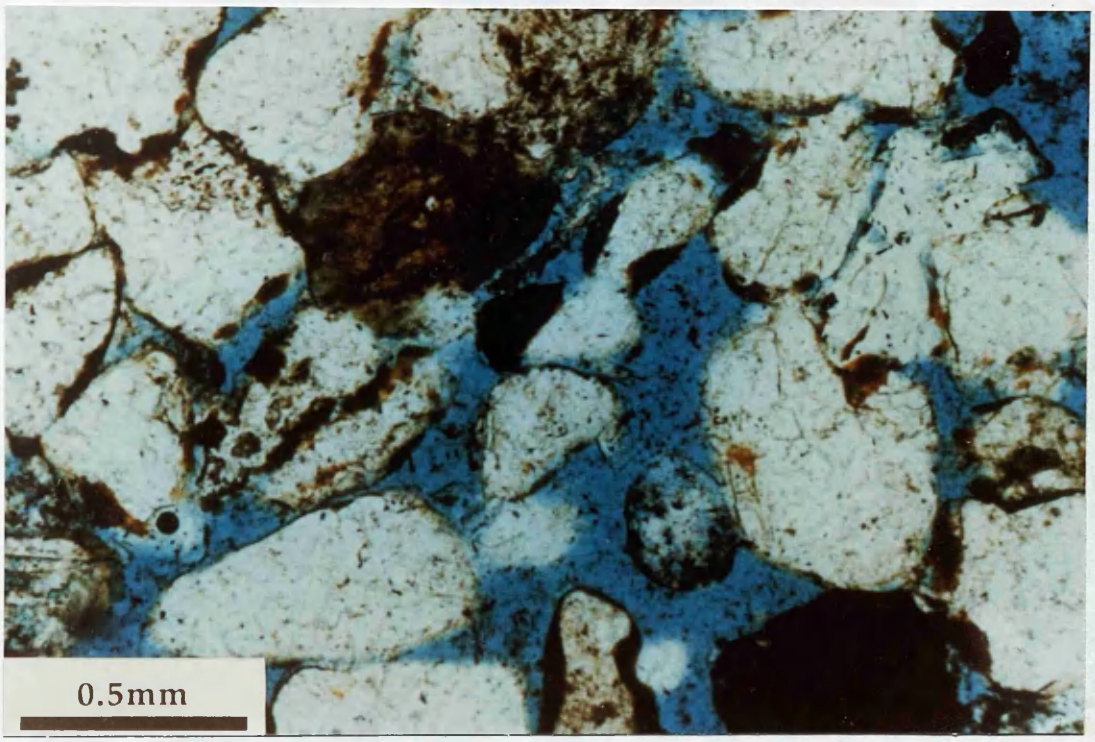

Figure 5.8 Photomicrograph of elongate pores which resulted from the dissolution of aggressive pore filling minerals. Plane polarized light. Well 49/26-5, 6670'.

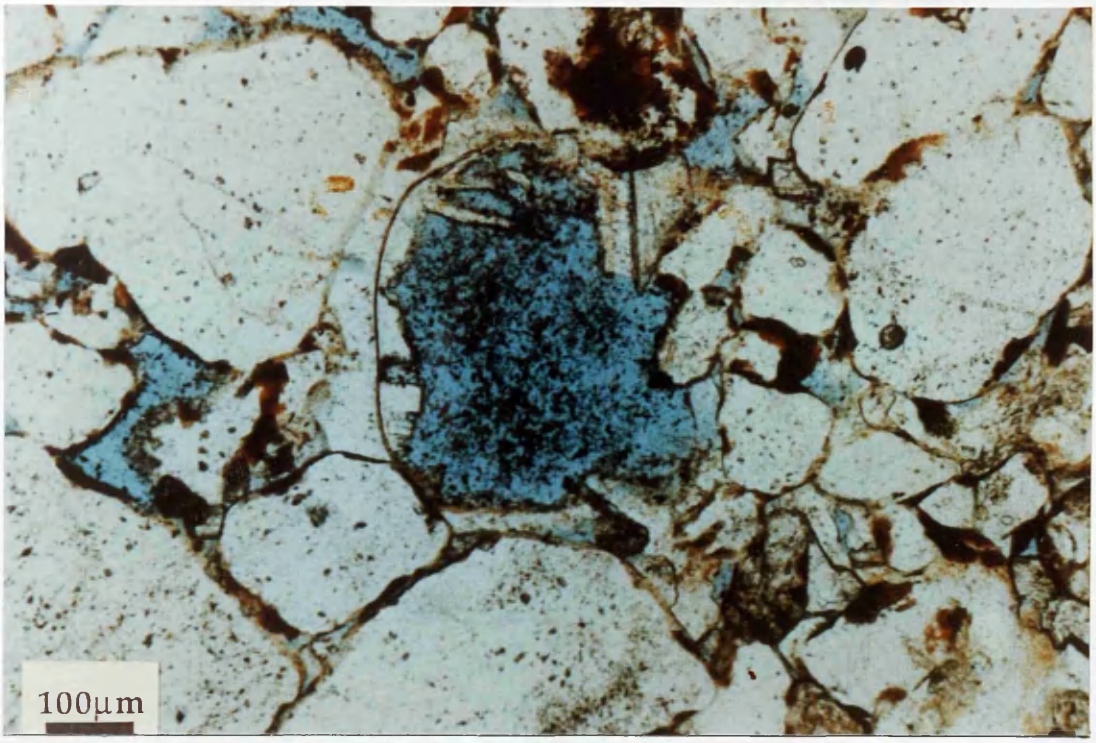

Figure 5.9 Photomicrograph of macropore produced by the near complete dissolution of a detrital plagioclase. Note the fresh appearance of K-spar overgrowth on dissolved plagioclase. Well 49/27-2, 6515'.

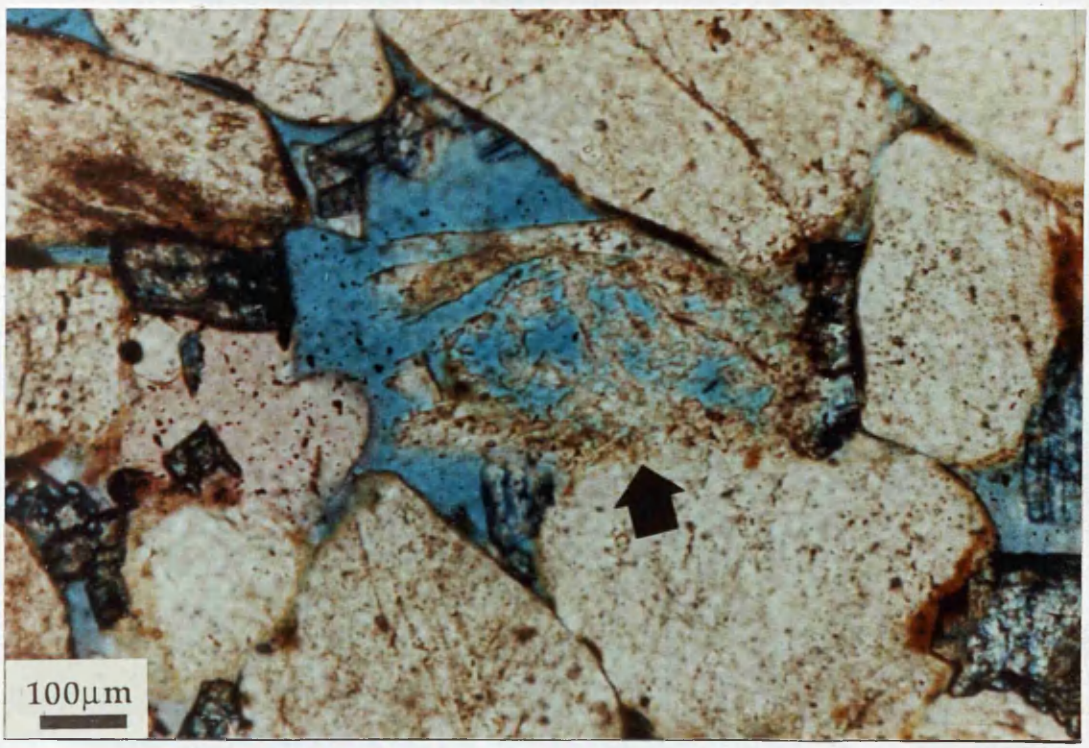

Figure 5.10 Photomicrograph of micropores generated by the partial dissolution of a detrital plagioclase grain. Well 49/27-2, 6396'.

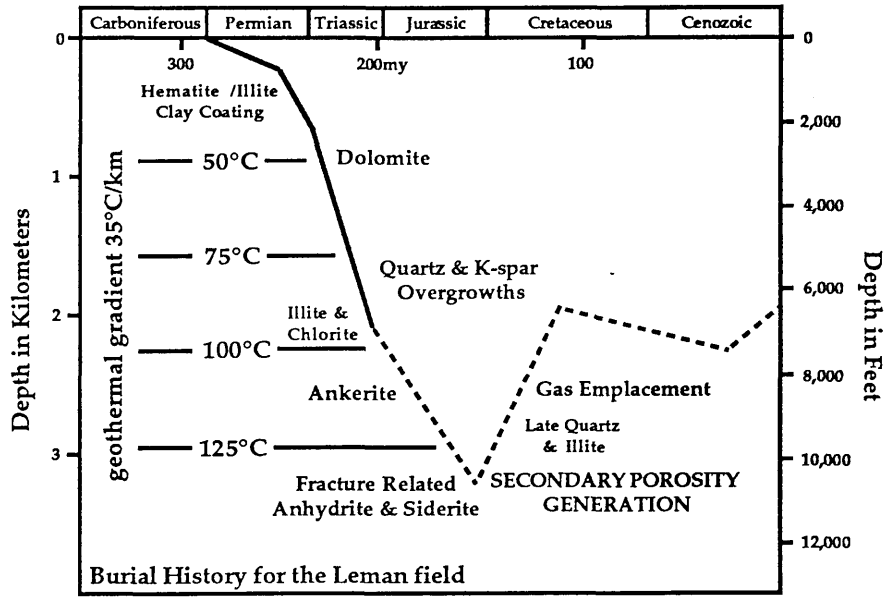

Figure 5.11 Burial curve for the Rotliegend Sandstone in the Leman field showing time and temperature of dolomite, ankerite and anhydrite precipitation and secondary porosity generation. The reconstructed burial curve is based on well logs 49/27-3 & 49/27–4, interval velocity data from Marie (1975), Glennie *et al.* (1978) and Bulat & Stoker (1987), and vitrinite reflectance data from Cope (1986).

Figure 5.12 Photo of narrow anastomosing fractures. Note that the sediments adjacent to the fractures have been whitened due to the the reduction of iron oxide grain coatings by reducing waters. The finer grained sediments, at the top of the sample, are not as extensively reduced, as the coarser grained sediments, due to their low porosities and permeabilities. These fractures commonly are found in regions of high secondary porosity and are thought to have been path ways for aggressive fluids. Scale bar = 2 cm. Well 49/27-4, 6934'.

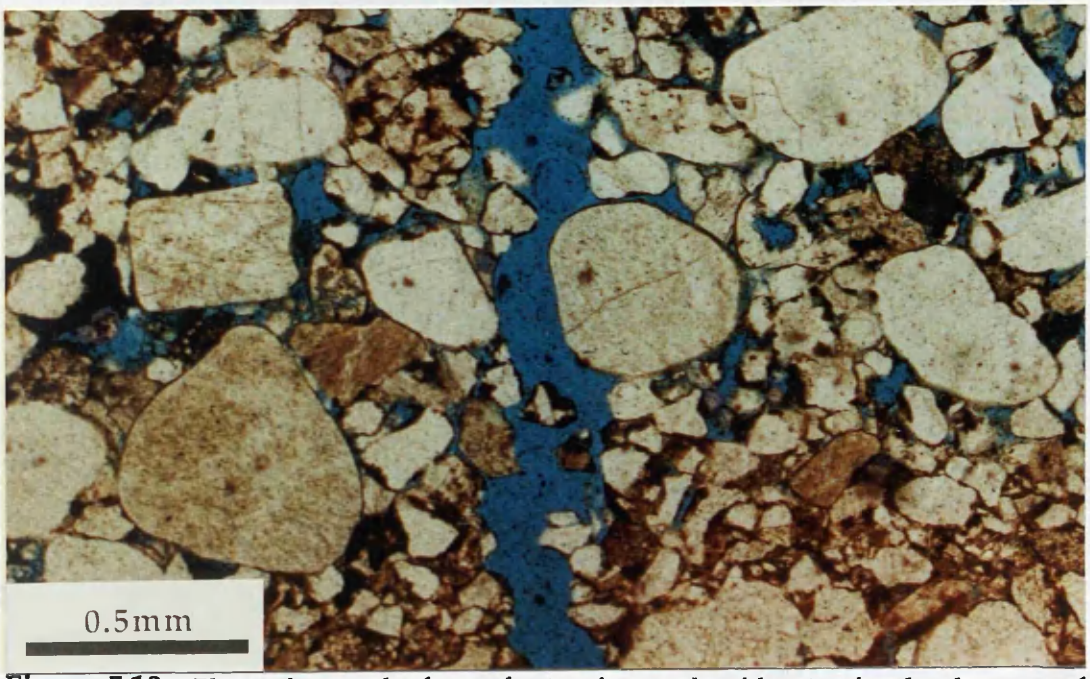

Figure 5.13 Photomicrograph of open fracture in sample with extensive development of secondary porosity. This is the same sample as shown in Figure 5.12 and this fracture is thought to have been a path way for aggressive fluids. Note the extensive development of secondary porosity in the coarser grained laminae. Well 49/27-4, 6934'.

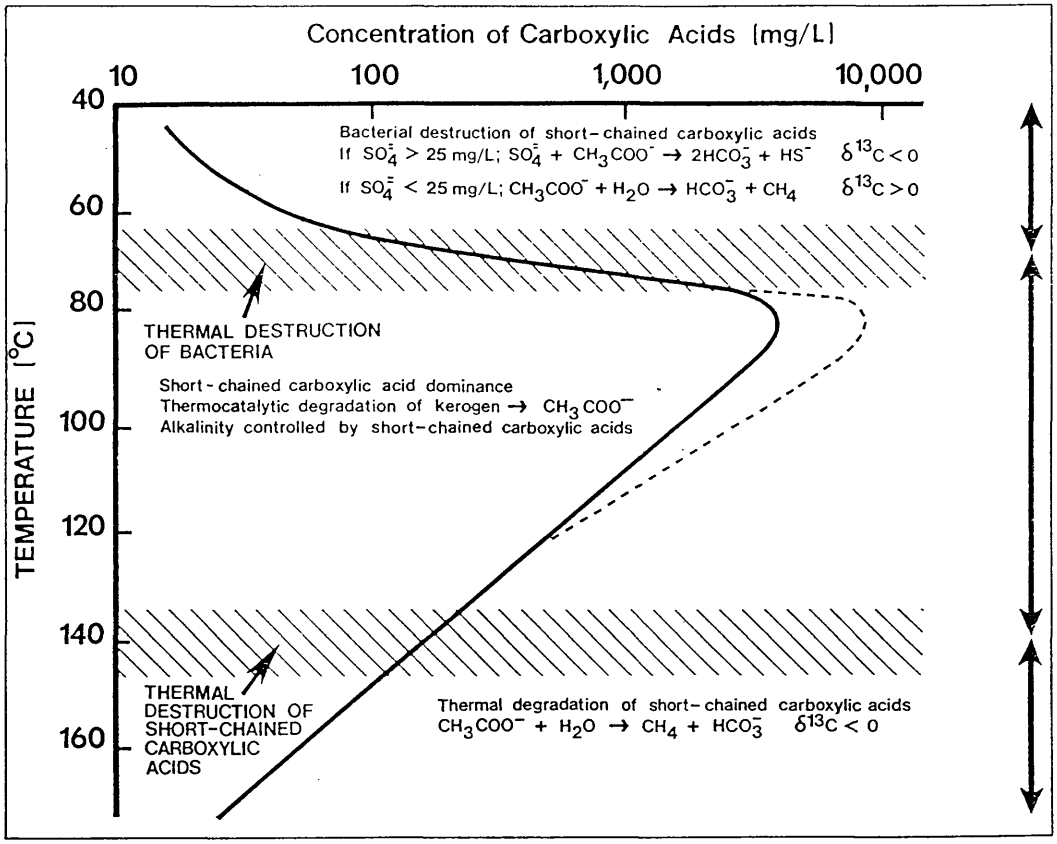

Figure 5.14 Concentration of carboxylic acids anions in oilfield waters vs. temperature. Concentration data are from Carothers and Kharaka (1978). Also shown are areas where bacterial degradation (<80°C) and thermal decarboxylation (>140°C) of carboxylic acids occur. Dashed line indicates maximum reported concentrations (Surdam *et al.*, 1984). (From Surdam *et al.*, 1989).

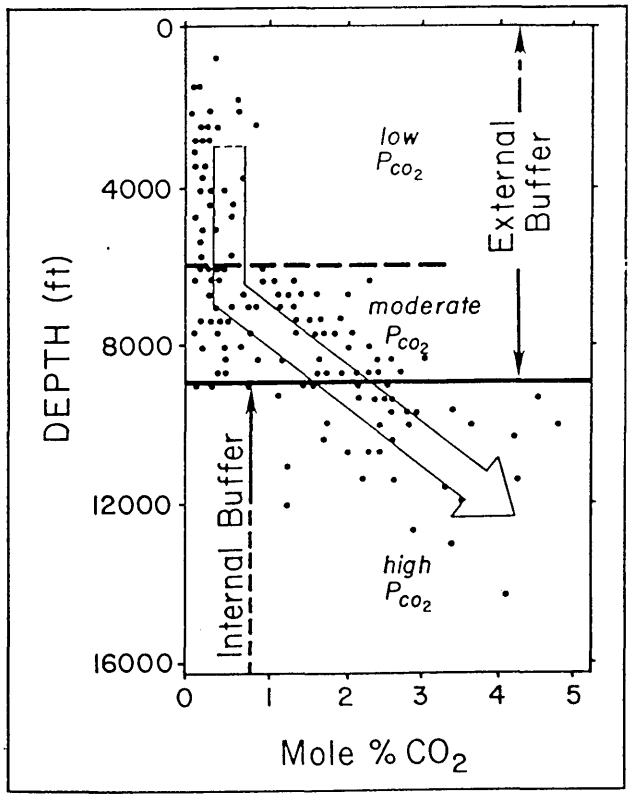

Figure 5.15 Mole % CO_2 from gases vs. depth of Wilcox Formation, Texas Gulf Coast. Mole % CO_2 data from Franks and Forester (1984). (From Surdam *et al.*, 1989).

CHAPTER 6

CHAPTER 6 SUMMARY AND CONCLUSIONS

6.1 CONCLUSIONS

The aim of this project was to document and decipher the diagenetic history of the Rotliegend Sandstone in the Leman field, focusing on the controls of authigenic mineral distribution and the evolution of pore fluids during burial diagenesis. This was accomplished applying geological, petrographic, geochemical and isotopic techniques and integrating the results from each to gain a better understanding of the complex diagenesis of the Rotliegend.

The sequence of major diagenetic events includes: compaction of detrital grains, dissolution of unstable detrital components, precipitation of authigenic cements, and development of secondary porosity. The major diagenetic minerals are hematite and mixed layered illite/smectite, dolomite, quartz, feldspar, chlorite, illite, ankerite, siderite and anhydrite.

Hematite: The first diagenetic minerals to precipitate were hematite (iron oxide) and smectitic clay which occur as thin coatings on detrital grains. The hematite/clay coatings are interpreted as having formed due to the alteration and dissolution of unstable iron silicates by oxidizing meteoric waters. The iron oxide cement is well developed throughout the Rotliegend except where later alteration by reducing fluids has removed it, as in the lower portion of well 49/26-5, or in the reworked dune deposits at the top of the Rotliegend, where the Late Permian marine incursion prevented the extensive development of hematite.

Dolomite: Two distinct generations of pervasive dolomite cement are recognized in the Rotliegend Sandstone. The first phase of dolomite is represented by microrhombic (10 to 30 μm) and rhombic (100 to 200 μm) Type I dolomite crystals. Microrhombic dolomite occurs as both coalesced aggregates of crystals and as individual pore lining rhombs. Rhombic dolomite commonly forms blocky, anhedral crystals, which reflect interfering growth during precipitation. Both grain sizes of

dolomite aggressively replace detrital grains. Examination under cathodoluminescence shows that the majority of microrhombic and rhombic dolomite is represented by brightly luminescent Type I dolomite. The uniform luminescence of both grain sizes of rhombic dolomite is consistent with the hypothesis that they are the same generation of cement. The chemistry of the Type I carbonate is also very uniform and is characterized by non-ferroan dolomite. The zoned bright luminescence and non-ferroan chemistry of the rhombic Type I dolomite is observed in all wells examined in the Leman field indicating the efficiency of the vertical and lateral communication of diagenetic fluids within the field during dolomite precipitation.

Type II dolomite is the second generation of dolomite cement recognized in the Leman field. It occurs as poikilotopic patches, corrosive overgrowths on earlier Type I dolomite, and individual pore lining rhombs. Overgrowths of Type II dolomite on earlier Type I dolomite rhombs indicates that the Type II is a slightly later generation of cement, although it is thought that both formed formed during early diagenesis. The Type II dolomite has extensively replaced detrital grains and this aggressive replacement has produced an "apparent" open texture in many of the samples studied. The Type II dolomite appears dull red to brownish red under cathodoluminescence and is significantly more ferroan (up to 4 mole % iron) than the non-ferroan Type I dolomite.

The distribution of authigenic dolomite cement in the Rotliegend Sandstone of the Leman field suggests that variations existed in the supersaturation of porewaters during burial and diagenesis. Three zones (A, B & C) are observed in the Rotliegend Sandstone in the Leman field on the basis of variations in the frequency of crystals and grain size of dolomite. Zone A is at the top of the Rotliegend and is characterized by a high frequency of crystals and extremely fine grained Type I dolomite. Zone B is located in the mid and lower portions of the sequence in the Leman field and consists of coarser grained Type I dolomite which has a lower frequency of nucleation sites than in Zone A. Zone C is located at

the base of the Rotliegend and is dominated by the coarsest size fraction of dolomite, which is Type II poikilotopic dolomite, and has the lowest frequency of nucleation sites.

The observed variations in grain size and frequency of nucleation sites in Zones A and B are consistent with decreasing supersaturation of the pore fluids with respect to Type I dolomite vertically in the Rotliegend, with the fluids at top being more supersaturated than in the lower portion of the sequence. In Zone C no Type I dolomite is observed, perhaps as a result of the complete dissolution of Type I dolomite in the lower portions of the Rotliegend dominated by poikilotopic Type II dolomite. Type II dolomite is significantly less abundant in Zones A and B where it only occurs as corrosive overgrowths on Type I dolomite. The vertical variation in the distribution of Type II dolomite reflects decreasing supersaturation with respect to dolomite moving away from the base of the Rotliegend, in contrast to the distribution of Type I dolomite which reflects decreasing saturation away from the top of the sequence.

Both Type I and II dolomite, from the unaltered red beds within the Rotliegend, have carbon isotope compositions ($\delta^{13}C$ values of approximately -1.5‰) which suggests that the fluids which precipitated dolomite were derived primarily from marine bicarbonate ($\delta^{13}C$ = 0 to +6‰) from the overlying Zechstein evaporites, although there also appears to have been a significant input of waters from the underlying Carboniferous shales ($\delta^{13}C$ = -10 to -25‰) at this time. $\delta^{18}O$ values for the dolomite range from -7.58 to -3.56‰ (PDB) and reflect precipitation from a mixed marine/meteoric water at temperatures ranging from 35-60°C, which corresponds to a burial depth of approximately 400 m to 1.2 km (1200 to 3300 ft) (Figure 6.1). This burial depth would have been attained during the Late Permian-Early Triassic when the basin was subsiding rapidly. $^{87}Sr/^{86}Sr$ ratios of the early dolomite ($^{87}Sr/^{86}Sr$ = 0.7077 to 0.7087) are only slightly more radiogenic then Late Permian sea water ($^{87}Sr/^{86}Sr$ = 0.7070) which is consistent with the hypothesis of the pore

fluids at this time being strongly influenced by an influx of marine waters.

Carbon and oxygen isotopic compositions were also measured for rhombic Type I dolomite from the discoloured whitened region at the base of the Rotliegend in well 49/26-5. Carbon isotope compositions for the dolomite from the discoloured region ($\delta^{13}C$ = -5.50 to -3.93‰) are significantly more depleted than the other Type I dolomites and this is thought to be due to a larger component of Carboniferous sourced waters and the incorporation of isotopically lighter carbon derived from the thermal maturation of organic matter in the underlying petroleum source rocks. $\delta^{18}O$ values, however, are similar for the Type I dolomites from both the unaltered and altered regions of the Rotliegend, suggesting that they formed at comparable temperatures and depths of burial. This supports the petrographic and geochemical information which suggests that they represent the same phase of cementation. The generation of isotopically light carbon at this time appears to have been very localized and it may have been related to channelized upward fluid motion from the Carboniferous along local faults in the Early Triassic.

Quartz and K-feldspar: Two generations of early authigenic quartz are recognized in the Rotliegend Sandstone. The earliest phase of quartz is represented by extremely small prismatic crystals which occur as "outgrowths" on detrital grains. Precipitation of the prismatic quartz was rapidly followed by formation of pore-filling syntaxial quartz which commonly engulfs earlier prismatic quartz, totally occluding porosity in some beds. Both types of early authigenic quartz are best developed along the centimeter thick, coarse grained, cross-stratified laminae of the avalanche deposits of the dune slip face. Selective development of authigenic quartz along coarse grained laminae of the dune slip face, which had the highest depositional permeabilities of any aeolian lithofacies, suggests that these beds sequestered more dissolved silica from migrating porewaters than less permeable horizons.

Quartz cement is volumetrically the most important cement in the Penrith Sandstone in NW England, occupying approximately 70% of

the depositional porosity. Diagenetic fabrics, authigenic mineral types and timing of cementation events in the Penrith Sandstone closely resemble those of Rotliegend Sandstone.

Oxygen isotope ($\delta^{18}O$ = +22.3 to +19.7‰) and fluid inclusion data (72 to 105°C), for both the Rotliegend and Penrith sandstones indicate that the greatest volume of of authigenic quartz precipitated at temperatures between 72 and 105°C from an evolved meteoric brine ($\delta^{18}O$ = -2‰ SMOW). These temperatures would have been attained at burial depths between 1.5 and 2 km (4900 to 6500 ft) during the Late Triassic (Figure 6.1).

The lack of sufficient intergranular pressure solution between quartz grains and the late timing of feldspar dissolution (post-dating quartz cementation) in both the Rotliegend and Penrith sandstones precludes the authigenic silica being derived internally and therefore suggests silica importation. Selective cementation of higher permeability beds by quartz suggests that silica was transported by migrating fluids, rather than diffusion. The temperatures of quartz precipitation (72° to 105°C) are coincident with the temperatures at which maximum silicate diagenetic reactions (80° to 120°C) would have been occurring in the deeper buried shales. Simple calculations indicate that compactional dewatering of the shales could not have supplied sufficient water for transporting the silica into the Rotliegend and Penrith sandstones, so it is thought that addational silica was imported by deep circulation of meteoric waters which were considerably modified by interaction with the rocks through which they passed. The waters which precipitated the quartz cement were probably part of an ascending limb of a regional meteoric water circulating system, such that as the water was circulated to deeper, hotter zones it became saturated with respect to quartz and then precipitated quartz cement as it rose, cooled and became oversaturated. The common occurrence of silicified veins in strongly quartz cemented sands suggests that faults may have acted as conduits for ascending meteoric fluids.

Authigenic K-feldspar is a minor cement which occurs both as

complete overgrowths, and as aggregates of small rhombic crystals. Authigenic feldspar and pore-filling quartz are commonly intergrown, suggesting that these two minerals were cogenetic.

Chlorite and illite: Iron-rich chlorite and illite are common authigenic minerals in the Leman field and post-date the precipitation of dolomite and quartz. Chlorite occurs as pseudohexagonal plates growing radially into pore space. Illite is present as wispy flakes which were formed by the merging and intergrowth of fibrous illite. Illite growth in the Leman field occurred during the middle Jurassic and since chlorite and illite are commonly intergrown they probably formed contemporaneously.

Ankerite and siderite: Ankerite and siderite are late diagenetic cements. Ankerite occurs as pore lining rhombs and also as replacive overgrowths on earlier Type I and II dolomites. The ankerite is compositionally zoned, but due to its high iron concentrations, an inhibitor to luminescence, zoning was not observed under cathodoluminescence. This zoning, seen by backscatter electron imaging, is characterized by concentric layers of strongly ferroan dolomite and ankerite. Generally, zones become more ferroan toward the margins of crystals. Ankerite is uniformly distributed throughout the stratigraphic section, indicating that the processes which affected the distribution and occurrence of dolomite did not influence its precipitation. This suggests that pore fluids were more homogeneous during the formation of ankerite.

$\delta^{13}C$ and $\delta^{18}O$ compositions for the late ankerite are more depleted than those of the dolomite from the unaltered red beds, but the $\delta^{13}C$ compositions of the ankerite (approximately -3.60‰) are very similar to the negative values of the dolomite from the discoloured region at the base of well 49/25-5. The light carbon isotope compositions of the ankerite are interpreted to reflect the generation of isotopically depleted carbon ($\delta^{13}C$ = -10 to -25‰) from the thermal maturation of organic matter in the underlying Carboniferous sediments. The uniformity of $\delta^{13}C$ values for the ankerite throughout the stratigraphic section indicates that this event

was not localized, in contrast to the early dolomite from the discoloured region at the base of well 49/26–5. Instead, prior to/or during ankerite growth the generation of isotopically light carbon was a more important event which affected the whole field. $\delta^{18}O$ values for the ankerite range from –11.70 to –9.60‰ and this shift in $\delta^{18}O$ compositions away from the oxygen values of the earlier dolomite indicates precipitation at higher temperatures. Precipitation temperatures for ankerite are thought to have been between 105° to 125°C from relatively $\delta^{18}O$ enriched brines ($\delta^{18}O$ = 0‰) at a depth of 2.3 km to 3 km (7500 to 10,000 ft) during the Jurassic (Figure 6.1). $^{87}Sr/^{86}Sr$ ratios for the ankerite ($^{87}Sr/^{86}Sr$ = 0.7089 to 0.7112) are significantly more radiogenic than the strontium isotope compositions of the earlier dolomite ($^{87}Sr/^{86}Sr$ = 0.7077 to 0.7087). This increase in radiogenic strontium in the ankerite reflects a significant input from silicate dissolution reactions in the underlying Carboniferous shales ($^{87}Sr/^{86}Sr$ = 0.720). Ankerite is therefore thought to have precipitated from fluids with a strong Carboniferous component, and to reflect the increasing importance of fluids and/or ions derived from the underlying shales during burial diagenesis.

Siderite is uncommon in the Rotliegend and is only found on the sides of mineralized fractures. This suggests that siderite precipitation was controlled by fluids and processes which were restricted to the fractures and did not extend into the sandstones themselves. Unlike the ankerite, the siderite is compositionally homogeneous and is unzoned.

Anhydrite: Anhydrite appears petrographically to have precipitated at the same time as the ankerite and siderite or slightly later. It is a pervasive cement in the Rotliegend and occurs as both intergranular poikilotopic and fracture-filling cements. Poikilotopic anhydrite is best developed along coarser grained laminae, suggesting that high porosities and permeabilities influenced its precipitation. Mineralized fractures with anhydrite are randomly distributed throughout the stratigraphic section. Both morphologies of anhydrite are interpreted as representing the same generation of cement.

$\delta^{34}S$ values for both intergranular and fracture-filling anhydrite in the Rotliegend from the Leman field are approximately +10‰, which coincides exactly with the $\delta^{34}S$ values of Late Permian Zechstein sulphate. The coincidence between the sulphur isotope compositions of the anhydrite in the Rotliegend and that of the Zechstein shows that the source of the sulphate in the Rotliegend was the stratigraphically overlying Zechstein. The strontium isotope compositions of the anhydrite (0.7093 to 0.7112) were not, however, derived solely from the overlying evaporites. Instead they suggest a mixing of radiogenic strontium from the underlying Carboniferous with strontium derived from the Zechstein. The oxygen isotope compositions of anhydrite cements ($\delta^{18}O$ = +14.04 to +15.99‰) reflect precipitation temperatures between 125° and 140°C from relatively $\delta^{18}O$ enriched brines ($\delta^{18}O$ = O‰), which occurred in the Leman field during early Cretaceous maximum burial of the Rotliegend at depths of between 3.5 and 4 km (11,500 to 13,100 ft) (Figure 6.1).

Secondary porosity: The main phase of mineral dissolution and the generation of secondary porosity occurred after the precipitation of late carbonate and sulphate cements and is therefore thought to have been associated with, or following the deepest burial of the Rotliegend Sandstone in the Leman field (Figure 6.1). Secondary porosity, which makes up approximately a third of the present porosity, formed by the dissolution of plagioclase, dolomite, ankerite and anhydrite. Textural evidence for mineral dissolution includes oversized and elongate pores, floating grains, corroded grain margins and authigenic cements. The fabrics and pore geometries produced by mineral dissolution suggest that secondary porosity generation was created by post-depositional leaching at depth by aggressive or undersaturated fluids. The source of the acid waters responsible for secondary porosity generation is thought to have been the maturation of the underlying Westphalian source rocks which resulted in the release of large volumes of CO_2. Mass balance calculations indicate that CO_2 generated by decarboxylation of the Westphalian source rocks can

account for 12% secondary porosity, yet an average of only 5% secondary porosity is observed in the Rotliegend. Therefore the observed secondary porosity in the Rotliegend could have been generated via CO_2 migration during maturation of the underlying Westphalian Coal Measures.

Late quartz and illite: Secondary porosity development in the Leman field was followed by precipitation of minor quartz and illite. The late generation quartz is characterized by small prismatic crystals which are commonly observed growing in secondary pores. Fibrous illite is often intergrown with the late quartz indicating its late precipitation.

Secondary porosity is preserved in the Rotliegend due to its late formation and the emplacement of hydrocarbons soon after its creation (Figure 6.1). This prevented any further diagenesis after the precipitation of minor quartz and illite.

Changing hydrologies and porewaters: From the above we can infer that the porewaters of the Rotliegend Sandstone in the Leman field have been significantly modified during burial diagenesis. The isotopic compositions of the diagenetic minerals provide a valuable record of the temperatures and porewater conditions during their formation and Figure 6.2 summarizes the evolution of porewater $\delta^{18}O$ conditions with respect to temperature during burial diagenesis.

The original pore fluids were probably meteoric waters derived from the arid environment in which the aeolian sands were deposited. It was during this early period that dissolution of iron-rich silicates and the reddening of the Rotliegend occurred with the formation of hematite/clay grain coatings. Permian meteoric waters probably had a oxygen isotope composition of between –5 and –4‰ (SMOW).

Carbon and strontium isotopic data for early dolomite cement indicate that upon flooding of the Southern Permian Basin by the Late Permian Zechstein seas, marine waters penetrated the Rotliegend Sandstone, displacing the depositional meteoric waters. During burial, Zechstein derived marine brines were gradually mixed with evolved meteoric fluids derived from the underlying Carboniferous, producing

vertically stratified porewaters. This stratification of the pore fluids produced the observed vertical variation in frequency and grain size of Types I and II dolomites. Burial temperatures calculated from oxygen isotope measurements of dolomite (35 to 60°C) suggest that the dolomite precipitated during the Late Permian-Early Triassic at depths between 400 m and 1.2 km (1300 to 4000 ft), assuming precipitation from mixed marine/meteoric derived waters with an oxygen isotope composition of −2‰.

Precipitation of extensive quartz cement in the Leman field and much of the southern North Sea basin suggests a change in the hydrology of the basin from gradual mixing of Zechstein and Carboniferous derived fluids to large scale movement of meteoric waters, at least with in the Rotliegend Sandstone. The fluids which precipitated quartz cement were probably part of an ascending limb of a regional meteoric water flow system which circulated evolved meteoric derived fluids through the underlying Carboniferous sediments and precipitated quartz as they rose. The extremely high salinities measured for fluid inclusions in quartz overgrowths and isotope data (C & Sr) for early and late carbonate cements, which pre-date and post-date quartz, indicate that the movement of fluids and/or diffusion of ions from the overlying marine Zechstein evaporites was important even during this period dominated by deep circulation of meteoric derived waters.

With increasing burial, deep circulation of meteoric derived fluids appears to have become less important and precipitation of illite and iron-chlorite is interpreted to have occurred from reducing waters derived from dewatering of the underlying shales. Illite and chlorite formation was followed by the extensive development of ankerite cement. Carbon and strontium isotope data indicate that ankerite also precipitated from porewaters with a strong Carboniferous component, reflecting the continued importance of fluids and/or ions from the underlying shales during burial diagenesis. The uniform stratigraphic distribution of ankerite suggests that these fluids were not stratified, as they were during earlier dolomite formation. The inferred shift in the oxygen isotope

composition of the porewaters at this time probably reflects the decreasing importance of meteoric waters, with isotopically light oxygen, and ^{18}O-^{16}O exchange between porewaters and minerals. Burial temperatures calculated from oxygen isotope measurements of ankerite (105 to 120°C) suggest that the ankerite precipitated during the Late Jurassic-Early Cretaceous at depths between 2.3 m and 3 km (7500 and 10,000 ft), assuming precipitation from waters with an oxygen isotope composition of 0‰.

Precipitation of intergranular anhydrite, fracture-filling anhydrite and siderite cements suggests an influx of fluids along faults and fractures from the overlying Zechstein evaporites during the deepest burial of the Rotliegend Sandstone. Although sulphur isotopes of intergranular and fracture-filling anhydrite strongly support the downward movement of fluids from the overlying evaporites, strontium isotope compositions indicate fluid movement from the underlying Carboniferous shales also occurred at this time. Oxygen isotope compositions suggest precipitation temperatures between 125° and 140°C from brines with a $\delta^{18}O$ of O‰ (SMOW) at depths of between 3.5 and 4 km (11,500 to 13,100 ft).

Lastly, acid waters generated by the maturation of organic matter in the Westphalian Coal Measures migrated into the Rotliegend along faults, microfractures and zones of high permeability following basin inversion. These waters were responsible for the formation of secondary porosity in the Rotliegend and the precipitation of minor quartz and illite in the resulting secondary pores.

6.2 SCOPE FOR FUTURE WORK

As a result of the work carried out in the course of this project, it has become apparent that there is scope for further research into several of aspects of this work. In the following paragraphs some of the possible lines for extension and expansion of this study are briefly outlined.

1) A detailed and accurate reconstruction of the burial history of the Rotliegend Sandstone in the Leman field is needed. The burial history presented in in this thesis is based on the data available at the time of study and includes data from released well logs, shale interval velocities and vitrinite reflectance. Some uncertainty, however, still exists however concerning the the depth of maximum burial and the timing of inversion events, and in order to better understand the important relationship between burial and diagenesis a more accurate burial history is needed.

2) Also related to construction of a more accurate burial history could be a detailed examination of the geothermal gradient during burial, and possible variations in geothermal gradients due changes in basin tectonics and hydrology. There is a distinct lack of data available on variations in geothermal gradients in the North Sea and therefore this study has assumed a constant geothermal gradient of 35°C/km. This is a reasonable assumption, but the geothermal gradient has probably varied due to rifting events and periods of deep penetration of cool meteoric waters.

3) A detailed fluid inclusion study of the various authigenic cements (i.e.dolomite, feldspar, quartz, ankerite, and anhydrite) would be be extremely useful as it may yield important information concerning the temperatures of cementation and could be further used in conjunction with existing oxygen isotope data for the above mentioned minerals to constrain geothermal gradients during burial diagenesis.

4) A study of present day formation water chemistry could be used to help constrain the source or sources of components involved in cementation and these data could be integrated with the isotopic data already collected for the various authigenic minerals to better model chemical changes in the porewaters during burial diagenesis.

5) Probably the most important future research needing to be completed with respect to the diagenesis of the Rotliegend Sandstone in the Leman field, and in the rest of the southern North Sea, is computer modelling of fluid movement in the subsurface during burial diagenesis. Such research could be used to better understand diagenesis, the movement of waters and ions through sedimentary rocks, and to help explain the observed sequence and quantity of diagenetic minerals.

6.3 FIGURES AND FIGURE CAPTIONS

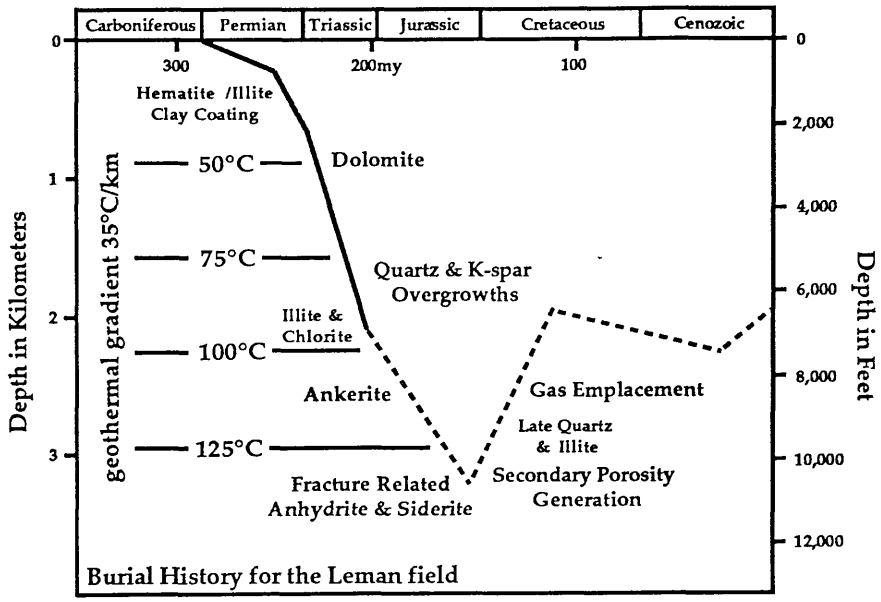

Figure 6.1 Burial curve for the Rotliegend Sandstone in the Leman field showing time and temperature of authigenic mineral precipitation and other major diagenetic events. The reconstructed burial curve is based on well logs 49/27-3 & 49/27-4, interval velocity data from Marie (1975), Glennie *et al.* (1978) and Bulat & Stoker (1987), and vitrinite reflectance data from Cope (1986).

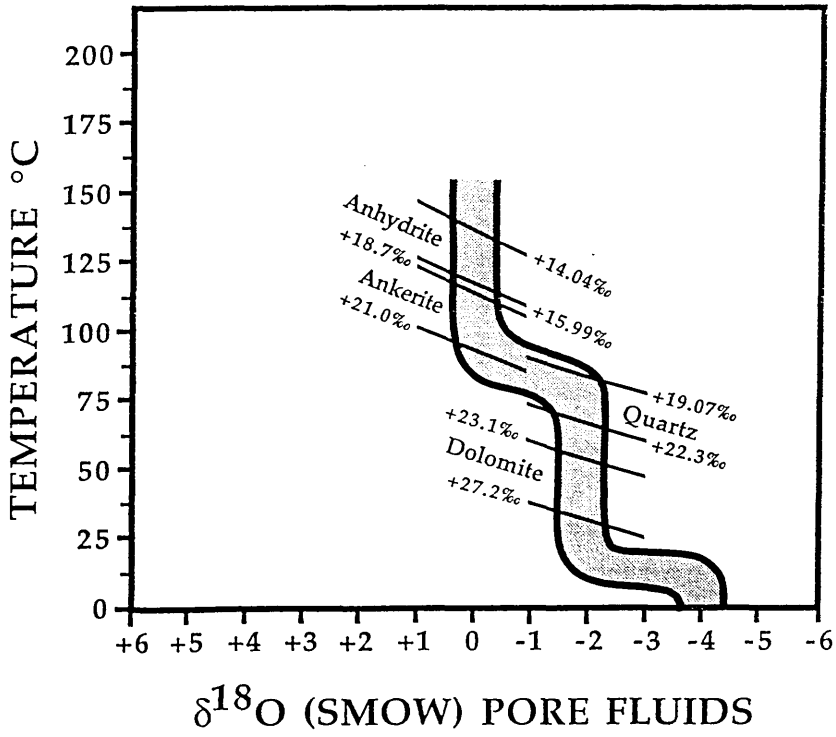

Figure 6.2 Idealized porewater evolution path ($\delta^{18}O$ vs temperature) for the Rotliegend Sandstone.

APPENDICES

Appendix A **List of Samples Selected from the RotliegendSandstone in the Leman field and the Penrith Sandstone from NW England. (Bold = ft, plain = m). Lithofacies key: sf/gf = sandflow/grainflow; wr = wind ripple; f/w = fluvial/wadi. (93 core samples)**

ROTLIEGEND CORE SAMPLES

49/26-5

6346 (1934.3) "Weisliegend"marine-reworked white sandstone, **Zone A**
6466 (1970.8) red sandstone, inclined planar beds (sf/gf) **Zone A**
6565 (2001) red sandstone, horizontal planar beds (wr) **Zone A**
6566 (2001.3) red sandstone, horizontal planar beds (wr) **Zone A**
6670 (2033) red sandstone, horizontal planar beds (wr) **Zone B**
6737 (2053.4) red sandstone, inclined planar beds (wr) **Zone B**
6387 (1946.6) red sandstone, horizontal planar beds (wr) **Zone B**
6925 (2110.7) white sandstone-altered region, horizontal planar beds (wr) **Zone B**
7040 (2145.8) white sandstone-altered region, horizontal planar beds (wr) **Zone B**

49/26-25

6350 (1935.5) red sandstone, horizontal planar beds (wr) **Zone A**
6471 (1972.4) red sandstone, horizontal planar beds (wr) **Zone A**
6500 (1981.2) red sandstone, horizontal planar beds (wr) **Zone A**
6585 (2007.1) red sandstone, horizontal planar beds (wr) **Zone B**
6649 (2026.6) red sandstone, inclined planar beds (wr) **Zone B**
6650 (2026.9) red sandstone, inclined planar beds (wr) **Zone B**
6700 (2042.2) red sandstone, hinclined planar beds (sf/gf) **Zone B**
6722 (2048.9) red sandstone, horizontal planar beds (wr) **Zone B**
6734 (2052.5) red sandstone, horizontal planar beds (wr) **Zone B**
6806 (2074.5) red sandstone, horizontal planar beds (wr) **Zone B**
6851 (2088.2) red sandstone, horizontal planar beds (wr) **Zone C**
6854 (2089.1) red sandstone, inclined planar beds (wr) **Zone C**
6960 (2121.4) red sandstone, horizontal planar beds (wr) **Zone C**
7007 (2135.7) red sandstone, horizontal planar beds (wr) **Zone C**

49/26-26

6363 (1939.9) Weisliegend"marine-reworked white sandstone
6395 (1949.7) red sandstone, inclined planar beds (sf/gf)
6442 (1964.0) red sandstone, inclined planar beds (sf/gf)
6458 (1968.9) red sandstone, inclined planar beds (sf/gf)
6466 (1971.3) red sandstone, inclined planar beds (sf/gf)
6485 (1977.1) red sandstone, inclined planar beds (sf/gf)

49/26-26

6579 (2005.8) red sandstone, horizontal planar beds (wr)
6585 (2007.9) red sandstone, inclined planar beds (sf/gf)
6606 (2014.0) red sandstone, horizontal planar beds (wr)
6609 (2014.9) white sandstone, horizontal planar beds (wr)
6677 (2036.7) red sandstone, inclined planar beds (wr)
6781 (2067.4) red sandstone, inclined planar beds (sf/gf)
6864 (2092.7) red sandstone, horizontal planar beds (wr
6906 (2105.5) white sandstone, horizontal planar beds (wr)
6913 (2107.6) red sandstone, inclined planar beds (sf/gf)
6982 (2128.6) white sandstone, inclined planar beds (sf/gf)
6995 (2132.6) white sandstone, inclined planar beds (sf/gf)
7065 (2154.0) red sandstone, horizontal planar beds (f/w)

49/26-B240

6933 (2113.7) red sandstone, inclined planar beds (sf/gf)
6945 (2117.4) red sandstone, inclined planar beds (sf/gf)
6988 (2130.5) red sandstone, inclined planar beds (sf/gf)

49/27-2

6286 (1916) "Weisliegend"marine-reworked white sandstone, **Zone A**
6305 (1921.8) white sandstone, inclined planar beds (sf/sf) **Zone A**
6317 (1925.4) red sandstone, inclined planar beds (sf/sf) **Zone A**
6345 (1934) red standstone, inclined planar beds (sf/sf) **Zone A**
6372 (1942.2) red sandstone, inclined planar beds (wr) **Zone A**
6396 (1949.5) red sandstone, horizontal planar beds (wr) **Zone A**
6418 (1956.2) red sandstone, inclined planar beds (sf/sf) **Zone A**
6440 (1962.9) red sandstone, inclined planar beds (sf/sf) **Zone A**
6463 (1970.4) red sandstone, inclined planar beds (sf/gf) **Zone A**
6480 (1975.1) red sandstone, inclined planar beds (wr) **Zone A**
6516 (1986.1) red sandstone, horizontal planar beds (wr) **Zone A**
6529 (1990) red standstone, horizontal planar beds (wr) **Zone B**
6552 (1997) red sanstone, horizontal planar beds (wr) **Zone B**
6623 (2018.7) red sandstone, horizontal planar beds (wr) **Zone B**
6697 (2041.2) red sandstone, inclined planar beds (wr) **Zone B**
6735 (2052.8) red sandstone, inclined planar beds (sf/sf) **Zone B**
6737 (2053.4) red sandstone, inclined planar beds (sf/sf) **Zone B**
6795 (2071.1) red sandstone, inclined planar beds (wr) **Zone B**
6850 (2087.9) red sandstone, horizontal planar beds (sf/sf) **Zone C**
6892 (2100.9) red sandstone, inclined planar beds (wr) **Zone C**
6910 (2106.2) red sandstone, inclined planar beds (wr) **Zone C**
7002 (2134.2) red sandstone, horizontal planar beds (wr) **Zone C**

49/27-3

6351 (1935.8) "Weisliegend" marine-reworked white sandstone **Zone A**
6369 (1941.3) "Weisliegend" marine-reworked white sandstone **Zone A**
6376 (1943.4) red sandstone, inclined planar beds (wr) **Zone A**
6479 (1974.8) red sandstone, horizontal planar beds (wr) **Zone A**
6535 (1992.4) red sandstone, inclined planar beds (sf/gf) **Zone A**
6560 (1999.5) red sandstone, inclined planar beds (sf/gf) **Zone A**
6602 (2012.3) red sandstone, inclined planar beds (sf/gf) **Zone A**
6715 (2046.7) red sandstone, horizontal planar beds (wr **Zone B**
6717 (2047.3) red sandstone, inclined planar beds (sf/gf) **Zone B**
6800 (2072.6) red sandstone, horizontal planar beds (wr) **Zone B**
6851 (2088.2) red sandstone, inclined planar w/ leached fracture (wr)**Zone B**
6870 (2094) red sandstone, horizontal planar w/ leached fractures (wr) **Zone B**
6894 (2101.3) red sandstone, massive **Zone B**
7017 (2138.8) red sandstone, inclined planar beds (sf/gf) **Zone B**

49/27-4

6463 (1969.9) red sandstone, inclined planar beds (sf/gf) **Zone A**
6670 (2033) red sandstone, horizontal planar beds (wr) **Zone A**
6851 (2088.2) red sandstone, horizontal planar beds (wr) **Zone B**
6934 (2113.5) red sandstone, inclined planar w/ leached fracture (wr) **Zone B**

ROTLIEGEND CORE PLUGS (Sample depths are in feet) **(37 core plugs)**

49/26-26

#15 (6364) "Weisliegend" marine-reworked white sandstone
#42 (6391) white sandstone, inclined planar beds (sf/gf)
#48 (6395) red sandstone, inclined planar beds (sf/gf)
#54 (6403) red sandstone, inclined planar beds (sf/gf)
#61 (6410) red sandstone, inclined planar beds (sf/gf)
#68 (6441) red sandstone, inclined planar beds (sf/gf)
#84 (6457) red sandstone, inclined planar beds (sf/gf)
#137 (6512) red sandstone, inclined planar beds (sf/gf)
#151 (6526) red sandstone, inclined planar beds w/ slump structure (sf/gf)
#159 (6534) red sandstone, inclined planar beds (sf/gf)
#163 (6556) red sandstone, inclined planar beds (sf/gf)
#169 (6562) red sandstone, inclined planar beds (sf/gf)
#207 (6600) red sandstone, horizontzl planar beds (wr)
#232 (6624) red sandstone, inclined planar beds (sf/gf)
#251 (6643) red sandstone, inclined planar beds (sf/gf)
#266 (6658) red sandstone, inclined planar beds (sf/gf)
#275 (6667) red sandstone, inclined planar beds (sf/gf)

49/26-26

#317 (6739) red sandstone, inclined planar beds (sf/gf)
#323 (6745) red sandstone, inclined planar beds (wr)
#329 (6751) red sandstone, horizontal planar beds (wr)
#332 (6754) red sandstone, inclined planar beds (sf/gf)
#334 (6756) red sandstone, inclined planar beds (wr)
#335 (6757) red sandstone, inclined planar beds (wr)
#338 (6760) red sandstone, horizontal planar beds (wr)
#342 (6764) red sandstone, inclined planar beds (wr)
#354 (6775) red sandstone, inclined planar beds (sf/gf)
#363 (6784) red sandstone, inclined planar beds (sf/gf)
#438 (6860) red sandstone, horizontal planar beds (wr)
#453 (6875) red sandstone, inclined planar beds (sf/gf)
#503 (6928) red sandstone, horizontal planar beds (wr)
#505 (6930) red sandstone, inclined planar beds (wr)
#608 (7067) white sandstone, horizontal planar beds (sf/gf)
#613 (7092) white sandstone, inclined planar beds (sf/gf)
#664 (7118) white sandstone, horizontal planar beds (f/w)
#685 (7139) white sandstone, horizontal planar beds (f/w)
#750 (7211) white sandstone, horizontal planar beds (f/w)
#756 (7217) white sandstone, horizontal planar beds (f/w)

PENRITH OUTCROP SAMPLES **(distance from fault)**

Nunnery Walks #1 red sandstone, inclined planar beds (sf/gf) **(1 metre)**
Nunnery Walks #2 red sandstone, inclined planar beds (sf/gf) **(3 metres)**
Nunnery Walks #3 red sandstone, inclined planar beds (sf/gf) **(5 metres)**
Nunnery Walks #4 red sandstone, inclined planar beds (sf/gf) **(10 metres)**
Nunnery Walks #5 red sandstone, inclined planar beds (sf/gf) **(15 metres)**
Nunnery Walks #6 red sandstone, inclined planar beds (sf/gf)
Nunnery Walks #7 red sandstone, inclined planar beds (sf/gf)

Kirkoswald #1red sandstone, inclined planar beds (sf/gf) **(1 metre)**
Kirkoswald #2red sandstone, inclined planar beds (sf/gf) **(5 metres)**
Kirkoswald #3red sandstone, inclined planar beds (sf/gf)

Shepherd's Hill Quarry #1 red sandstone, inclined planar beds (sf/gf)
Shepherd's Hill Quarry #2 red sandstone, inclined planar beds (sf/gf)

Appendix B Point count data for Rotliegend and Penrith sandstones

Well	49/26-5							49/26-25		
Depth (feet)	6346	6466	6566	6670	6737.5	6925	7040	6585	6649	6722
Detrital										
mono x-tal qtz	47.7	45.9	49.3	47.1	47.5	50.4	51.0	45.2	50.6	51.8
poly x-tal qtz	16.3	12.3	13.7	15.3	13.5	14.2	12.5	11.4	13.5	15.6
k-spar	4.6	8.3	6.3	2.7	4.0	3.5	5.7	6.5	1.9	6.1
plagioclase	1.6	1.7	1.1	0.5	0.7	1.0	0.5	Tr	1.1	1.9
rx fragments	6.1	7.2	5.0	6.9	7.3	7.5	6.4	5.5	4.9	9.2
heavy minerals	Tr-S	Tr	—	Tr-Z,S	Tr-S,R	—	Tr	—	Tr-R	T-R,S
Authigenic										
dolomite	7.0	4.3	3.0	4.2	6.1	4.5	6.5	3.7	4.3	3.5
ankerite	2.3	1.7	4.1	3.1	1.9	2.5	4.9	0.8	1.7	1.4
anhydrite	4.3	1.1	4.5	6.8	1.1	Tr	2.1	0.7	Tr	Tr
quartz	1.1	5.2	1.2	0.9	2.7	1.5	1.3	1.3	0.9	0.6
k-spar	0.3	1.1	0.7	Tr	0.3	—	Tr	—	Tr	1.0
clay	0.9	1.7	1.2	1.7	1.4	0.9	1.1	0.9	1.1	1.7
porosity	7.0	11.2	9.5	12.5	13.4	14.2	8.1	23	10.0	7.2

Well	49/26-25		49/26-26							
Depth	6854	6965	6395	6458	6467	6534	6643	6754	6860	6913
Detrital										
mono x-tal qtz	44.8	50.7	47.2	45.6	43.0	48.1	46.9	45.2	49.0	45.3
poly x-tal qtz	15.9	14.8	12.6	11.4	12.7	14.3	10.2	11.5	14.1	11.4
k-spar	4.9	4.1	5.5	6.6	6.9	4.3	7.1	6.4	8.8	7.1
plagioclase	1.2	1.8	0.8	2.1	1.5	1.1	Tr	2.1	0.9	Tr
rx fragments	5.1	7.8	7.5	5.8	8.6	7.8	5.2	4.5	6.3	6.3
heavy minerals	Tr	—	Tr-Z	Tr-S	Tr	Tr	Tr	—	Tr-R,S	Tr
Authigenic										
dolomite	10.1	4.8	Tr	1.2	1.7	3.6	Tr	1.2	3.1	0.9
ankerite	3.1	4.1	2.8	Tr	2.0	6.0	1.9	Tr	1.7	Tr
anhydrite	1.1	2.1	Tr	Tr	2.1	TR	7.4	5.5	4.5	3.2
quartz	2.8	Tr	15.1	17.8	12.1	1.6	11.5	8.5	3.0	17.8
k-spar	Tr	Tr	1.1	1.9	0.9	—	0.9	1.2	Tr	2.1
clay	1.8	0.7	0.7	1.0	0.5	1.2	0.6	0.5	2.1	0.7
porosity	8.2	9.1	7.2	6.9	8.8	12.1	8.1	12.4	4.9	5.4

Well	49/26-B240		49/27-2							
Depth	6933	6945	6286	6305	6317	6372	6396	6418	6516	6623
Detrital										
mono x-tal qtz	43.8	45.7	43.5	50.6	48.0	51.0	46.9	47.7	47.0	48.3
poly x-tal qtz	14.9	11.8	13.6	13.4	14.7	14.3	11.2	11.5	13.8	10.4
k-spar	4.9	3.1	6.5	1.6	7.9	4.3	2.1	5.4	5.8	7.1
plagioclase	1.2	1.8	0.8	2.1	1.5	1.1	Tr	2.1	0.9	Tr
rx fragments	4.1	7.8	8.5	7.8	6.6	7.8	4.2	6.5	7.3	8.3
heavy minerals	Tr	—	Tr-Z	Tr-S	Tr	Tr	Tr-Z,S	—	Tr-R,S	Tr
Authigenic										
dolomite	2.1	3.1	2.7	2.2	6.6	5.4	3.3	3.3	4.3	0.9
ankerite	2.0	2.6	0.6	0.6	2.7	2.7	12.0	1.2	3.8	Tr
anhydrite	6.3	Tr	12.3	7.3	4.0	—	3.7	0.8	0.9	Tr
quartz	11.8	8.1	3.0	0.7	0.6	0.8	2.9	11.5	6.3	1.3
k-spar	0.8	1.1	0.5	Tr	—	—	0.9	1.2	1.6	0.7
clay	1.8	0.7	0.5	0.6	2.1	1.2	0.6	1.4	1.4	1.1
porosity	7.0	15.1	7.5	12.3	5.3	12.4	12.1	8.4	7.1	24.9

Well	49/27-2									49/27-3
Depth	6681	6697	6737	6795	6850	6892	6910	6943	7002	6351
Detrital										
mono x-tal qtz	47.8	48.9	44.7	40.6	48.1	50.0	49.7	40.3	53.3	47.5
poly x-tal qtz	12.5	18.0	12.8	18.2	14.5	11.2	12.0	15.8	10.9	12.5
k-spar	4.3	7.4	9.1	1.9	4.3	6.5	2.9	7.1	2.7	6.0
plagioclase	1.4	2.1	0.9	0.8	0.9	1.1	Tr	1.7	2.3	Tr
rx fragments	9.5	8.2	5.9	4.5	7.2	5.5	8.2	6.1	7.3	5.5
heavy minerals	Tr	Tr-Z,S	Tr-S	—	Tr	Tr	Tr-S	Tr	Tr-Z,S	Tr-S,R
Authigenic										
dolomite	4.3	4.3	5.0	1.8	3.2	3.5	5.2	2.1	5.2	6.0
ankerite	2.0	1.8	4.3	—	7.1	4.1	—	1.0	3.4	13.0
anhydrite	1.0	—	2.3	—	—	1.6	—	—	3.7	1.5
quartz	2.4	Tr	3.7	0.9	Tr	1.9	1.4	0.8	0.6	2.0
k-spar	0.6	—	0.4	0.6	—	0.8	0.3	—	Tr	1.5
clay	0.9	1.9	2.1	1.1	1.3	0.6	2.3	2.1	2.3	1.1
porosity	13.4	9.3	6.9	26.2	9.6	13.2	18.0	22.0	8.3	5.4

Well	49/27-3					49/27-4			
Depth (feet)	6369	6560	6717	6851	7017	6463	6670	6851	6934
Detrital									
mono x-tal qtz	50.1	51.3	48.4	48.7	46.0	42.6	49.6	50.0	48.4
poly x-tal qtz	11.3	13.2	12.2	16.7	14.8	11.3	15.3	15.2	12.2
k-spar	7.8	4.5	6.3	8.5	3.4	5.7	4.1	3.6	3.1
plagioclase	1.4	1.0	1.1	1.3	1.3	1.9	1.2	2.1	1.3
rx fragments	9.2	6.2	5.1	8.2	8.4	9.4	10.2	7.9	5.4
heavy minerals	Tr-S	Tr-S	Tr	—	Tr-S,R	Tr	Tr-S	Tr	—
Authigenic									
dolomite	1.5	4.9	3.7	3.0	4.6	0.8	3.1	3.8	2.9
ankerite	0.6	7.0	9.3	1.5	7.3	—	5.2	4.1	1.5
anhydrite	—	2.1	1.2	—	2.1	—	Tr	5.8	3.1
quartz	2.9	1.4	0.8	2.5	1.1	20.2	0.8	1.3	1.0
k-spar	1.5	0.6	2.2	0.6	0.4	5.6	—	0.6	0.6
clay	1.1	2.1	1.7	1.0	2.0	0.4	2.6	1.4	2.4
porosity	12.6	6.7	9.3	8.2	8.6	1.8	7.9	4.2	18.1

Location	Nunnery Walks				
Sample	NW#1	NW#2	NW#3	NW#4	NW#5
Detrital					
mono x-tal qtz	50.1	47.3	48.4	49.5	46.0
poly x-tal qtz	11.3	12.2	12.2	16.7	14.8
k-spar	3.1	2.2	4.3	6.5	3.4
plagioclase	1.4	1.0	1.1	1.3	1.3
rx fragments	3.5	4.2	1.8	5.1	3.5
heavy minerals	Tr	Tr	Tr	TR	Tr
Authigenic					
dolomite	—	—	—	—	—
ankerite	—	—	—	—	—
anhydrite	—	—	—	—	—
quartz	17.5	19.1	23.6	19.2	14.6
k-spar	2.4	1.9	2.2	2.2	1.9
clay	1.1	2.1	2.3	0.9	1.1
porosity	10.1	9.4	5.6	6.0	13.4

Appendix B Additional point count data for the Rotliegend Sandstone in well 49/26-26. These samples were examined to provide additional data on the distribution of quartz cement in the field.

Well 49/26-26 Sample (depth in feet)	% quartz cement	lithofacies
6363'	3.3	m
6364'	3.7	m
6376	1.9	m
6391'	19.6	sf/gf
6410'	9.5	sf/gf
6441'	2.1	sf/gf
6492'	2.2	gf
6466'	1.8	wr
6512'	5.3	sf/gf
6526'	2.0	sf/gf
6624'	12.0	sf/gf
6631	2.1	wr
6658'	8.3	sf/gf
6667'	6.1	sf/gf
6739'	3.3	gf
6745'	7.1	wr
6751'	0.5	wr
6756'	15.3	sf/gf
6760'	1.1	wr
6764'	1.5	wr
6775'	7.2	sf/gf
6782'	4.2	wr
6784'	3.8	sf/gf
6865'	2.3	wr
6928'	1.1	wr
6930'	5.1	sf/gf
7067'	14.7	sf/gf

Well 49/26-26 Sample (depth in feet)	% quartz cement	lithofacies
7092	5.0	f/w
7118'	3.1	f/w
7139'	2.2	f/w
7211'	2.6	f/w
7217'	3.6	f/w

Appendix C **Summary of Microprobe Analyses for Carbonate and Sulphate Minerals in the Rotliegend Sandstone in the Leman field.**

(Well/depth in ft.)	$CaCO_3$	$MgCO_3$	$FeCO_3$	$MnCO_3$
Well 49/26-5				
6565'				
Type I dolomite	58.80	40.20	0.37	0.63
	59.19	39.83	0.42	0.56
ankerite	55.78	36.24	7.38	0.60
	57.02	37.38	5.08	0.52
	57.58	37.21	4.65	0.56
	54.90	28.53	16.0	0.57
siderite	3.85	7.10	88.58	0.47
	4.37	7.40	87.70	0.53
	4.60	7.90	87.05	0.45
	4.40	7.75	87.30	0.55
anhydrite (fracture)	40.90	—	—	59.10
	42.30	—	—	57.70
anhydrite (pore)	43.10	—	—	47.90
	41.70	—	—	58.30
Well 49/26-25				
6854'				
Type II dolomite	57.34	38.79	3.37	0.50
	57.80	37.55	4.00	0.65
	57.50	39.10	2.90	0.50
	57.45	38.75	3.30	0.50
	56.80	38.41	4.05	0.74
	57.96	38.05	3.40	0.63
	56.45	38.85	4.05	0.65
Ankerite	54.00	27.60	17.50	0.90
	54.54	31.42	13.40	0.64

(Well/depth in ft.)	$CaCO_3$	$MgCO_3$	$FeCO_3$	$MnCO_3$
Well 49/25-25				
6925				
Type I dolomite	59.83	39.34	0.28	0.55
	57.57	41.80	0.11	0.52
Well 49/26-25				
7040'				
Type I dolomite	58.95	39.60	0.42	0.63
	59.38	39.77	0.27	0.58
	59.65	39.72	0.21	0.42
Well 49/27-2				
6317'				
Type I dolomite	59.15	40.20	0.20	0.65
	58.97	39.98	0.34	0.71
	58.95	40.20	0.39	0.46
TypeII dolomite	57.95	39.45	2.25	0.45
	58.15	38.60	3.75	0.80
ankerite	56.55	33.15	9.55	0.67
Well 49/27-2				
6737'				
Type I dolomite	58.30	40.80	0.20	0.50
	59.02	40.20	0.12	0.58
	59.20	40.70	0.10	0.65
	59.30	40.50	0.20	0.63
	58.90	40.70	0.30	0.61
	58.80	40.45	0.10	0.65
	58.40	40.70	0.30	0.50
	58.20	40.90	0.20	0.70
Type II dolomite	57.80	39.60	2.20	0.35
	57.30	38.73	3.47	0.50
	57.40	39.37	2.60	0.63
Ankerite	56.70	33.20	9.50	0.52
	55.90	34.4	8.50	1.20
	52.5	27.3	19.6	1.0
	53.60	28.20	17.26	0.94

(Well/depth in ft.)	$CaCO_3$	$MgCO_3$	$FeCO_3$	$MnCO_3$
Well 49/27-2				
6737'				
ankerite	56.30	35.50	7.62	0.58
	55.66	32.36	11.0	1.0
	52.85	24.95	21.10	1.10
	52.69	26.61	19.70	1.10
	53.98	28.73	16.37	1.02
	51.38	32.10	24.60	0.92
	52.95	26.75	19.30	1.10
Anhydrite (pore)	41.50	—	—	58.50
	42.10	—	—	57.90
Well 49/27-2				
6892'				
Type II dolomite	57.47	37.8	4.05	.068
	57.38	38.70	3.40	0.52
	56.91	39.10	3.40	0.59
	57.08	38.87	3.60	0.45
ankerite	54.55	31.42	13.40	0.63
	53.95	27.60	17.56	0.89
Well 49/ 27-3				
6560'				
Type I dolomite	58.90	40.55	—	0.55
	59.37	39.70	0.25	0.68
ankerite	53.69	22.80	22.75	0.75
	54.30	21.60	23.45	0.65
	55.0	24.80	19.05	1.15
Well 49/27-3				
6717'				
ankerite	55.30	32.50	11.41	0.79
	52.24	25.22	21.91	0.63
	53.01	28.30	17.59	1.10

,Appendix DSummary of Isotope Results For AuthigenicMinerals in the Rotliegend Sandstone in the Leman Field.

Appendix D.1 **Carbon and oxygen isotope values for dolomite and ankerite in the Rotliegend Sandstone in the Leman field, Quadrant 49. D=dolomite and A=ankerite.**

Lab #	Sample	$\delta^{13}C$	$\delta^{18}O$ (PDB)	$\delta^{18}O$ (SMOW)
C2924	6681 (27-2) D	-1.28	-2.73	28.05
C2926	6892 (27-2) D	-1.53	-5.22	25.48
C2927	6516 (27-2) A	-4.93	-9.85	20.71
C2928	6681 (27-2) A	-3.10	-9.37	21.20
C2929	6737 (27-2) A	-3.11	-8.10	22.52
C2930	6892 (27-2) A	-3.26	-9.42	21.15
C2944	6737 (27-2) D	-2.78	-3.92	26.87
C2946	6681 (27-2) A	-4.72	-9.73	20.63
C2971	6737 (27-2) A	-3.71	-8.89	21.68
C2972	6892 (27-2) A	-2.97	-9.59	20.99
C2973	6566 (26-5) A	-4.35	-10.80	19.71
C2991	6670 (26-5) A	-4.17	-10.45	20.07
C3095	6854 (26-25) A	-4.68	-9.96	20.63
C3103	7040 (26-25) A	-4.46	-9.34	21.20
C3104	6722 (26-25) A	-4.19	-9.35	21.18
C3105	6965 (26-25) A	-4.64	-8.84	22.31
C3107	7040 (26-25) A	-4.68	-10.16	20.38
C3150	6585 (26-25) A	-2.45	-7.89	22.73
C3151	6925 (26-5) A	-2.64	-10.18	20.37
C3152	6965 (26-25) A	-3.00	-9.20	21.38
C3153	6466 (26-5) A	-5.92	-10.10	20.44
C3154	6566 (26-25) D	-2.40	-6.07	24.08
C3155	6670 (26-5) D	-1.36	-4.70	26.02
C3158	6722 (26-5) D	-1.63	-5.04	25.66
C3164	6892 (27-2) D	-0.90	-3.07	27.70

Lab #	Sample	$\delta^{13}C$	$\delta^{18}O$ (PDB)	$\delta^{18}O$ (SMOW)
C3165	6649 (26-25) D	-1.59	-5.33	25.52
C3166	7040 (26-25) D	-5.20	-7.42	22.59
C3167	6566 (26-5) D	-2.77	-4.85	25.85
C3168	6737 (27-2) D	-0.86	-3.07	27.70
C3169	6466 (26-5) D	-2.60	-5.84	24.15
C3170	6566 (26-5) A	-4.35	-8.62	21.28
C3172	6585 (26-25) D	-1.49	-3.74	27.01
C3174	6854 (26-25) D	-1.03	-6.63	24.03
C3175	7040 (26-5) D	-5.89	-8.97	21.61
C3176	6585 (26-25) A	-2.51	-8.32	22.37
C3177	6649 (26-25) A	-3.06	-8.75	21.84
C3180	6851 (27-4) D	-2.23	-4.12	26.61
C3181	6932 (27-4) D	-2.52	-6.33	24.38
C3198	6932 (27-4) A	-2.13	-5.89	24.98
C3199	6670 (27-4) D	-1.00	-3.81	27.04
C3201	6317 (27-2) D	-0.90	-3.62	27.29
C3522	7017 (27-3) A	-3.25	-9.83	+20.73
C3523	6717 (27-3) A	-3.10	-9.71	+20.85
C3525	6670 (27-4) D	-1.00	-4.60	+26.11
C3526	6851 (27-4) D	-2.23	-4.92	+25.79
C3527	7017 (27-3) D	-1.71	-5.32	+25.38
C3531	6560 (27-3) D	-1.79	-5.64	+25.05

Appendix D.2 **Uncorrected $^{87}Sr/^{86}Sr$ and $^{87}Rb/^{86}Sr$ ratios and Sr and Rb concentrations for dolomite, ankerite and anhydrite cements in the Rotliegend Sandstone in the Leman field, Quadrant 49.**

Sample depth in ft (well)	Sr (PPM)	$^{87}Sr/^{86}Sr$ ($\pm 2SE \cdot 10^5$)	Rb (PPM)	$^{87}Rb/^{86}Sr$
Dolomite				
6670' (26-5)	86	0.70843 ±140	3.5	0.11838
6681' (27-2)	25	0.70886 ±208	2.8	0.32299
6737' (27-2)	18	0.70892 ±159	0.8	0.12476
6965' (26-25)	225	0.70882 ±89	2.9	0.03711
Ankerite				
6566' (26-5)	100	0.71035 ±132	3.9	0.11442
6585' (26-25)	59	0.70924 ±165	1.7	0.08584
6854' (26-25)	76	0.71175 ±140	3.9	0.14992
6892' (27-2)	18	0.70994 ±600	1.5	0.23184
7040' (26-25)	88	0.71014 ±86	0.4	0.01416
Anhydrite				
6305' (27-2)	1206	0.70927 ±3	0.805	0.00193
6395' (26-26)	1000	0.70936 ±3	0.485	0.00140
6566' (26-5)	2235	0.70949 ±3	0	0
6606' (26-26)	2149	0.71123 ±3	0	0
6982'(26-26)	1559	0.70949 ±3	0.653	0.00123
7066' (26-26)	1517	0.70979 ±3	0	0

Appendix D.3. Summary of isotope data for quartz cement in the Rotliegend Sandstone in the Leman field and Penrith Sandstone in NW England.

Well no.	depth (ft)	size fraction	$\delta^{18}O$ total quartz
Rotliegend Sandstone			
49/26-5	6459	<30μm	16.7
		30-53μm	16.6
		53-85μm	17.2
49/26-26	6395	30-53μm	17.3
		53-85μm	17.7
		53-85μm	17.0
		85-100μm	17.1
49/26-26	6458	30-53μm	17.8
		30-53μm	18.5
		30-53μm	18.1
		53-85μm	18.1
		53-85μm	18.3
		53-85μm	18.8
		53-85μm	18.0
		85-100μm	18.2
		85-100μm	18.0
49/26-26	6467	30-53μm	18.1
		30-53μm	17.4
		53-85μm	16.7
		85-100m	17.4
		53-85μm	16.9
		85-100μm	19.1
		85-100μm	19.2
49/26-B240	6933	30-53μm	18.6
		53-85μm	18.1

Well no.	depth (ft)	size fraction	$\delta^{18}O$ total quartz
49/26-B240	6933	85-100m	17.9
49/26-B240	6945	30-53μm	-19.0
		53-85μm	18.9
		53-85μm	18.9
		53-85μm	18.1
		85-100μm	17.6
		85-100μm	18.5
49/26-B240	6988	30-53μm	19.5
		30-53μm	18.3
		53-85μm	19.3
		53-85μm	19.4
		85-100μm	19.1
		85-100μm	19.2
49/27-2	6418	30-53μm	17.5
		53-85μm	17.3
		85-100μm	18.3
49/27-2	6463	30-53μm	16.7
		53-85μm	17.8
		85-100μm	15.6
49/27-3	6535	30-53μm	17.3
		53-85μm	17.5
		53-85μm	18.7
Detrital Quartz			12.9
			13.9
			12.2
			12.6
			13.1
			12.7
			13.5

Well no.	depth (ft)	size fraction	$\delta^{18}O$ total quartz
Penrith Sandstone			
Nunnery Walks #1		<30m	18.3
		30-53μm	18.9
		30-53μm	18.7
		53-85μm	21.1
		53-85μm	19.0
		85-100m	18.2
Nunnery Walks #2		30-53μm	20.8
		53-85μm	19.8
		85-100μm	17.5
Nunnery Walks #3		<30m	17.9
		30-53μm	18.8
		53-85μm	20.5
		85-100μm	19.8